ELASTIC STRESS MODELLING AND PREDICTION OF GROUND CLASS USING A BAYESIAN BELIEF NETWORK AT THE KEMANO TUNNELS

by

Josephine S. Morgenroth

B.Sc.E., Queen's University, 2014

A THESIS SUBMITTED IN PARTIAL FULFILLMENT OF

THE REQUIREMENTS FOR THE DEGREE OF

MASTER OF APPLIED SCIENCE

in

THE COLLEGE OF GRADUATE STUDIES

(Civil Engineering)

THE UNIVERSITY OF BRITISH COLUMBIA

(Okanagan)

August 2016

The undersigned certify that they have read, and recommend to the College of Graduate Studies for acceptance, a thesis entitled:

ELASTIC STRESS MODELLING AND PREDICTION OF GROUND CLASS USING A BAYESIAN BELIEF NETWORK AT THE KEMANO TUNNELS

submitted by Josephine Morgenroth in partial fulfilment of the

requirements of the degree of Master of Applied Science.

Dr. Dwayne Tannant – School of Engineering, UBC-O
Supervisor, Professor

Dr. Rehan Sadiq – School of Engineering, UBC-O
Supervisory Committee Member, Professor

Dr. Sumi Suddiqua – School of Engineering, UBC-O
Supervisory Committee Member, Professor

Dr. Joshua Brinkerhoff, School of Engineering, UBC-O
University Examiner, Professor

Dr. Erik Eberhardt – Earth and Ocean Sciences, UBC-V
External Examiner, Professor

August 8, 2016

Date Submitted to Grad Studies

Abstract

The Kemano hydroelectric facility was constructed in the 1950s to supply power to the aluminum smelter in Kitimat, on the west coast of British Columbia. The Kemano project includes a 16 km long water conveyance tunnel that set world record advance rates in the 1950s, and 8 km of a partially completed tunnel.

A risk management strategy was developed in the late 1980s in case of collapse of the first water conveyance tunnel, and by 1990 the excavation of a second tunnel parallel to the first had begun. Work halted in 1991 due to environmental litigation and change in political climate. In 2011 the owner of the Kitimat smelter and the Kemano hydroelectric facility announced plans to continue work on the tunnel that was left unfinished.

This thesis is a collaboration with Hatch Ltd., a consultant to the owner, to determine the ground conditions and support requirements that should be anticipated in completing the backup tunnel. Three dimensional finite element elastic stress modelling was completed in order to determine the in-situ stress conditions as well as the boundary stresses around the tunnel. The modelling results were used to estimate where stress-induced problem areas should be expected, for example at chainages 10+700 to 12+700 in the backup tunnel.

The results of the stress modelling were incorporated into a Bayesian Belief Network that was developed for the Kemano tunnels. It was built using widely accepted empirical relationships in rock mechanics, expert judgement and conditional relationships between inputs. This network predicts the ground class at a user-defined chainage, based on a database that was developed from project literature. The user is also able to input new data as it becomes available, for example during the tunnel advance. The predictions from the network align with what can be seen in the excavated portion of the backup tunnel, for example accurately predicting the need for steel sets at chainage 8+510. The predicted ground class was plotted as a function of chainage, and may be used as a comparison to the support requirements that have been determined thus far.

Preface

Chapters 3 and 4 are based on work conducted in UBCO's Rock Mechanics Lab by Dr. Dwayne Tannant and myself, Josephine Morgenroth. I was responsible for synthesizing data collected from the industry sponsor about the Kemano hydroelectric facility into a usable digital form, building and running the finite element models, and building the Bayesian Belief Network to predict ground class at the Kemano tunnels.

A version of the first half of Chapter 3 was presented at the 2015 Tunnelling Association of Canada workshop in Kingston, Ontario entitled Challenges and Innovations in Tunnelling, and has been published. Morgenroth, J., Tannant, D. D., & Kellaway, M. (February 2016). Submitted as *Tunnel stress modelling and rock support for two hydroelectric tunnels in British Columbia*, published as *Fine tuning.* Tunnels and Tunnelling North America, pp. 34-39.

Ethics approval from the UBC Research Ethics Board was not required for this research.

Table of Contents

List of Figures

List of Tables

Acknowledgements

This research would not have been possible without the support of the Natural Science and Engineering Research Council of Canada (NSERC) and Hatch Ltd., who partnered with my supervisor for an NSERC Engage Grant that is designed to build relationships between industry and academic institutions. Thanks in particular to Sean Hinchberger and Mark Kellaway of Hatch, who championed my involvement in this project.

I'd like to acknowledge the academic support and guidance of my supervisor, Dr. Dwayne Tannant. Thank you for helping me turn this project into the broad and interesting research topic it became.

I'd also like to recognize the members of my supervisory committee, Drs. Rehan Sadiq and Sumi Siddiqua, for their assistance, attention and valuable time.

I offer my gratitude to my fellow graduate students who helped me when I was on the brink of throwing my computer out the window and giving up entirely: Wenbo Zheng, Sam Nunoo, and Oleg Sharbarchin, among many others.

Dedication

To my parents and my siblings, Katrina and Sebastian, for encouraging me to pursue my passion and for teaching me that there are no mistakes, only learning opportunities.

To Claire D'Amico, Ylena Quan, Melissa Weaver, Natalie Narbutt, Liske Bruinsma and Rachel Wilson for being my long distance support network, and for listening to me rant on days when it felt like no progress was made and my continued effort was in vain.

To Jinhee Lee and Mallory Alcock, for not only putting up with my fluctuating enthusiasm for my research, but also for being occasional accomplices in my procrastination.

Chapter 1. Introduction

1.1 Problem Description

Hatch Ltd., the industry sponsor on this thesis, is in the prefeasibility stage of the construction of a 16 km water conveyance tunnel, which was partially completed in the early 1990s. This is the second tunnel to be constructed at the Kemano hydroelectric facility which is located near Kitimat in western British Columbia, and is referred to as the T2 tunnel. The complicated logistics associated with the scale of the project and its remote location necessitate accurate material and quantity estimates for excavation of upstream portion of the T2 tunnel. Fortunately, the first Kemano tunnel (T1) is only 300 m north of T2 and runs approximately parallel to it, providing insight into the ground conditions. Construction records from T1 show that the main challenge with tunnelling through the rock in this area is not the rock mass strength, but rather the pervasive fault-related structure and associated infilling throughout the area. Several minor and one major collapse have occurred in T1 since it was built in the early 1950s, so T2 will serve as a risk mitigation strategy as well as providing extra power generation capacity.

Characterizing the rock mass that will be excavated is a challenge in all tunnelling projects, as there are many inherent geotechnical uncertainties, for example groundwater, stress concentrations, and discontinuity characteristics. There is a wealth of data for the Kemano project area resulting from the T1 excavation records and the T2 downstream drive records, so the challenge becomes applying the data in a meaningful way to predict the rock mass conditions that will be encountered during the T2 upstream drive.

1.2 Research Objectives

The main objective of this research was to determine the ground conditions and associated required rock support along the unexcavated portion of the Kemano T2 tunnel, as well as evaluate the dominant failure mechanisms. The secondary objectives were two-fold: to develop and use a probabilistic tool called a Bayesian Belief Network to handle inherent geotechnical uncertainties and predict the ground class at a given chainage, and to build a 3D stress model of the Kemano area to determine in-situ and tunnel boundary stresses along the tunnel alignments.

This thesis provides a point of comparison for the ground class predictions and support design completed to date, as well as providing a 3D stress model that may be used in future works.

1.3 Research Methodology

The main scope of this project is to evaluate the geotechnical attributes that contribute to the overall stability and ground support design in the Kemano tunnel. This was done using a probabilistic modelling tool called a Bayesian Belief Network, which handles the inherent uncertainty of tunnelling projects by applying conditional dependencies and expert judgement to input parameters. The scope of this thesis was focused on geotechnical, topographical and geometrical aspects of the tunnel, which were captured by widely accepted empirical relationships in rock mechanics. The network does not include operational or logistical considerations such as the costing of materials and quantities, site mobilization and demobilization, contract types (ex. design-build, fixed price, turnkey), excavation advance methods and associated rates, or human factors.

Part of the scope of this thesis was to evaluate the in-situ stresses along the Kemano tunnel alignments using 2D and 3D elastic stress models, for use as inputs into the Bayesian Belief Network. The models were chosen to be elastic and not plastic because of the associated computational cost for such a large model, and also because the elastic stresses were sufficient for their intended use in the Bayesian Belief Network. Locked in tectonic stresses were not considered in the models, and average rock mass material properties were applied as they are essentially uniform in the immediate project area, as all the rock types are crystalline and most are intrusive.

1.4 Project Setting

The Kemano project is a unique part of Canadian history, as it was the largest privately funded construction project in Canada at its time of construction. A detailed account of its political and construction history as well as a more detailed geological summary can be found in Appendix A: Context of the Kemano Project.

1.4.1 Physiography and Climate

The Kemano hydroelectric power generating facility is located approximately 70 km southeast of Kitimat, British Columbia in the Coast Mountains. The site is extremely remote, requiring access by water taxi or helicopter.

The Coast Mountains are characterized by narrow ranges that trend north and northwest which are transected by deep northeast trending valleys. The flooding of these valleys by the Pacific Ocean creates the elongated pattern of fiords on the west coast of British Columbia. The Kemano area is located in the range that marks the eastern edge of the Coast Mountains (Stuart, 1960). The Kemano area does not have the coastal protection afforded by mountainous islands from wet westerly winds, as is the case for much of coastal British Columbia (Stuart, 1960). This results in a high annual precipitation of nearly 4 m, 10% of which falls as snow (Environment Canada, 2015).

1.4.2 Kemano Site

Kemano town is situated at the junction of the Kemano River and Horetzky Creek in Kemano Valley, approximately 60 m above sea level. During the 1950s construction, when the bulk of the infrastructure was completed, the camp housed 6,000 workers and their families (Kendrick, 2012). It included a school, a bank, a small shop, a post office, a golf course and a church (KMA, 2010). When the powerhouse was automated and the community was shut down in 2000, the residents moved out and the buildings were burned down as a training exercise for fire departments from all over B.C. (NRC Canada, 2003). Today, there are contractor and permanent residences, an office building, a recreation centre and a mechanic's shop.

The Kemano powerhouse is located 427 m inside Mount DuBose and houses eight vertical axis generators. Each generator has a capacity of 112 MW, for a total of 896 MW. On-site operators work in weekly shifts consisting of twelve crew members.

The 16 km long, 8 m diameter T1 water conveyance tunnel was constructed in the 1950s using drill and blast technology. It trends approximately northeast-southwest, with the intake at the east end at Tahtsa Lake, and the west end terminating at the penstock tie-in at

what is called 2600' Level. The 2600' Level is the main access portal to the tunnel, penstocks and guard valve chamber, and is aptly named as it is 2600' (790 m) above sea level. Horetzky adit, approximately at the halfway point, offers another access point to the tunnels. T2 is similar in orientation to T1, however the excavated downstream end of the T2 tunnel (7+881 to 16+158) was constructed in the 1990's using a 5.73 m diameter tunnel boring machine (TBM) starting from the Horetzky adit and excavating toward 2600' Level. It remains uncompleted.

1.5 Regional Geology

The Kemano area is at the eastern border of the Coast intrusions, which are composite batholiths underlying the Coast Mountains. The general geological sequence of the area is as follows (Stuart, 1960):

- pre-Middle Jurassic igneous rocks (the Tahtsa Complex)
- Middle and Lower Jurassic volcanic and sedimentary rocks, some metamorphosed (the Gamsby Group)
- Cretaceous sandstones and shales
- post-Middle Jurassic granitic gneisses and massive igneous rocks (the Coast Intrusions)

A detailed account of the regional formations can be found in Appendix A: Context of the Kemano Project.

1.6 Tunnel Geology

As T1 and T2 are approximately 300 m apart, the tunnels pass through similar geologic units. However, the structural geology varies from tunnel to tunnel. The geologic units as well as the abundance of tectonic structure in the area pose different challenges to the design, construction, and support of each tunnel.

The generalized geology along the T1 tunnel alignment can be seen in Figure 1. The Horetzky Complex was encountered at approximately the midpoint of the T1 tunnel, and was described as more closely jointed, sheared and fractured than the Horetzky Dyke (Hatch Ltd., August 2015). Two major shears were encountered during tunnel construction, one dipping

northeast and the other northwest. The Horetzky Dyke, now recorded as the Mortella Pluton, was intersected by the central part of T1. It was found to be in contact with the Gamsby Group, Horetzky Complex, Tahtsa Complex and Dubose Stock (Mortella Pluton), due to its steeply dipping attitude. During T1 construction, more intense fracturing was noted near the contact with the Gamsby Group. Contact with the Tahtsa Complex was considered to be distinct and sharp, while contact with the Horetzky Complex is sheared and weathered over approximately 1 m (Hatch Ltd., August 2015). Observations of the Tahtsa Complex during T1 excavation indicate that many of the fractures and shears are annealed, resulting in a relatively consistent, competent rock mass. Foliation was not noted to be well developed, however highly fractured and sheared areas exhibited numerous calcite veins (Hatch Ltd., August 2015).

Seven major faults were identified along the T1 alignment, six trending approximately north-south and the seventh trending approximately east-west. In addition, shear seams are prevalent along the tunnel alignment, particularly in the Tahtsa Complex. The thickness of these can vary from tens of millimetres to tens of metres, and are typically healed with secondary mineralization (Hatch Ltd., August 2015).

Table 1 shows the breakdown of T1 by lithology, following a report entitled *The Geology of the Kemano-Tahtsa Area* (Stuart, 1960).

Table 1: Lithology along the T1 tunnel alignment.

	Tahtsa Complex	***Gamsby Group***	***Horetzky Dyke/Complex***	***Mortella Pluton***
Chainage	0+000 to 5+000, 6+282 to 7+723	7+723to 9+725	5+000 to 6+282, 9+725 to 13+427	13+427 to 16+185
Total length of unit	6440 m	2000 m	4980 m	2760 m
Percent of tunnel	40%	12%	31%	17%

A longitudinal sections along T2 can be seen in Figure 2 and Figure 3. T2 is partially excavated to date. The downstream half of the tunnel was excavated in the 1990s by TBM, from a heading at the Horetzky adit, which is approximately the halfway point.

The majority of the structural discontinuities encountered during the T2 downstream drive resulted from cooling and shrinkage of fractures associated with the intrusive bodies, contact metamorphism between the Horetzky Dyke and Horetzky Complex, and rebound effects from glacial recession. In general, the rock mass quality along the downstream drive is good to excellent, being overall strong and competent except where localized shears and faults occur (Bechtel Canada, Inc., 1991).

Excavation conditions were very favourable and no major delays or problems were encountered due to rock failures. The areas of lowest rock mass quality can be attributed to stress relief zones (particularly from 11+669 to 12+500) and fault zones (the most significant encountered at 8+500). Significant water seepage was noted only in two locations, coinciding with fault zones (chainages 8+500 and 15+060) (Bechtel Canada, Inc., 1991).

Table 2 shows the breakdown of T2 by lithology, following Volume IV of the Suspension Report produced in 1991 (Bechtel Canada, Inc., 1991).

Table 2: Lithology along the T2 tunnel alignment.

Tahtsa Complex	***Horetzky Dyke***	***Horetzky Complex***	***Mortella Pluton***
0+000 to 2+950	2+950 to 6+830, 9+145 to 12+945	6+830 to 9+145	12+945 to 16+185
2950 m	7680 m	2315 m	3240 m
18%	47%	14%	20%

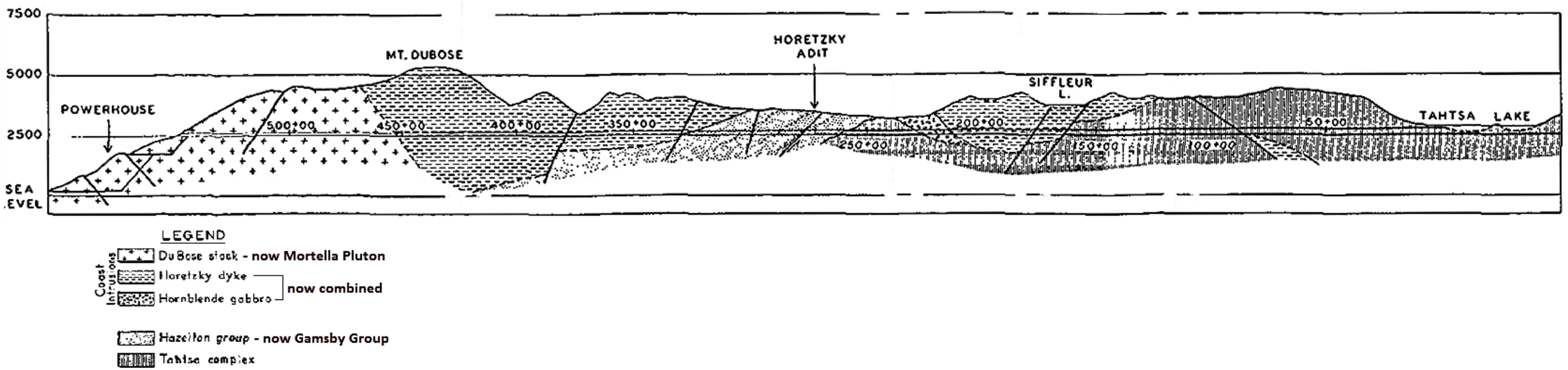

Figure 1: Longitudinal section along T1, showing geology and topography (Stuart, 1960).

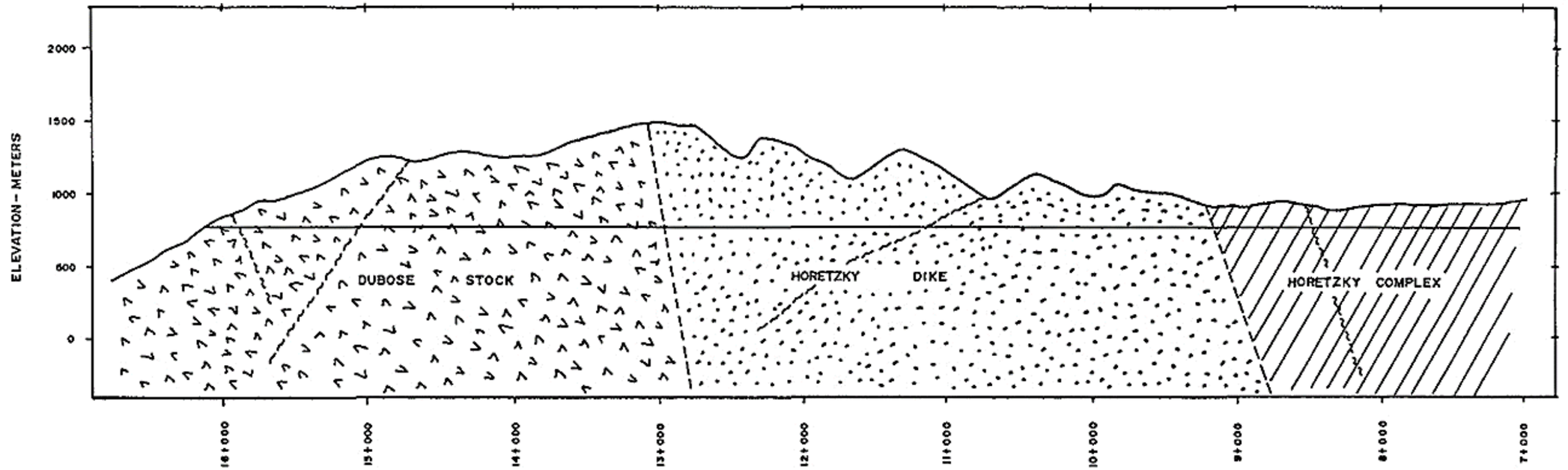

Figure 2: Longitudinal section of downstream T2, showing geology (Bechtel Canada, Inc., 1991).

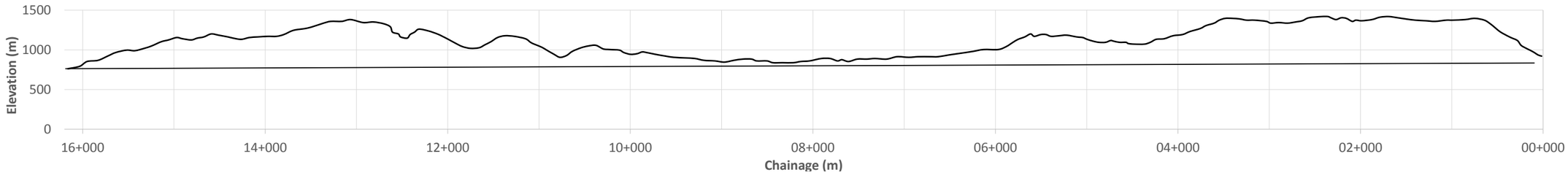

Figure 3: Longitudinal section of T2 tunnel alignment, showing topography.

Chapter 2. Review of Literature

2.1 Risk Assessment Methods

Risk is the probability of an event occurring combined with the severity of the consequence of its occurrence. In general, a risk assessment consists of establishing the context of the risk, identifying and analyzing the risks, prioritizing the risks and finally manage the risks. There are many approaches to do this. Including both qualitative and quantitative knowledge is important in order to get an accurate representation of the whole system. Fault Tree Analysis, Event Tree Analysis, and Failure Mode and Effects Analysis are approaches to identifying failure modes and their effects on a system. However, these methods can only analyze one failure mode at a time, and not an entire interdependent system where some events may depend on the state of other events. This is where the advantage of using a Bayesian Network becomes apparent. Bayesian Networks are able to evaluate the conditional probabilities between multiple events, or nodes, giving rise to much larger and more complex risk models.

2.1.1 Fault Tree Analysis

Fault tree analysis is a top down, deductive form of risk modelling, meaning that it starts at the event of interest and looks backward to assess the cause of an undesired state of a system. This is an interesting solution for obtaining a complete risk, reliability or maintenance analysis, as it allows consideration of dependencies between events as well as the incorporation of various types of knowledge (technical, organizational, decisional, human). However, Fault Tree Analysis struggles to handle multiple failures that affect components of the system, which lead to numerous consequences on the system (Weber et al., 2012). Fault Tree models are also limited in that they are only able to assess one top level event at a time. Several authors (Castillo et al., 1997; Portinale & Bobbio, 1999; Bobbio et al., 2001, 2003; Mohadevan et al., 2001) have shown that a Fault Tree model can be translated into a Bayesian Network, however the reciprocal is not true.

2.1.2 Event Tree Analysis

Event Tree Analysis takes the form of a bowtie diagram, showing whether or not an event has occurred, and whether or not the system has failed. This analysis identifies and

quantifies possible outcomes of an initiating event. This makes Event Tree Analysis a valuable qualitative as well as quantitative risk assessment tool, as it graphically represents the possible scenarios resulting from an event, as well as providing a probability of occurrence for an event and its consequences (Aven, 2008). Like Fault Tree Analysis, Event Tree Analysis can only handle one top level event at a time, meaning that multiple models are required to assess the consequences of multiple events.

2.1.3 Failure Mode and Effect Analysis

Failure Mode and Effect Analysis (FMEA) is a systematic way of assessing how a system might fail. This allows the user to assess the relative impacts of different failure mechanisms and identify parts of the system that need maintenance or need to be replaced. The FMEA approach allows the user to identify potential failure mechanisms, assess the associated risks, and prioritize which problems to address first (Lee, 2001). As with the previous risk assessment tools discussed, the FMEA method is designed to investigate one failure mode at a time, and does not take into account conditional probabilities between these mechanisms.

2.1.4 Bayesian Belief Networks

Bayesian statistics and subjective expected utility (a combination of a personal utility function and a personal probability distribution) first emerged in the 1960s, having origins in probability theory, decision theory and problems in Artificial Intelligence (Sousa & Einstein, 2012). As applied to tunnelling projects, the majority of risk analysis systems, including Bayesian Networks, deal only with “random” (common) geological and construction uncertainties. Additional risks due to specific geotechnical uncertainties are not included (Sousa & Einstein, 2012).

Bayesian Belief Networks can be applied at any stage of risk analysis to replace fault and event trees, as they are designed to model general dependency phenomena (Sousa & Einstein, 2012). These networks are compact, graphical representation of a joint distribution based on simplifying assumptions where some variables are conditionally independent of others (Sousa & Einstein, 2012). The variables together with the directed links form a directed acyclic graph (DAG).

Bayesian Belief Networks consist of several essential components:

- a set of random variables that make up the nodes of the network,
- a set of directed links between nodes that reflect cause-effect relationships,
- finite, mutually exclusive states for each variable, and
- each random variable is connected to a conditional probability table, except for variables on the root nodes which have prior probabilities.

Inference is required to compute answers to queries made to the Bayesian Network and obtain results. There are two main classes of inference: *a priori* and *posterior* (Sousa & Einstein, 2012). *A priori* inferences deduce the probability distribution of a given variable. This type of query is used during the design phase of a tunnel to assess the probability of failure under design conditions, for example geology or hydrology. *Posterior* inferences deduce the distribution of variables given observational evidence, for example updating the probability of tunnel failure as data become available. This type of query is used to update the knowledge of the state of the variable when other variables are observed.

More so than most other areas of civil engineering, tunnelling is characterized by high degrees of uncertainty. These uncertainties stem from the unpredictability of geological conditions, and the subjective construction processes and methodologies chosen by project engineers. There are also several interdependent variables that affect the cost and schedule of tunnelling projects, many of which are difficult to quantify. Factors such as reliability of equipment, skill and morale of workers, excavation sequence and support requirements are challenging to measure and simultaneously have the potential to significantly impact major decisions. For example, the realization of the project, the alignment and configuration of the tunnel, support requirements, excavation methodology and sequence, and the necessity of additional geotechnical exploration work. For this reason, it is important to formalize the uncertainties associated with these variables, and to define them probabilistically to determine the overall uncertainty of the project. One of many methods that can be applied to achieve this is a Bayesian Belief Network.

2.2 Why use Bayesian statistics in geotechnical engineering?

Geotechnical engineers of all education and experience levels are familiar with the uncertainty that is encountered very early on in the design process, which is an essential part of the iterative site investigation and rock mass characterization processes. Many different data types are encountered within this discipline, each with their own degree of certainty and limitations on what further information can be extracted (Figure 4). There is typically improved certainty when moving from prefeasibility and feasibility stages of design where only minimal data are collected, to subsequent engineering design and construction stages when more data are collected and added to the design and decision making process. Even quantities that can be measured with accuracy, for example unconfined compressive test, have an inherent spatial variability that result in not being able to pin down a single, deterministic value. On the other end of the scale, geotechnical engineers often deal with qualitative values that contain a great deal of subjectivity, such as degree of weathering in the RMR system. It is important to keep in mind that while many of the standard geotechnical software suites can handle input parameters with great precision, it is almost never the case that they are known with this degree of certainty.

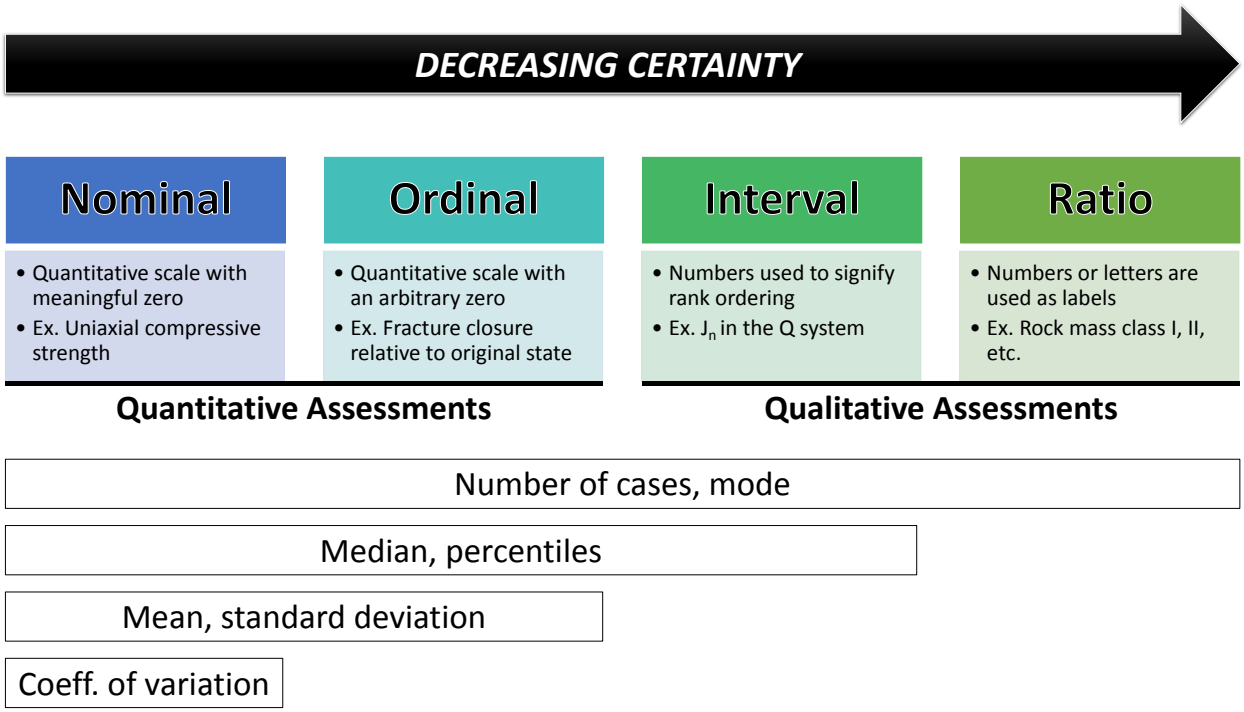

Figure 4: Scales of measurement and the data that are possible to extract at different levels of certainty, adapted from Stevens (1946) and Harrison (2016).

Of particular sensitivity is the junction between qualitative and quantitative data types, where there is an overlap of aleatory variability (natural random variation) and epistemic uncertainty (inability to measure a phenomenon) (Figure 5). This is precisely where Bayesian statistics fits in, due to its ability to combine qualitative information, such as expert judgement, and quantitative data, such as project specific data obtained from site investigations. Bayesian statistical methods should be useful for tunnel design precisely due to this ability to handle an assortment of data: quantitative and deterministic, as well as qualitative and vague. This methodology is also well suited to manage gaps and unknowns in datasets. Bayesian Belief Networks are an appropriate choice for the Kemano case study, because despite its richness in data as far as tunnelling projects go it still involves a myriad of data types and data qualities.

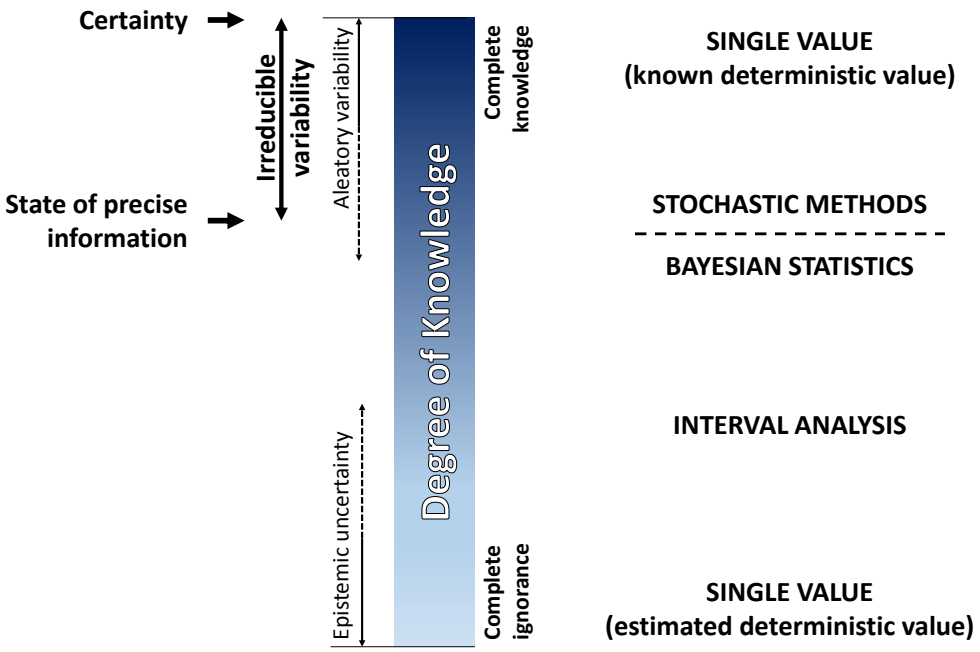

Figure 5: Spectrum of analytical techniques, adapted from Harrison (2016).

2.3 Bayesian Networks for Tunnelling

2.3.1 Decision Aids for Tunnelling (DAT)

The Decision Aids for Tunnelling (Einstein et al., 1992) was developed with the primary goal of simulating the actual construction of a tunnel or network of tunnels. There are two main components of the DAT: a geology module and a construction module.

The geology module creates probabilistic geologic/geotechnical profiles indicating the probability of encountering particular conditions at a particular location along the tunnel axis. This module requires objective geological data as well as subjective estimates from experts as inputs. The user must subdivide the tunnel into geologic zones/units and represent uncertainty in lengths of zones, as well as their transition probabilities. The profiles for all parameters are combined into ground class profiles, where each possible combination of parameters is a ground class.

The construction module simulates the construction process through each ground class. This defines initial and permanent support, as well as the best suited excavation method. Construction is simulated by advancing round by round through one of the geologic profiles, where each round is associated with a particular construction time and cost corresponding

to a particular ground class. This cost and time data is taken from a triangular distribution. This is repeated for the entire set of profiles, generating a set of cost-time pairs which can be plotted to produce a cost-time scattergram representing simulated cost-time pairs for building the tunnel.

The DAT was revised in 2002 (Haas & Einstein, 2002) to include an updating component. As actual progress data becomes available more accurate predictions can be made, either by replacing predictions with actual progress or by refining previously made predictions. Of course, uncertainty about the excavated part of the tunnel is significantly reduced. The main source of uncertainty is the unexcavated upstream part of the tunnel, and therefore as the tunnel advances the overall project uncertainty decreases. It is important to note that significant updating effort lies in data collection during construction. As much of the required data is collected as part of the construction process, it is essential to minimize the additional efforts required for data acquisition. In general terms, the updating process is completed using Equation 1 (Haas & Einstein, 2002).

$$P'' = f(P'; I) \qquad \text{Equation 1}$$

P'' is the posterior prediction, P' is the prior prediction, and I is the new information. A Markov process is used to describe the uncertainties in the geologic/geotechnical parameters, because it can generate parameter state sequences that reflect both the user's knowledge and uncertainties. A more detailed discussion of the mathematical model can be found in Haas & Einstein (2002).

The Decision Aids for Tunnelling (Einstein et al., 1992) encompass binary technical data as well as user interpretations and insight, making them unique as far as Bayesian Networks that have been developed for tunnelling applications. The main obstacle to applying the DAT to active projects is that it does not take into account extraordinary failure events, which can have severe consequences but a low probability of occurring.

2.3.2 Risk analysis during tunnel construction using Bayesian Networks: Porto Metro case study

A methodology was developed to systematically assess and manage risks associated with tunnel construction and applied to Porto Metro in Portugal (Sousa & Einstein, 2012). The

methodology combines two models based on Bayesian Networks, a geological prediction model as well as a construction strategy decision model, including an updating component. The authors' purpose was to address specific geotechnical risk by: a) developing methodology for identifying risk (even low probability), and b) performing a quantitative risk analysis to identify minimum risk construction strategies.

The emphasis of the Decision Support System is on the construction phase where the geological prediction model predicts conditions ahead of the tunnel face, then making it possible to decide on the optimal construction strategy for the updated geologies. This decision is based on maximized utility and minimized risk. The geology prediction model predicts the characteristics of a particular ground class at a particular slice of the tunnel using construction variables, and then uses these data to predict the conditions at the next slice of the tunnel.

The basic structure of construction strategy decision model (Figure 6) consists of the following components.

- Chance nodes: 1) geological condition – possible ground conditions at the face of the tunnel, and 2) failure mode – probability of different failure modes.
- Decision node: construction strategy – determined by the user.
- Utility node: total cost – sum of costs associated with construction strategies and the utilities associated with failure.

The authors of this paper augmented the construction strategy decision model to include more parameters to better suit their Porto Metro case study, including parameters such as piezometric level, ground condition at face, and level of damage resulting from failure.

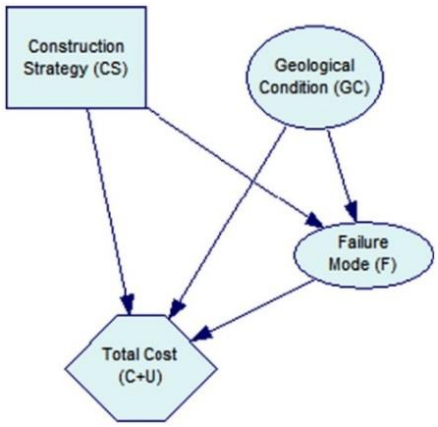

Figure 6: Basic structure of construction strategy decision model (Sousa & Einstein, 2012).

The augmented model was successfully applied to a case study, where tunnel boring machine (TBM) performance data were used to predict geology, which was then in turn used to help decide the lowest risk construction methodology. Through application to the Porto Metro tunnel, where several collapses occurred, it was shown that the model can predict changes in geology and adjust the recommended construction strategy accordingly. An important feature of the model developed by Sousa & Einstein (2012) is that there was an abundance of previous data from the Porto Metro project to calibrate the geological predictions. In other tunnelling projects, this wealth of information may not be available.

2.3.3 Dynamic Bayesian Network for Probabilistic Modelling of Tunnel Excavation Processes

A dynamic Bayesian Network (Špačková & Straub, 2013) was developed for probabilistic assessment of tunnel construction performance, as the authors believed that no previous models fulfilled all the requirements deemed important for realistic estimation of time and construction. Špačková and Straub state that a tunnel construction model should provide the following.

1. Correct modelling of common factors that systematically influence the construction process, which the authors believe lead to stochastic (random) dependence among random variables at different phases of excavation and may pose significant influence on construction time. Examples of this include human and organizational factors.

2. Consideration of the risks associated with extraordinary events. Despite the small probabilities associated with these events, for example collapse or flooding, their consequences have catastrophic delays on schedule and heavy implications on cost.
3. Incorporation of data available from previous projects in similar conditions, so that knowledge is systematically managed.
4. Facilitation of easy updating of predictions with new information as it becomes available.
5. Proper understanding and description of model assumptions and simplifications, especially because probabilistic modelling cannot be tested with experimentation.

The authors point out that many of these requirements could be satisfied with Monte Carlo Simulation, however they propose that a Dynamic Bayesian Network (DBN) is more efficient at updating predictions based on additional observations. The DBN presented by Špačková & Straub (2013) includes extraordinary events as well as human and organizational factors.

This DBN for modelling uncertainties associated with tunnelling is well defined in terms of the input variables, which fall into four categories: 1) geotechnical conditions, 2) construction process, 3) extraordinary events, and 4) overall excavation time. The DBN is shown in Figure 7, and the variables are described in Table 3.

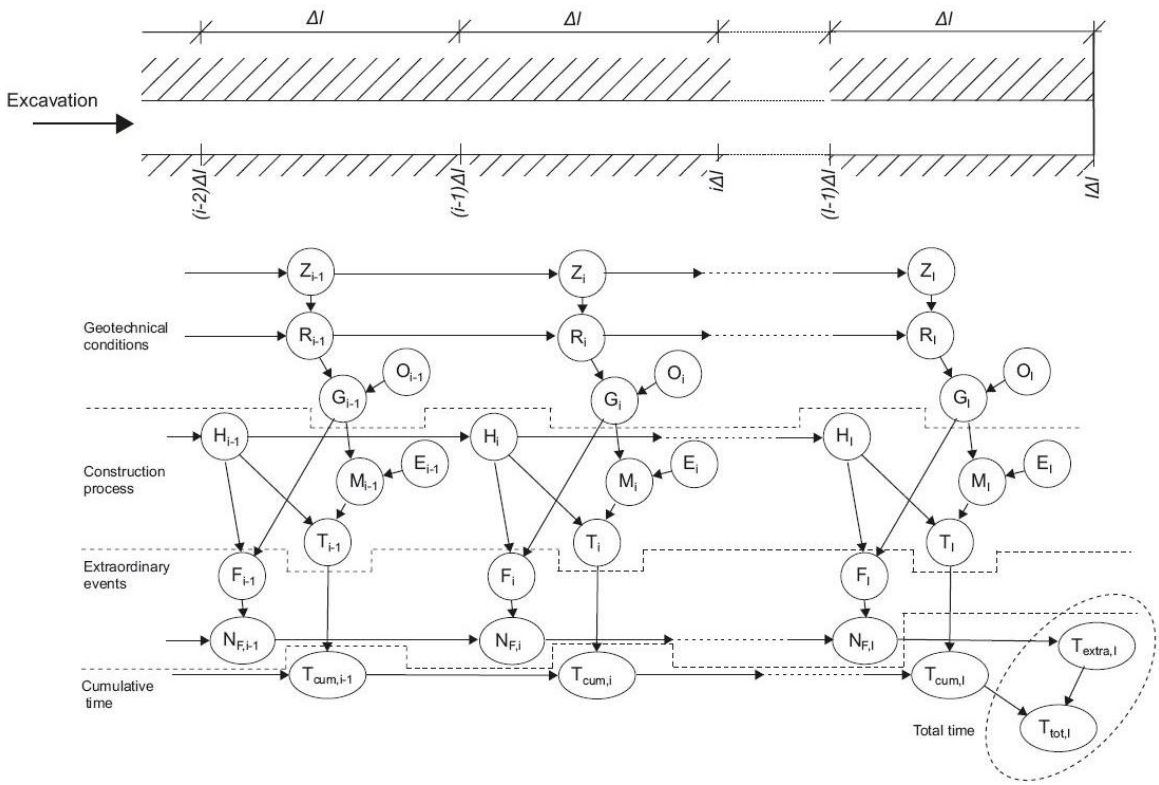

Figure 7: Dynamic Bayesian Network for tunnel excavation (Špačková & Straub, 2013).

Table 3: Input variables for Dynamic Bayesian Network for tunnel excavation (Špačková & Straub, 2013).

Id.	*Variable*	*Type*	*States of the variable*
Z	Zone	Random/discrete	1, 2, . . . , 8
R	Rock class	Random/discrete	I, II, III, IV, V
O	Overburden	Determ./discrete	Low, medium, high
G	Ground class	Random/discrete	L-I, L-II, L-III, L-IV, L-V, M-I, M-II, M-III, M-IV, M-V, H-I, H-II, H-III, H-IV, H-V
H	Human factor	Random/discrete	Favorable, neutral, unfavorable
E	Geometry	Determ./discrete	1 (begin/end), 2 (typical), 4 (chemical plant), 5 (Emergency Parking Places [EPP])
M	Construction method	Random/discrete	P.1, P.2, P.3, P.4, P.5, P.6, P.2–1, P.2–2, P.2–3, P.EPP
T	Unit time	Random/discretized	0, t_{int}, $2t_{int}$, . . . , 15 (days)*
F	Failure mode	Random/discrete	Failure, no failure
N_F	Number of failures	Random/discrete	0, 1, 2, 3, 4, >5
T_{cum}	Cumulative time	Random/discretized	0, t_{int}, $2t_{int}$, . . . , 1,830 (days)**
T_{extra}	Delays caused by failures	Random/discretized	15, t_{int}, $2t_{int}$, . . . , $t_{extra,99.9}$ (days)***
T_{tot}	Total time	Random/discretized	0, t_{int}, $2t_{int}$, . . . , $(1{,}830 + t_{extra,99.9})$ (days)

*t_{int} is the discretization interval of time variables. In the application example it is $t_{int} = 0.5$ days.
**Upper bound of cumulative time = 122 × 15 = (number of segments) × (upper bound of unit time).
***$t_{extra,99.9}$ is the 99.9 percentiles of T_{extra}.

This DBN is evaluated in three steps.

1. All continuous variables are discretized. For example, any variables describing unit time are converted into random variables in a discrete space.

2. Some nodes are eliminated generically from all slices to simplify the computations. The effects of the removed variables are implicit in the reduced DBN model.
3. The modified Frontier algorithm is applied to evaluate the DBN, as described in detail in Špačková & Straub (2013).

The tunnel cost and schedule predictions can be updated at a particular point using the data from other slices. In particular, the probability distribution of a variable in slice *i* is updated using evidence from all the slices preceding it. Again, the Frontier algorithm is required to accomplish this. The cumulative time of the tunnel excavation can be computed by summing the cumulative times at each slice, as well as any delays caused by extraordinary events.

The DBN developed by Špačková & Straub (2013) is unique in that a random variable "human factor" is included to represent the correlation between performance at different stages of construction and the overall quality of the planning and execution, which influence the entire project. In addition, most existing models do not allow for the occurance of extraordinary failure events.

This model is based on the DAT (discussed previously), with modification to how the intrinsic uncertainties in the construction process are represented. The authors state that an area for future improvement is the construction method (M) variable, which should be revised to more realistically reflect the changes of construction technology as the excavation progresses. The current model assumes full flexibility in transitioning between technologies, when in reality there are significant time delays and cost associated with these modifications.

The application of the Frontier algorithm in the DBN developed by Špačková & Straub (2013) allows the user to deal with large quantities of disrete random variables that result from the discretization of continuous random variables. This results in a more efficient evaluation of the DBN.

2.4 Topography-Induced Stress and Failure Mechanisms

2.4.1 Topography and Stress

In general, the simplifying assumption that principal stresses are horizontal and vertical can be made that when the ground surface is horizontal. This is no longer the case when varying topography is introduced. Principal stresses are parallel and perpendicular to overlying topography close to ground surface in the absence of surface loads. With increasing depth, principal stresses approach the same orientations as when the ground surface is horizontal. Tectonic stresses are generated by the movement of crustal material, and are of particular interest in mountain ranges as they behave differently than they would in non-mountainous regions.

Research conducted by Tan et al. (2004) introduced the idea of a "tectonic stress plane" (TSP), a plane near the earth's surface that delineates the depth at which the effect of topography on stress disappears. Above the TSP both tectonic and non-tectonic effects on stress can be expected, and below the TSP only undisturbed tectonic stress exists, aside from the influence of faults and folds (Tan et al., 2004). This research found that valley width affects stress concentration values, but not the TSP depth. At the relatively shallow depth of 500 m, the Kemano tunnels are assumed to be above the local TSP, and topography is expected to affect the tangential boundary stresses.

Studies of gravitational stresses in long symmetric ridges and valleys, of which the Coast Mountains are a good example, have been conducted in order to delineate the nature of topography's impact of stresses (Pan, Amadei, & Savage, 1994). The large variation in geometry and associated deep-cut valleys cause the horizontal tectonic stresses on the sides of mountains to disappear (Zhang et al., 2012). These deep-cut valleys create a free surface relative to the mountain. When the slope is greater than 45° the gravitational stress can cause stress concentrations at the valley bottom (Tan et al., 2004).

2.4.2 Overstressing in Hard Rock Tunnelling

Overstressing, or failure resulting from the stresses induced by a tunnel excavation, can result in spalling and slabbing. Deep hard rock tunnels in steep mountainous terrain may be subject to this brittle failure mechanism just behind the advancing tunnel face during TBM

excavation (Brox, 2012). This is applicable to the Kemano case study, as the T1 and T2 tunnels are located in the Coast Mountains proximal to a valley wall.

Work has been done by Brox (2012) to classify overstressing severity using a ratio of the maximum tangential wall stresses around a tunnel and the rock mass' uniaxial compressive strength, as well as delineating the required support for each class (Table 4). This work was based on previous work done to predict depth of spalling in underground excavations (Martin et al., 2001; Martin & Christiansson, 2009; Diederichs et al., 2010).

Table 4: Overstress classification (Brox, 2012).

Overstressing Class	σ_{max}/σ_c	***Description***	***Relative Overstress Depth, r/a***	***Support***
1	0.45	Minor	~1.0	Spot bolts
2	0.60	Moderate	1.25	Pattern bolts/mesh
3	0.90	Severe	1.60	Pattern bolts/channels
4	1.20	Extreme	1.95	Steel ribs/mesh
5	1.60	Possible rockbursts	2.40	Continuous full profile system

It should be noted that the installation of support for spalling failure is extremely time sensitive, as the longer the ground is left unsupported and unconfined the more space the rock mass has to deform into. Steel ribs are recommended for Brox's overstressing Class 4, which take a long time to install relative to shotcrete, rock bolts and mesh, allowing the rock mass to deform more than is desirable. Steel ribs are also generally installed with room to allow the rock mass to deform and settle into a stable equilibrium, which makes them more applicable to raveling rockmass failure than to spalling.

Brox applied his classification scheme to several tunnels around the world, including the Kemano T2 tunnel (Table 5). The classifications correspond to direct observations and anecdotal information (Brox, 2013).

Table 5: Examples of overstress classification around the world (Brox, 2013).

Project	***Year***	***Excavation Method***	***Length (km)***	***Size (m)***	***Overburden (m)***	***Actual Overstress***
Alfalfal	1990	Drill & Blast	4.5	5	1150	Rockburst
Lesotho Transfer	1990	TBM	45	5	1300	Severe
Rio Blanco	1990	TBM	11	6.5	1200	Severe

Kemano T2	1991	TBM	8	6	650	Minor
Vereina	1996	TBM	21	6.5	1500	Extreme
Manapouri	2002	TBM	10	10	1200	Minor
Casecnan	2002	TBM	21	6.5	1400	Moderate
Loetschberg	2005	D&B/TBM	34	8	2000	Rockbursts
El Platanal	2008	Drill & Blast	12	6	1800	Rockbursts
Ashlu	2009	TBM	4	4.1	600	Moderate
Olmos	2010	TBM	14	5	2000	Rockbursts
Jinping	2011	TBM	16	12	2500	Rockbursts

2.4.3 Predicting Depth of Spalling

It is generally accepted that when the stresses on a tunnel boundary reach the rock mass strength, failure occurs. In good quality rock this failure typically takes the form of spalling, which involves extensional, stress-induced splitting, which forms slabs in the direction of the maximum tangential stress on the tunnel boundary. These slabs may vary from a few millimetres to several centimetres in thickness for circular underground openings ranging from 1 to 5 m in diameter. Progressive spalling can result in V-shaped notches that form diametrically opposite each other, and are sometimes mistaken for wedges (Martin & Christiansson, 2009). Estimating depth of spalling can be crucial to the design of tunnel support elements.

It is unlikely that the orientation and magnitudes of the principal stresses are known at early stages of design, so a relatively simple way of estimating brittle failure was developed by Martin et al. (2009). Martin based his work on two extensive in situ experiments which were carried out to investigate brittle failure: AECL's (Atomic Energy of Canada Ltd.) Mine-by Experiment (Martin et al., 2001) and SKB's (Svensk Kärnbränslehantering AB) Äspö Pillar Stability Experiment (Andersson, 2005). Both experiments aimed to further constrain the stress magnitude required to initiate brittle failure. The grain size of the rock has a significant effect on the stress magnitude required to initiate failure (Martin et al., 2001).

For both experiments, lab tests were carried out to determine the onset of dilation (or crack initiation) and the unconfined compressive strength (UCS) of the intact rock. According to Martin et al. (2009), the mean uniaxial compressive strength, rather than the full range, was found to provide better correlation to field observations. Comparing the crack initiation and UCS values to the stress at which spalling was initiated (rock mass spalling strength, σ_{sm}), it

was determined that the crack initiation value provides a lower bound for rock mass spalling strength, occurring at 0.4 to 0.6 of the mean uniaxial compressive strength for crystalline rock (Martin & Christiansson, 2009). The relationship used to establish the depth of spalling is shown in Figure 8.

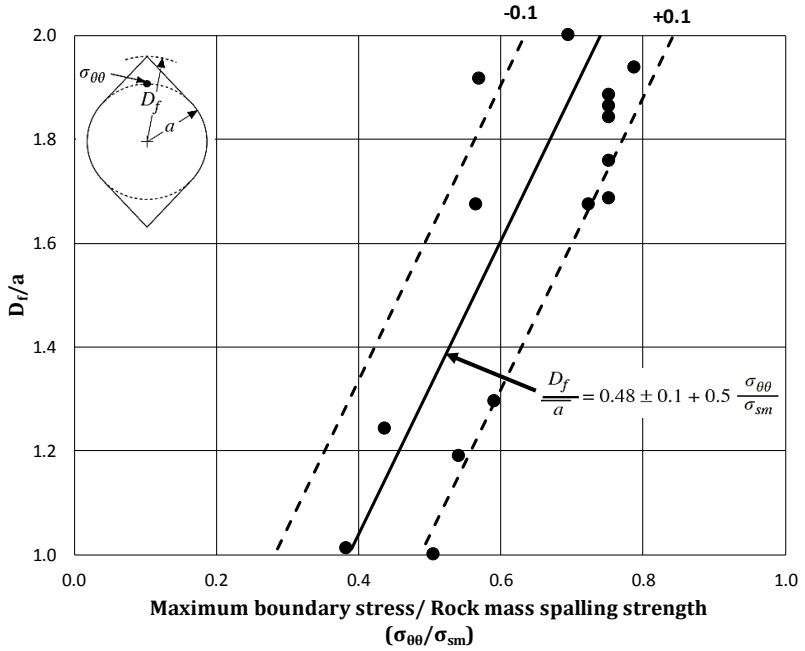

Figure 8: Empirical relationship used to establish the severity of the hazard, i.e., the depth of spalling (adapted from Martin & Christiansson, 2009).

The tunnel specific depth of spalling can be estimated from the empirical correlations described by Martin et al. (2001) and given by Equation 2.

$$s_d = a\left(0.5\,\frac{\sigma_{\theta\theta}}{\sigma_{sm}} - 0.52\right) \qquad \text{Equation 2}$$

The depth of spalling measured from the tunnel boundary is s_d, a is the radius of the tunnel, $\sigma_{\theta\theta}$ is the magnitude of the maximum tangential stresses on the boundary of an underground opening (typically found based on an elastic stress solution,; e.g., Kirsch (1898) equations, or using simple boundary element or finite element numerical modelling), and σ_{sm} is the rock mass spalling strength as described above. The SKB experiment found that the existence of fractures did not significantly affect the average depth of spalling calculated by this equation.

This work was extended by Diederichs, Carter, & Martin (2010) to delineate the severity of the spalling behaviour if it does occur, through the addition of several more case histories.

2.4.4 Rock Mass Ravelling Failure

Ravelling is a gravity controlled failure mechanism, which results from low shear strength and interlocking structure in the rock mass, as well as low tangential stress around the excavation. Important parameters controlling this behaviour are: orientation and degree of fracturing, roughness, aperture and infill of discontinuities, strength of the rock mass, water pressure, stress conditions, and excavation geometry (Goricki, 2013). Thapa, et al. (2009) states that ravelling can manifest as a successive failure mechanism, where small blocks fall out and can progress to result in significant failure in the crown.

Kinematic and mechanical models are typically used to analyze the potential for ravelling to occur. The behaviour of this gravity-induced failure is particularly sensitive to the discontinuity properties and stress conditions, which are rarely known with certainty (Goricki, 2013). It is common to randomly predict these parameters for deep tunnels, and to update the support decision as the excavation advances. The exact prediction of the limit equilibrium of a ravelling rock mass is difficult, but a recognizable pattern can be developed from analytical models and site observations.

The boundary between gravity-induced ravelling and discontinuity-controlled fallouts is also difficult to define, although practically speaking does not have a significant impact on support design. This concept is confirmed in a publication concerning the Caldecott 4th Bore, located in Oakland, California, where support selection was based on ground behaviour and condition, with allowance for adjustments to support design due to variations in ground behaviour (Thapa, et al., 2009).

Beyond describing the symptoms of this phenomenon (ie. progressive failure), very little work has been published to delineate exactly how contributing factors must coalesce to result in ravelling, as has been done for spalling. Most authors can agree that rock mass conditions, structure and groundwater are the most important driving factors, and that boundary stress conditions are secondary (Goricki, 2013; Thapa, et al., 2009; Csuhanics & Debreczeni, 2012).

Work done for empirical design of crown pillars in the mining sector by Carter et al., (2008) is the closest analogy for characterizing progressive gravity driven failure in rock

excavations. Carter developed an expression that captured an intuitive scaling principle: as the size of the undergrond excavation increases, so does the degree of risk for failure of a structure's roof or "crown pillar" (Equation 3).

$$Crown\ Stability = f\left(\frac{T\sigma_h\theta}{SL\gamma u}, Q\right) \qquad \text{Equation 3}$$

Where T is the crown pillar thickness, σ_h is the horizontal in situ stress, and θ is the dip of the foliation or of the underlying opening. An increase in any of these increases the stability for given rock mass. The crown span is S, L is the overall strike length of the opening, γ is the specific gravity of the rock in the crown, u is the groundwater pressure, and Q is the tunnel quality index (Grimstad & Barton, 1993). An increase in any of these decreases the stability of a crown pillar.

Equation 3 can be split into the rock mass characteristics (denomenator) and the underground opening geometry (numerator). This led to development of the basic deterministic approch of comparing the critical rock mass competence where failure might be expected, to the dimensions of the exacation geometry, where the Scaled Span is determined by Equation 4.

$$C_s = S\left(\frac{\gamma}{T(1+S_R)(1-0.4cos\theta)}\right)^{0.5} \qquad \text{Equation 4}$$

Where S is the crown pillar span (m) and S_R is the span ratio (S/L, crown pillar span/crown pillar strike length).

However, Martin's work was developed for steeply dipping openings (represented by θ), and was found to break down on shallow dip openings, such as a tunnel (Carter et al., 2008). The methodology was revised to address shallow dip openings, however it was determined that failure in shallowly dipping stopes was initiated predominantly by hangingwall delamination and/or voussoir arch buckling, which are not generally applicable to long, narrow openings like tunnels. This is where this metholodogy deviates from applicability to this research, and was therefore not used directly for further work contained in this thesis. However, the concept of using two main groupings of factors (rock mass characteristics and underground opening geometry) to assess the potential for ravelling failure was explored further and eventually used to develop a ravelling failure expression (see Section 4.2.3.10).

The principles of Terzaghi's work on estimating rock load is relevant to the discussion of progressive gravity-induced failure, as he spent a lot of time characterizing how tunnels through different rock masses support the load above them by redistributing stresses around the opening (Proctor, Terzaghi, & White, 1946). *Rock load* is defined as the height of the mass of rock which tends to drop out of the roof, or the loads to which the tunnel liner may be subject. If no support is installed, the unsupported mass of rock drops into the tunnel incrementally and results in an irregular chimney-like structure above the tunnel until the tunnel is completely filled in.

Terzaghi discussed how several types of rock masses carry the rock load above a given tunnel geometry, but here the discussion will be focused on the three that are relevant to Kemano: (1) massive, moderately jointed rock, (2) moderately blocky rock, and (3) very blocky, shattered rock.

Tunnels through moderately jointed, massive rocks commonly have blocks formed by intersecting joints that are so closely interlocked that they have little freedom of movement. Over time stress relaxation may allow these blocks to fall out if left unsupported, however with support installed the risk of this type of failure is much less. Depending on the orientation and spacing of joints, the load on the crown may be estimated from the weight of rock defined by a thickness of 0-0.25 times the tunnel span (Figure 9).

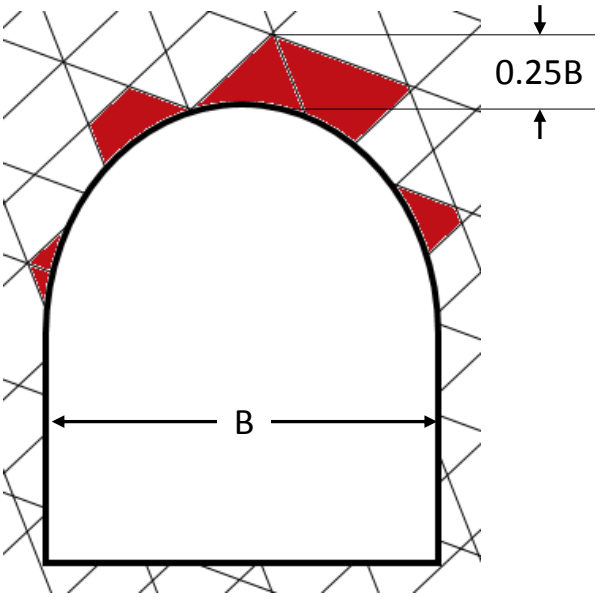

Figure 9: Overbreak experienced by a tunnel in a massive, moderately jointed rock mass if left unsupported (Proctor, Terzaghi, & White, 1946).

Tunnels in blocky and seamy rock have weakness due to the fact that the blocks between joints are not interconnected or interlocked. Such rock has little to no cohesion, and the load on the roof is analogous to arching experienced by sand. Therefore, the load on the roof if the tunnel is at considerable depth is independent of depth, and instead depends on the width and the height of the tunnel. The loads on the roof of a tunnel in blocky and seamy rock will increase with time and distance from the tunnel advance (Proctor, Terzaghi, & White, 1946).

Terzaghi was the first to pioneer a rational basis for rock loads, however as time progressed and this methodology was being applied in practice, it became apparent that the loads Terzaghi set forth were ultraconservative. This is because they failed to capture the intrinsic capacity of the rock, which in some cases has a higher uniaxial compressive strength than the concrete meant to support it (King, 1996). Deere et al. (1967) proposed modified rock load values, building on a relationship between Deere's Rock Quality Designation and the support required for tunnels in rock. The new values are about 20% below Terzaghi's method for drill and blast tunnels, and the values for machine-bored tunnels are a further 25% below the drill and blast values. Deere's adjustments to Terzaghi's rock loads are meant for tunnels 20 to 40 ft (6.1 to 12.2 m) in diameter, and since the tunnel diameter at Kemano is 5.73 m, the original values were used.

The rock loads from Terzaghi's work that are relevant to the rockmass conditions at Kemano are summarized in Table 6.

Table 6: Rock Loads, where B is span width and H is span height (Proctor, Terzaghi, & White, 1946).

Rock mass	***Rock Load***
Massive, moderately jointed	0 to 0.25 (B)
Moderately blocky rock	0.25 to 0.35 (B+H)
Very blocky, shattered rock	0.35 to 1.10 (B+H)

These rock loads can be used as a proxy for the extent of ravelling a particular rock mass will undergo, given the tunnel's geometry and the rock mass conditions at that location.

Chapter 3. Modelling the Effects of Topography on Tunnel Stress

Overlying topography causes stress magnitudes and orientations to vary along a tunnel alignment (Amadei et al., 1995; Amadei & Stephansson, 1997), and may become crucial factors for tunnel design if they influence the tunnel performance and support requirements. Regions of relatively high or low stress concentrations occur at the excavation boundary, implicating the design of rockbolt pattern and spacing, shotcrete thickness, mesh installation and even the cross-sectional geometry chosen for the excavation. This is important when studying the Kemano tunnels because T1 and T2 exist in slightly different stress regimes despite being only 300 m apart, which can be attributed to the proximity of the Horetzky Creek Valley to the south.

2D and 3D finite element models were constructed to determine the tangential and in situ stress magnitudes and orientation around the tunnels. The 2D models consist of cross sections taken at various topographically representative chainages along the tunnel alignment, while the 3D model was built using a contour map of the surrounding mountains encompassing a 10 x 20 km area. The results of these models were compared to determine if 3D finite element modelling, which is more time consuming and computationally expensive, is required, or if 2D modelling suffices.

3.1 2D Finite Element Modelling using RS2

2D numerical modelling of the tunnels and surrounding area was completed for five cross sections to estimate the in situ stresses at the tunnel axis prior to the tunnel excavation, as well as the tangential wall stresses post excavation.

3.1.1 2D Model Set Up

RS2 9 Modeller (RocScience Inc., 2015) was used to create five 2D finite element models of the tunnel cross-section and the surrounding mountains, Mount DuBose and East Jaw, as well as the topographic low represented by Horetzky Creek. The models have an exterior boundary extending laterally to include the Horetzky Creek Valley, down to sea level and up to 3 km above sea level. The lower corners of the exterior boundary of the model were pinned, the lower edge allowed lateral deformations only, and the vertical edges allowed only vertical deformations. In the models, a gravity field stress was applied, with a unit

weight of 27 kN/m^3 for all rock masses. The models were run elastically. The initial stress ratio was set to 1 since no detail on the stress regime is known. This was considered to be reasonable as the Kemano project is in the prefeasibility stage of design, and because the main goal was to model the in situ state of stress caused by topography without the tectonic stress influences. Rock mass parameters applied to the model represent the average properties for the formations present, which are primarily granodiorite. The values were based on work completed by Klohn Leonoff Consulting Engineers (1991) and Stuart (1960), and are summarized in Table 7. The Hoek-Brown strength paramaters were not used to allow yielding to occur in the model, but if the model was run plastically regions of over stressing could be used to assessed.

Table 7: Material properties used in 2D stress modelling of T1 and T2.

UCS (MPa)	m_b	***s***	***a***	***Young's Modulus (GPa)***	***Poisson's Ratio***
150	6.94988	0.0117	0.5028	45	0.3

Figure 10 shows a plan view of where the representative tunnel cross sections were taken, while Figure 11 through Figure 15 show the cross sections that were modelled.

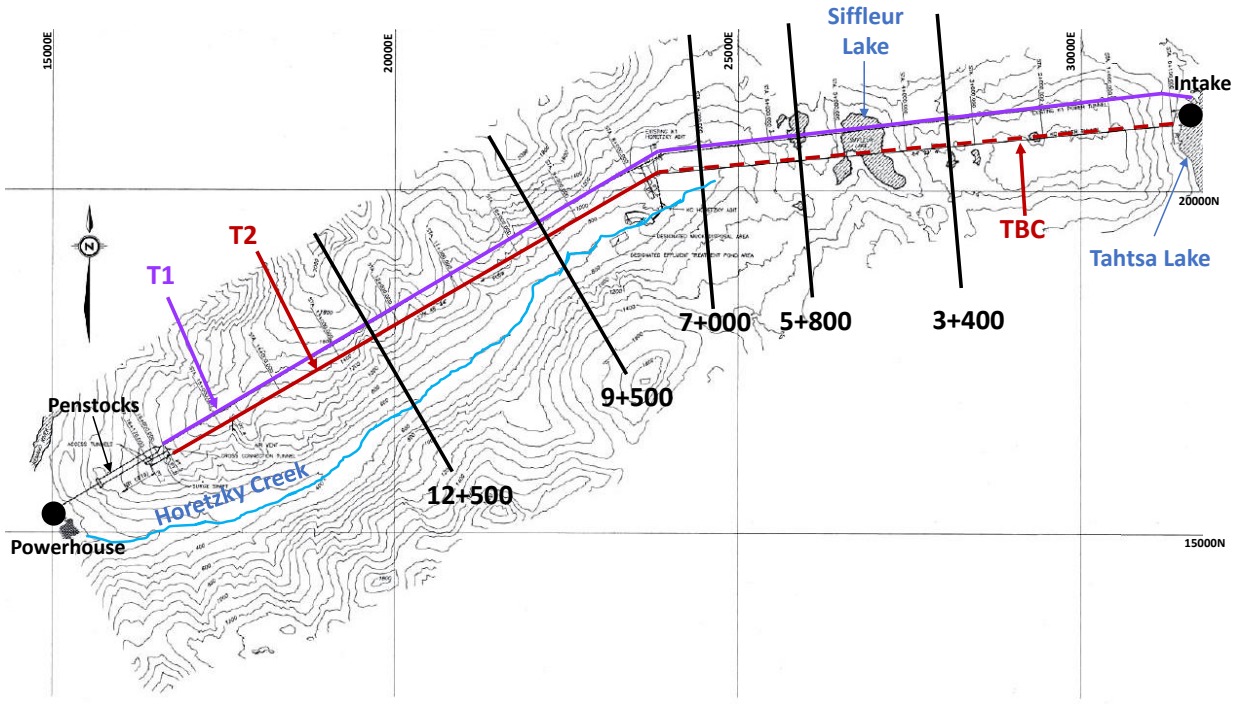

Figure 10: Locations of representative sections, overlain on 100 m contour map of the tunnel alignments.

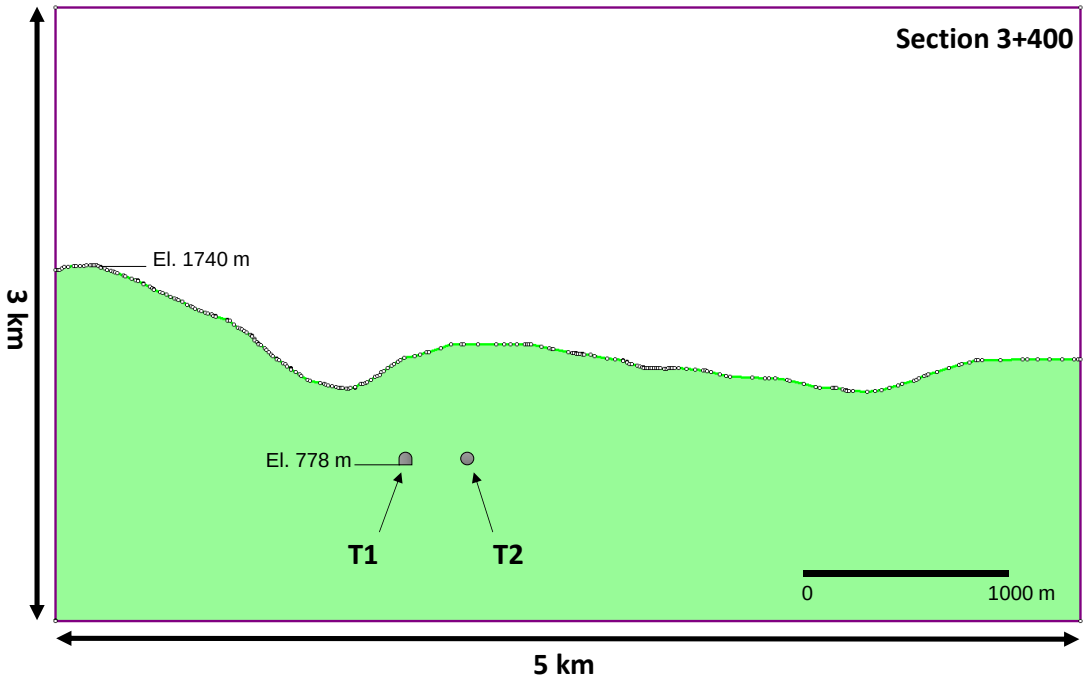

Figure 11: Model at chainage 3+400 (tunnels not to scale), showing extent of external boundary.

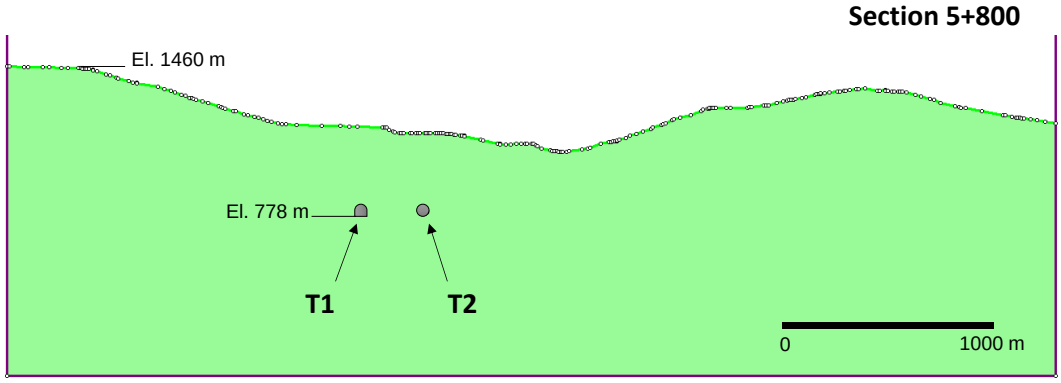

Figure 12: Model at chainage 5+800 (tunnels not to scale).

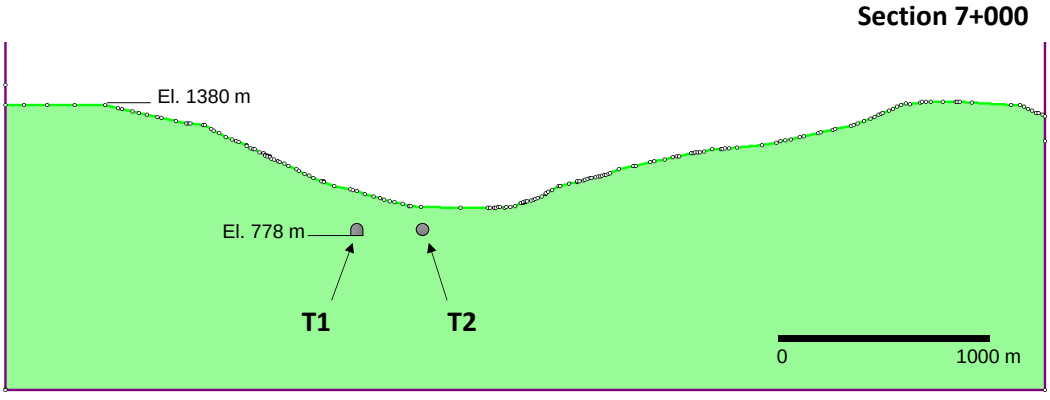

Figure 13: Model at chainage 7+000 (tunnels not to scale).

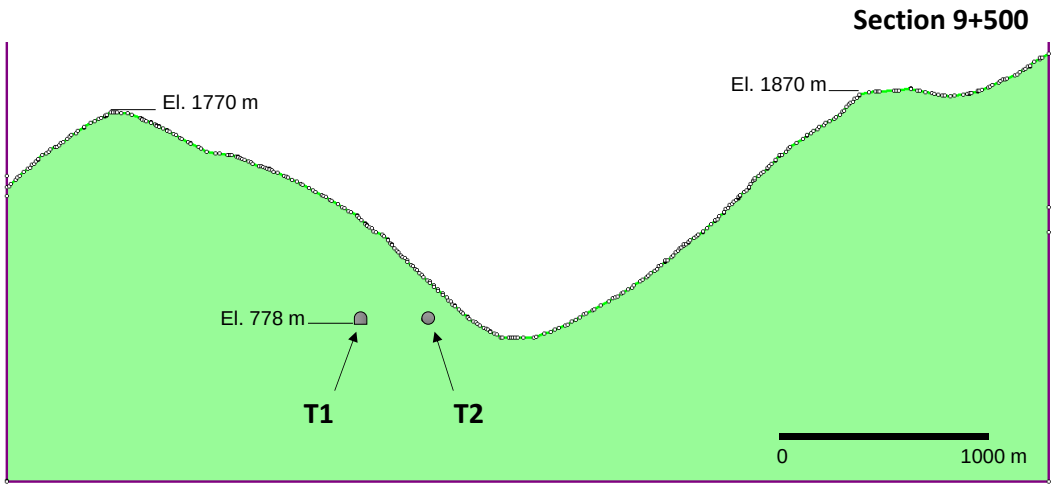

Figure 14: Model at chainage 9+500 (tunnels not to scale).

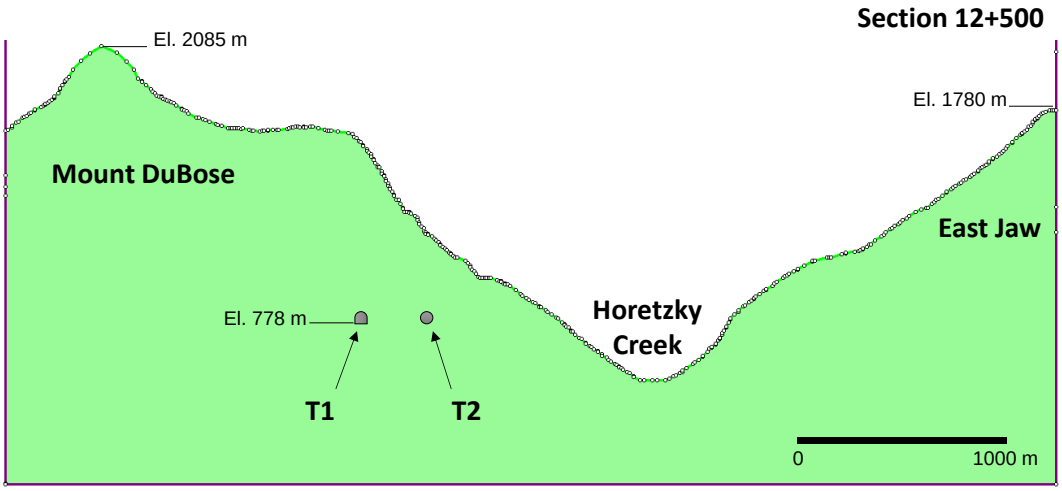

Figure 15: Model at chainage 12+500 (tunnels not to scale).

3.1.2 2D In situ Stress Results

The major and minor principal stress magnitudes at the tunnel locations prior to tunnel excavation were queried and extracted from the 2D finite element models. The stress magnitudes were queried at the centre of each tunnel and were analyzed using a subset of Kirsch's equations (Equation 5) to obtain the maximum and minimum tangential wall stresses (Kirsch, 1898).

$$\sigma_{max} = 3\sigma_1 - \sigma_3$$
$$\sigma_{min} = 3\sigma_3 - \sigma_1 \qquad \text{Equation 5}$$

For profiles taken across the Horetzky Creek valley, in both T1 and T2, the higher compressive stress concentrates in the top right quadrant and bottom left quadrant of the

tunnel profile, while the tensile stress concentrates in the top left quadrant and the bottom right quadrant looking upstream (eastward). This was most extreme where the Horetzky Creek Valley wall was closer to T2, as shown in Figure 16. This change in stress concentrations can be attributed to the change in proximity of the Horetzky Creek valley.

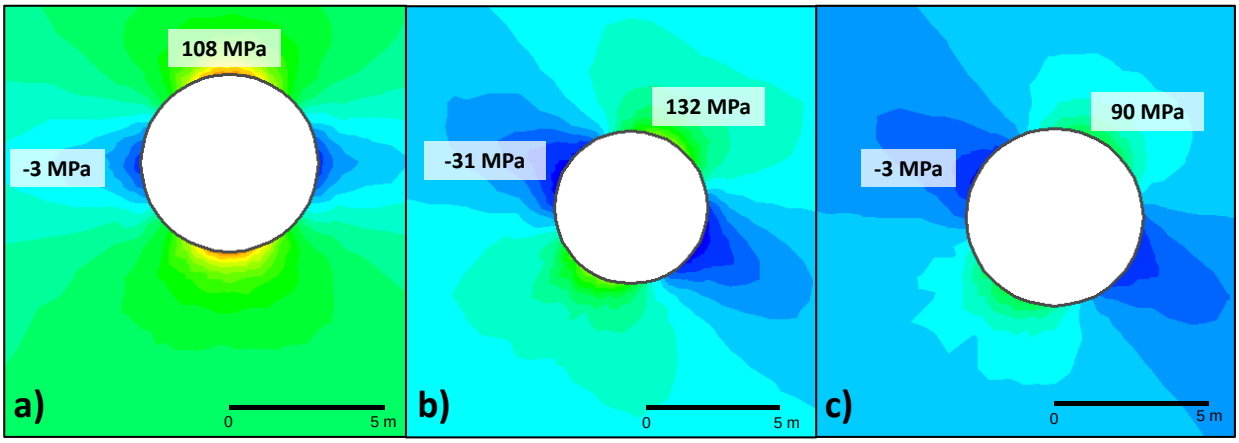

Figure 16: Major principal stress contours around T2 at a) 3+400, b) 9+500 and c) 12+500.

Model results are shown in Table 8. At sections 9+500 and 12+500, the ratios of major to minor principal stress (k) in T2 are approximately double those in T1 because T2 is much closer to the Horetzky Creek valley. The depth of cover at T2 for both these sections is less than the depth of cover at T1. At each of the other sections, the k ratios at T1 and T2 are similar as both tunnels have similar depths of cover and lateral confinement.

Table 8: Principal stresses from RS2 9 Modeller and resulting tangential stress and *k* ratio.

Cross-section Chainage		***Principal Stress***		***k***	***Angle of σ_1****	***Tangential Stress***	
		σ_1 (MPa)	***σ_3 (MPa)***			***σ_{max} (MPa)***	***σ_{min} (MPa)***
3+400	*T1*	42.0	14.6	2.9	-3.1°	111.3	1.9
	T2	40.3	12.6	3.2	0.1°	108.4	-2.6
5+300	*T1*	41.4	11.1	3.7	-4.5°	113.0	-8.0
	T2	42.2	10.2	4.1	-3.2°	116.5	-11.6
7+000	*T1*	46.8	6.4	7.3†	-10.1°	134.1	-27.6
	T2	52.8	6.1	8.6†	-5.4°	152.2	-34.4
9+500	*T1*	39.8	8.8	4.5	-24.2°	110.5	-13.3
	T2	45.7	4.8	9.5††	-28.1°	132.2	-31.2
12+500	*T1*	31.8	14.8	2.1	-28.7°	80.5	12.7
	T2	*33.6*	*10.3*	*3.3*	*-29.0°*	*90.5*	*-2.8*

** Negative value denotes counter clockwise rotation from the crown when looking down the tunnel axis from west to east.*

† Multiple intrusive bodies as well as the low depth of cover at 7+000, combined with the elastic material properties, result in extremely high k values and tensile stress in the rock mass. Due to the elastic rebound resulting from the valley's erosion, the minor principal stress near the tunnels is low, and subsequently the k values are high.

†† The proximity of the Horetzky Creek Valley to T2 at chainage 9+500 results in high principal stresses, and therefore an extremely high k ratio.

The results of the 2D finite element modelling emphasized the effect of the Horetzky Creek valley on the ratio between the principal stress magnitudes in T1 and T2. Where the tunnel is located close to the valley wall, the stress concentrations indicate that the rock mass is susceptible to spalling and/or ravelling.

3.2 3D Finite Element Modelling using Abaqus

The 2D elastic stress modelling of the T1 and T2 tunnels give a snapshot of the distribution of stresses along the tunnel alignments, however because the eventual aim is to use stress data as an input to a Bayesian Belief Network, a more continuous dataset is preferable. A 3D topographical stress model was developed to allow for extraction of major and minor stress orientations and magnitudes at any "slice" along the tunnel alignment.

3.2.1 3D Model Set Up

A 3D solid of the terrain surrounding T1 and T2 was generated from the 20 m interval contour map of the Kemano area (Autodesk, Inc., 2014), provided by Hatch Ltd. To create the solid, the contours were exploded into polyline segments and a surface was draped to form

a 3D Triangular Irregular Network (TIN). The surface representing the topography was then extruded to form a 3D solid of the mountains in the Kemano area. Once it was verified that the solid existed in the appropriate coordinate system (i.e. UTM coordinates), it was exported to an ACIS file that could be imported into the 3D finite element software Abaqus/CAE (DSSC, 2013).

The 3D solid was treated as a continuous, homogeneous, isotropic, linear-elastic (CHILE) material (Hudson & Harrison, 2000) with a density of 2700 kg/m^3, Poisson's ratio of 0.3, and Young's Modulus of 45 GPa, which represents the average for the rock types known to be present at Kemano (Figure 17). The presence of faults and dykes in the rock mass, which are known to affect the stress field, are not accounted for in the stress model but are accounted for more specifically in the Bayesian Belief Network developed as part of this thesis by the rock mass characterization nodes (e.g. Structure, Joint Infilling, Joint Weathering). The edges of the model were seeded, and then the solid was meshed with over 10,000 tetrahedral elements (Figure 18). A gravity load of 9.81 m/s downward was applied to all the elements. Boundary conditions were applied to the sides and bottom of the 3D solid to prevent movement of nodes out of plane, and all the edges were pinned to restrict node movement. The 3D topographical model was run elastically.

The 3D stress tensors along the T1 and T2 tunnel alignments were extracted by inputting the 3D coordinates of T1 and T2 as "paths" into the model (Figure 18). A path is a series of user defined points in Abaqus, along which data can be extracted (DSSC, n.d.). The 3D stress tensor was extracted at 50 m intervals along the T1 and T2 paths.

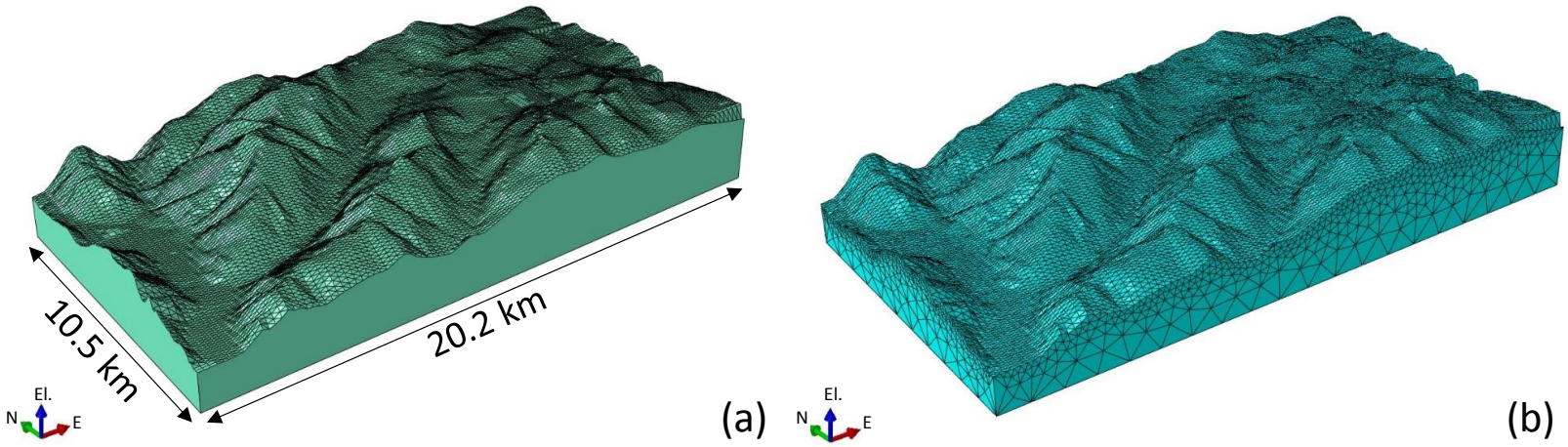

Figure 17: 3D elastic stress model development in Abaqus: (a) 3D solid with material properties assigned, (b) meshing of solid (DSSC, 2013).

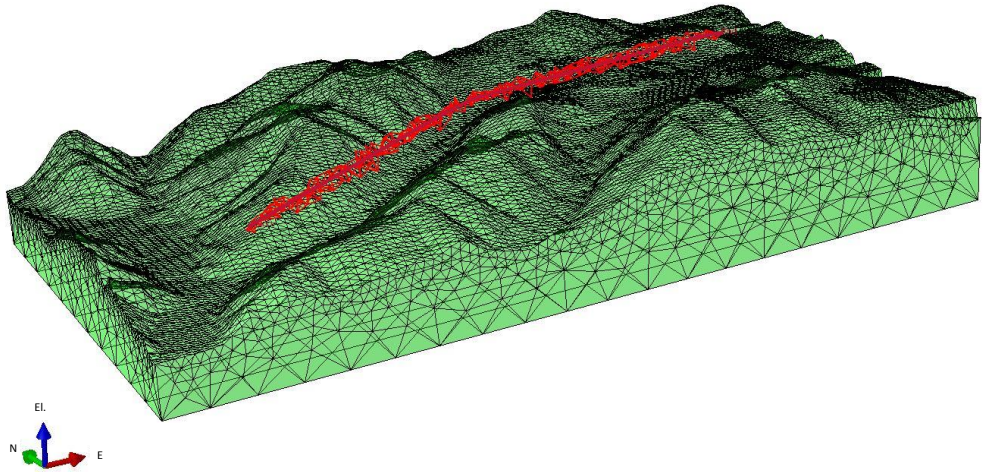

Figure 18: The 3D topographical model in Abaqus, showing the T1 "path" along which stress tensors were extracted (DSSC, 2013).

3.2.2 Transformation of 3D Stress Tensor

The 3D stress tensors obtained at 50 m intervals along T1 and T2 from Abaqus were transformed to determine the magnitude and orientation of the maximum and minimum principal stresses in the plane perpendicular to the tunnel (σ_1, σ_2 and θ). This was done by transforming the stress tensor about the z-axis, so that the x-axis became parallel to the tunnel axis. Equation 6 can be applied to perform this transformation (Housner & Vreeland, 1965).

$$\sigma' = R(\alpha) * \sigma * R(\alpha)^T \qquad \text{Equation 6}$$

Where $R(\alpha)$ is the rotation matrix for rotation about the z-axis by angle α, σ is the 3D tensor representing the state of stress at a given point, and $R(\alpha)^T$ is the transpose of the rotation matrix. Equation 7 shows this transformation equation in matrix form (Housner & Vreeland, 1965).

$$\sigma' = \begin{bmatrix} cos(\alpha) & -sin(\alpha) & 0 \\ sin(\alpha) & cos(\alpha) & 0 \\ 0 & 0 & 1 \end{bmatrix} * \begin{bmatrix} \sigma_x & \tau_{yx} & \tau_{zx} \\ \tau_{xy} & \sigma_y & \tau_{zy} \\ \tau_{xz} & \tau_{yz} & \sigma_y \end{bmatrix} * \begin{bmatrix} cos(\alpha) & sin(\alpha) & 0 \\ -sin(\alpha) & cos(\alpha) & 0 \\ 0 & 0 & 1 \end{bmatrix} \qquad \text{Equation 7}$$

Because the tunnels have doglegs and are not strictly linear, the rotation angle (α) changes slightly for various segments along T1 and T2. These varying rotation angles are summarized in Table 9, and were obtained from an AutoCAD drawing of the tunnels provided by Hatch Ltd.

Table 9: Rotation about the z-axis required for x-axis to be parallel to tunnel axis, where a positive value denotes a CCW rotation.

Tunnel	*From Chainage (m)*	*To Chainage (m)*	*Angle of Rotation (α)*
T1	0+000	0+270	-15°
	0+270	0+570	-2°
	0+570	7+880	7°
	7+880	7+890	16°
	7+890	8+960	26°
	8+960	16+765	30°
T2	0+000	7+610	6°
	7+610	7+640	10°
	7+640	7+665	8°
	7+665	7+695	15°
	7+695	16+200	30°

Once the rotation is performed, the following stress tensor is obtained (Equation 8).

$$\sigma' = \begin{bmatrix} \sigma_x{}' & \tau_{yx}{}' & \tau_{zx}{}' \\ \tau_{xy}{}' & \sigma_y{}' & \tau_{zy}{}' \\ \tau_{xz}{}' & \tau_{yz}{}' & \sigma_y{}' \end{bmatrix} \quad \text{Equation 8}$$

The tensor in the y-z plane now represents the state of stress in the plane perpendicular to the tunnel (Equation 9).

$$\sigma' = \begin{bmatrix} \sigma_y{}' & \tau_{zy}{}' \\ \tau_{yz}{}' & \sigma_z{}' \end{bmatrix} \quad \text{Equation 9}$$

Then basic 2D stress transformation equations (Brady & Brown, 1985) can be used to determine the major principal stress (σ_1), minor principal stress (σ_2) and the orientation of σ_1 (θ) (Equation 10).

$$\sigma_{1,3} = \frac{\sigma_y + \sigma_z}{2} \pm \frac{\sqrt{(\sigma_y + \sigma_z)^2 + 4\tau_{yz}^2}}{2} \quad \text{Equation 10}$$
$$tan(2\theta) = \frac{2\tau_{yz}}{\sigma_y - \sigma_z}$$

The stress rotation and transformation for all the tensors extracted along T1 and T2 were completed using MATLAB (MathWorks©, 2014), the code written for this can be found in Appendix B: MATLAB Code.

3.2.3 3D In situ Stress Results

The principal stress ratios for T1 and T2 are shown in Figure 19 plotted against the ground surface. The stress regime is close to hydrostatic where the depth of cover is low, and higher horizontal stress is encountered toward the middle of the tunnel where there is higher lateral confinement. The differences between the stresses are more extreme in the T2 tunnel due to its closer proximity to the Horetzky Creek Valley.

Similar to work done previously with the 2D models, the maximum and minimum tangential stresses were calculated using Kirsch equations along each tunnel at 50 m intervals. These are shown in Figure 20 and Figure 21 as a function of tunnel chainage. The ground surface is also plotted here for visualization purposes. The magnitudes of the tangential stresses are similar in T1 and T2, as expected. The fluctuations in the tangential stresses reflect the

change in the overlying topography, in particular reaching a local low where the depth of cover results in smaller in situ stresses near the Horetzky Adit. The maximum tangential stress is not high relative to the rock strength. This is because the tunnel is at a shallow depth relative to some mine tunnels, and therefore stress-induced spalling is expected to be minimal and not catastrophic. However, the minimum tangential stress between approximately 6+000 and 8+000 is tensile, which when combined with the pervasive structure and soft joint infill in the rock mass may result in gravity-induced failures. Since this failure is controlled by structure, the low and tensile tangential stress may cause progressive ravelling failure at these locations.

The orientation of the maximum principal stress is heavily affected by the proximity of the Horetzky Creek Valley wall. The principal stress orientations for T1 and T2 are shown in Figure 24 and Figure 25. The colours of the points indicate the relative magnitudes of the relevant tangential stress, and give an indication of how likely the failure mechanism (spalling or ravelling) is to occur. For the most sections of the tunnel there is medium or low potential for those failure mechanisms to occur, however there are localized areas of high failure potential.

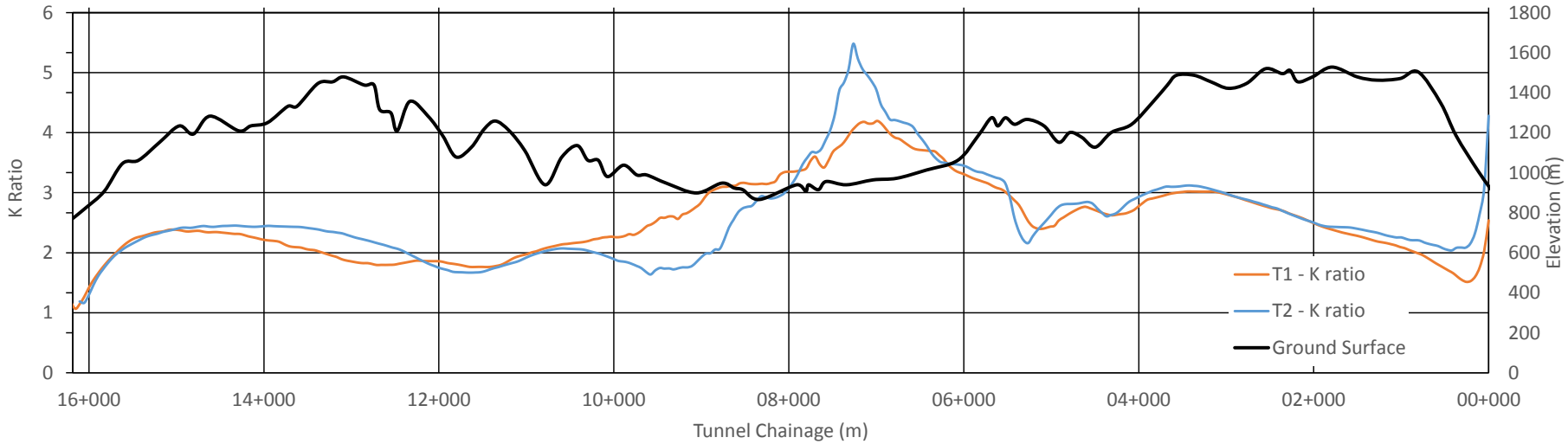

Figure 19: Principal Stress Ratios (k values) for T1 and T2 plotted with ground topography.

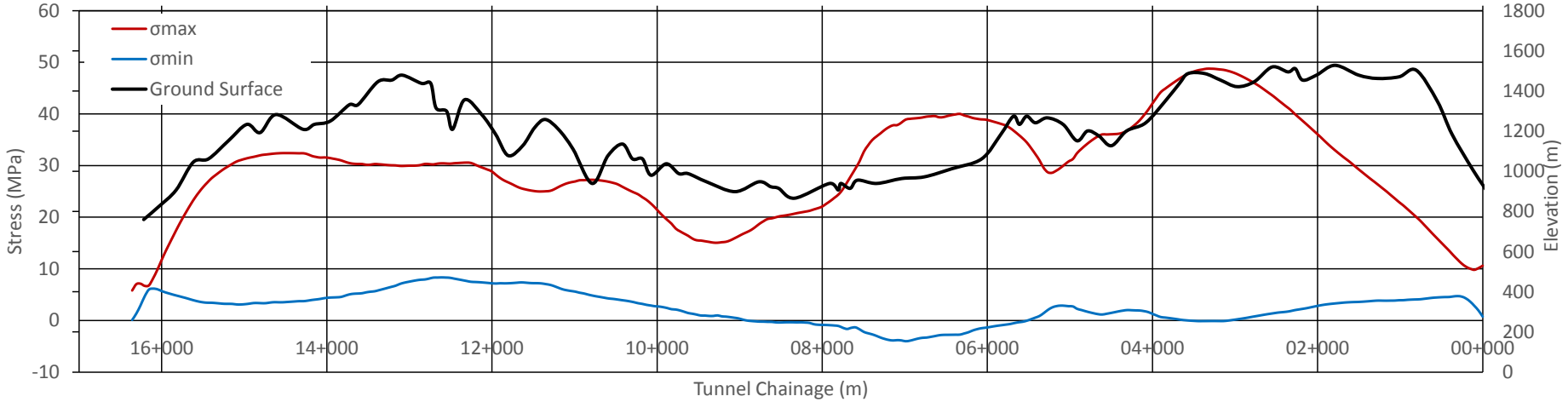

Figure 20: Tangential stresses around T1 at 50 m intervals as a function of tunnel chainage.

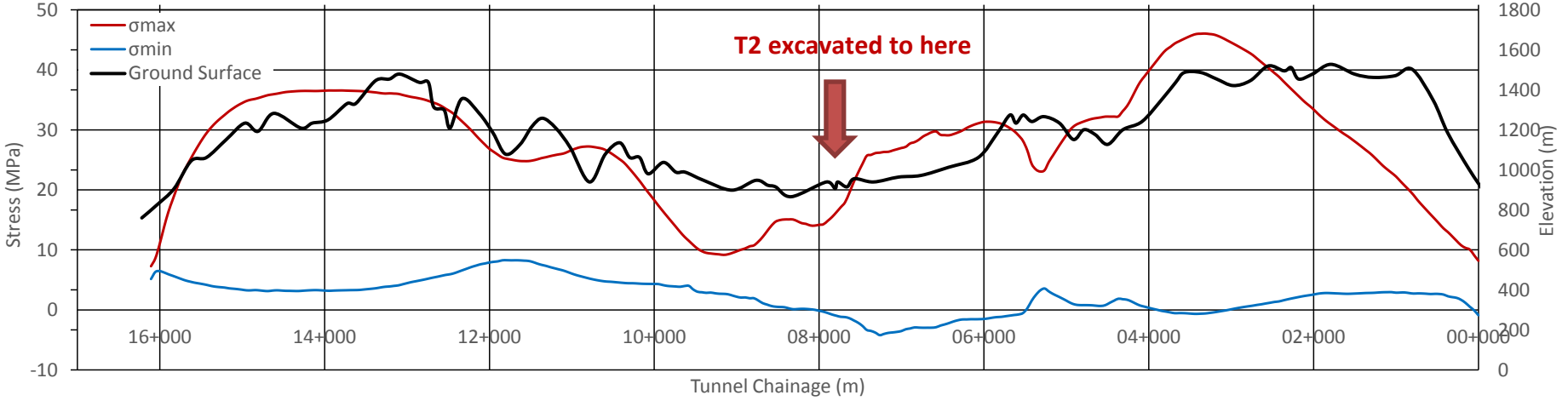

Figure 21: Tangential stresses around T2 as a function of tunnel chainage.

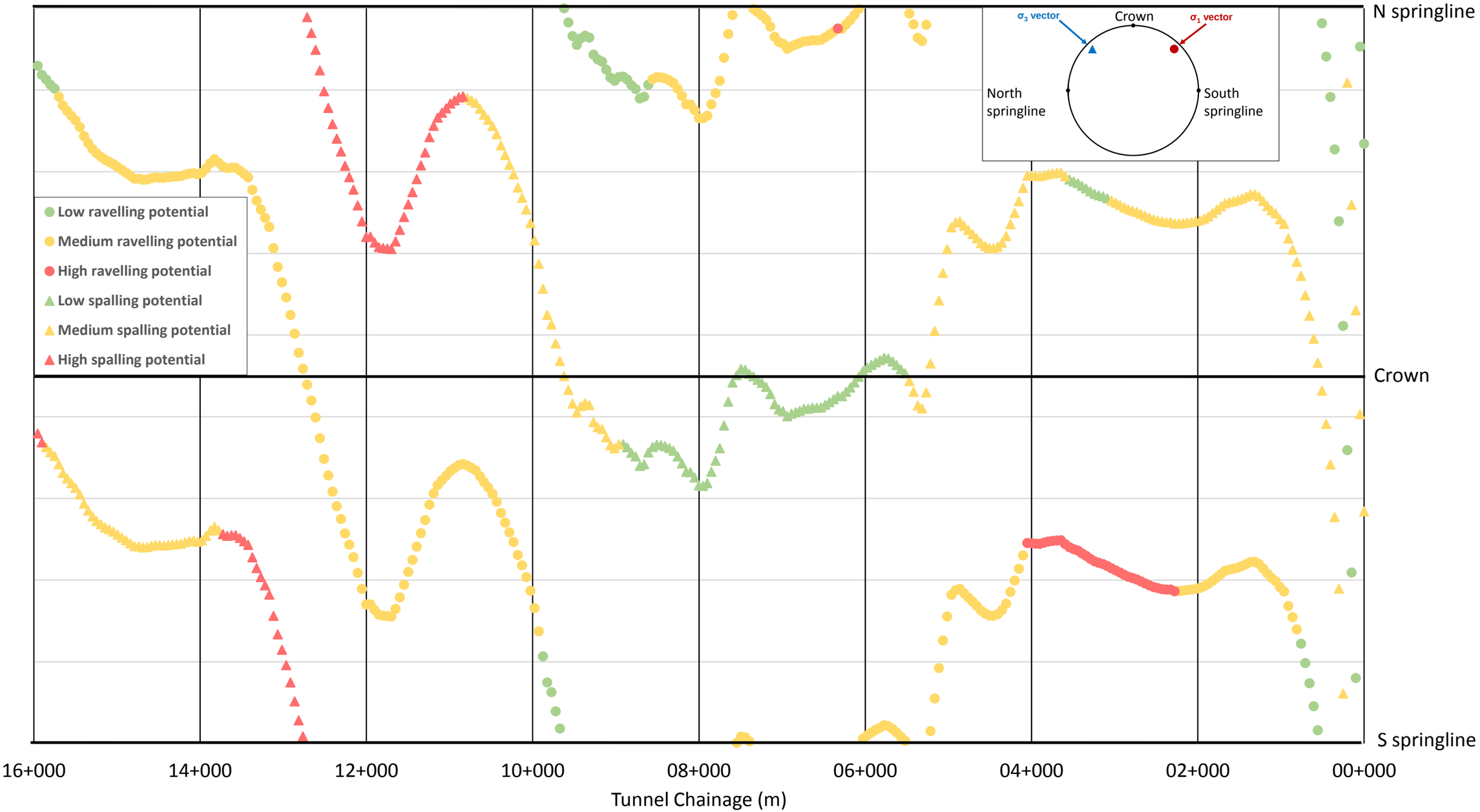

Figure 22: Orientation of the σ_1 and σ_3 vectors vs. T1 chainage, colour coded to show likelihood of failure mechanism.

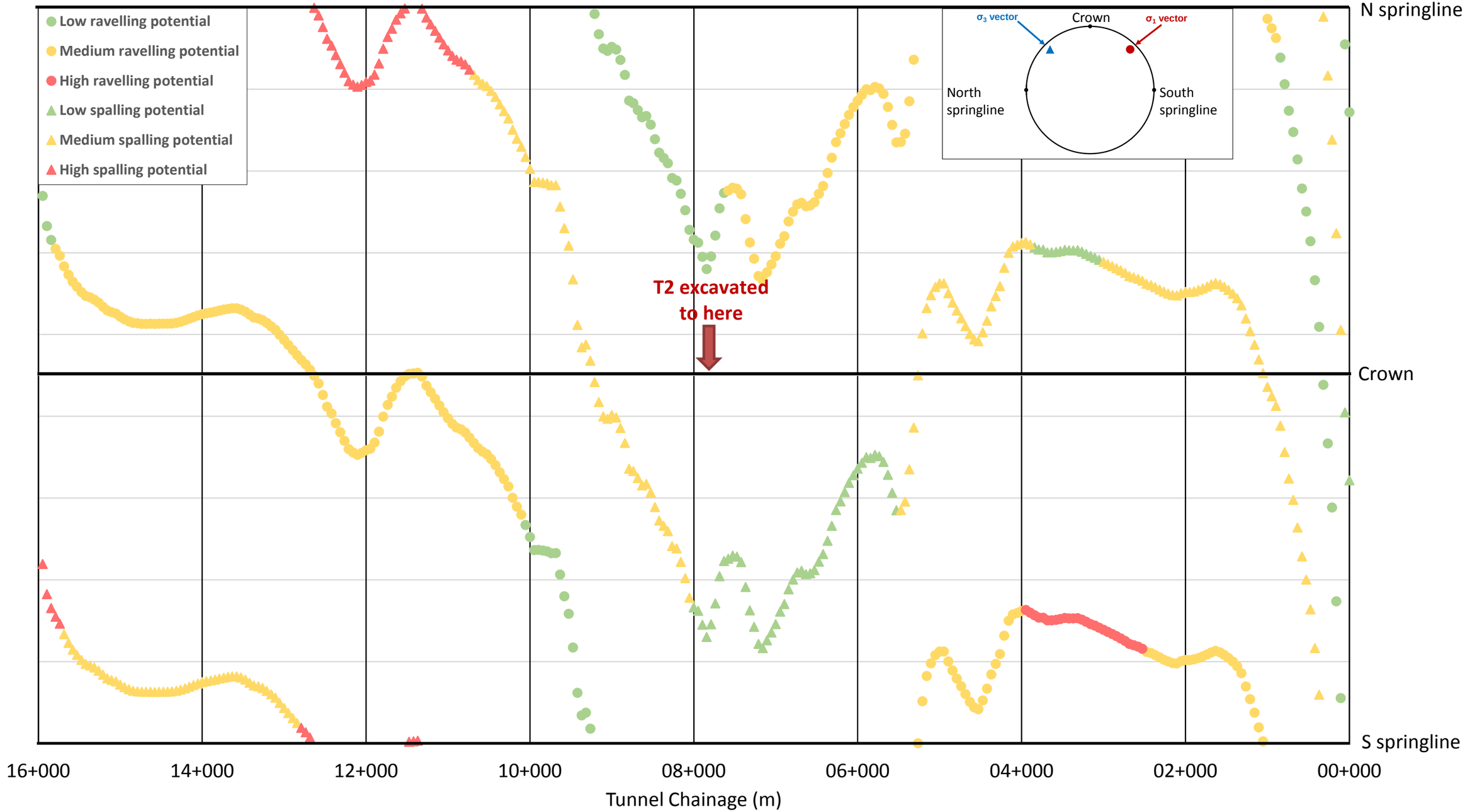

Figure 23: Orientation of the σ_1 and σ_3 vectors vs. T2 chainage, colour coded to show likelihood of failure mechanism.

3.3 Comparison of 2D and 3D Modelling

The orientations and overall trend of the stresses obtained by the 2D and 3D modelling are comparable (Figure 24 and Figure 25), however the stress magnitudes obtained differ significantly. This can be attributed to the lack of influence of the changing topography in the third dimension for the 2D models. As the models were run under plane strain assumptions, with an out-of-plane stress ratio of 1 (the simplest assumption), the 2D models are not able to capture the change in the depth of cover along the tunnel axis. 2D stress models require stress increases to only occur within the 2D plane, resulting in higher values than in a 3D model where stresses have an extra dimension to be redistributed into. The 2D models also don't include the change in proximity to the Horetzky Creek Valley, which is believed to have a significant influence on the stresses.

For this reason, it has been concluded that 3D stress modelling is essential in cases such as Kemano, where the tunnels are not deep enough to escape the influence of varying topography.

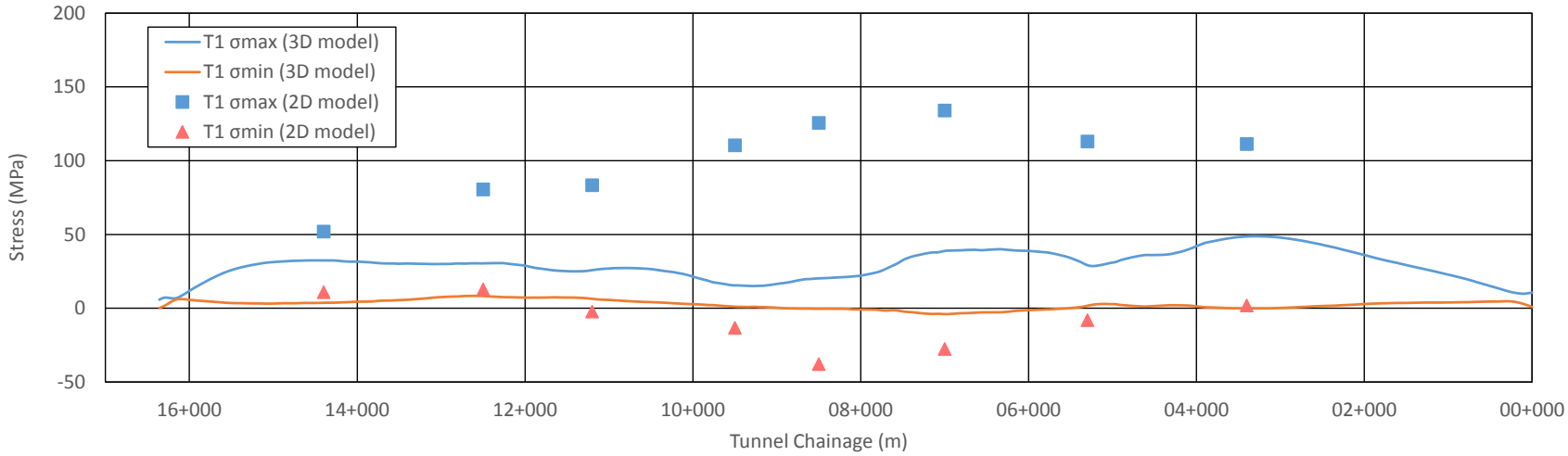

Figure 24: Comparison of tangential stress results from 2D and 3D modelling of T1.

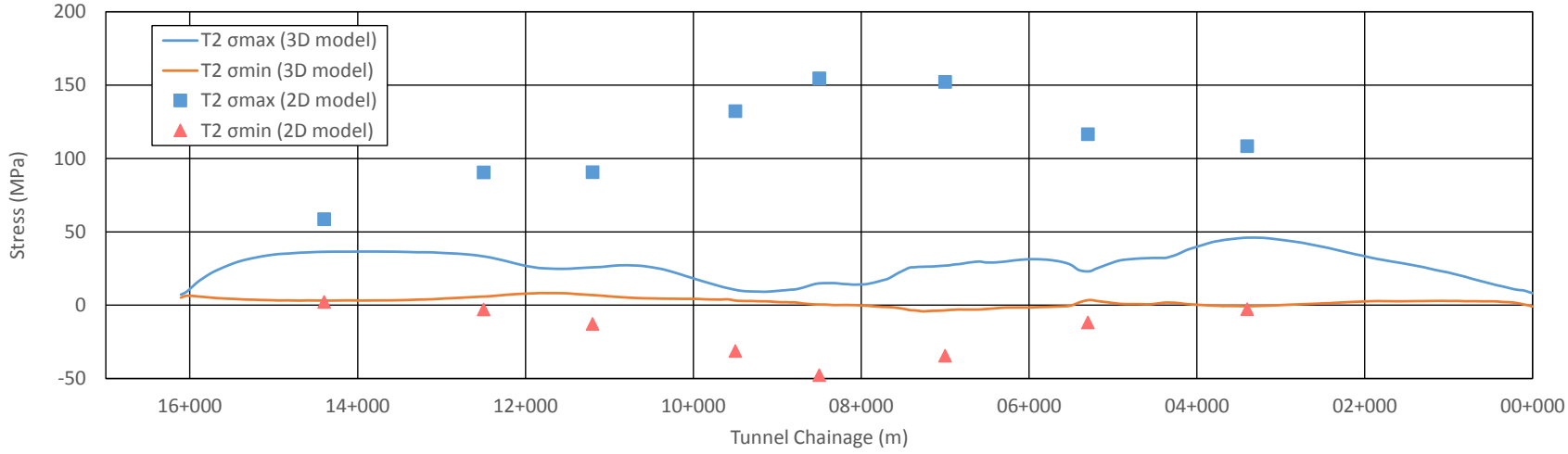

Figure 25: Comparison of tangential stress results from 2D and 3D modelling of T2.

3.4 Implications of Stress on Tunnel Performance and Ground Support

The results of the 2D models indicate that the upstream half of T2 may be more challenging to excavate than the downstream completed half. The predicted tangential stresses vary widely around the tunnel, which may result in the need for more rock support. Geological reports regarding the tunnel alignment indicate that the geology throughout the upstream T2 tunnel is more complicated than the downstream portion, as there are multiple shear zones, faults and intersecting veining (Stuart 1960, Bechtel Canada, Inc. 1991). Ravelling of the rock mass can therefore be expected where there are low tangential stresses and a high concentration of discontinuities. Spalling can be expected where there are localized highs in tangential stress

The 3D modelling results indicate that the next phase of tunnel excavation, between stations 8+000 and 4+000 may prove to be the most challenging of the entire project. This can be inferred by the high principal stress ratios resulting from high lateral confinement, which will result in high tangential wall stresses and possible spalling. Overall, as the tunnel excavation approaches Tahtsa Lake (lower chainages) the Horetzky Creek valley disappears, resulting in a lower *k* value and therefore less critical tangential stresses.

The results from the 3D modelling allow the tunnel alignments to be broken into three distinct zones based on similar *k* ratios (Figure 19), tangential stresses (Figure 20 and Figure 21), and stress concentrations (Figure 22 and Figure 23). This is summarized in Table 10, with Figure 26 for reference.

Table 10: Summary of 2D and 3D model results for three distinct geotechnical zones.

Chainage	***Model Result***	***T1***	***T2***
0+000 to 5+000	*k* ratio	In situ stress is close to hydrostatic, as the depth of cover and confinement are similar.	In situ stress is close to hydrostatic, as the depth of cover and confinement are similar.
	Tangential stresses and stress concentrations	High tensile stress in the right shoulder (approx. 2+200 to 4+000) may result in ravelling. Medium compressive stress along the left shoulder may result in spalling/crushing.	High tensile stress in the right shoulder (approx. 2+500 to 3+900) may result in ravelling. Medium compressive stress along the left shoulder may result in of spalling/crushing.
5+000 to 10+000	*k* ratio	The in situ stress ratio peaks at 7+260 with a value of 5.5, where the tunnel is close to surface and the effect of the Horetzky Creek Valley has become much shallower, resulting in high confinement.	The in situ stress ratio peaks at 6+990 with a value of 4.2, which is lower than the T2 ratio at the same location because there is a larger depth of cover at T1.
	Tangential stresses and stress concentrations	Medium to high tensile stress along the left springline (approx. 5+000 to 8+500) may result in ravelling.	Medium tensile stress in the left shoulder (approx. 5+300 to 7+600) may result in ravelling. Medium compressive stress between the left and right shoulders (approx. 8+000 to 10+000) may result in spalling/crushing.
10+000 to >16+000	*k* ratio	In situ stress is close to hydrostatic, as the depth of cover and confinement are similar.	In situ stress is close to hydrostatic, as the depth of cover and confinement are similar.

Chainage	*Model Result*	*T1*	*T2*
	Tangential stresses and stress concentrations	Medium tensile stress between the left and right shoulders (approx. 9+900 to 15+000) may result in ravelling. High compressive stress in the right springline (approx. 12+700 to 13+600) and left springline (approx. 10+800 to 12+700) may result in spalling/crushing.	Medium tensile stress between the left and right shoulders (approx. 10+000 to 15+800) may result in ravelling. High compressive stress in both springlines (approx. 10+700 to 12+700) and in the left shoulder at the portal may result in spalling/crushing.

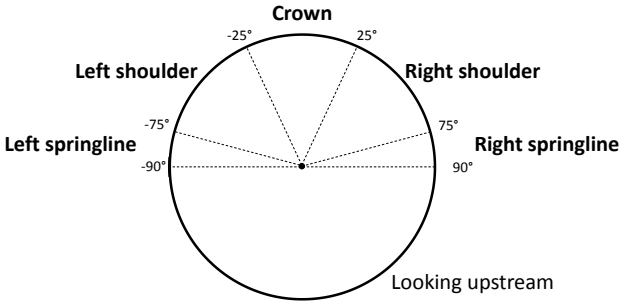

Figure 26: Definition of major principal stress orientations.

3.4.1 Verification of Model Results with Site Observations

Site observations of rock mass failures and fallen ground during the 2015 site inspection program confirm the predicted chainages where relatively high or low tangential stresses will occur around the tunnel. Site investigations of the excavated half of T2 (7+500 to 16+158) found rock mass failure in the form of spalling on the top right (looking eastward) and ravelling on the top left (looking eastward) of the tunnel profile. During the site investigations, the spalling and/or ravelling were primarily observed between chainages 8+500 and 12+500. The spalling mechanism is attributed to high stress tangent to the tunnel wall and crown, while the ravelling is associated with the low and sometimes tensile stresses and pre-existing geological structures. The locations of these failure mechanisms are consistent with the orientation of the major and minor principal stresses determined by the finite element models. A photo of an area where ravelling occurred is shown in Figure 27 while Figure 28 shows an area with spalling.

Figure 27: Ravelling of rock mass at a chainage of approximately 8+850.

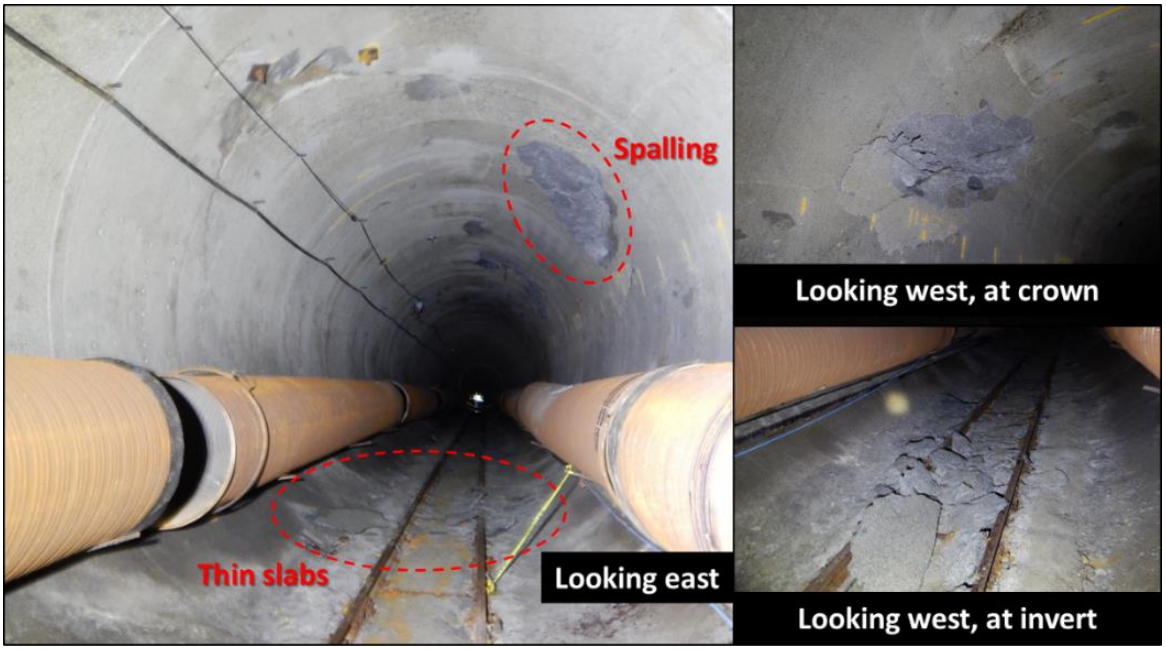

Figure 28: Spalling of rock mass at a chainage of approximately 11+730.

Chapter 4. Bayesian Belief Network

4.1 Netica

4.1.1 Building the Network

It is important that the user map out the proposed network and linkages before beginning to construct the network in Netica, a Bayesian Belief Network software (Norsys Software Corp., 2014). This will allow the creator to have a concept of types of nodes and the functional relationships they may want to apply. Once this is complete, the network can be created in Netica. There are three types of nodes that can be used:

1. Nature node – A variable of interest that cannot be directly controlled by the user. If the node has a functional relationship with its parents, it is a *deterministic node*, whereas if the node is probabilistic it is called a *chance node.*
2. Utility node – Also known as a *value node*, this is a node whose expected value is to be maximized while the network searches for the best decision rule for the decision node.
3. Decision node – A variable that represents a choice under the control of the user. The net solves for the best decision rule while optimizing the expected utility.

Each node is classified as either discrete or continuous. A discrete node has a well-defined set of possible values, corresponding to a digital quantity. Discrete variables have *states* assigned, which may be an integer or real number. They may also be qualitative, for example "male, female" or "true, false." Continuous variables may take on any value between two other values, and corresponds to an analog quantity. Continuous nodes do not have state values, but when they are discretized they have *state levels* or *thresholds* instead. These are used to partition the range of the variable into intervals.

A conditional probability table (CPT) is stored within each node, and contains the probabilities of that node given all possible combinations of parent node values. The CPT dictates that nodes relation to all its parent nodes, and subsequently affects the CPTs of its children. These conditional probabilities are entered as percentages, and are user defined. The addition of new information, or *findings*, may be entered into the network to update the CPTs (this is discussed in detail below).

Once the network is built and the CPT tables are completed, the network must be compiled. By selecting Network → Compile, Netica will compile and update the network. There is an option of a quick compile, which auto-compiles any file that is set to auto-update, or an optimized compile, which works out an efficient structure for the internal junction tree used for belief updating. The quick compile function does a minimum-weight search for a good elimination order, and the optimized compile searches for the best elimination order using a specialized algorithm which is a combination of minimum-weight search and stochastic search (for a detailed explanation of these algorithms see Neumann & Witt, 1998).

4.1.2 Entering New Findings and Updating the Network

Belief updating, or *probabilistic inference*, can be applied to a network when new information (*beliefs* or *posterior probabilities*) becomes available. Introducing the new data into the network results in Netica filtering the information through the network to determine new probabilities for the states of all subsequent nodes. Netica has the capability to update automatically after a new finding is entered, and the network has been compiled. The user may choose to turn off this automatic updating if several findings are entered at once, as recompiling between entries may be time consuming.

Findings (or *evidence*) are entered into the network by right-clicking on the node that is to be updated. There are several methods of updating the node, depending on the nature of the new information:

1. If the information received is conclusive that a node resides within a certain state, a 100% probability of that state occurring can be assigned. This is done by right-clicking on the node and selecting the appropriate state. For a continuous node, if the exact numeric value of the state is known it can be entered by right-clicking and entering the known value.
2. A *calibration* can be made if the new data changes the probability of each of the states occurring based on all observations made.

$$P(Node = state | All\ Observations)$$

3. A *likelihood finding* can be used to update a discrete node if the new information is uncertain. The user can assign one probability for each state of the node, which is the probability that the actual observation would be made if the node were in that state.

$$P(All\ Observations|Node = state)$$

4. A *negative finding* can be assigned to a particular state if it is certain that the node does not fall in this state. This is done by entering a likelihood of zero for the state. It is possible to have more than one negative finding for a given node.

In the event that the user enters a finding that is inconsistent, Netica will report them. This is done through a consistency check of the findings during belief updating. There are three types of inconsistencies:

1. Several findings for different nodes can be inconsistent with each other.
2. Several findings for the same node can be inconsistent with each other.
3. A single finding can be inconsistent with the net itself.

If the user wished to remove, or *retract*, a finding from the network, this can be done by right-clicking on the node and choosing "unknown". This is equivalent to never having entered the finding. Whenever a positive finding (knowledge that some variable definitely has a particular value) is entered, all the previous findings for that node are automatically retracted first. However, if more than one likelihood finding is entered for a node, Netica will query if the previous finding(s) are to be removed, or if they should accumulate. Accumulating the findings allows the user to enter several independent pieces of evidence for the same node.

Netica has the ability to save all the positive findings of a network to a case. This contains the set of all findings entered into the nodes of a network, which can later be re-entered into the network. A case can be created by selecting Cases → Save Case As, prompting Netica to extract all the current findings in the net. The case can be read back into a network and be modified by selecting Cases → Get Case. Case files may consist of a database of cases, which can be randomly generated and may be called a simulation or sampling. Conversely, Netica can take a case file to learn the CPTs of a particular network. This is done by creating the

nodes and linkages, and then adding the case file in order for the network to learn the conditional probabilities (Cases → Learn → Incorp Case File).

4.2 Bayesian Network for Kemano

4.2.1 Network Setup

The Bayesian Belief Network for Kemano is made up of empirically established relationships in rock mechanics as well as expert judgement specific to this project. Input data were mined from historic tunnel excavation records and geological baseline reports to populate some of the nodes. The vagueness that is inherent with many geotechnical parameters gave rise to the need for a certain amount of judgement to be built into the network. The overall network design can be seen in Figure 29, with colour coded nodes to indicate the source of the data used to determine their states. Many of the nodes are shown as belief bars, which display the likelihood of that node falling into any of its states. If the node is continuous, Netica displays its average value given the current states of its parents. Nodes calculated deterministically based on their parents are displayed as labeled boxes.

Two main failure mechanisms were evaluated in order to predict the ground class at a given chainage: spalling and ravelling. The network was targeted at these two failure mechanisms in particular as these were the main failure types observed during site investigations in July of 2015 (see Section 3.4.1).

Spalling is a stress-induced failure mechanism, and as such it was important to get an approximation of the stress magnitudes and orientations along the tunnel alignments. This came from the 3D stress modelling (see Section 3.2). The other important inputs are the tunnel geometry, and the unconfined compressive strength of the rock.

Ravelling has not been as rigorously defined with empirical relationships as spalling (see Section 2.4.4). The discussion of important driving factors (i.e., rock mass blockiness or fracture frequency, tunnel span, groundwater, boundary stresses) that appears repeatedly in published literature was used to derive a relationship that may be used to determine whether or not ravelling occurs at a given chainage. This relationship was derived with Kemano in mind, but may also be applicable to other tunnelling projects.

Separate from the main network is a miniature network that utilizes the orientation of the major principal stress to tell the user where around a tunnel the failures would occur.

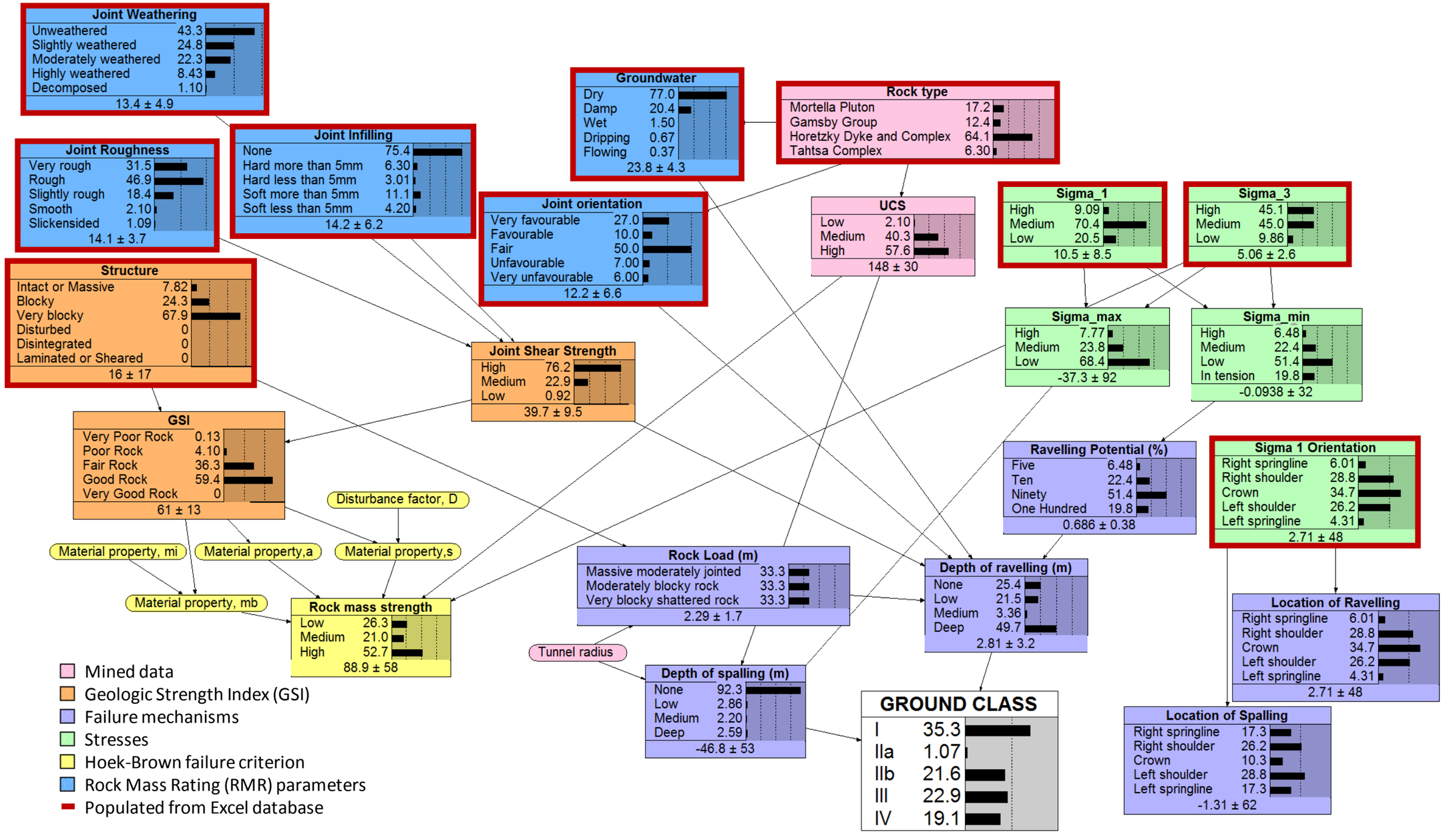

Figure 29: Bayesian Belief Network for the Kemano case study, showing nodes, conditional relationship and probability distributions.

A wealth of data are available for the Kemano project, largely due to the long history of the project starting in the late 1940s. The challenge with streamlining the data for use in the Bayesian Network was to convert the data into a meaningful digital form, as most records exist only in analog form. A Kemano-specific database was developed and populated with known information mined from reports, drive records, mapping sheets, and photographs (see Appendix D: Kemano Specific Database). This database contains data from chainages 0+000 to 16+186 in 25 m increments, with the following row headers: Rock type, maximum principal stress (σ_1), minimum principal stress (σ_3), stress orientation (θ), Structure, Joint Roughness, Joint Infilling, Joint Weathering, Groundwater, and Joint Orientation. In some cases for the upstream T2 tunnel, which is not excavated yet, data for the RMR parameters are not populated. In these cases, a distribution is applied that represents the most likely condition of the rock mass at the tunnel alignment.

When new information becomes available as the tunnel advances, the user should update the database with the new inputs and re-run the network to obtain the new ground class predictions.

4.2.2 Parent Nodes

The nodes in this section contain data that may be used as a direct input. These reflect data that are independent of other nodes, in other words do not have conditional dependencies associated with them.

4.2.2.1 Rock Type

A geological report entitled *The Geology of the Kemano Tahtsa* Area prepared by Stuart (1960) details the geology in the Kemano region, as well as the geology immediately along the T1 tunnel alignment. This combined with the Geotechnical Baseline Report produced by Hatch Ltd. (2012), which gave details on the geology along the T2 tunnel, allowed a direct link to be made between tunnel chainage and Rock Type.

The Rock Type node depends on the user's input (chainage of interest), and is a discrete and deterministic node. The possible states are shown in Table 11.

Table 11: States of Rock Type Node.

States
DuBose Stock
Gamsby Group
Horetzky Dyke and Complex
Tahtsa Complex

4.2.2.2 Tunnel Radius

This node is used to calculate the depth of spalling at a given chainage. For tunnel boring machine (TBM) excavations it is a fixed "finding" in the Bayesian Belief Network, and in the case of Kemano the TBM excavation has a diameter of 2.865 m (Klohn Leonoff Consulting Engineers, 1991). In order to be generally applicable to various tunnelling projects, the node is a continuous nature node, however it is treated as a deterministic node for Kemano as the tunnel geometry is known with certainty. The possible states are shown in Table 12.

Table 12: States of Tunnel Radius Node.

States	*Range*
Small	0 – 3 m
Medium	3 – 6 m
Large	6 – 9 m

4.2.2.3 Joint Orientation

The Joint Orientation node takes into account the orientation of discontinuities relative to the tunnel axis, in accordance with Bieniawski's RMR system (Bieniawski, 1989). It is a discrete nature node. The user of the network is able to select the state of this node if the favourability of the joint orientation is known, based on the RMR system (Table 13).

Table 13: Guidelines for determining effect of discontinuity orientations in tunnelling (Bieniawski, 1989).

Strike of Discontinuity	*Dip of Discontinuity*	*State*
Strike perpendicular to tunnel axis (Drive with dip)	20° to 45°	Favourable
	45° to 90°	Very Favourable
Strike Perpendicular to tunnel axis (Drive against dip)	20° to 45°	Unfavourable
	45° to 90°	Fair
Strike parallel to tunnel axis	20° to 45°	Fair
	45° to 90°	Very unfavourable
Irrespective of strike	0° to 20°	Fair

The user is expected to make a decision using their expert judgement and the information available to them, or if nothing is known, these data will be populated from the Excel database. The original RMR ratings had to be scaled up and reversed for use in the ravelling depth equation, as described in Section 4.2.3.10. The possible states are shown in Table 14.

Table 14: States of the Joint Orientation node, based on the RMR system (Bieniawski, 1989).

States	***RMR Rating***	***Rating used to calculate Ravelling***
Very favourable	0	21
Favourable	-2	18
Fair	-5	9
Unfavourable	-10	4
Very Unfavourable	-12	0

For the Kemano study area, the structural data available had to be refined in order to be streamlined into the Joint Orientation node. The tunnel mapping completed as part of the T2 downstream drive included discontinuity mapping (shears, joints, fault zones), description of lithology and structural features, drawings of installed rock support and drain holes, as well as information on tunnel advance rates and penetration rate (ASCL, 1990). An example of this is shown in Figure 30. The dip and dip direction of the discontinuities along the tunnel were recovered by digitizing three points along the trace of the discontinuities in plan view, specifically the points where the feature crosses both springlines and where it crosses the crown. The orientation of a plane can be calculated from these three points, and therefore the trend and plunge of the pole to the feature can be recovered once these data were digitized from the drawings (assuming that the discontinuities are planar features). The points on the plane were digitized as shown in Figure 31 and tabulated as shown in Table 15.

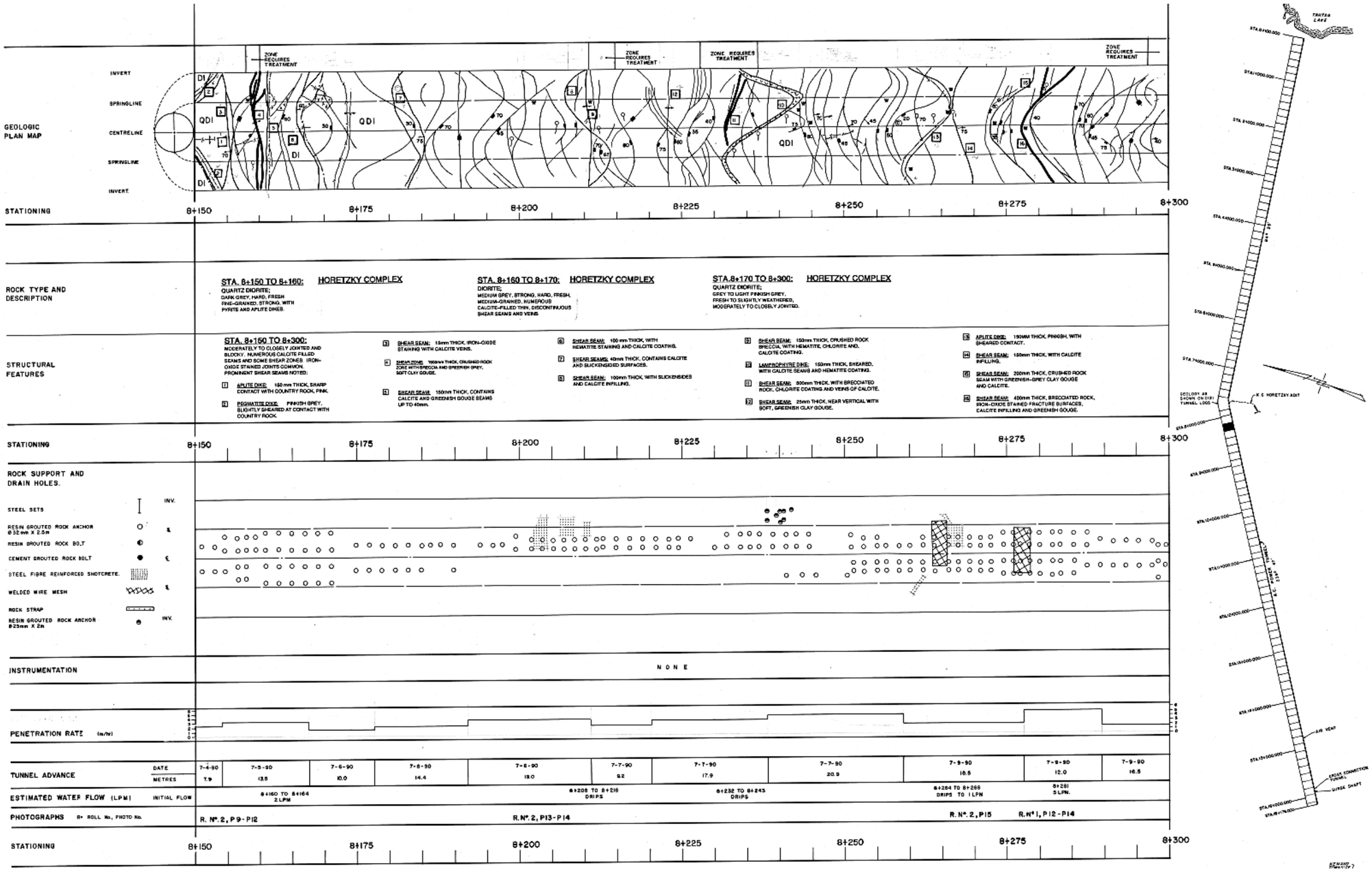

Figure 30: Example of a T2 mapping sheet adapted for use in the Joint Orientation node (ASCL, 1990).

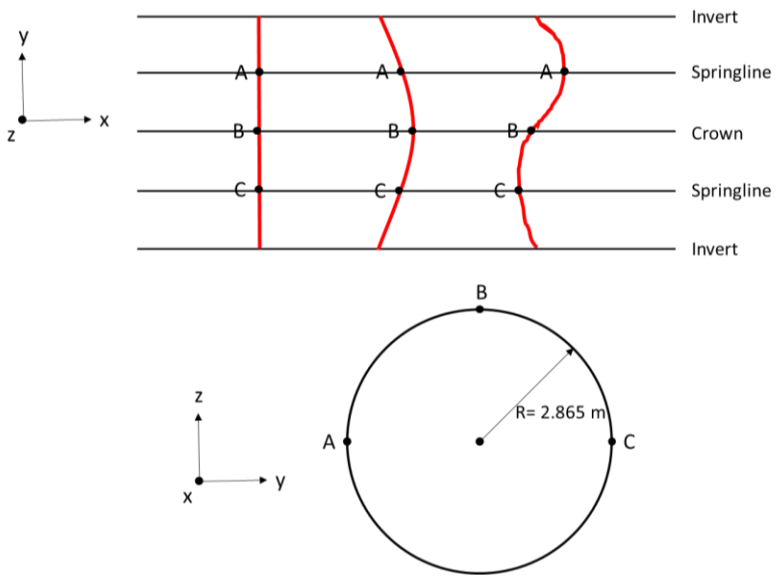

Figure 31: Convention for digitizing structural features from T2 geological mapping.

Table 15: Convention for tabulating structural features from T2 geological mapping.

Data Point Label	***X***	***Y***	***Z***
A	x_A = Chainage at A	y_A = -R	z_A = R
B	x_B = Chainage at B	y_B = 0	z_B = 2R
C	x_C = Chainage at C	y_C = R	z_C = R

Once the discontinuities were digitized in this format, it was possible to perform the vector math required to calculate the trend and plunge of the pole to the discontinuity. This was completed following the methodology set out by Groshong in his textbook, *3-D Structural Geology* (1999). Treating point A as the origin, the vectors $\overrightarrow{AB}$ and $\overrightarrow{AC}$ can be found using a Dot Product (Equation 11 and Equation 12).

$$\overrightarrow{AB} = [(x_B - x_A), (y_B - y_A), (z_B - z_A)]$$
$$\overrightarrow{AB} = \left[x_{\overrightarrow{AB}}, y_{\overrightarrow{AB}}, z_{\overrightarrow{AB}}\right] \quad \text{Equation 11}$$

$$\overrightarrow{AC} = [(x_C - x_A), (y_C - y_A), (z_C - z_A)]$$
$$\overrightarrow{AC} = \left[x_{\overrightarrow{AC}}, y_{\overrightarrow{AC}}, z_{\overrightarrow{AC}}\right] \quad \text{Equation 12}$$

The cross product of these two vectors, which by definition lie in the plane of the discontinuity, is the vector normal to the feature (Equation 13, illustrated in Figure 32).

$$\vec{N} = \overrightarrow{AB} \times \overrightarrow{AC}$$
$$\vec{N} = \left[\left(y_{\overrightarrow{AB}} z_{\overrightarrow{AC}} - y_{\overrightarrow{AC}} z_{\overrightarrow{AB}}\right), \left(x_{\overrightarrow{AB}} z_{\overrightarrow{AC}} - x_{\overrightarrow{AC}} z_{\overrightarrow{AB}}\right), \left(x_{\overrightarrow{AB}} y_{\overrightarrow{AC}} - x_{\overrightarrow{AC}} y_{\overrightarrow{AB}}\right)\right] \quad \text{Equation 13}$$
$$\vec{N} = \left[x_{\vec{N}}, y_{\vec{N}}, z_{\vec{N}}\right]$$

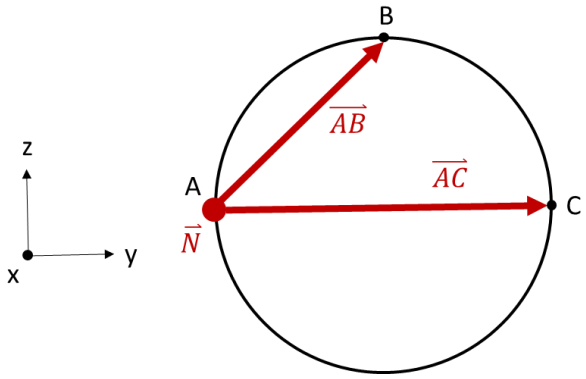

Figure 32: Cross product of vectors $\overrightarrow{AB}$ and $\overrightarrow{AC}$ result in a vector, $\vec{N}$, which is the pole to the discontinuity.

It is important that the z component of $\vec{N}$ be positive in order for the vector to be "pointing" in the correct direction, so a formula is programmed into the spreadsheet to perform this check, and switch the signs of all the components if necessary.

Since the vector normal to the plane is known, the direction cosines can be calculated and used to obtain its trend and plunge. The cosine of the angle between $\vec{N}$ and the x-axis (α), y-axis (β), and z-axis (γ) are calculated by dividing the appropriate component of $\vec{N}$ by its total length (Equation 14).

$$\cos\alpha = \frac{x_{\vec{N}}}{\sqrt{x_{\vec{N}}^2 + y_{\vec{N}}^2 + z_{\vec{N}}^2}}$$
$$\cos\beta = \frac{y_{\vec{N}}}{\sqrt{x_{\vec{N}}^2 + y_{\vec{N}}^2 + z_{\vec{N}}^2}} \quad \text{Equation 14}$$
$$\cos\gamma = \frac{z_{\vec{N}}}{\sqrt{x_{\vec{N}}^2 + y_{\vec{N}}^2 + z_{\vec{N}}^2}}$$

The plunge (δ) of the pole to the feature can now be calculated using Equation 15 (Groshong, 1999).

$$\delta = 90° - \cos^{-1}(\gamma) \quad \text{Equation 15}$$

The trend or azimuth (θ) of the pole is slightly more complicated, as it is dependent on which quadrant of the compass rose it falls into (Groshong, 1999). First θ' is calculated using Equation 16. The resulting value is then corrected based on Table 16.

$$\theta' = tan^{-1}\left(\frac{cos\ \alpha}{cos\ \beta}\right) \qquad \text{Equation 16}$$

Table 16: Corrections applied to calculated azimuth values (Groshong, 1999).

Azimuth	***cos(α)***	***cos(β)***	***θ***
000° to 090°	+	+	θ'
090° to 180°	+	-	180°+ θ'
180° to 270°	-	-	180°+ θ'
270° to 360°	-	+	360°+ θ'

Once this methodology was applied to all the discontinuities digitized from the mapping, it was possible to plot the poles on a stereonet (Figure 34). It should be noted that there is an inherent bias in tunnel mapping in which discontinuities that are perpendicular to the tunnel axis are observed and mapped preferentially. Three major joint sets are apparent from the stereonet (plunge → trend): Set 1, 12° → 238°, Set 4, 48° → 056°, and Set 5, 20° → 064°. Three minor sets were also noted: Set 2, 49° → 242°, Set 3, 13° → 280°, and Set 6, 13° → 022°.

The discontinuities are largely perpendicular to the tunnel alignment and steeply dipping, although there is quite a bit of scatter in the data. The possible impact of the discontinuities on the tunnel stability using Table 13 were determined by tunnel chainage and used to populate the Excel input database for the downstream T2 (Figure 33). The same distribution of orientations was used to estimate the impact of discontinuity orientations for the upstream half of T2 where mapping is not available. The mapping of T1 and of downstream T2, as well as the available geologic reports, support that the orientations of the discontinuities are consistent in the vicinity of the Kemano tunnels.

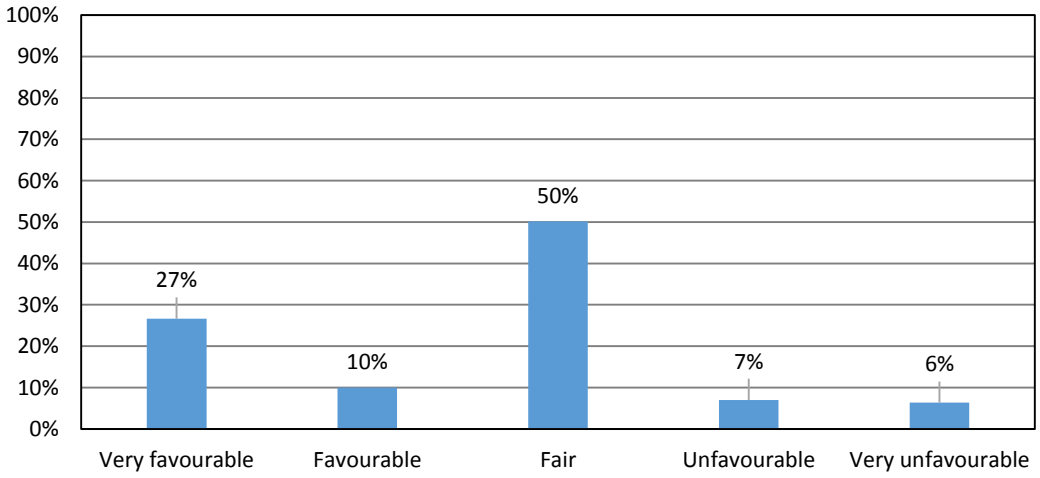

Figure 33: Distribution of discontinuity orientations along the T2 tunnel alignment.

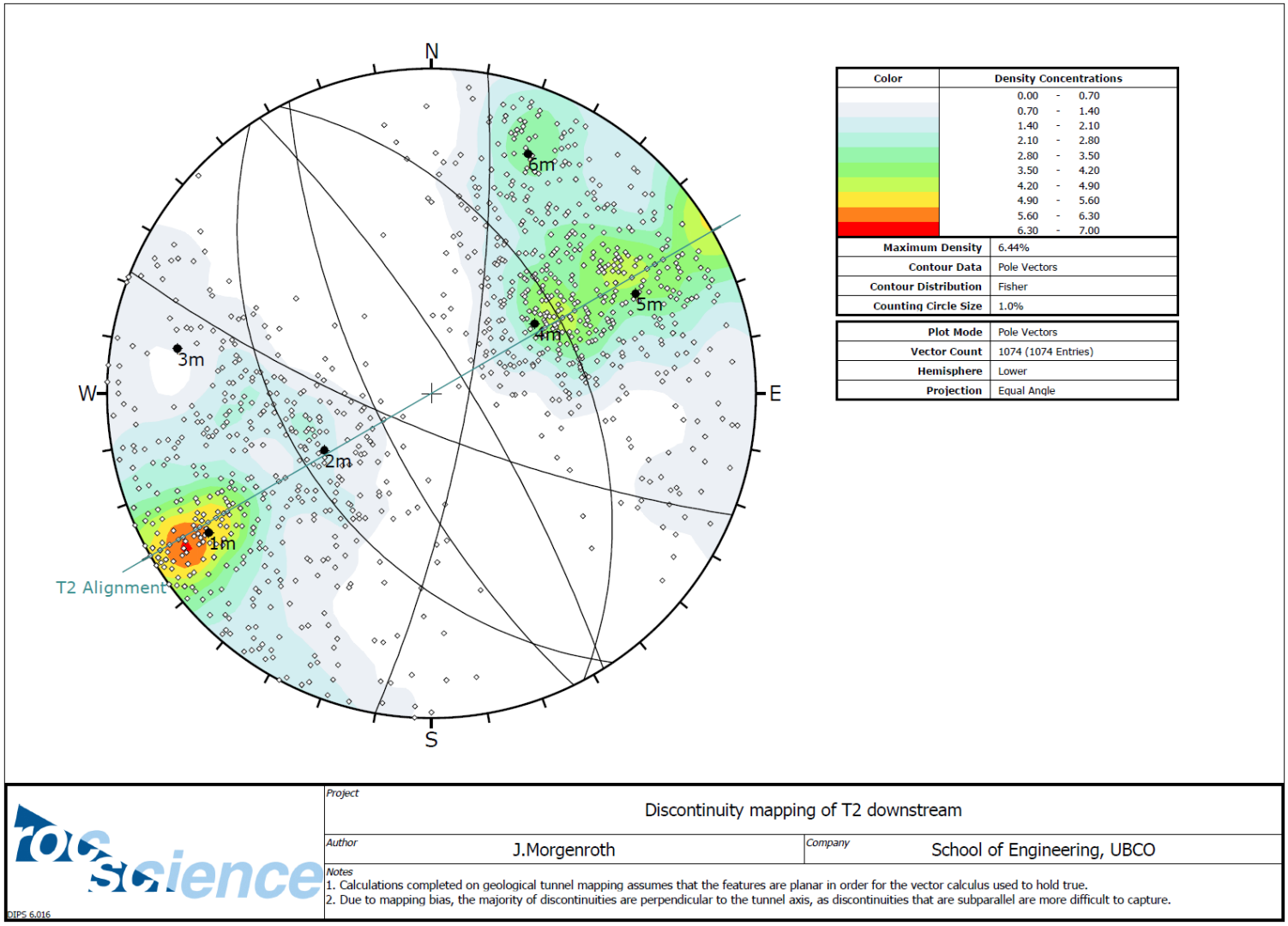

Figure 34: Discontinuity mapping of T2 downstream, showing major sets and tunnel alignment.

4.2.2.4 Structure

The Structure node follows the rankings given by the rock mass classification scheme developed by Hoek & Marinos (2000) called the Geological Strength Index, or GSI. It is a continuous nature node, and is user defined. The states are shown in Table 17.

Table 17: States of the Structure node.

States	***Range***
Intact or Massive	>30 m
Blocky	15 – 30 m
Very Blocky	1 – 15 m
Disturbed	n/a for Kemano
Disintegrated	n/a for Kemano
Laminated or Sheared	n/a for Kemano

Discontinuity intensity, or the volumetric count of discontinuities, is useful for determining structure of a rock mass but was not available in the dataset provided for Kemano. The digitized dataset of discontinuities was adapted to assess the Structure node. First the 1D fracture frequency was obtained in the form of number of discontinuities per metre of tunnel, and then this was converted into three dimensional fracture intensity following the work of Dershowitz & Herda (1992).

To do this, the number of fractures per length of tunnel (P_{11}) was converted into fracture spacing (S_f), which is just its inverse (Equation 17) (Dershowitz & Herda, 1992).

$$S_f = \frac{1}{P_{11}} \qquad \text{Equation 17}$$

Dershowitz & Herda note that while P_{11} and S_f are dependent upon the orientation of the fractures, they are not dependent on their size. As a result, they are scale independent and do not depend on the region in which they are defined. The dependence these variables have on orientation can be nullified by performing a correction factor for the relative orientation of the scanline, represented by the tunnel in this case. The angle between the scanline and the mean pole of the fractures can be determined and used to convert the fracture spacing into the number of fractures in a volume, P_{32} (Equation 18) (Dershowitz & Herda, 1992).

$$P_{32} = \frac{C_{PS}}{S_f}$$ Equation 18

In the case of the discontinuities at Kemano, the mean orientation of the discontinuities is approximately perpendicular to the tunnel alignment, and therefore no correction factor is required to calculate the 3D fracture intensity – it is the same as the 1D fracture intensity. This volumetric fracture intensity can now be treated as a proxy for blockiness. Figure 35 shows the calculated 3D fracture intensity plotted as a function of tunnel chainage, which was used for the downstream/excavated portion of T2.

The upstream dataset proved to be more difficult to obtain, as the tunnel has not yet been excavated. Since the T1 and T2 tunnels are only 300 m apart, an assumption was made that the discontinuity intensity could be mapped linearly from T1 to T2 (this was checked against the downstream data and proved to be appropriate). A plot of the shears and faults in the T1 tunnel exists (HMM, 2010), and a similar method as was described above was used to approximate the fracture frequency. However, this resulted in a coarser dataset, because digitizing was done in 500 m increments. Due to the coarseness of the dataset, fracture spacing was not used as a direct input, but rather the spacing values were binned using relative magnitudes to arrive at “Massive/Intact”, “Blocky” and “Very Blocky” designations for each 500 m section (see Appendix D: Kemano Specific Database).

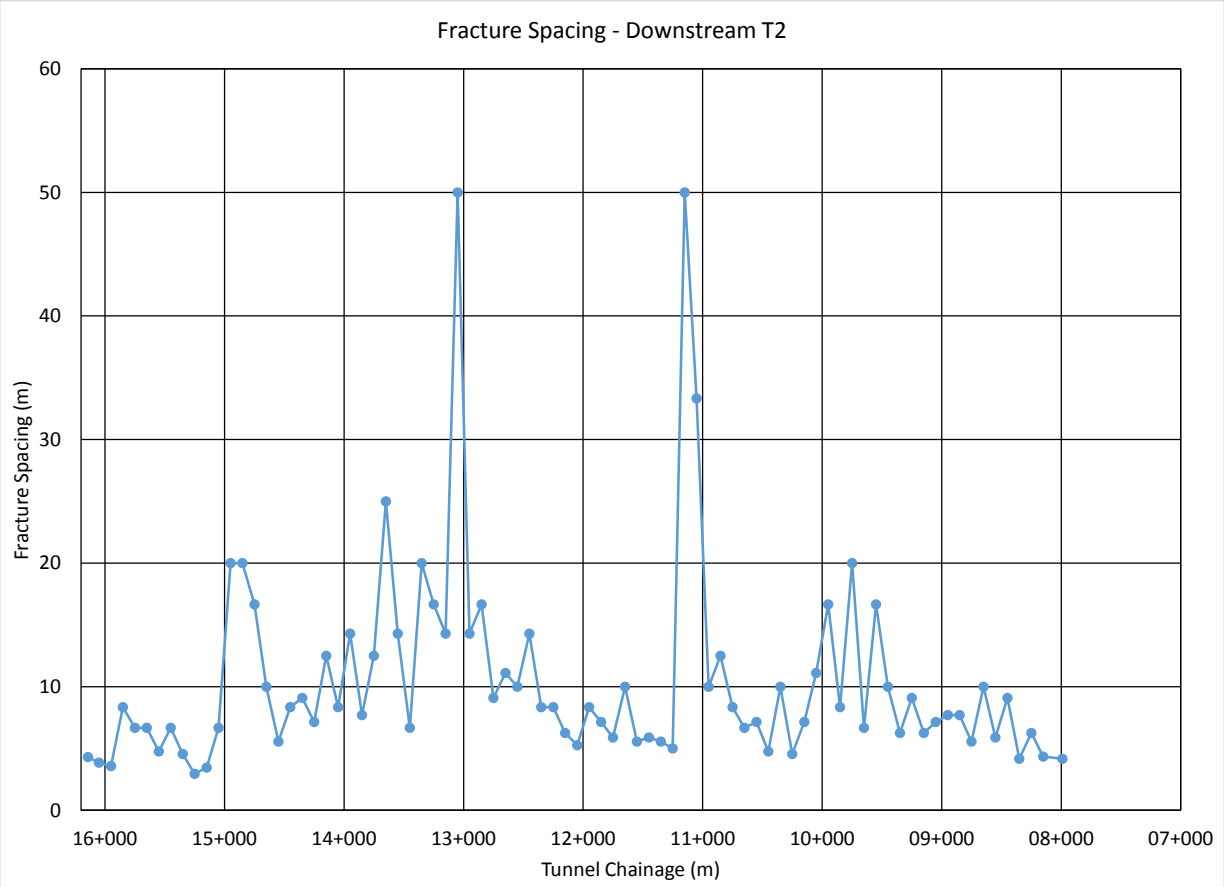

Figure 35: 3D fracture spacing as a function of tunnel chainage for the downstream (excavated) portion of T2.

4.2.2.5 Joint Infilling

The Joint Infilling node accounts for the infilling or gouge of discontinuities in the rock mass, according to the Bieniawski (1989) RMR ratings. It is a discrete nature node. As discussed in in Section 4.2.3.1, the rating was scaled up to account for the fact that discontinuity persistence and aperture were not included in estimating joint shear strength. The unusual values for the states were used to preserve the original proportionality of the parameters and their possible states from the RMR system. The possible states are shown in Table 18.

Table 18: States of the Joint Infilling node, based on the RMR ratings (Bieniawski, 1989).

States	*Original RMR Rating*	*Rating used to calculate Joint Shear Strength*
None	6	17.54
Hard <5mm	4	11.69
Hard >5mm	2	5.85
Soft <5mm	2	5.85
Soft >5mm	0	0

At Kemano, samples of joint and shear infill were taken during 2015 site investigations (Hatch Ltd., October 2015). Data for infill are only available for the excavated portion of T2. Where data existed they were used to populate the Excel database at the appropriate chainage. Since there are no data available for the upstream half of T2, a distribution based on the data from the downstream drive was applied (Figure 36).

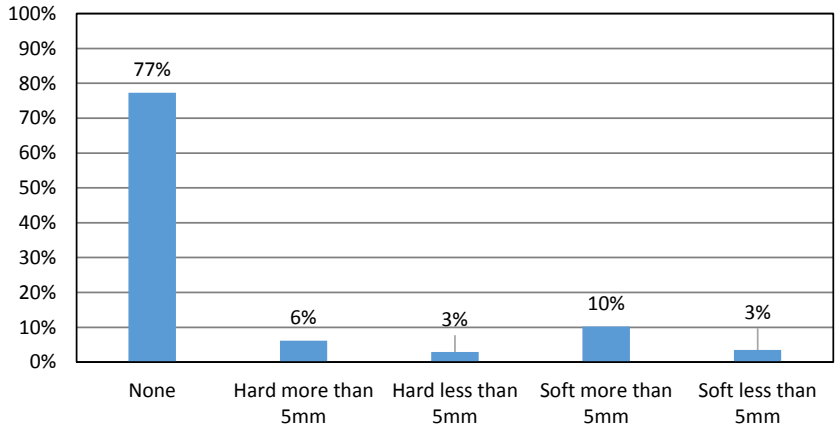

Figure 36: Distribution of discontinuity infilling along the T2 tunnel alignment.

4.2.2.6 Joint Weathering

The Joint Weathering node takes into account the degree of weathering of discontinuities in the rock mass, in accordance with Bieniawski's RMR ratings (Bieniawski, 1989). It is a discrete nature node. As discussed in Section 4.2.3.1, the rating have been scaled up to account for the fact that discontinuity persistence and aperture were not included in estimating joint shear strength. The unusual values for the states were used to preserve the original proportionality of the parameters and their possible states from the RMR system.

Similar to the Joint Infilling node, the user can make an expert judgement on the likely states of this node, or choose to use the built in distribution based on the downstream drive. The states are shown in Table 19.

Table 19: States of the Joint Weathering node, based on the RMR ratings (Bieniawski, 1989).

States	***Original RMR Rating***	***Rating used to calculate Joint Shear Strength***
Unweathered	6	17.54
Slightly weathered	5	14.62
Moderately weathered	3	8.77
Highly weathered	1	2.92
Decomposed	0	0

The distribution of weathering along the downstream portion of T2 was determined using the field mapping done during the 2015 site investigations (Hatch Ltd., 2015). This distribution is applied to the unexcavated portion of T2, in the absence of user supplied data (Figure 37).

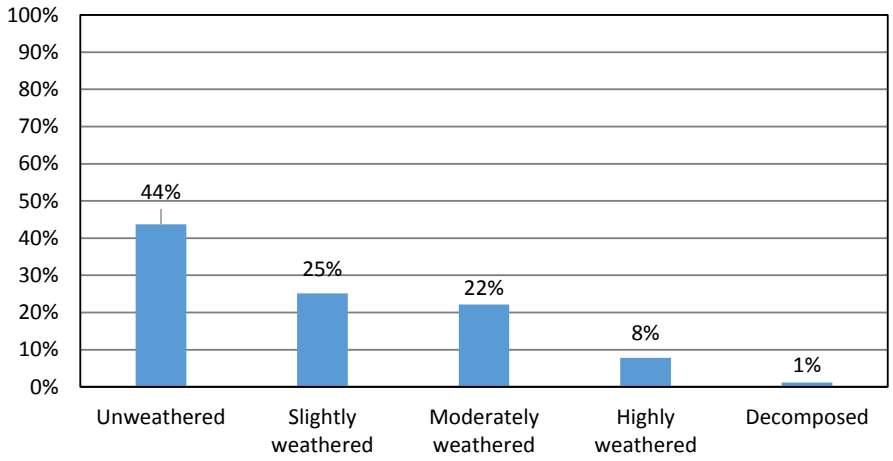

Figure 37: Distribution of discontinuity weathering along the T2 tunnel alignment.

4.2.2.7 Joint Roughness

The Joint Roughness node takes into account the irregularities on the surfaces of discontinuities in the rock mass, in accordance with the Bieniawski (1989) RMR ratings. It is a discrete nature node.

As discussed in Section 4.2.3.1, the rating have been scaled up to account for the fact that discontinuity persistence and aperture were not included in estimating joint shear strength.

The unusual values for the states were used to preserve the original proportionality of the parameters and their possible states from the RMR system. This node is also user defined, and if nothing is known about the discontinuity roughness the data are taken from a predetermined distribution. The states are shown in Table 20.

Table 20: States of the Joint Roughness node, based on the RMR ratings (Bieniawski, 1989).

States	***Original RMR Rating***	***Rating used to calculate Joint Shear Strength***
Very Rough	6	17.54
Rough	5	14.62
Slightly Rough	3	8.77
Smooth	1	2.92
Slickensided	0	0

The discontinuity roughness distribution was obtained from observations and mapping done during the 2015 site investigations (Hatch Ltd., 2015). This distribution can be seen in Figure 38.

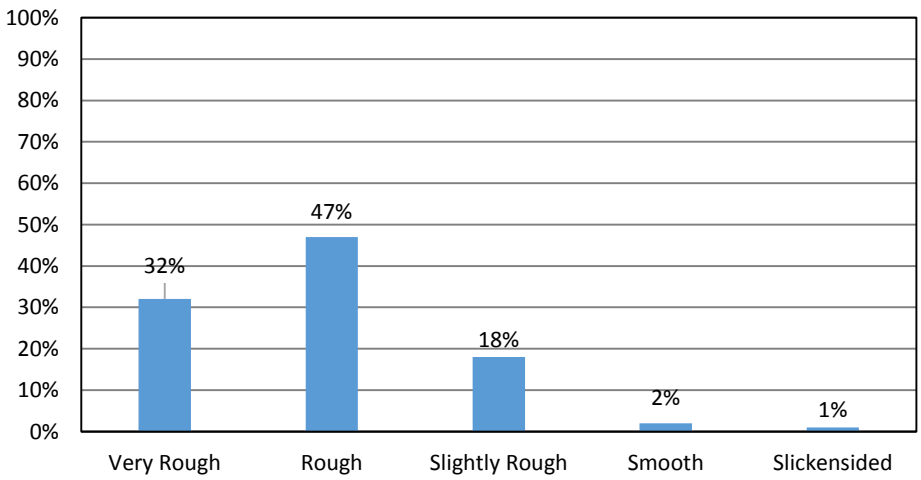

Figure 38: Distribution of discontinuity roughness along the T2 tunnel alignment.

4.2.2.8 Groundwater

The Groundwater node takes into account the groundwater inflow along discontinuities in the rock mass, in accordance with the Bieniawski (1989) RMR ratings. It is a continuous nature node.

Groundwater inflow is difficult to quantify prior to excavation, and therefore an option has been given that it can be input by the user to update the network as the tunnel advances. If

nothing is known, a distribution correlating to the rock type and the measured groundwater inflow from the downstream T2 drive is assigned (Figure 39).

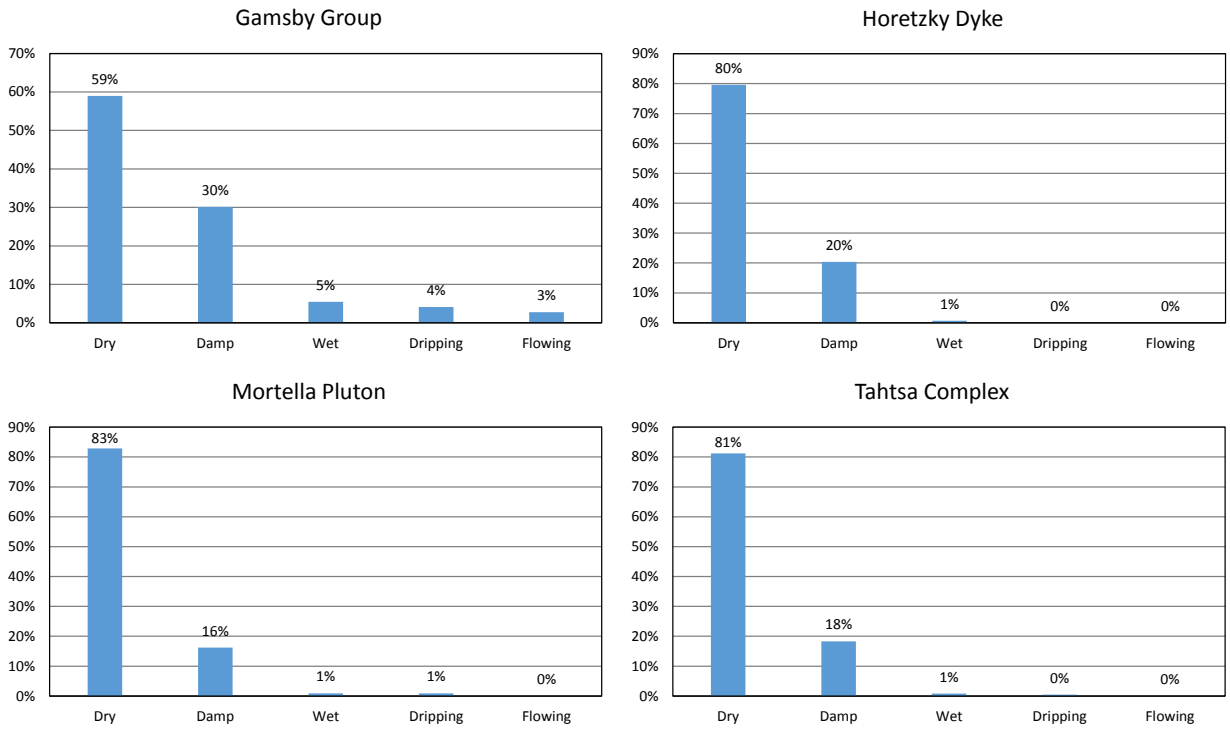

Figure 39: Histograms showing distribution of groundwater inflow for each rock type (ASCL, 1990).

The original RMR ratings needed to be scaled up for used in the depth of ravelling calculation, as described in Section 4.2.3.10. The states of the groundwater node are shown in Table 21.

Table 21: States of the Groundwater node, based on the RMR ratings (Bieniawski, 1989).

States	***Range***	***RMR Rating***	***Rating used to calculate Ravelling***
Dry	0 L/min	15	26
Damp	<10 L/min	10	17.33
Wet	10 – 25 L/min	7	12.13
Dripping	25 – 125 L/min	4	6.93
Flowing	>125 L/min	0	0

4.2.2.9 Unconfined Compressive Strength (UCS)

The unconfined compressive strength of the rock is an important parameter used to calculate rock mass strength, and in the case of this network is also used to estimate the tensile strength of the rock. For Kemano, the UCS values were obtained from lab testing conducted

prior to the downstream T2 drive (KLCE, 1991; Bechtel Canada, Inc., 1991). This is a continuous nature node, and the states are shown in Table 22.

Table 22: States of the UCS node.

States	*Range*
Low	20 – 140 MPa
Medium	140 – 160 MPa
High	160 – 250 MPa

4.2.2.10 Magnitude of Major and Minor Principal Stresses (σ_1 and σ_3)

The magnitudes of the major and minor principal stresses along the tunnel alignment were obtained from 3D stress modelling completed in Abaqus, as described in Chapter 3. These nodes are continuous nature nodes. The states are shown in Table 23 and Table 24.

Table 23: States of the Major Principal Stress node.

States	*Range*
Low	< 7 MPa
Medium	7 – 15 MPa
High	> 15 MPa

Table 24: States of the Minor Principal Stress node.

States	*Range*
Low	< 2 MPa
Medium	2 – 5 MPa
High	> 5 MPa

4.2.2.11 Orientation of Major and Minor Principal Stresses (ϑ)

The orientation of the major and minor principal stresses along the tunnel alignment were obtained from 3D stress modelling completed in Abaqus, as described in Chapter 3. This node is a continuous nature node, and the states are shown in Table 25.

Table 25: States of the Stress Orientation node.

*States**	*Range*
Right springline	-90° to -75°
Right shoulder	-75° to -25°
Crown	-25° to +25°
Left shoulder	+25° to +75°
Left springline	+75° to +90°

** Definition of failure locations:*

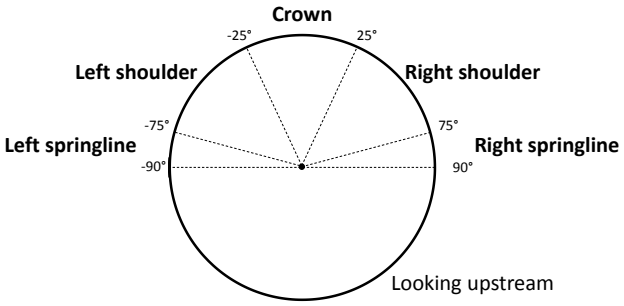

4.2.3 Child Nodes

The states of the nodes described in this section rely on conditional dependencies with their parent nodes. In some cases empirical relationships that are widely accepted in rock mechanics were used to build the links, and in other cases Conditional Probability Tables (CPTs) were built using expert judgement and the support of published literature.

4.2.3.1 Joint Shear Strength

Joint shear strength has been quantified following the Rock Mass Rating (RMR) System (Hudson & Harrison, 2000). The joint shear strength, or "condition of discontinuities", depends on discontinuity persistence, aperture, roughness, infilling and weathering. For the purposes of the Kemano Bayesian Network, only the latter three factors were included due to limited information to delineate persistence and aperture. As a result, the remaining three contributing factors were scaled to comprise the entirety of the Joint Shear Strength parameter in the RMR system (Table 26). This was then further scaled up to 31% of the factors contributing to ravelling, as described in Section 4.2.3.11. This unusual value was used to preserve the original proportionality of the parameters and their possible states from the RMR system, and to simplify the Ravelling expression.

Table 26: Values used to calculate Joint Shear Strength, based on RMR system (Bieniawski, 1989).

Parameter	***Weight (/53)***	***States***	***Original RMR weighting***	***Value used in Joint Shear Strength calculation***
Joint Infilling	17.54	None	6	17.54
		Hard <5mm	4	11.69
		Hard >5mm	2	5.85
		Soft <5mm	2	5.85
		Soft >5mm	0	0
Joint Weathering	17.54	Unweathered	6	17.54
		Slightly weathered	5	14.62
		Moderately weathered	3	8.77
		Highly weathered	1	2.92
		Decomposed	0	0
Joint Roughness	17.54	Very Rough	6	17.54
		Rough	5	14.62
		Slightly Rough	3	8.77
		Smooth	1	2.92
		Slickensided	0	0

The states of the Joint Shear Strength Node are shown in Table 27.

Table 27: States of the Joint Shear Strength node.

States	***Range***
Low	0 – 17.54
Medium	17.54 – 35.08
High	35.08 – 53

The Conditional Probability Table for this node can be found in Appendix C: Conditional Probability Tables. This table was populated using a point estimation method.

4.2.3.2 Geological Strength Index (GSI)

This node follows the rock mass classification scheme developed by Hoek and Marinos called the Geological Strength Index, or GSI (Marinos et al., 2005). This classification scheme relies on only two input parameters: blockiness (which translates roughly to the number of discontinuity sets, their spacing and their orientation relative to each other) and joint shear strength (Figure 40). The states of this node are shown in Table 28.

Table 28: States of the GSI node (Marinos et al., 2005).

States	***Range***
Very Poor Rock	0 – 20
Poor Rock	20 – 40
Fair Rock	40 – 60
Good Rock	60 – 80
Very Good Rock	80 – 100

The Conditional Probability Table for this node can be found in Appendix C: Conditional Probability Tables. This table was created by digitizing the work of Hoek & Marinos (2000).

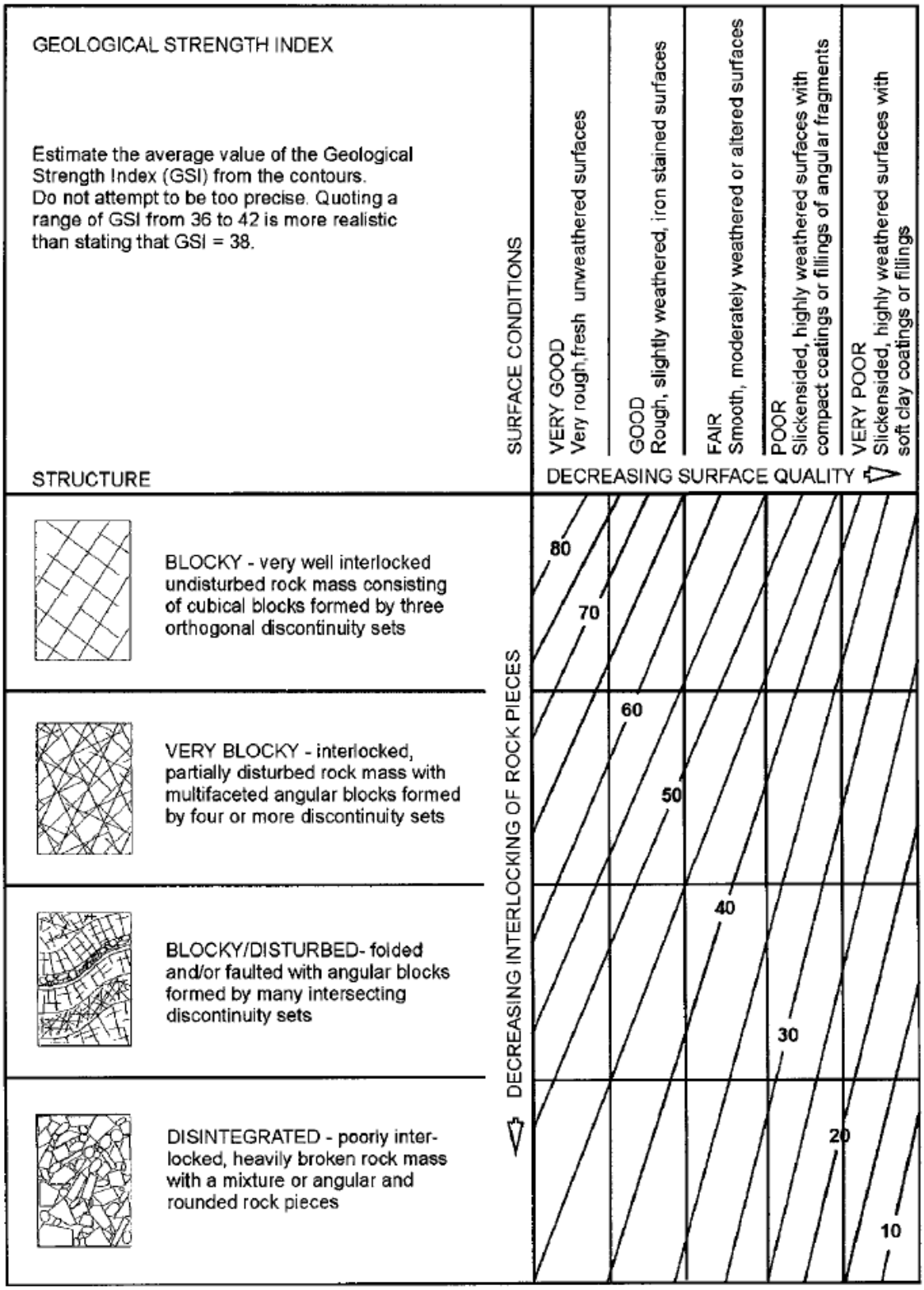

Figure 40: Estimates of Geological Strength Index GSI based on geological descriptions (Marinos & Hoek, 2000).

4.2.3.3 Hoek-Brown Parameters (D, s, a, m_i, m_b)

The rock mass strength parameters were determined using the Hoek-Brown failure criterion (Hoek, 2002). The Disturbance Factor (*D*) accounts for the amount of damage caused to the rock by the excavation method. It is a discrete nature node, and is determined by the method of excavation (Table 29).

Table 29: Guidelines for estimating Disturbance Factor, *D* (Hoek, 2002).

Description of rock mass	***D***
Excellent quality controlled blasting or excavation by tunnel boring machine causes minimal disturbance to the confined rock mass surrounding a tunnel.	0
Mechanical or hand excavation of tunnels in poor quality rock masses (no blasting) causes minimal disturbance to the surrounding rock mass.	0
Where squeezing problems in a tunnel causes significant floor heave, disturbance can be severe unless a temporary invert is placed.	0.5
Small scale, good blasting in civil engineering slopes causes modest rock mass damage, particularly if controlled blasting is used. However, stress relief results in disturbance.	0.7
In some softer rocks, excavation can be carried out by ripping and dozing and the degree of slope disturbance is less.	0.7
Very poor quality blasting in a hard rock tunnel causes severe local damage, extending 2 to 3m, in the surrounding rock mass.	0.8
Small scale, poor blasting in civil engineering slopes causes rock mass damage, and stress relief results in disturbance.	1
Very large open pit mine slopes suffer significant disturbance due to heavy production blasting and also stress relief from overburden removal.	1

For the Kemano T1 tunnel, a D = 0.8 is selected due to the drill and blast excavation method used. For the T2 tunnel, D = 0 is selected because the tunnel is excavated by TBM. The states are shown in Table 30.

Table 30: States of Disturbance Factor node (Hoek, 2002).

States	***Value***
Excellent	0
Minimal	0.5
Severe damage	0.8

The Hoek-Brown parameters m_i (*i* for intact) and m_b (*b* for broken) are analagous to friction. m_b is calculated based on m_i and *GSI (*Equation 19*).*

$$m_b = m_i * exp\left(\frac{GSI - 100}{28}\right)$$ Equation 19

These nodes are both continuous nature nodes. The possible states for the m_i node was kept generally applicable to all possible rock types (Table 31), and m_b is calculated based on the state of m_i.

Table 31: States of m_i node (Hoek, 2002).

States	*Value*
Low	0-15
Common	15-25
High	25-35

The rock mass in the Kemano is part of an intrusive complex, and granites have an m_i value ranging from 20-35. An average value of 27.5 was applied and treated as a deterministic input in this case.

The Hoek-Brown parameter s and a are continuous nature nodes. These are calculated based on the GSI predicted by the Bayesian Network, and s also depends on the Disturbance Factor. The parameter s is calculated using Equation 20, and the parameter a is calculated using Equation 21.

$$s = exp\left(\frac{GSI - 100}{9 - 3D}\right)$$ Equation 20

$$a = 0.5 + \left(\frac{e^{-\frac{GSI}{15}} - e^{-\frac{20}{3}}}{6}\right)$$ Equation 21

The states of these nodes are shown in Table 32 and Table 33.

Table 32: States of s (Hoek, 2002).

States	*Range*
s low	< 2e-4
s normal	2e-4 to 0.006
s high	0.006 to 1

Table 33: States of a (Hoek, 2002).

States	*Range*
a low	0 - 0.5
a common	0.5 – 0.51
a high	0.51 - 1

The disturbance factor is deterministic and therefore does not have a CPT. CPTs for the *s* and *a* nodes can be found in Appendix C: Conditional Probability Tables. These tables were populated using a point estimation method.

4.2.3.4 Rock Mass Strength

The Hoek-Brown rock mass strength is calculated using Equation 22 (Hoek, 2002). This parameter is not used further in the network, however it can be useful to geotechnical engineers for design purposes, and was therefore included as a secondary output.

$$\sigma_1' = \sigma_3' + UCS * \left(m_b \frac{\sigma_3'}{UCS} + s \right)^a \qquad \text{Equation 22}$$

This is a continuous nature node, and the states are shown in Table 34.

Table 34: States of the Rock Mass Strength node (Hoek, 2002).

States	***Range***
Low	< 60 MPa
Medium	60 – 120 MPa
High	> 120 MPa

The Conditional Probability Table for this node can be found in Appendix C: Conditional Probability Tables. This table was populated using a Monte Carlo Simulation, conducted with the Excel add-in Crystal Ball (Oracle, 2014).

4.2.3.5 Tangential Stresses (σ_{max}, σ_{min})

The tangential stresses around the tunnels are calculated using Kirsch equations (Equation 5). This is done in Netica using the in situ stresses that resulted from the 3D modelling. These nodes are continuous nature nodes, and the states are shown in Table 35 and Table 36.

Table 35: States of the σ_{max} Node.

States	***Range***
High	> 60 MPa
Medium	30 – 60 MPa
Low	< 30 MPa

Table 36: States of the σ_{min} Node.

States	*Range*
High	> 20 MPa
Medium	10 – 20 MPa
Low	0 – 10 MPa
In tension	< 0 MPa

The Conditional Probability Tables for these nodes can be found in Appendix C: Conditional Probability Tables. These tables were populated using a Monte Carlo Simulation, conducted with the Excel add-in Crystal Ball (Oracle, 2014).

4.2.3.6 Depth of Spalling

As outlined in Section 2.4.3, the probable depth of spalling was calculated in Netica following the work by Martin, Christiansson, & Söderhäll (2001). Relative to other tunnel projects around the world, the depth of spalling observed in T1 and in the excavated portion of T2 at Kemano is relatively low, with a maximum depth of about 0.5 m observed in the excvated portion of T2. The ranges for this node were adusted according to this maximum value for Kemano (Figure 41).

$$\frac{r}{a} = \frac{2.865\ m + 0.5\ m}{2.865\ m} = 1.2$$

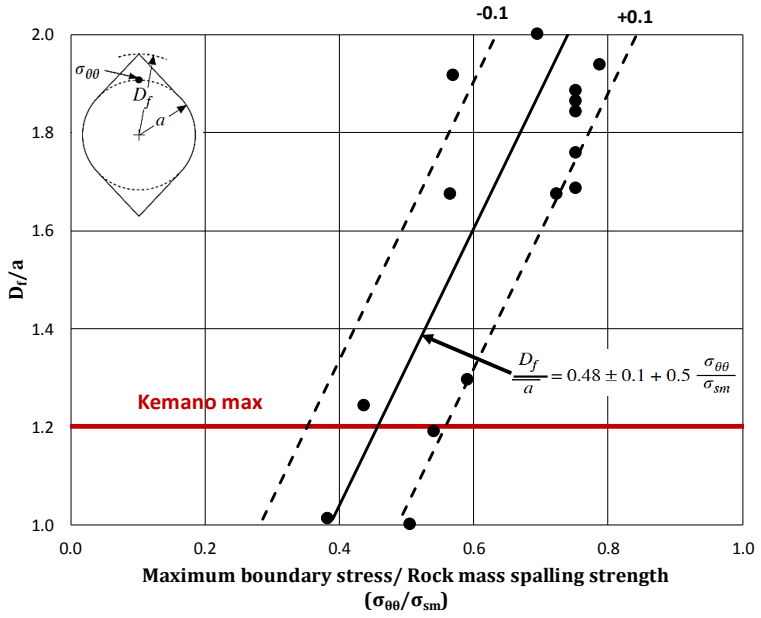

Figure 41: Maximum depth of spalling observed in the field (adapted from Martin & Christiansson, 2009).

The Depth of Spalling node is a continuous nature node, and the states are shown in Table 37.

Table 37: States of Depth of Spalling Node.

States	*Range*
None	0 m
Low	0 – 0.2 m
Medium	0.2 – 0.5 m
Deep	> 0.5 m

The Conditional Probability Table for this node can be found in Appendix C: Conditional Probability Tables. This table was populated using a Monte Carlo Simulation, conducted with the Excel add-in Crystal Ball (Oracle, 2014).

4.2.3.7 Location of Spalling

The location of spalling is determined by the orientation of the major principal stress at a given tunnel chainage. The location orthogonal to this orientation corresponds to where spalling may occur. This is a continuous nature node, and the states are shown in Table 38.

Table 38: States of Location of Spalling Node.

*States**	*Range*
Right springline	-90° to -75°
Right shoulder	-75° to -25°
Crown	-25° to +25°
Left shoulder	+25° to +75°
Left shoulder	+75° to +90°

** Definition of failure locations:*

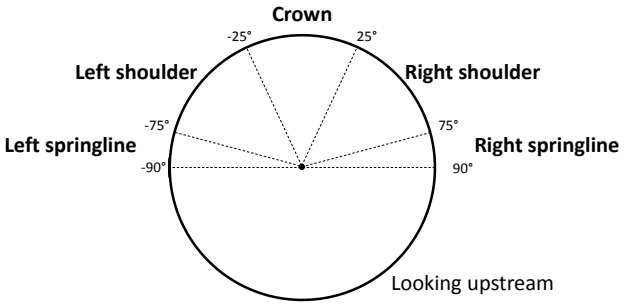

The Conditional Probability Table for this node can be found in Appendix C: Conditional Probability Tables.

4.2.3.8 Ravelling Potential

The Ravelling Potential node represents whether or not the stress conditions tangent to the tunnel opening are conducive for ravelling. Low stress conditions are known to contribute

to ravelling failure, namely when the tangential stress is tensile or in low compression. In the case of tensile tangential stress, there is no compressive arch and the blocks or wedges are free to slide out of the tunnel crown or shoulder. Low compressive tangential stress may allow ravelling to occur if the weight of a block is able to overcome the shear resistance provided by the joints defining the block boundaries, which in turn depends on the normal stress acting on the joints. If the tangential stress is high enough it will clamp the blocks and therefore ravelling failure is not possible. If the tangential stress is compressive and higher than UCS, crushing or spalling may initiate.

An order of magnitude of the value of the tangential stress that begins to allow for block ravelling in the roof of a tunnel can be approximated using a simple clamped block model (Figure 42).

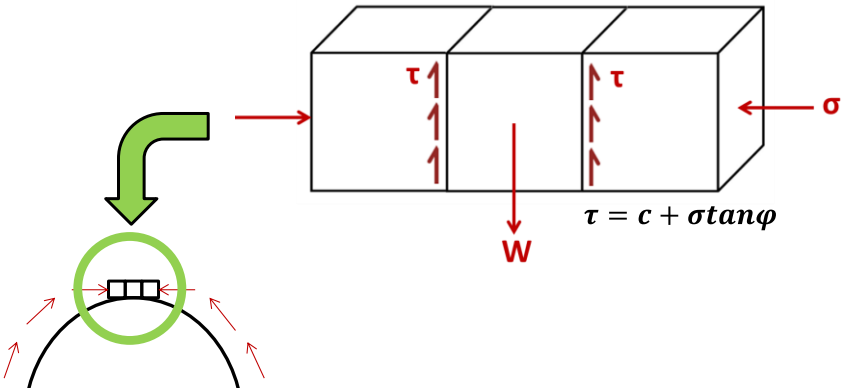

Figure 42: Low compressive tangential stress may allow blocks to ravel due to lack of clamping to keep the blocks in place.

This model consists of a cubic metre block held in place by vertical joints on two sides. The shear strength of the joints on each side are assumed to be governed by the Mohr-Coulomb shear strength criterion with no cohesion (to account for the clay infill and low shear strength seen locally at Kemano). The stress acting on the block is its self-weight. For vertical force equilibrium, a tangential compressive stress of less than 1 MPa is required to just keep the block in place. The minimum tangential stress is more important than the maximum tangential stress for this evaluation, because the minimum tangential stress is always lower

and therefore the ravelling failure will always initiate here, and then perhaps propagate to the location of maximum tangential stress if it is also in low compression.

It can be shown through this simple analytical model that low stress can allow a block to fall out of the crown of a tunnel and result in ravelling failure. Since it is not easy to determine the exact stress that results in sufficient clamping to keep the block in place, a percentage of Terzaghi's Rock Load (Section 4.2.3.9) is used in the Ravelling expression (Section 4.2.3.10) depending on whether the minimum tangential stress is High, Medium, Low or In Tension. Ravelling Potential is a deterministic nature node, and the states are shown in Table 39.

Table 39: States of the Ravelling Potential Node.

States	***Value – Percentage of Rock Load***
High	5%
Medium	10%
Low	90%
In tension	100%

4.2.3.9 Rock Load

This node is based on Terzaghi's work on determining the height of the mass of rock which will tend to drop out of the roof of a tunnel, discussed in Section 2.4.4. Terzaghi's original work is based solely on how blocky and seamy a rock mass is, and the ranges for the rock loads given are based on his expert judgement. The high value in each of the ranges corresponds to wet or saturated rock mass conditions, but since groundwater is accounted for later in the Ravelling expression (Section 4.2.3.10, Equation 23) the low (dry) value is used for the purposes of this node. The span width and span height are both the diameter of the tunnel, which is 5.73 m in the case of Kemano. This is a discrete nature node, and the states are shown in Table 40. The states are based on the methodology described in Section 2.4.4.

Table 40: States of Rock Load node.

States	***Value***
Massive to moderately jointed	0 * 5.73 = 0 m
Moderately blocky rock	0.25 * (5.73+5.73) = 2.9 m
Very blocky to shattered rock	0.35 * (5.73 + 5.73) = 4.0 m

The Rock Load is deterministic and therefore does not have a CPT.

4.2.3.10 Depth of Ravelling

As discussed in Section 2.4.4, there has been little work done to delineate the precise circumstances that result in ravelling, a gravity-driven failure mechanism. It is known that important factors are: the tunnel span, degree of fracturing, joint infill and cohesion, discontinuity shear strength, groundwater, imposed stress conditions, and strength of the rock (Thapa, et al., 2009; Goricki, 2013). These factors coalesce in a variety of ways to result in ravelling, but much of this information is difficult to obtain prior to a tunnel's excavation. For the purposes of this thesis, and for input into the Kemano Bayesian Network, a proportional approach was used to determine whether ravelling occurs, analogous to a factor of safety calculation. Equation 23 was developed to define the depth of ravelling, R_D, resulting from the coalescing of these factors.

$$R_D = Ravelling\ Potential\ * \overbrace{\frac{1}{(J_o + J_s + J_w)}}^{Rock\ mass\ characteristics} * Rock\ Load \qquad \text{Equation 23}$$

Where the Ravelling Potential term represents whether the tangential stresses around the tunnel are conducive to ravelling, J_o is Joint Orientation, J_s is Joint Shear Strength, and J_w is Groundwater. Table 41 shows the breakdown of the rock mass characteristic parameters used in the rock mass characteristics portion of this calculation.

Table 41: Summary of rock mass characteristics used to calculate Ravelling, their states and values used in the calculation.

Parameter	***Weight (/100)***	***States***	***Original RMR weighting***	***Scaled value used in Ravelling calculation***
Joint Orientation (J_o)	12	Very favourable	0	21
		Favourable	-2	18
		Fair	-5	9
		Unfavourable	-10	4
		Very unfavourable	-12	0
Joint Shear Strength* (J_s)	53	Low	-	0 – 17.54
		Medium	-	17.54 – 35.08
		High	-	35.08 – 53
Groundwater (J_w)	26	Dry - 0 L/min	15	26
		Damp - <10 L/min	10	17.33
		Wet - 10 – 25 L/min	7	12.13
		Dripping - 25 – 125 L/min	4	6.93
		Flowing - >125 L/min	0	0

** The value of Joint Shear Strength used in Ravelling calculation depends on values of Joint Infilling, Joint Weathering and Joint Roughness, as described in Section 4.2.3.1.*

The Rock Load term gives the resulting value of the ravelling expression a dimension in metres, which reflects the depth of ravelling that can occur as a result of the stresses, rock mass conditions, and geometry of the tunnel. The states of the Ravelling node are shown in Table 42.

Table 42: States of the Ravelling Node.

States	***Range***
None	0
Low	0 – 0.5 m
Medium	0.5 – 1 m
High	> 1 m

The Conditional Probability Table for this node can be found in Appendix C: Conditional Probability Tables. This table was populated using a point estimation method.

4.2.3.11 Location of Ravelling

The location of ravelling is determined by the orientation of the major principal stress at a given tunnel chainage. This orientation corresponds to where ravelling may occur. This is a continuous nature node, and the states are shown in Table 43.

Table 43: States of Location of Ravelling Node.

States*	***Range***
Right springline	-90° to -75°
Right shoulder	-75° to -25°
Crown	-25° to +25°
Left shoulder	+25° to +75°
Left shoulder	+75° to +90°

** Definition of failure locations:*

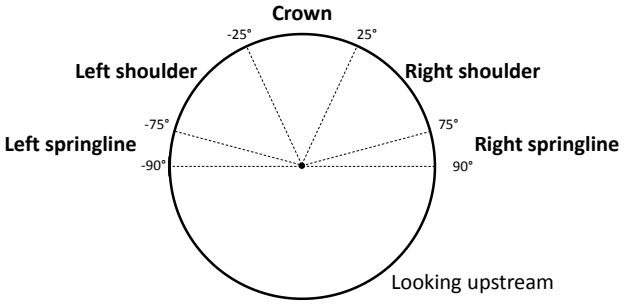

The Conditional Probability Table for this node can be found in Appendix C: Conditional Probability Tables.

4.2.3.12 Ground Class

The Ground Class prediction for a given tunnel chainage depends on the predicted depth of spalling and ravelling. The possible consequences of the different combinations of these two rock mass failure modes were based on site observations of the downstream portion the T2 tunnel. The severity of the failure and therefore the corresponding levels of ground support are based on expert judgement and the final support design produced by Hatch for the excavated half of the T2 tunnel (Hatch Ltd., May 2015). The possible states of the Ground Class are summarized in Table 44.

Table 44: States of Ground Class node.

States	*Ground Behaviour*
Class I	No failure
Class IIa	Low to medium depth of spalling
Class IIb	Low to medium depth of ravelling
Class III	Medium to high depth of spalling and/or ravelling
Class IV	High depth of spalling and/or ravelling

This node is not driven by an empirical relationship nor populated from the Excel database (see Section 4.2.1), but rather it relies completely on the Conditional Probability Table (CPT) that was designed using expert judgement and previous work on the Kemano project (Table 45).

Table 45: Conditional Probability Table for the Ground class node.

Depth of Ravelling	*Depth of Spalling*	*I*	*IIa*	*IIb*	*III*	*IV*
None	*None*	100	0	0	0	0
None	*Low*	50	50	0	0	0
None	*Medium*	20	60	0	20	0
None	*Deep*	0	20	0	40	40
Low	*None*	50	0	50	0	0
Low	*Low*	60	20	20	0	0
Low	*Medium*	0	50	20	30	0
Low	*Deep*	0	10	0	30	60
Medium	*None*	20	0	50	30	0
Medium	*Low*	0	20	40	40	0
Medium	*Medium*	0	20	20	60	0
Medium	*Deep*	0	10	10	30	50
Deep	*None*	0	0	40	40	20
Deep	*Low*	0	10	20	30	40
Deep	*Medium*	0	0	0	40	60
Deep	*Deep*	0	0	0	20	80

In general, the rock mass quality observed in the downstream T2 tunnel was good to very good, with only localized areas of failure (Hatch Ltd., October 2015). For this reason is was anticipated that approximately 50% of the tunnel would be unlined.

4.3 Sensitivity Analysis

Netica has the ability to run a sensitivity of any node to the findings of any other node in the network. This allows the user to determine which nodes are completely independent of each other, and how much a finding at one node will likely change the beliefs at another.

Netica calculates three sensitivity measures.

- *Mutual information* is the expected reduction of entropy at the node of interest due to a finding entered at another node (or itself). The value is 0 if the nodes are independent of each other.
- *Percent* compares the reduction of entropy from the finding at a given node versus a finding entered directly at the node of interest. The value is 0 if the nodes are independent of each other.
- *Variance of beliefs*, the expected change squared of the beliefs at the node of interest over all its states, due to a finding at another node. The value is 0 if the nodes are independent of each other.

The sensitivity measures calculated pertaining to the Ground Class node are presented in Table 46.

Table 46: Sensitivity analysis results for the Ground Class node.

Rank	***Node***	***Mutual Information***	***Percent***	***Variance of Beliefs***
1	σ_1	0.09945	4.92	0.0057116
2	σ_3	0.06308	3.12	0.0057966
3	Joint Shear Strength	0.0409	2.02	0.0036961
4	Joint Infilling	0.01764	0.873	0.0016709
5	GSI	0.01076	0.532	0.0011286
6	Joint Weathering	0.00514	0.255	0.0005506
7	Joint Roughness	0.00325	0.161	0.0003536
8	UCS	0.00299	0.148	0.000254
9	Joint orientation	0.0013	0.0642	0.0000855
10	Rock type	0.00108	0.0532	0.0000765
11	Groundwater	0.00077	0.0379	0.0000508
12	Structure	0.00075	0.0372	0.000086

Aside from the immediate parents to Ground Class (omitted from this analysis), the major principal stresses are the most sensitive parameters as they contribute to determining the severity of the failure mechanisms. The minimum tangential stress (σ_{min}), which is calculated

from Kirsch equations using the principal stresses, is important for the ground class prediction because it is a highly sensitive parameter to the depth of ravelling. This is because the value of σ_{min} determines the modification factor, Ravelling Potential, which is applied in the Ravelling expression.

The other parameters significant to the ground class prediction can be divided into three main categories: joint shear strength, rock strength, and structure.

The Joint Shear Strength, as well as Joint Infilling and GSI are the next most sensitive parameters after the in situ stresses. These parameters are all associated with the condition of the rock mass and how broken up it is. Their relatively high rank in sensitivity reaffirms the notion that careful rock mass characterization is vital to the design of underground rock support (Hoek & Brown, 1997). Joint Infilling, Weathering and Roughness are combined to form Joint Shear Strength, which in turn is a major contributing factor in the Ravelling expression. For this reason, the site investigations at Kemano for the detailed design phase should focus on geological mapping of the conditions of the discontinuities. The high sensitivity of the Joint Shear Strength to the Ground Class prediction indicates the importance of delineating these parameters with a higher degree of confidence, resulting in a more constrained prediction.

The Unconfined Compressive Strength (UCS) appears in the middle of the rankings in terms of sensitivity. The UCS is an important input into the spall depth prediction. Although spalling is not prevalent at Kemano, in terms of the BBN and a generic tunnel it is important to have some valid UCS measurements along the tunnel alignment in order to constrain the spall depth predictions.

Of the ultimate parent nodes, Structure is the least sensitive parameter. However, Structure and Joint Shear Strength make up GSI, which is of high sensitivity to the ground class predictions.

Chapter 5. Scenario Analysis

For validation purposes, select locations along the T2 tunnel alignment were assessed using the Bayesian Belief Network. Three locations along the excavated portion were chosen where failure has occurred and been documented because photographs exist to verify the network's output. One location that has not been excavated was chosen as an exercise in comparison to a similar chainage in the T1 tunnel.

5.1 Scenario 1 – Chainage 15+900

The first scenario is located at chainage 15+900, about 300 m from the 2600' level portal, next to the penstocks inside Mount DuBose. At this location, the rock is heavily veined and the discontinuity surfaces are stained with oxidation. Initial support consisted only of spot bolting. A small fall of ground occurred 10 years after construction, so during site investigations in the summer of 2015 an A-frame was set up in order to allow the tunnel inspection crew safe passage. Steel sets were installed after the fall of ground to add additional support, however the timber lagging is now falling out which allowed more material to displace. If the unstable nature of the rock mass had been identified at the time of construction, and appropriate primary support was installed, it is possible that the rock mass would not have raveled further to the state it is in now. Photographs of the tunnel at this chainage are shown in Figure 43.

Figure 43: Rock mass at chainage 15+900, showing the A-frame and condition of discontinuities (Hatch, 2015).

Based on the photographs taken on site, as well as the results of the stress modelling and data extracted from the project reports, appropriate input parameters were selected for use in the BBN (Table 47).

Table 47: Inputs into BBN for Scenario 1.

Rock type	***σ_1 (MPa)***	***σ_3 (MPa)***	***θ (°)***	***Structure***	***J_{infill}***	***$J_{weather}$***	***J_w***	***J_{orient}***
Mortella Pluton	7	4	37	Very blocky	Soft, >5 mm	Moderately weathered	Dry	Unfav-ourable

When this data is input into the BBN, the Ground Class prediction is as shown in Table 48.

Table 48: Ground Class prediction for Scenario 1.

Ground Class	*Probability*
Class I	16%
Class IIa	1%
Class IIb	45%
Class III	32%
Class IV	6%

The result from the network reflects the need for spot treatment at this location, but the likelihood for needing shotcrete from 10 o'clock to 2 o'clock is a close second. The network also predicts the location of ravelling failure correctly, in the right shoulder looking upstream. If the support specifications for Class IIb (Section 6.2) had been installed initially, the progressive failure might have been prevented.

5.2 Scenario 2 – Chainage 13+665

Scenario 2 is located at chainage 13+665, approximately 2.5 km from the 2600' level portal. The rock quality here is so good it was been described as being as smooth as the inside of the barrel of a shotgun by the inspection crew. There are almost no visible discontinuities, and the few that are visible are tightly healed with no infilling. No ground support has been installed, with the exception of the occasional spot bolt. It is believed that these spot bolts were installed as a precautionary measure, and upon closer inspection it becomes clear that they were not necessary. The rock quality is so high here that there are visible grooves from the cutter heads and marks from the TBM gripper pads on the walls (Figure 44).

Figure 44: Rock mass at chainage 13+665, showing the grooves and marks left by the TBM.

As with Scenario 1, the input parameters for the BBN were obtained from the Excel database populated from reports, the stress modelling, as well as photographs. These inputs are shown in Table 49.

Table 49: Inputs into BBN for Scenario 2.

Rock type	***σ_1 (MPa)***	***σ_3 (MPa)***	***θ (°)***	***Structure***	***J_{infill}***	***$J_{weather}$***	***J_w***	***J_{orient}***
Mortella Pluton	14	6	16	Intact or Massive	None	Unweathered	Dry	Fair

When this data is input into the BBN, the Ground Class prediction is as shown in Table 50.

Table 50: Ground Class prediction for Scenario 2.

Ground Class	***Probability***
Class I	98.5%
Class IIa	0%
Class IIb	0.5%
Class III	0.5%
Class IV	0.5%

As was expected, the BBN is predicting that the tunnel can remain unlined at this chainage, as no failure of any type is expected. The photographs taken during the site investigations in 2015 show that even though the tunnel has been dewatered since its construction 25 years ago, it is in excellent condition.

5.3 Scenario 3 – Chainage 8+510

Scenario 3 is located at chainage 8+510 just before the junction with the Horetzky adit, almost at the end of the completed downstream bore. A large fall of ground occurred here during construction of the tunnel due to a combination of veining with weak infill and high groundwater inflow, resulting in the installation of approximately 20 steel ribs. The rock mass here is poor to very poor, and there is caving occurring in some locations behind the ribs (Figure 45). A large volume of failed material has been failing progressively behind the ribs, pushing out the timber lagging and resulting in increasingly larger caving. The high groundwater inflow has washed out the failed material, as evidenced by the debris found in the invert of the tunnel as much as 50 m away from the end of the ribs.

Figure 45: Rock mass at chainage 8+510, showing caving behind the steel sets and the failed debris in the invert.

The inputs for the BBN at this chainage are shown in Table 51.

Table 51: Inputs into BBN for Scenario 3.

Rock type	***σ_1 (MPa)***	***σ_3 (MPa)***	***θ (°)***	***Structure***	***J_{infill}***	***$J_{weather}$***	***J_w***	***J_{orient}***
Gamsby Group	6	2	58	Very blocky	Soft, >5mm	Decomposed	Flowing	Fair

When this data is input into the BBN, the Ground Class prediction is as shown in Table 52.

Table 52: Ground Class prediction for Scenario 3.

Ground Class	***Probability***
Class I	22%
Class IIa	1%
Class IIb	46%
Class III	27%
Class IV	4%

The network predicts the need for spot treatment for ravelling failure, and also has the ability to show that a large depth of ravelling is the issue at this chainage (0.7 m) as opposed to spalling (93% in the None state). The second highest ground class calls for springline to springline shotcrete and mesh, which indicates that the potential failure is on the more critical side and perhaps extra ground support is necessary. The slightly under conservative prediction at this chainage indicates and opportunity to further fine-tune the network as part of future work. Field observations confirm that progressive failure has resulted in ravelling material from springline to springline over time. The network also shows that ravelling will occur at the right shoulder, which is confirmed by the photos.

5.4 Scenario 4 – Chainage 4+700

The final scenario is located in the unexcavated portion of the T2 tunnel at 4+700, which is approximately the same chainage as a known collapse in the T1 tunnel (Figure 46). This collapse was cause by a large fault zone, and the cavern resulting from this failure is approximately 10-20 ft (3-6 m) long, 40-50 ft (12-15 m) high, and 70-75 ft (21-23 m) wide (Figure 47, Figure 48). The debris from the failed volume traveled as far as 100 m along the tunnel before coming to rest. This section of tunnel is located in the Horetzky Dyke, and where the rock mass has been described as being highly sheared and slightly altered in some locations. The 3D stress modelling completed (see Section 3.2) indicates that the stress regime at the onset of the upstream T2 bore will be the most challenging of the entire excavation.

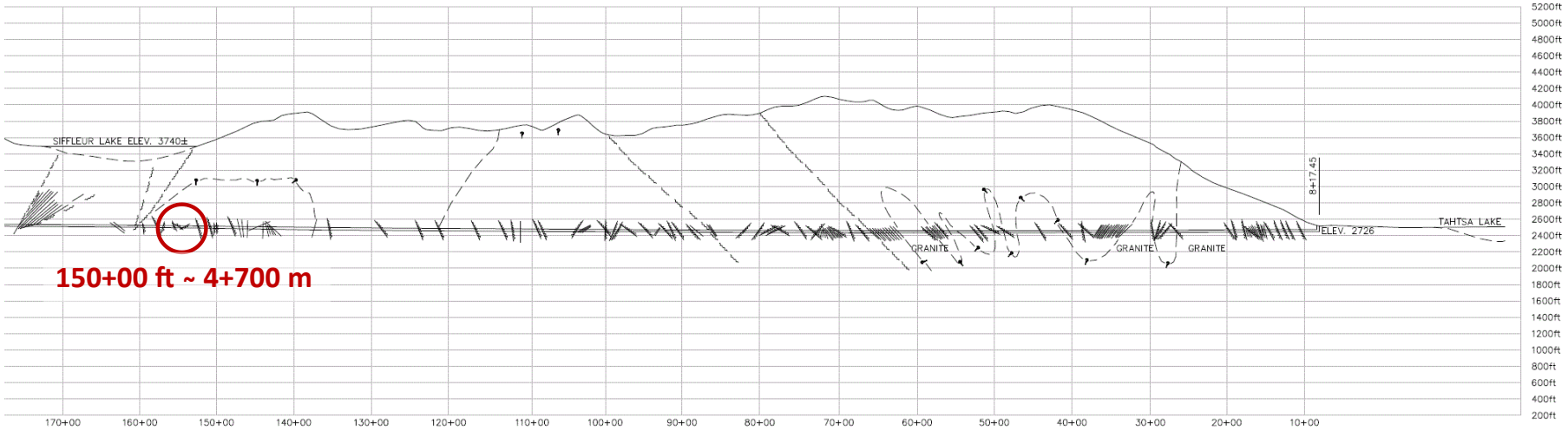

Figure 46: Location of known collapse in T1 at chainage 150+00 ft, which is approximately 4+700 m in T2 (HMM, 2010).

Figure 47: Failure located near chainage 4+700 in the T1 tunnel caused by unstable fault material (HMM, 2010).

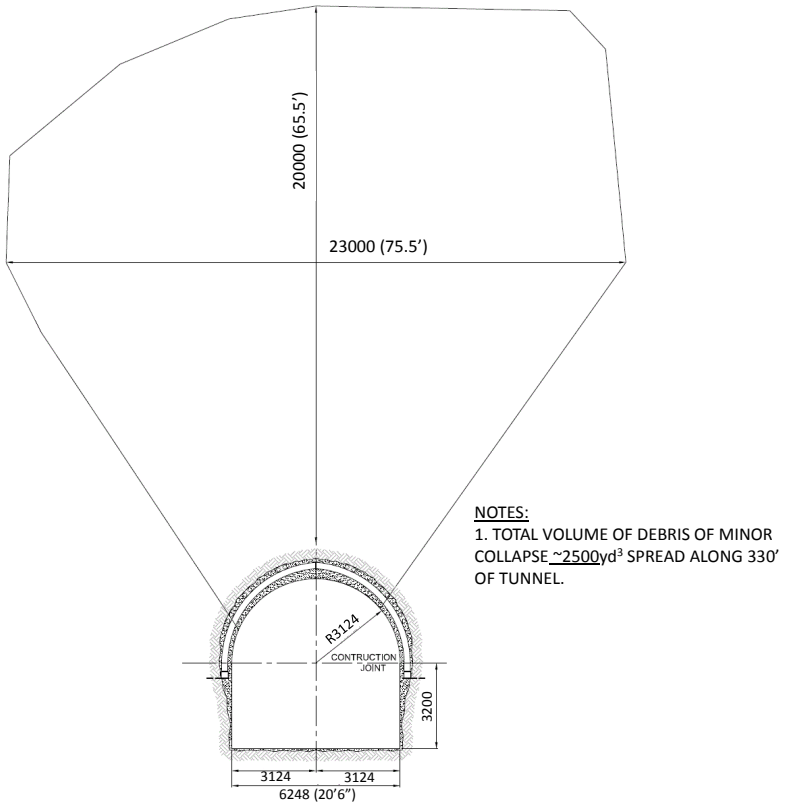

Figure 48: Cross section of caving at location of T1 tunnel failure (HMM, 2010).

The inputs for the BBN at this chainage are shown in Table 53.

Table 53: Inputs into BBN for Scenario 4.

Rock type	***σ_1 (MPa)***	***σ_3 (MPa)***	***θ (°)***	***Structure***	***J_{infill}***	***$J_{weather}$***	***J_w***	***J_{orient}***
Horetzky Dyke	12	4	-78	Very blocky	Soft, >5 mm	Slightly weathered	Dry	Unknown

When this data is input into the BBN, the Ground Class prediction is as shown in Table 54.

Table 54: Ground Class prediction for Scenario 4.

Ground Class	***Probability***
Class I	1%
Class IIa	1%
Class IIb	13%
Class III	28%
Class IV	57%

The network predicts the need for full perimeter support with the possibility of installing steel sets, resulting from both a deep depth of spalling (> 0.5 m) in the crown as well as a deep depth of ravelling (5 m). This prediction coincides with the results of the 3D stress modelling, as well as with a major collapse at a similar chainage in the parallel T1 tunnel. In particular, the extreme depth of ravelling coincides with what has been called an “ice cream cone failure” at a similar chainage in T1, which is known to be progressively caving (ITASCA, 2015).

Chapter 6. Results

6.1 Ground Class

The ground class predictions along the T2 tunnel were made in 25 m increments using the Bayesian Belief Network described in Section 4.2.1 and using the Kemano specific database, included in Appendix D: Kemano Specific Database. Topography has a notable effect of the boundary stresses along the T2 alignment (see Section 2.4). This was verified by the 3D models, and has implications for the ground class and required support along the tunnel. In addition to the imposed state of stress, rock mass quality was an important factor that made the difference between stable or unstable rock mass. The poor rock mass quality in some areas can be attributed to weak discontinuity infilling, as well as fault zones and associated shears.

The results of the ground class prediction were plotted on a composite of drawings originally created by Hatch (Figure 49). This drawing includes an abundance of additional data that may be used to validate the predictions made. The original drawing for the downstream T2 (Hatch Ltd., 2015) includes information on the lithology, the shear and fault locations, the water inflow intensity, the areas of historic overstress and collapses, the original temporary support installed, as well as the recommendations made as a result of the 2015 site investigations of the excavated half of the tunnel. There is no similar drawing of the upstream part of T2, as it has not been excavated yet, but there is a full profile drawing of the full T1 tunnel profile (HMM, 2010). It includes locations of faults and shears on a larger scale, the original installed support and the repairs that were made in 1961 after some major collapses. As the T1 and T2 tunnels are only 300 m apart, the assumption was made that the locations of significant geological features could be laterally extrapolated from one tunnel to the other.

All of this data was plotted with the most probable and second most probable ground classes predicted by the Kemano BBN. The second most probable ground class was only plotted if it was within 20% of the most probable prediction, to illustrate how close the difference between the predictions was. An example of this can be seen at chainage 15+600, where the most probable ground class is Class IIb at 47% and the second most probable is Class III at 30%. Conversely, if the most probable prediction was the highest by a large margin, nothing

is plotted for the second most probable ground class, for example at chainage 13+600. In some cases the two most likely ground classes were very close, a matter of a few percent, for example at 3+800, which may indicate how critical the severity of failure is within that class. In other words where two classes are only separated by a few percent the ground class may fall into either of the two classes, and the BBN prediction should not be taken as the definitive appropriate design at a location. This may help the user determine whether that particular location needs special attention when the advancing face approaches.

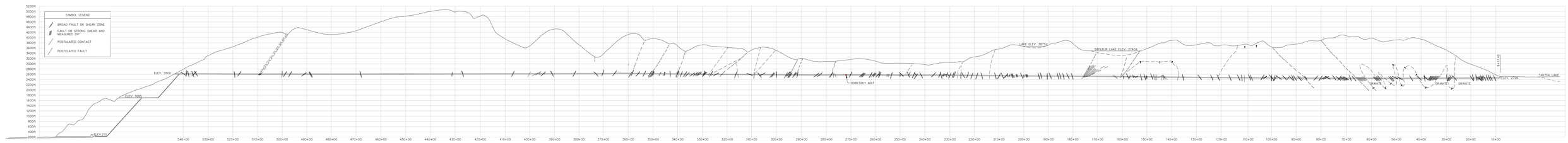

ROCK TYPE LEGEND
GRANITE, GRANODIORITE AND QUARTZ DIORITE
MEDIUM GRAINED DIORITE
GREENSTONE COMPLEX, INCLUDING INTERMIXED DIORITE AND PORPHYRITIC DIORITE DYKE TYPES AND SOME LAYERED SECTIONS
METAMORPHOSED SEDIMENTS – LAYERED ROCKS, QUARTZITE, SCHIST, TUFF AND SOME LIMESTONE AND FINE GRAINED, DARK VOLCANICS

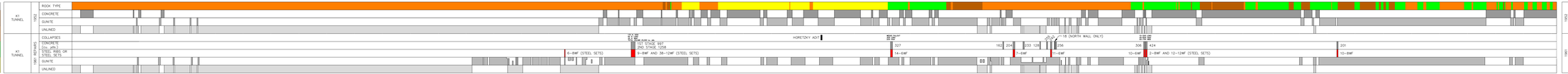

SUMMARY PERCENTAGES	
CONCRETE	~50%
GUNITE	~40%
UNLINED	~50%

SUMMARY PERCENTAGES	
CONCRETE	5,051 cu. yds.
STEEL RIBS	119 RIBS
GUNITE	-- ft.
UNLINED	-- ft.

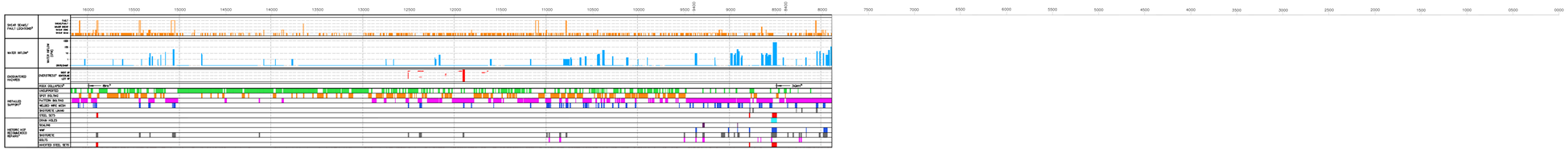

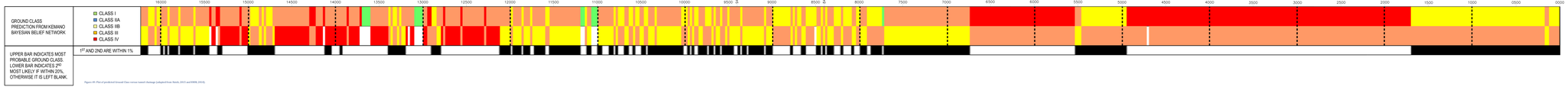

GROUND CLASS PREDICTION	SUMMARY PERCENTAGES
CLASS I	2%
CLASS IIA	0%
CLASS IIB	27%
CLASS III	41%
CLASS IV	30%

Figure 49: Plot of predicted Ground Class versus tunnel chainage (adapted from Hatch, 2015 and NWM, 2015).

6.2 Support Classes

Using visual observations during the 2015 site investigations, an assessment was made that some spot treatment in areas of minor spalling and ravelling may be required. This would consist of rock bolts as well as a combination of shotcrete and welded-wire mesh, or just fibre-reinforced shotcrete. In a few extreme circumstances, the addition of steel sets may be required. The support classes have a direct relationship to the predicted ground classes, as shown in Table 55. These ground classes are based on preliminary ground support design (Hatch Ltd., May 2015), as well as field observations during the 2015 site investigations and expert judgement regarding what can be considered reasonable support for the given ground conditions.

Table 55: Proposed support classes for Kemano T2 tunnel.

Support Class	***Dowels/Bolts***	***Shotcrete****	***Welded Wire Mesh or FRS****	***Other***
Class I	Unsupported			
Class IIa & IIb	2.5m long, 25mm dia. grouted dowels, 1.5 m c/c 10 to 2 o'clock	75 mm min.	None	None
Class III	2.5m long, 25mm dia. grouted dowels, 1.2 m c/c springline to springline	75 mm min.	#6 gauge wire or FRS	None
Class IV	2.5m long, 25mm dia. grouted dowels, 1 m c/c 7 to 5 o'clock	100 mm min.	#4 gauge wire or FRS	Steel sets***

**If spalling is the dominating failure mechanism, immediate installation of shotcrete is crucial in order to create a stabilizing confining stress before spalling can propagate.*
***Fibre Reinforced Shotcrete.*
****The need for steel sets should be assessed on a case by case basis by a geotechnical engineer.*

In these support classes, it appears as if similar severities of spalling and ravelling failure are treated identically. This is not the case. Although the final installed support may make it difficult to distinguish between the two mechanisms, the theory behind how the rock mass is supported for each is different. In the case of spalling, immediate confinement after excavation is crucial. Spalling initiates and propagates almost immediately after the advancing face passes, so installing shotcrete and mesh as soon as possible is critical to prevent spalling from initiating and for the long term stability of the rock mass. Steel sets are

not effective in preventing spalling from occurring, as they take a long time to install and are installed with a gap between them and the rock mass. In the case of ravelling failure there is less time sensitivity, as the shotcrete and mesh serve to catch and hold the failed material in place so that progressive failure is inhibited. In locations of severe ravelling, steel sets may be installed to preserve the original shape of the tunnel.

Based on the most probable ground classes predicted by the BBN, the breakdown of support requirements for T2 is summarized in Table 56.

Table 56: Percentage of tunnel in each Ground Class.

Ground Class	***% of Tunnel***	
Class I	2 %	29% Unlined
Class IIa	0 %	
Class IIb	27 %	
Class III	41 %	71% Lined
Class IV	30 %	

Overall, the ground class predictions result in approximately 71% of the T2 tunnel needing some form of final liner (Classes III and IV), while the predominant support required is springline to springline lining with bolts and welded wire mesh (Class III). Spalling failure (Class IIa) turned out to be a minor concern, and was not the predominant failure mechanism at any of the chainages assessed. Only 2% of the tunnel requires no support at all. These results are meant to be a first estimate, and the specific support design should be further assessed by a geotechnical engineer on a case by case basis.

Empirical rock support recommendations were developed based on ubiquitous rock mass classification schemes in the late 1980s and early 1990s. In particular, the publishers of both the tunnelling quality index, Q (Grimstad & Barton, 1993) and the Rock Mass Rating, RMR (Bieniawksi, 1993) created support estimates for the spectrum of rock qualities covered by their rock mass classification systems and correlations can be found between the two. It is therefore expected that the empirical support estimates that these methodologies predict would also be comparable with the results from the BBN. The scenarios discussed in Chapter 5 were plotted on the empirical support plots to compare the BBN predictions to the Q and RMR support recommendations.

Since most of the parameters needed to calculate Q were readily available in the Excel database, Q was calculated (Equation 24) for each of the scenarios (

Table 57) and correlated to the corresponding RMR value so it could be plotted on Bieniawski's support recommendations plot.

$$Q = \left(\frac{RQD}{J_n}\right)\left(\frac{J_r}{J_a}\right)\left(\frac{J_w}{SRF}\right) \quad \text{Equation 24}$$

Table 57: Tunnel Quality Index for each Scenario.

Scenario	*RQD*	J_n	J_r	J_a	J_w	*SRF*	*Tunnel Quality Index, Q*	
1	60	4	1	15	1	1	1	Poor to Very Poor
2	100	0.5	4	0.75	1	1	>1000	Exceptionally Good
3	40	5	1	20	0.33	1	0.132	Very Poor to Extremely Poor
4	20	9	0.5	20	0.33	1	0.0183	Extremely Poor

For comparison to Bieniawski's support recommendations (Bieniawski, 1993), the maximum tangential stresses (σ_{max}) and uniaxial compressive strengths (UCS) used to calculate the y-axis of Bieniawski's empirical support plot are shown in Table 58.

Table 58: Values used to calculate y-axis on Bieniawski's empirical support figure.

Scenario	σ_{max}	*UCS*	σ_{max}/UCS
1	16.32	174.79	0.09
2	36.50	174.79	0.21
3	14.97	150.00	0.10
4	31.85	149.90	0.21

Figure 50 shows the scenarios from Chapter 5 plotted against Bieniawski's empirical support recommendations (Bieniawksi, 1993). The empirical support estimates mirror the ground class predictions from the Kemano BBN, where the most unstable scenario (Scenario 4) is recognized as needing the most rock support. Conversely, Scenario 2 is recognized as needing generally no support, as verified by field observations.

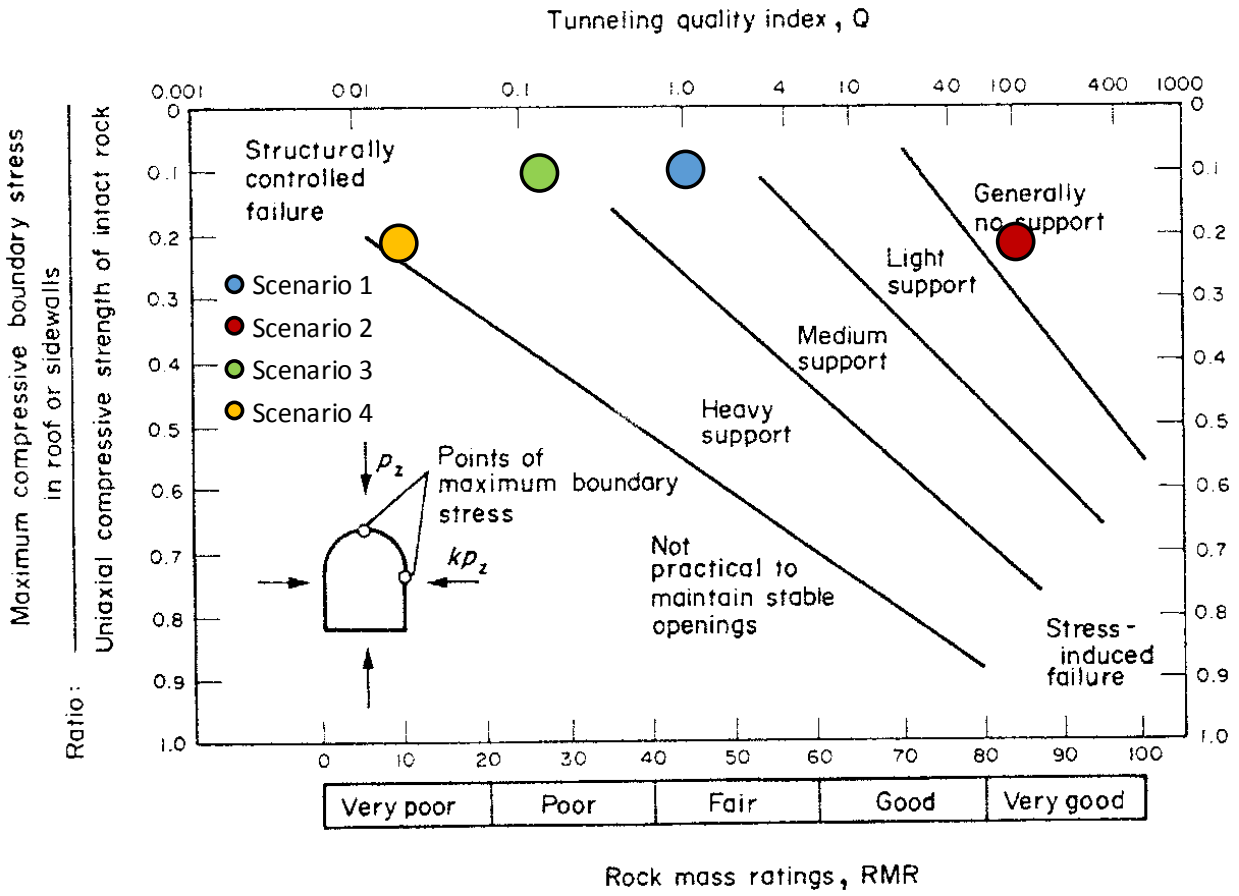

Figure 50: Scenarios analyzed compared to empirical support estimate based on Q and RMR (adapted from Bieniawksi, 1993).

Grimstad & Barton (1993) developed support recommendations based on the Q system. This methodology includes an Excavation Support Ratio (ESR), which expresses safety requirements for the purpose of the excavation. The tunnel diameter of T2 is 5.73 m, and an ESR of 1.0 was applied because T2 is a power tunnel. Figure 51 shows the scenarios from Chapter 5 plotted against the empirical support recommendations from Grimstad & Barton. These empirical rock support recommendations capture the possible necessity of increased shotcrete thickness and or closer bolt spacing as the ground conditions worsen, however they do not include the potential need for steel sets, which is included in the Kemano support classes (Section 6.2).

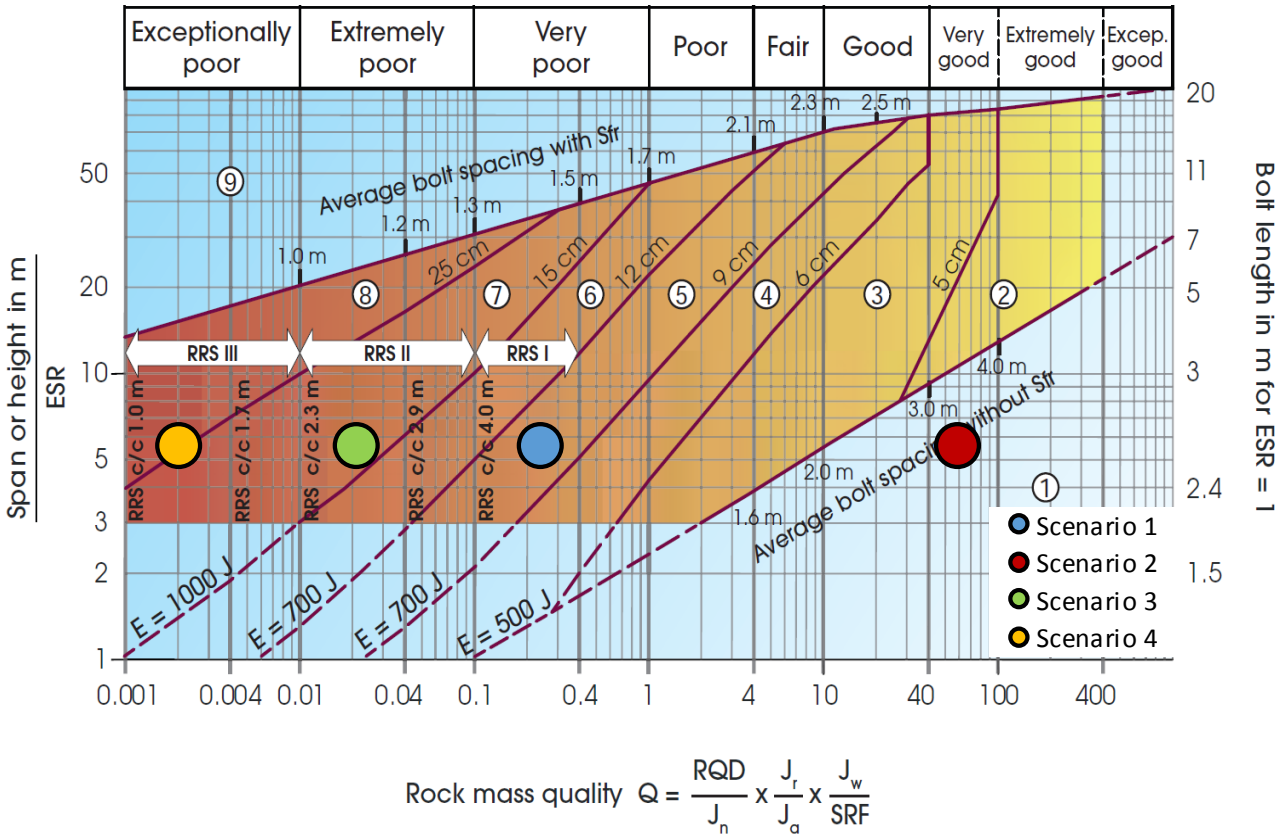

Support categories

① Unsupported or spot bolting
② Spot bolting, **SB**
③ Systematic bolting, fibre reinforced sprayed concrete, 5-6 cm, **B+Sfr**
④ Fibre reinforced sprayed concrete and bolting, 6-9 cm, **Sfr (E500)+B**
⑤ Fibre reinforced sprayed concrete and bolting, 9-12 cm, **Sfr (E700)+B**
⑥ Fibre reinforced sprayed concrete and bolting, 12-15 cm + reinforced ribs of sprayed concrete and bolting, **Sfr (E700)+RRS I +B**
⑦ Fibre reinforced sprayed concrete >15 cm + reinforced ribs of sprayed concrete and bolting, **Sfr (E1000)+RRS II+B**
⑧ Cast concrete lining, **CCA** or **Sfr (E1000)+RRS III+B**
⑨ Special evaluation

Bolts spacing is mainly based on Ø20 mm

E = Energy absorbtion in fibre reinforced sprayed concrete

ESR = Excavation Support Ratio

Areas with dashed lines have no empirical data

RRS - spacing related to Q-value

I — **Si30/6 Ø16 - Ø20 (span 10m)**
D40/6+2 Ø16-20 (span 20m)

II — Si35/6 Ø16-20 (span 5m)
D45/6+2 Ø16-20 (span 10m)
D55/6+4 Ø20 (span 20m)

III — D40/6+4 Ø16-20 (span 5 m)
D55/6+4 Ø20 (span 10 m)
D70/6+6 Ø20 (span 20 m)

Si30/6 = Single layer of 6 rebars, 30 cm thickness of sprayed concrete

D = Double layer of rebars

Ø16 = Rebar diameter is 16 mm

c/c = RSS spacing, centre - centre

Figure 51: Scenarios analyzed compared to empirical support estimate based on Q (adapted from Grimstad & Barton, 1993)

6.3 Spalling

Despite the relative unimportance of spalling as a failure mechanism at the Kemano tunnels, the empirical relationship developed by Martin et al. (2001) was used to check the depth of stress-induced spalling predicted by the Kemano BBN. This was done by plotting data from the four scenarios (Table 59) from Kemano to the empirical depth of spalling figure from Martin et al. (2001) as seen in Figure 52.

Table 59: Martin's depth of failure parameters for four scenarios.

Scenario	*Chainage*	$\sigma_{\theta\theta}$ *(MPa)*	σ_{sm}* *(MPa)*	*a (m)*	D_f** *(m)*
1	15+900	16	87.4	2.865	2.97
2	13+665	37	87.4	2.865	2.87
3	8+510	15	75.0	2.865	2.97
4	4+700	32	75.0	2.865	3.22

** σ_{sm} is 0.4-0.6 of the UCS, as discussed in Section 2.4.3. A value of 0.5 times the UCS was used here.*
*** Depths of failure obtained from Kemano BBN predictions.*

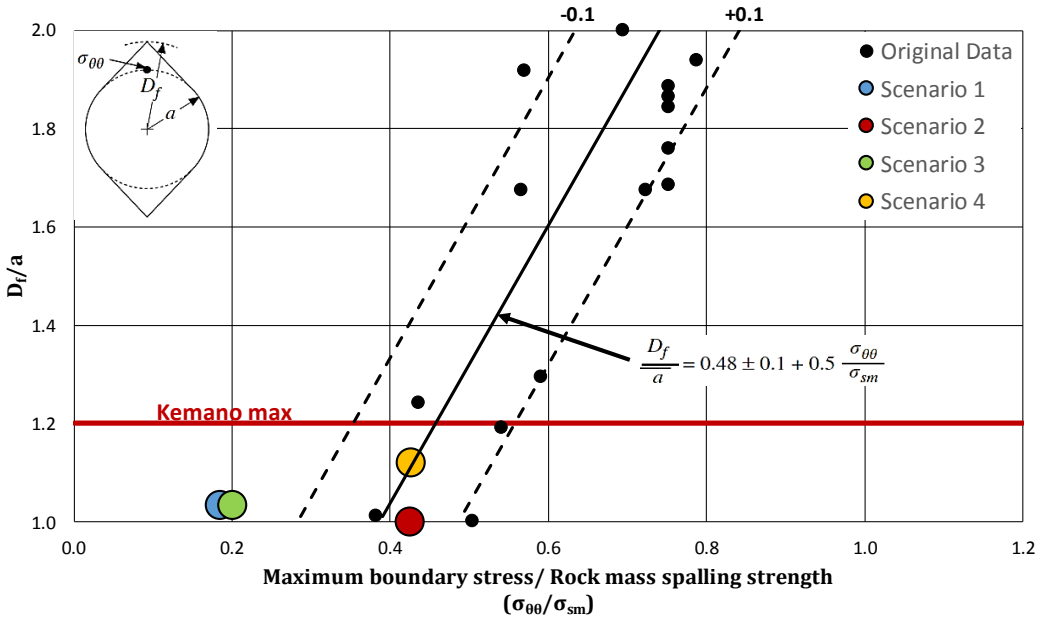

Figure 52: Data from scenarios plotted to predict depth of failure (adapted from Martin et al., 2001).

The data followed the general trend of the relationship presented by Martin et al. (2001). The slight deviations of scenarios may be attributed to either the uncertainty in the tangential stresses resulting from the coarseness of the 3D modelling, or to the impreciseness of the UCS resulting from the scarcity of data. These departures from the empirical relationship may elicit further callibration of the BBN as part of future works.

6.4 Discussion of Results

The ground class predictions made by the Kemano BBN agree closely with the empirical support recommendations developed for the Q and RMR systems (Grimstad & Barton, 1993; Bieniawksi, 1993). Keeping in mind that these recommendations were developing for ravelling and squeezing ground, these support classes should be treated as a first estimate and the detailed design of the ground support should be completed based on the dominant failure mechanism at the given chainage by a qualified geotechnical engineer on a case-by-case basis. The predicted depths of failure from the BBN informs which failure mechanism is the dominant one, and how time sensitive the support installation is. If spalling is the dominant predicted mechanism, early application of shotcrete is crucial in order to provide immediate confinement and to prevent spalling from initiating. If ravelling is the dominant failure mechanism, there is less time pressure to install support immediately. In that case the support does not prevent the failure from initiating, but rather keeps the failed material in place to prevent progressive ravelling from occurring. The BBN combines the two failure mechanisms in order to predict the ground class, however it may be useful for design purposes to keep them separate with their own distinct support classes. This represents an opportunity to develop how the network presents its outputs as part of future works.

The spall depth predictions also follow the empirical relationship developed by Martin et al. (2001). This validates that the Bayesian Belief Network and its built-in conditional relationships make a good first estimate of the required ground support, as well as predicting the depth of spalling failure within an appropriate margin of error.

The empirical support recommendations for the plotted scenarios matched the support design discussed in Section 6.2, with the exception of Grimstad and Barton's (1993) plot not including steel sets for Scenario 4. At this chainage the BBN predicted a ground class of Class IV, which would require steel sets, however the need for increased support is accounted for in Grimstad and Barton's (1993) recommendations by thicker shotcrete. Rock bolt spacings for all the Support Classes agree with the recommendations made by Grimstad and Barton (1993). Bieniawski's (1993) recommendations are more comparative than quantitative, but these also agree with the relative severity of failure expected for the four scenarios analyzed.

The spall depth predicted by the BBN falls within the appropriate range as described by Martin et al. (2001), with some minor deviations that may be attributed to data gaps within the 3D stress models or UCS measurements. Despite the deviations, the data points from the scenarios loosely follow the empirical trend, however these discrepancies may be treated as an opportunity to fine tune the BBN.

It is reassuring that the BBN provides similar predictions as the empirical support recommendations, however it also provides some additional information about the failure mechanisms that they do not. It specifically gives the expected depths of spalling and ravelling at a given location, and can easily handle a distribution of input values instead of just deterministic ones. The Bayesian approach is effective at handle uncertainty and allows the user to avoid simply using an estimated deterministic value, something that geotechnical engineers should be eliminating from standard practice (Harrison, 2016).

Chapter 7. Conclusions

The outcomes of this research and the conclusions from this thesis will prove valuable to the industry sponsor as the prefeasibility stage of the Kemano T2 upstream drive concludes, and as the detailed design and the construction stages begin.

Both 2D and 3D elastic finite element stress modelling for the entire mountain range overlying the Kemano tunnels were completed as part of this thesis, which had not been done before for this project. The 2D models were found to result in much higher stresses than the 3D model, due to its inability to capture the changing topography and therefore changes in the out-of-plane stress. This led to the conclusion that 3D elastic stress modelling is more reliable and closer to reality than 2D modelling. It is therefore imperative to include 3D modelling in tunnelling projects where topography is believed to have a significant impact on the in situ stresses, i.e. where the tunnel is situated above the "tectonic stress plane" described by Tan et al. (2004). The 3D models help to determine the effects of topography on the in-situ stresses and therefore stresses on the tunnel boundary.

The 3D stress modelling results aligned with the observed spalling and ravelling failures in the downstream drive of the T2 tunnel, specifically the stress orientations and magnitudes are reasonable for the failures observed. This was a validation that the boundary conditions and model set up are also reasonable. Plotting the maximum principal stress orientations and as well as the in situ and Kirsch stress magnitudes as a function of tunnel chainage showed a few areas of concern for the upstream drive of T2. In particular, the most challenging stress conditions around the tunnel start at the onset of boring from the Horetzky adit toward the Tahtsa intake and extend for approximately 2 km, where large depths of spalling and ravelling are anticipated. This is approximately the same location in T1 where large collapses were experienced. For this reason extra care and forethought are necessary when planning the excavation of this portion of the tunnel.

A major outcome of this research is the Kemano specific Bayesian Belief Network (BBN). The network was built incorporating as many empirical relationships as possible that are widely accepted in the field of rock mechanics, as well as some expert judgement and a new expression for gravity-induced ravelling failure that encapsulated discussions in the

literature. The network is built to handle variable levels of data richness, from everything being completely unknown besides the tunnel geometry, to having great detail about the rock mass characteristics and stress conditions. It is possible to leave many of the nodes with a uniform distribution, however it is preferable to make a reasonable guess if possible.

The ground class prediction as an outcome of the network is most sensitive to the major principal stresses and Joint Shear Strength, as well as Joint Infilling and GSI. This reinforces the necessity for good delineation of in situ stress conditions and rigorous rock mass characterization.

Following extensive literature review of gravity-driven failure mechanisms, it became clear that no definitive empirical relationship has been developed for rock mass ravelling. This is likely because there are so many factors at play: tunnel span, rock mass internal friction, cohesion and strength, groundwater regime, in-situ stress, rock mass structure, weathering, infilling, and so on. Each rock mass behaves differently, and so this behaviour is difficult to characterize and predict. As part of the research contained in this thesis, an attempt was made to encapsulate the factors that contribute to this failure mechanism in an expression. A combination of discussions in literature based on case studies was combined with Terzaghi's work on Rock Loads to obtain an expression that could estimate the depth of ravelling in a given rock mass. This expression has three separate modifying terms: the ratio of tangential stress to rock mass strength, a factor composed of RMR terms that approximate shear strength, and the Rock Load defined by Terzaghi, which depends on the tunnel geometry and rock mass conditions.

The outputs of the Kemano BBN were compared to widely recognized empirical support recommendations based on the Q tunneling index and the Rock Mass Rating systems, as well as empirical spall depth predictions. The BBN predictions matched these empirical plots reliably, with the added benefit of predicting the expected depths of spalling and ravelling failure. The BBN also handles variability in input parameters more efficiently than the empirical charts.

The final output of the BBN is a plot of most probable ground class as a function of tunnel chainage. This was used as a point of comparison against the support design and

recommendations completed to date. The network proved to be reliable in predicting problem areas, and correlated closely with the observations made in the downstream half of T2. Less data are available for the upstream half, as it has not yet been excavated, but the ground class predictions provide a useful estimate of what can be expected when the next phase of the tunnel excavation begins. In particular, it has been noted that the first few kilometres of excavation from the Horetzky Adit toward the Tahtsa Intake will have some of the most challenging geotechnical conditions of the entire tunnel.

7.1 Contributions

There are three main deliverables that are useful to the industry sponsor from this thesis, none of which have been completed previously: the 3D stress model, the Bayesian Belief Network, and the predicted ground classes as a function of tunnel chainage.

To date, the only numerical modelling that has been completed for the Kemano project is the FLAC3D modelling of the major collapses in T1 (ITASCA, 2015). Modelling for the entire tunnel has not been completed until now. This model is useful for visualizing the effects of the overlying topography on the tunnel boundary stresses, as well as getting an approximate magnitude and orientation of the in-situ stresses along the tunnel.

The Bayesian Belief Network developed for Kemano is another major deliverable to the industry sponsor. The BBN can be adapted to a variety to tunnelling projects, as the rock mechanics principles that govern the network remain the same. The network can also be updated as excavation progresses so that new information is taken into account. Alternatively, if nothing is known about a particular rock mass parameter then the user has the option of applying a uniform distribution or an educated guess.

The final output of the network is a plot of ground class versus tunnel chainage for the Kemano project. The support recommendations should be taken as a first estimate, giving an approximate idea of where problems might occur, for example at 4+700 (see Section 6.1). This output is useful to the industry sponsor as it can be used as a comparison to the tunnel support design that was chosen using other methods, and may be a tool for refining the material and quantities estimates.

This thesis makes a contribution to the field of rock mechanics through the creation of an expression to calculate the depth of ravelling that may occur in a rock mass. Ravelling is defined as the gravity-induced failure mechanism that results from the coalescence of structure with weak infill, groundwater inflow, and low stress conditions. This expression developed may be considered to be conservative because it incorporates Terzaghi's pioneering work on rock loads which do not account for the rock's capacity. However, Deere's recommended adjustments do not apply to the Kemano tunnels as the diameter is too small. The expression takes into account that discontinuities and their shear strength properties are widely accepted as being more important contributing factors to the ravelling failure mechanism than low tangential stress conditions. The output of the ravelling expression was calibrated using scenarios from the Kemano tunnel where photographs and site observations were available to validate the calculated value.

7.2 Recommendations

It is recommended that future research on probabilistic tunnel modelling and ground class prediction include the operational and logistical considerations that were omitted from this research. This might include the costing of materials and quantities, site mobilization and demobilization, contract types (ex. design-build, fixed price, turnkey), excavation advance methods and associated rates, or human factors. These are considered to be crucial variables in tunnel design (Špačková & Straub, 2013).

Although the best efforts were made to include all the relevant information available for the Kemano project, there are still many data gaps that were unavoidable. While this is a relatively data rich project, a luxury many other tunnelling projects do not have, there is still inherent uncertainty associated with all the geotechnical parameters. Further rock mass characterization and more rigorous 3D stress analysis would yield better ground class predictions. Many of the RMR parameters are not well constrained, and should be recorded during the tunnel advance. During the next stage of data collection, particular emphasis should be put on discontinuity condition mapping, particularly of infill location and prevalence. Also, the discontinuity mapping that exists for T2 should be digitized more completely to ensure that minor structures are not overlooked. So far only major structures

were digitized. The 3D stress analysis could be improved with better understanding of the boundary conditions, in particular the locked in tectonic stresses that were ignored here. In addition, running the model plastically with lithological structure and boundaries may result in stress predictions that are closer to reality.

The equation used to define the depth of rock mass ravelling (see Section 4.2.3.10) is just a starting point. Little work has been done to define the expected depth of failure arising from this gravity-driven mechanism; this could be another whole thesis in and of itself. The relative proportions of the input parameters should be verified using case histories, and the application of Terzaghi's "Rock Load" to this case should be verified for pertinence to this failure mechanism. The expression as a whole should be applied to known and thoroughly understood projects to judge its competence in describing ravelling as a gravity- and structure-driven failure mechanism.

A Graphic User Interface for the BBN could be developed as part of future works. This would allow the user to manipulate the input parameters and specify the chainage of interest, and then run the BBN for only that chainage. The GUI should allow the user to update the input parameters if they are known more definitively. It would result in better ease of use because the user would not have to interface with Netica directly, but rather could update the database from Excel and run the BBN in the background to get the ground class prediction.

References

Alcan B.C. Operations. (n.d.). *A History of Kitimat-Kemano Project*. (IEEE) Retrieved March 13, 2015, from http://www.ieee.ca/millennium/kitimat/kitimat_history.html

Alcan Kemano agreement can be cancelled, packed meeting told. (1994, February 21). *The Fisherman*.

Alcan Smelters and Chemicals Ltd. (1990). *Kemano Completion Project - Power Tunnel Geologic Map.*

Amadei, B., & Pan, E. (1995). Role of topography and anisotropy when selecting unlined pressure-tunnel alignment. *Journal of Geotechnical Engineering, 121*(12), pp. 879-885.

Amadei, B., & Stephansson, O. (1997). *Rocks stress and its measurement.* Dordrecht: Springer Science+Business Media.

Andersson, C. (2005). Äspö pillar stability experiment. (T. Franzen, Ed.) *Bergmeckanikdag*, 69-78.

Autodesk, Inc. (2014). AutoCAD 2015 J.51.0.0.

Aven, T. (2008). *Risk analysis assessing uncertainties beyond expected values and probabilities.* Noboken, NJ: Chichester, England. Retrieved from http://site.ebrary.com/id/10297957

Bechtel Canada, Inc. (October 1991). Volume IV - Power Tunnel Construction Report. In *Kemano Completion Project.*

Bieniawski, Z. T. (1989). In J. Wiley, *Engineering Rock Mass Classifications* (p. 251).

Bieniawski, Z. T. (1993). Chapter 22 - Classification of rock masses for engineering: the RMR system and future trends. In *Comprehensive Rock Engineering* (Vol. Vol. 3, pp. 553-573).

Bobbio, A., Montani, S., & Portinale, L. (2003). Parametric dependability analysis through probabilistic horn abduction. *Uncertainty in Artificial Intelligence*, pp. 65-72.

Bobbio, A., Portinale, L., Minichino, M., & Ciancameria, E. (2001). Improving the analysis of dependable systems by mapping fault trees into Bayesian networks. *Reliability Engineering and System Safety, 3*, pp. 249-260.

Brady, B., & Brown, E. (1985). *Rock Mechanics for Underground Mining.* Dordrecht, the Netherlands: Kluwer Academic Publishers.

Brox, D. (2012). *Evaluation of Overstressing of Deep Hard Rock TBM Excavated Tunnels in BC.* Montreal: Tunneling Association of Canada.

Brox, D. (2013). *Evaluation of Overstressing of Deep Hard Rock Tunnels.* Geneva, Switzerland: World Tunnel Congress 2013.

Burrows, M., & Lane, D. (n.d.). *Kemano Completion Project Background.* T. Buck Suzuki Environmental Foundation.

Carter, T., Cottrell, B., Carvalho, J., & Steed, C. (2008). *Logistic Regression improvements to the Scaled Span Method for dimensioning Surface Crown Pillars over civil or mining openings.* Mississauga, ON: American Rock Mechanics Association.

Castillo, E., Solares, C., & Gomez, P. (1997). Tail uncertainty analysis in complex systems. *Artificial Intelligence*, pp. 395-419.

Christensen, B. (1995). *Too Good to Be True: Alcan's Kemano Completion Project.* Vancouver: Talonbooks.

Crippen Consultants. (March 1982). Report on Geotechnical Aspects of Design of Tunnel, Powerhouse and Associated Structures. In *Kemano Completion Project Report No. 22.*

Csuhanics, B., & Debreczeni, A. (2012). *The connection between rock wall raveling and in situ rock mass strength - a study on the influencing factors.* Miskolc, Hungary: University of Miskolc, Institute of Mining and Geotechnical Engineering.

Dassault Systemes Simulia Corp. (2012). *Abaqus 6.12 Glossary.* Providence, RI: Simulia.

Dassault Systemes Simulia Corp. (2013). Abaqus/CAE 6.13-1. Providence, RI: Simulia.

Deere, D. U., Peck, R. B., Monsees, J. E., & Schmidt, B. (1967). *Design of Tunnel Liners and Support Systems.* Springfield, Virginia: Customer Services Clearing-house, U.S. Department of Commerce.

Dershowitz, W. S., & Herda, H. H. (1992). Interpretation of fracture spacing and intensity. *The 33th U.S. Symposium on Rock Mechanics (USRMS)* (pp. 757-767). Santa Fe, New Mexico: American Rock Mechanics Association.

Diederichs, M. (2007). Mechanistic interpretaton of practical application of damage and spalling prediction criteria for deep tunnelling. *The 2003 Canadian Geotechnical Colloquium* (pp. 1082-1116). Can. Geotech. J.

Diederichs, M. S., Carter, T., & Martin, D. (2010). Practical rock spall prediction in tunnels. *Proceedings of International Tunneling Association World Tunnel Congress.* International Tunneling Association.

Dolmage, V. (1951). *Geology of the Kemano-Tahtsa Tunnel.*

Dolmage, V., & Campbell, D. D. (1961). *Report on Kemano Tunnel Inspection and Repair 1961 Geology.* Vancouver, BC.

Environment Canada. (2015, September 22). *Temperature and Precipitation Chart for 1981 to 2010 Canadian Climate Normals KEMANO*. Retrieved from Canadian Climate Normals 1981-2010 Station Data: http://climate.weather.gc.ca/climate_normals/results_1981_2010

Gent, D. (2014, February 8). *Kemano & Kitimat British Columbia, Canada ca 1953-1957*. Retrieved March 30, 2015, from http://gent-family.com/Kemano/kemanotunnel.html

Ghate, A. (1991). Building Canada's Coast Mountains: The Challenging Kemano Hydro Project. *Hydro Review, 10*(7), 24-32.

Goricki, A. (2013). Engineering aspects of geotechnical tunnel design. In M. Kwaśniewski, & D. Łydżba, *Rock Mechanics for Resources, Energy and Environment.* London: Taylor & Francis Group.

Grimstad, E., & Barton, N. (1993). Updating the Q-System for NMT. *Proc. Int. Symp. On Sprayed Concrete - Modern Use of Wet Mix Sprayed Concrete for Underground Support.* Oslo, Norwegian Concrete Assn.: Fagernes (ed. Kompen, Opsahl and Berg).

Groshong, R. H. (1999). Chapter 2: Location, Attitude and Thickness. In *3-D Structural Geology - A Practical Guide to Surface and Subsurface Map Interpretation* (pp. 67-68). Berlin, Germany: Springer-Verlag Berlin Heidelberg.

Haas, C., & Einstein, H. (2002). Updating the Decision Aids for Tunneling. *Journal of Construction Engineering and Management*, 40-48.

Hard Rock at Kitimat. (1952). *Mining Engineering*, 1044-1045.

Harrison, J. (2016, April 14). Limit state design and rock engineering. *Technical presentation for the Okanagan Section of the Canadian Geotechnical Society*. Kelowna, BC.

Hatch Ltd. (August 2015). *SWP-07 - Geotechnical Characterization of T2 Tunnel.*

Hatch Ltd. (June 2012). *Kemano Geotechnical Baseline Report.*

Hatch Ltd. (May 2015). *SWP-06 - De-Risking Alternatives Order of Magnitude Study Report.*

Hatch Ltd. (May 2015). *SWP-07 - Pre Feasibility Study Project Execution Plan.*

Hatch Ltd. (November 2008). *Kemano Tunnel Maintenance - Gate 1 Estimate.* Vancouver, BC.

Hatch Ltd. (October 2015). *Kemano 2015 Site investigations - 2015 Field Data Compilation Report.* Vancouver, BC.

Hatch Mott MacDonald. (June 2010). *Tunnel Cleaning Project Study Report - DRAFT.*

Hobbs, D. W. (1964). The tensile strength of rocks. *International Journal of Rock Mechanics and Mining Sciences, 1*, 385-396.

Hoek, E. (2002). Hoek-Brown failure criterion - 2002 edition. *NARMS-TAC Conference*, (pp. 267-273). Toronto.

Hoek, E., & Brown, E. T. (1997). Practical estimates of rock mass strength. *International Journal of Rock Mechanics and Mining Sciences, 34*(8), 1165-1186.

Hoek, E., Kaiser, P. K., & Bawden, W. F. (1995). *Support of Underground Excavations in Hard Rock.*

Housner, G. W., & Vreeland, T. J. (1965). *The Analysis of Stress and Deformation.* Division of Engineering and Applied Science, California Institute of Technology.

Hudson, J. A., & Harrison, J. P. (2000). *Engineering Rock Mechanics - An Introduction to the Principles.* Elsevier.

Hutchinson, J. D., & Diederichs, M. S. (1996). *Cable bolting in Underground Mines.* Bitech.

ITASCA Consulting Group Inc. (2015, September 30). Memorandum - Study of Tunnel Crown Collapse Potential in Blocky and/or Faulted Ground in Support of Kemano T1 Tunnel Risk Assessment. *Ref. 15-2976-66M*.

Kendrick, J. (2012, February 16). *Kitimat: Making It Happen*. (Royal B.C. Museum) Retrieved March 12, 2015, from http://www.livinglandscapes.bc.ca/northwest/kitimat/happen.html

King, E. H. (1996). Chapter 7: Rock Tunnels. In J. O. Bickel, T. R. Kuesel, & E. H. King, *Tunnel Engineering Handbook* (2nd Edition ed., pp. 122-152). Norwell, Massachussetts: Chapman & Hall.

Kirsch, G. (1898). Die theorie der elastizitat und die bedurfnisse der festigkeitslehre. *Zeitschrift des Vereines deutscher Ingenieure, 42*(28), pp. 797-807.

Kitimat Museum & Archives. (2010, December 20). *Alcan Project History*. Retrieved March 12, 2015, from http://www.kitimatmuseum.ca/node/37

Klohn Leonoff Consulting Engineers. (August 1991). KC Power Tunnel Geological and Geotechnical Report. In *Kemano Completion Project.*

Klohn Leonoff Consulting Engineers. (August 1991). Power Tunnel Design Report. In *Kemano Completion Project.*

Lee, B. H. (2001). Using Bayes belief networks in industrial FMEA modeling and analysis. *Reliability and Maintainability Symposium, 2001*, pp. 7-15. Retrieved from http://doi.org/10.1109/RAMS.2001.902434

Mahadevan, S., Zhang, R., & Smith, N. (2001). Bayesian networks for system reliability reassessment. *Structural Safety, 23*(3), pp. 231-251.

Marinos, P., & Hoek, E. (2000). GSI – A geologically friendly tool for rock mass strength estimation. *Proc. GeoEng2000 Conference*, (pp. 1422-1442). Melbourne.

Marinos, V., Marinos, P., & Hoek, E. (2005). The geological strength index: applications and limitations. *Bulletin of Engineering Geology and the Environment*, 55-65.

Martin, C. D., & Christiansson, R. (2009). Estimating the potential for spalling around a deep nuclear waste repository in crystalline rock. *International Journal of Rock Mechanics and Mining Sciences*, 219-228.

Martin, C. D., Christiansson, R., & Söderhäll, J. (2001). *Rock stability considerations for siting and constructing a KBS-3 repository: based on experiences from Äspö HRL, AECL's URL, tunnelling and mining.* Stockholm, Sweden: Svensk Kärnbränslehantering AB.

MathWorks©. (1984-2014). MATLAB R2014b (8.4.0.150421) 64-bit.

Morgenroth, J. (2014). *Calculation - Kemano T1 Tunnel Data Review.* Hatch Ltd.

Morgenroth, J., Tannant, D. D., & Kellaway, M. (2016, February). Tunnel stress modelling and rock support for two hydroelectric tunnels in British Columbia. *Tunnels and Tunneling North America*, pp. 34-39.

National Research Council Canada. (2003, February 1). *Burning up the town!* (NRCC) Retrieved March 12, 2015, from http://www.nrc-cnrc.gc.ca/eng/achievements/highlights/2003/kemano.html

Neumann, F., & Witt, C. (1998). *Bioinspired Comuptation in Combinatorial Optimization - Algorithms and Their Computational Complexity.* Berlin, Germany: Springer.

Norsys Software Corp. (2014). Netica "5.18" 64 Bit.

Oracle. (2014). Oracle Crystal Ball 11.1.2.4.000 (32-bit).

Pan, E., Amadei, B., & Savage, W. (1994). Gravitational Stresses in Long Symmetric Ridges and Valleys in Anisotropic Rock. *International Journal of Rock Mechanics and Mining Sciences and Geomechanics, 31*(4), 293-312.

Portinale, L., & Bobbio, A. (1999). Bayesian networks for dependability analysis: an application to digital control reliability. *Proceedings of the 15th conference on uncertainty in artificial intelligence* (pp. 551-558). San Francisco: Morgan Kaufmann Publishers.

Proctor, R. V., Terzaghi, K., & White, T. L. (1946). *Rock tunneling with steel supports.* Youngstown, Ohio: Commerical Shearing & Stamping Co.

Rankin, M., & Finlay, A. (1992). *Alcan's Kemano Project: Options and Recommendations.* Victoria, B.C.

RocScience Inc. (2015). RS2 9 Modeler version 9.008 64-bit. Toronto, Canada.

Sorenson, J. (2012, April 12). Kemano water tunnel to be completed 20 years later. *Journal of Commerce*. Retrieved from http://www.journalofcommerce.com/Projects/News/2012/4/Kemano-water-tunnel-to-be-completed-20-years-later-JOC049746W/

Sousa, R., & Einstein, H. (2012). Risk analysis during tunnel construction using Bayesian Networks: Porto Metro case study. *Tunnelling and Underground Space Technology*, 86-100.

Špačková, O., & Straub, D. (2013). Dynamic Bayesian Network for probabilistic modeling of tunnel excavation processes. *Computer-Aided Civil and Infrastructure Engineering*, 1-21.

Stevens, S. S. (1946). On the theroy of scales of measurement. *Science, 103*(2684), pp. 677-680.

Stevenson, G. W. (1999). Empirical Estimates of TBM in Hard Rock. *Rapid Excavation and Tunneling Conference Proceedings.*

Stuart, R. A. (1960). *Geology of the Kemano-Tahtsa Area.* British Columbia Department of Mines and Petroleum Resources.

Stueck, W. (2012, September 6). Rio Tinto Alcan revisits Nechako Valley tunnel. *The Globe and Mail*. Retrieved from http://www.theglobeandmail.com/news/british-columbia/rio-tinto-alcan-revisits-nechako-valley-tunnel/article556769/

Tan, C. X., Wang, R. J., & Sun, Y. (2004). Numerical modelling estimation of the 'tectonic stress plane' (TSP) beneath topography with quasi-U-shaped valleys. *International Journal of Rock Mechanics and Mining Sciences*, 303-310.

Thapa, B. B., Marcher, T., McRae, M. T., John, M., Skovajsova, Z., & Momenzadeh, M. (2009). NATM strategies in the U.S. - Lessons learned from the initial support design for the Caldecott 4th bore. *Rapid Excavation and Tunneling Conference Proceedings* (pp. 96-107). SME.

Weber, P., Medina-Oliva, G., Simon, C., & Iung, B. (2012). Overview on Bayesian networks applications for dependability, risk analysis and mainenance areas. *Engineering Applications of Artificial Intelligence, 4*, pp. 671-682. Retrieved from http://doi.org/10.1016/j.engappai.2010.06.002

Wood, D. (2012, October 15). Alcan Smelters and Chemicals Ltd Feeds While Nechako River Chokes. *Watershed Sentinel*. Retrieved from http://www.watershedsentinel.ca/content/alcan-smelters-and-chemicals-ltd-feeds-while-nechako-river-chokes

Young, D. (October 2008). *KC Power Tunnel Design Considerations for Hydraulic Analysis.*

Zhang, C., Feng, X., & Zhou, H. (2012). Estimation of in situ stress along deep tunnels buried in complex geological conditions. *International Journal of Rock Mechanics and Mining Sciences*, 139-162.

Appendices

Appendix A: Context of the Kemano Project

Construction History

Between 1951 and 1954, six thousand construction workers built Kenney Dam, Skins Lake spillway, Kemano tunnel (including the intake, two penstocks and tailrace channel), the subterranean powerhouse, and the transmission line to Kitimat. Sixteen people died during tunnel excavation (Kendrick, 2012).

In May of 1949, 93.9% of B.C. residents were in favour of the Kemano hydroelectric generating facility (Rankin & Finlay, 1992). In its day, it was the largest privately funded construction project in Canada, costing $500 million in 1950, or more than $3.3 billion in today's currency. In 1950 the B.C. government gave the Aluminum Company of Canada, now Rio Tinto Alcan, the Nechako River (a headwater of the Fraser River) water rights (Burrows & Lane, n.d.). The facility was then constructed from 1951 to 1954 to supply power to the Rio Tinto Alcan aluminium smelter in Kitimat, B.C. Eight 112 MW generators were originally installed, resulting in the facility having a total capacity of 896 MW (Rankin & Finlay, 1992).

The diversion of the Fraser River (Rankin & Finlay, 1992) and blocking eastward flowing Nechako River were required in order to reverse the flow of a 13000 km^2 drainage area [6]. To achieve this massive change in the hydrogeological regime, Kenney Dam was constructed. Kenney Dam was the largest sloping clay core dam in the world at the time, raising water 97 m at its face (Rankin & Finlay, 1992).

The water from the Nechako reservoir was diverted through a 16 km long tunnel through Mt. DuBose to create an 860 m head differential (Alcan B.C. Operations, n.d.). The water is then routed through two penstocks and the subterranean powerhouse, after which it empties into the Kemano River (Hard Rock at Kitimat, 1952). The electricity generated travels through an 80 km transmission line to Kitimat, B.C. where it powers a large aluminium smelting facility (Hard Rock at Kitimat, 1952).

In the late 1980s, Rio Tinto Alcan proposed an expansion called the Kemano Completion Project (KCP). This expansion was meant to increase the capacity of the facility by

construction of a second 16 km tunnel and third penstock, as well as installing four turbine-generator units and additional transmission (Ghate, 1991). In addition, since the original infrastructure was beginning to deteriorate, this secondary tunnel was to allow for the completion of repair work and still maintain regular operation levels. Due to regulatory complications, work was suspended in the early 1990s (Burrows & Lane, n.d.). Work has not resumed since then, although RT Aluminium Group is in the conceptual stages of restarting work as a part of the Kitimat Modernization Project.

Construction of Underground Works

As with any underground excavation work, rock mass classification and reasonable geological assumptions are the basis for the excavation and support design. The geological conditions determine excavation shape, method, alignment, cost and schedule of the excavation. At the Kemano hydroelectric facility, the rock is predominantly diorite and granodiorite (see Section 0). The rocks in the Kemano area are of varying homogeneity, as some areas are fractured due to fault and shear zones while others are uniform in composition.

Powerhouse

The powerhouse was constructed underground due to national security concerns in the post-WWII climate, and was designed to be secure against air raids and landslides (KMA, 2010). The powerhouse cavern is 335 m long by 25 m wide by 36 m high, and lies 427 m back from the mountain face (Hard Rock at Kitimat, 1952).

The cavern excavation began with the driving of a 450 m long exploratory drift and two horseshoe-shaped access and tailrace tunnels to serve the excavation work (Hard Rock at Kitimat, 1952). The tailrace tunnel would eventually be enlarged to drain water from the turbines and out into the tailrace channel. Bolting of the powerhouse roof was completed in the fall of 1952. An 8 m square mucking tunnel was driven the length of the cavern, and seven shafts (3 m wide and 24 m long) were drilled to the exploratory drift below to allow for the blasting of the cavern using dynamite (Hard Rock at Kitimat, 1952). In the summer and fall of 1953, the steel columns and beams were constructed, and concrete was poured. By the

beginning of 1954, the interior of the powerhouse was mostly complete and the tailrace portal had been enlarged.

The first three generators came online in the summer of 1954 (Ghate, 1991). By the end of 1955, all eight turbine generators had been installed in the powerhouse, producing a continuous output of 1,250,000 kW and required an installed capacity of 1,750,000 kW (Kitimat Museum & Archives, 2010). This was over three times the capacity of all of B.C. in 1937. The tailrace channel was completed by 1955 rendering the powerhouse fully complete.

Penstocks

Two circular penstock tunnels were driven horizontally from the powerhouse for 150 m before angling upward at 48° from the horizontal to meet the 16 km conveyance tunnel at the 2600' level (Hard Rock at Kitimat, 1952). Two additional excavation headings were started at 1700' level to intersect the penstocks by means of an adit, at which points they travel horizontally for 312 m before angling upwards again. The final steel penstock lining is 3.35 m in diameter (Hard Rock at Kitimat, 1952). To resist the 8270 kPa water pressures, the rock around the penstocks was grouted and the void between the rock and steel liner was filled with concrete (Hard Rock at Kitimat, 1952).

T1 Tunnel

The 16 km, 8 m diameter conveyance tunnel diverts water from West Tahtsa Lake westward to Kemano hydroelectric facility (Hard Rock at Kitimat, 1952). The tunnel was excavated from two headings and met within an inch when the excavations were joined (Gent, 2014). Since the rock at West Tahtsa consists of blocky porphyries and andesites, it was necessary to reinforce the walls of the tunnel with timber and steel sets (Hard Rock at Kitimat, 1952). All sections requiring support were lined with concrete, and any timber sets were replaced with steel before the completion of the project (Hard Rock at Kitimat, 1952). Drill and blast tunnelling advance rates averaged to approximately 3-4 m per shift, with a world record of 282 ft/6 day week and 61 ft/24 hours set on February 25th, 1953 (Hard Rock at Kitimat, 1952).

The tunnel has survived two large collapses over its 60+ year life, one in 1958 and the other in 1961. The collapse in 1958 resulted in a partial shutdown of water flow through the tunnel, and the 1961 collapse put the aluminum smelter in Kitimat offline (Stueck, 2012).

T2 Tunnel

The Kemano Completion Project (KCP) was an expansion plan originally proposed by Rio Tinto Alcan in the late 1980s. It includes the construction of a second intake and water conveyance tunnel, a third penstock, a powerhouse extension with four additional turbine-generator units, a second tailrace and separate transformer gallery, and additional transmission lines (Ghate, 1991).

Excavation of the backup tunnel began in 1991 and was undertaken by a joint venture consisting of Guy F. Atkinson Construction and Peter Kiewit Construction (Sorenson, 2012). The tunnel would have been 16.1 km long and a 5.73 m diameter, and was designed to be a secondary water conveyance tunnel before excavation was halted due to environmental litigation (see section 0 - Political Obstacles for details). Before construction was suspended, tunnel advance rates ranged between 3.2 mm to 4.7 mm per revolution of the tunnel boring machine (TBM) cutter head (Stevenson, 1999), or an average of 28 meters per day (Ghate, 1991). The TBM was so efficient that it reached its first milestone two months ahead of schedule, on June 25th 1991. The smoother walls also resulted in lower hydraulic losses than the original drill and blast tunnel (Ghate, 1991).

In 2011, Rio Tinto Alcan announced its proposal to finish the work that was started in the 1990s (Stueck, 2012), namely finishing the remaining 8 km of the backup tunnel. This expansion is meant to increase capacity and support the $3.3 billion dollar Kitimat Modernization Project to update the existing aluminum smelter (Sorenson, 2012). A spokesperson for RTA emphasized that this revitalized KCP project differs from the 1990s version of the project in that its main purpose is risk mitigation, not water intake (Sorenson, 2012). Paul Henning, RTA's vice-president of B.C. operations, stated that there were three options: do nothing, shut down the tunnel while the smelter update was being completed, or build a backup tunnel (Stueck, 2012). Mr. Henning explained that a full shutdown could last between six and nine months and affect over 1,000 employees, so the backup tunnel was the

preferable option. Inspections in 2010 and 2011 using submersible remotely operated vehicles (ROVs) showed that there were no major problem areas, although the ROV was not able to access all parts of the tunnel (Stueck, 2012). While expert analysis of the data collected suggests the tunnel is in good shape (Sorenson, 2012), there is no way to know this for certain, which validates RTA's reasoning to approach the completion of the backup tunnel as a risk mitigation strategy (Stueck, 2012).

Geologic Setting

Glaciation

Alpine glaciers as well as perennial snowfields are common on higher peaks and ridges in the Kemano area. Evidence of previous glaciations is present in the form of erosional features in the U-shaped valleys. Horizontally oriented striations and glacial grooves generally trend parallel to Kemano Valley. Hanging valleys are also common, producing spectacular waterfalls where the walls of Kemano Valley are near vertical. Deposits of glacial materials are rare, found only in the form of a few small terminal and recessional moraines related to present-day glaciers (Stuart, 1960).

Regional Geology

The Kemano area is at the eastern border of the Coast intrusions, which are composite batholiths underlying the Coast Mountains. The general geological sequence of the area is as follows (Stuart, 1960):

- post-Middle Jurassic granitic gneisses and massive igneous rocks (the Coast Intrusions)
- Cretaceous sandstones and shales
- Middle and Lower Jurassic volcanic and sedimentary rocks, some metamorphosed (the Gamsby Group)
- pre-Middle Jurassic igneous rocks (the Tahtsa Complex)

The Tahtsa Complex

The Tahtsa Complex is pre-Middle Jurassic in age, regionally exposed in the core of a large dome. The rocks are igneous in origin, being comprised of hornblende diorite and quartz

diorite intruded by quartz monzonite stock, granodiorite dykes and basic dykes (Stuart, 1960).

Hornblende diorite makes up 75% of the Tahtsa Complex. It is inhomogeneous in texture, grain size and degree of alteration, and contains narrow veinlets of quartz diorite. This dominant variety of diorite is most often found to be medium grained, granitic in texture, medium to dark grey in colour when fresh and greenish-grey where altered. It contains equals parts hornblende and plagioclase with up to 10% quartz, which is most often only visible in thin section. The distribution of grain size from fine to coarse, though most commonly medium, creates a darker and lighter spectrum of rock colour and contributes to the overall appearance of inhomogeneity. Accessory minerals include apatite, sphene, zircon, magnetite, ilmenite, and pyrite. Most exposures of the diorite are sheared and fractures with a chlorite-epidote alteration that has affected practically all the diorite (Stuart, 1960).

Quartz diorite is a prevalent but minor component of the Tahtsa Complex. It most often occurs as narrow, discontinuous stringers filling joints and fractures. Locally it is sometimes sufficient to isolate a block of diorite and give a brecciated appearance. The quartz diorite is variable in grain size and mineral composition, occurring medium to fine grained most often and consisting primarily of quartz and plagioclase. Accessory minerals are rare but include apatite, magnetite, zircon and sphene (Stuart, 1960).

Quartz monzonite occurs in the southeastern part of the Tahtsa Complex as a large, tabular body south of Tahtsa Lake, outside the Kemano area. It is grey to dark pink in colour, and either medium grained, fine grained, or fine grained porphyritic in texture (Stuart, 1960).

Granodiorite dykes less than 15 meter wide occur in vaguely defined belts that trend approximately north-northeast in the Kemano area. The dykes are closely spaced locally and contain wedge and slab shaped blocks of diorite where dykes intersect. The granodiorite is light grey to pink, medium to coarse, and consists primarily of grey quartz and white feldspar. Accessory minerals are not common, but include apatite, magnetite, zircon and rarely ilmenite (Stuart, 1960).

Basic dykes occur throughout the Tahtsa complex, but are most common in the quartz monzonite and granodiorite intrusion. They are randomly oriented and may be a few centimeters to a few meters wide. The dykes are dark green to black, and may be aphanitic, fine grained or porphyritic. Plagioclase and hornblende are the dominant minerals, pyroxene and quartz occur in minor amounts, and accessory minerals include apatite, sphene, and magnetite (Stuart, 1960).

The Gamsby Group (formerly Hazelton Formation)

The Gamsby Group consists of volcanic, metavolcanic and metasedimentary rocks of Middle to Lower Jurassic age. It overlies the Tahtsa Complex uncomformably, and is truncated to the north and the west by intrusive rocks (Stuart, 1960).

Massive lavas are the most prevalent constituent of the volcanic rocks comprising the Gamsby Group and underlying the Kemano area. These rocks are light to dark green, and are occasionally found in shades of purple and red. Most commonly the rocks are aphanitic and porphyritic in texture, though occasionally they may be amygdaloidal. Most of these rocks are moderately to strongly altered, and are comprised of sericitized plagioclase, chlorite and magnetite, with occasional amphibole or quartz. Volcanic rocks in the Gamsby Group in massive, subangular to angular breccias, and more rarely occurring green crystal tuffs (Stuart, 1960).

Metamorphic rocks occupy the western part of the Gamsby Group underlying the Kemano area. These rocks are so highly metamorphosed that it is difficult to determine whether their precursor is sedimentary or volcanic. The metamorphic rocks present are generally greenschist and amphibolite facies. The Mortella Pluton is credited as the chief agent of metamorphism as the magma from which it crystallized was richest in volatiles, which permeated the country rock and promoted recrystallization (Stuart, 1960).

Rocks of the greenschist facies are light to dark green in colour, weakly to strongly schistose, and very fine grained. They are composed of albite, chlorite, calcite, magnetite, minor quartz, and locally abundant epidote. The greenschist facies metamorphism in the Kemano area is attributed to low grade dynamothermal (regional) metamorphism (Stuart, 1960).

Rocks of the amphibolite facies are dark grey or greyish-green in colour and are fine to medium grained. Parallel alignment of mafic minerals gives a gneissic appearance, but this is not accompanied by the schistosity of the greenschist facies rocks. Dominant minerals are amphibole, biotite, epidote, feldspar and quartz, with amphibole, biotite and garnet occurring as small porphyroblasts in fine grained rocks. The higher grade amphibolite facies are found in narrow zones adjacent to intrusive bodies. The amphibolite facies metamorphism may be a result of either thermal (contact) metamorphism or medium to high grade dynamothermal metamorphism (Stuart, 1960).

Coast Intrusions

The Coast Intrusions forms dykes and stocks in the Gamsby Group and the Tahtsa Complex. Three separate intrusions outcrop on Mount DuBose and intersect the T1 and T2 tunnel alignments: the Kemano gneiss, the Horetzky Dyke and the Mortella Pluton. All are post-Middle Jurassic in age (Stuart, 1960).

The Kemano Gneiss is the oldest of the three intrusions, and is comprised of well-foliated quartz diorite gneiss. The gneiss contains a variety of fine to medium grained, dark grey, medium grey and light grey crystalline rocks. The dark and light phases are strongly foliated and form a banded gneiss, where the dark phase is dominant and the light phase forms the well-defined bands. Banding is mostly parallel to foliation, however the bands swell and pinch locally. The dark and light phases only differ in proportions of mineral constituents. The main minerals constituents are andesine, quartz, biotite, hornblende, minor potash feldspar, and accessory apatite, magnetite, zircon and sphene (Stuart, 1960).

The Horetzky Dyke is a steeply dipping tabular body that intrudes the Tahtsa Complex, the Gamsby Group and the Kemano Gneiss. It is composed of grey medium grained diorite and quartz diorite. It is approximately 2.4 km wide and dipping 75° south at Mount DuBose, decreasing gradually in width and dip eastward toward Tahtsa Lake. Hornblende, plagioclase, quartz and minor potash feldspar are the major mineral constituents. Accessory minerals include apatite, sphene, zircon, and magnetite associated with biotite. Very minor alteration is evident throughout the Horetzky Dyke (Stuart, 1960).

The Mortella Pluton, formerly the Dubose Stock, is a roughly circular pluton that intrudes the Gamsby Group, the Kemano Gneiss, and the Horetzky Dyke. It is made up of light grey, medium to coarse grained, biotite-hornblende quartz diorite. The rock is primarily composed of quartz and plagioclase feldspar, with lesser amounts of biotite and hornblende, and scattered sphene crystals. The biotite crystals in the quartz diorite form a strong foliation and are often oriented parallel to the walls of the stock. The boundary between the Mortella Pluton and the Horetzky Dyke can be easily observed in the T1 and T2 tunnels. The contact, approximately 900 m wide, is characterized by large wedge-shaped and angular blocks of the Horetzky Dyke are enclosed in the quartz diorite of the Mortella Pluton. The Mortella Pluton can be distinguished from the Horetzky Dyke by its foliation, coarser grain size, lower mafic content, and dominance of biotite over hornblende (Stuart, 1960).

Structural Geology

The primary structures found in the Tahtsa Complex are sheared and fractured zones. This is particularly abundant in the diorite. These zones are characterized by abundant slickensiding and alteration, and are found in two dominant sets – one striking north-northeast, the other north-northwest. These trends are not found in the Gamsby Group. The granodiorite and quartz monzonite are highly fractures but not sheared, indicating that they were emplaced after the shearing event (Stuart, 1960).

The Gamsby Group strata have been regionally folded on north-northeast trending axes, locally folded adjacent to intruded bodies, and have been domed. The major folds are symmetrical and of approximately the same order of magnitude through the Kemano area. The low amplitude folds adjacent to the intrusive bodies indicate lateral thrusting during intrusion. The broad dome is elongated and striking slightly west of north. The disparity between the trend of the dome and the trend of the folds indicates that they formed independently (Stuart, 1960).

The Coast Intrusions all contain strongly oxidized zones of shearing likely representing faults that strike slightly west of north, but most do not cross lithostatic boundaries or show signs of displacement. Those that show evidence of displacement show small relative movement that is not measureable. The normal fault that forms part of the western boundary of the

Tahtsa Complex is older that the Horetzky Dyke. The remainder of the faults in the area are of similar orientation and sense of displacement, and are believed to have taken place concurrently with the intrusion of the Horetzky Dyke (Stuart, 1960).

Construction Challenges

During the original construction of the Kemano hydroelectric facilities, 13.3 million m^3 of rock was removed for the tunnel and powerhouse (Ghate, 1991). The massive scale of the project earned it the unofficial title of "eighth wonder of the world," due to its massive scope and the capital involved (Ghate, 1991). However, another reason why this project was so novel in its time is due to its extremely remote location. The project site is only accessible by boat or helicopter, and its only land connection to anything else is the transmission line right-of-way, which passes over very steep, rocky terrain. The area is also known for grizzlies, black bears and mountain goats.

Many of the earlier construction challenges due to remoteness have been alleviated through technological advances over the past 60 years. These technological advances are particularly apparent in the differences between the 1950s tunnel and the 1990s KCP tunnel. The second tunnel alignment is parallel to the existing one, but approximately 300 m to the south. The TBM was advancing at 28 meters per day, which is three times faster than the crews in the 1950s were able to achieve with traditional drill and blast techniques.

Those working on the Kemano Completion Project were especially proud of their low lost-time accident frequency, which was about one quarter of the industry average according to the Worker's Compensation Board of British Columbia. This is particularly remarkable because of the unusually hard working conditions resulting from the dangerous underground work and steep, rocky transmission line right-of-way (Ghate, 1991).

Another severe construction challenge during the KCP was posed by the necessity to blast and excavate the new penstock next to the existing, operational power plant. Several adjustments were made to ensure that the blast vibrations had no impact on the plant, including: detailed design of blast patterns, giving adequate warning to the station's control room operators, and taking very thorough seismic measurements. Despite these precautions, there were some vibration-induced shutdowns of the generating units. A "blast

wall" was constructed to protect the powerhouse, consisting of a steel mesh, a steel barricade, and a polyethylene cover (Ghate, 1991).

Political Obstacles

In 1978 Alcan expanded its power generation, which reduced the Nechako River to a trickle and endangered the habitats of Chinook and sockeye salmon (Burrows & Lane, n.d.). The federal Department of Fisheries and Oceans (DFO) got a court injunction shortly thereafter in order to force Alcan to leave enough water in the Nechako to sustain the salmon and sockeye habitats (Burrows & Lane, n.d.).

The conceptual planning of the Kemano Completion Project began in the 1980s, when Alcan resolved to double its power capacity by diverting the rest of the Nechako River (Burrows & Lane, n.d.). Only the authority of the DFO stood in the way, sending the dispute to trial. Alcan was engaged in environmental studies, public discussions and legal negotiations throughout the 1980s, which culminated in the 1987 Kemano Settlement Agreement (Ghate, 1991). This allowed Alcan to cut the Nechako River water levels to 30% of the natural flow in the short term, and to 13% in the long term once the cold water release was completed at Kenney Dam (Burrows & Lane, n.d.). The lowered water levels pose numerous risks to the fish spawning habitats, including higher water temperatures, putting more stress on returning salmon and a higher probability of disease. If there is not enough water covering the incubating salmon eggs in the winter, they can be damaged by freezing or lack of oxygen. The purpose of the cold water release facility was to convey cold water from the Nechako reservoir into the river in order to lower the water temperatures (Burrows & Lane, n.d.).

As well as incorporating the cold water release facility to protect the salmon population, several stages of mitigation were taken to control and water runoff from construction activities (Ghate, 1991). Settling ponds, oil separators and absorbers, filtering and pH adjustment were all employed to treat any waste water.

In October of 1990, the Rivers Defense Coalition and the Carrier-Sekani Tribal Council filed suits against the federal government aiming to overthrow the 1987 Kemano Settlement Agreement and requiring the Kemano Completion Project to undergo a full environmental review (Ghate, 1991). On May 16th, 1991, federal court Justice Allison Walsh effectively

quashed the Kemano Settlement Agreement by ruling that a public review was required. Alcan immediately began slowing down work, and by October 1991 the work was at a complete standstill.

Kemano Project Timeline

1949	- Surveyors from McElhanney Company began topographic surveys for Kenney Dam and survey controls for the tunnel drilling (Gent, 2014)
1951	- Boring of the tunnel begins on October 22nd from the west end of Tahtsa Lake, and on November 2nd from the powerhouse end (Gent, 2014)
1952	- Kenney Dam is constructed to dam the Nechako River (KMA, 2010) - Formation of the Tunnel and Rock Workers Union of B.C. on August 14th (Gent, 2014) - Excavation of powerhouse begins in the spring, roof of cavern is supported by October (KMA, 2010)
1953	- World records set for tunnel driving of 282 ft/6 day week and 61 ft/24 hours on February 25th (KMA, 2010) - Penstock liners are lowered and welded in place by the fall (KMA, 2010) - Tailrace channel is completed in September (KMA, 2010)
1954	- Powerhouse excavation is completed (KMA, 2010) - First generator goes into operation (Gent, 2014)
1967	- All eight generators go online (Gent, 2014)
1978	- Alcan increases water diversion and block Nechako River (Burrows & Lane, n.d.)
1979	- Alcan announces plans to proceed with Kemano Completion Project (Burrows & Lane, n.d.)
1980	- Carrier-Sekani Tribal Council requests an Environmental Assessment of KCP (Burrows & Lane, n.d.)

	- DFO goes to court to force Alcan to increase Nechako water flows with an interim injunction, but Alcan files a counter-claim stating that the provincial government does not have the constitutional authority to demand this (Burrows & Lane, n.d.)
1985	- The Rivers Defence Coalition is formed and tries to intervene in the constitutional case in the B.C. Supreme Court, but is denied intervener status (Burrows & Lane, n.d.)
1986	- DFO paper recommends minimal flows to be double those recommended by Alcan (Burrows & Lane, n.d.)
1987	- Constitutional case is settled out of court through a special Settlement Agreement that allows the water flows that Alcan originally recommended (Burrows & Lane, n.d.)
1988	- Rivers Defense Coalition sues DFO in federal court to have Settlement overturned (Burrows & Lane, n.d.)
1990	- Rivers Defense Coalition goes to federal government for an order forcing Alcan to conduct an Environmental Review, but the federal government specifically exempts Alcan from Environmental Review process (Burrows & Lane, n.d.)
1991	- Federal Court rules that KCP requires an Environmental Review and voids the 1987 Settlement, Alcan suspends KCP construction (Burrows & Lane, n.d.)
1992	- Alcan and the federal government appeal the Federal Court decision at the Federal Court of Appeal and win (Burrows & Lane, n.d.) - Rivers Defense Coalition appeals to the Supreme Court of Canada but leave to appeal is not granted (Burrows & Lane, n.d.)

1993	-	Provincial review is launched, and Alcan's exemption from the Environmental Review process is found unconstitutional and illegal (Burrows & Lane, n.d.)
1994	-	Federal government announces that KCP is to face a full environmental review (The Fisherman, 1994)
1995	-	Following the release of the B.C. Utilities Commission report on KCP, Premier Mike Harcourt (NDP) cancels the project (Wood, 2012)
2011	-	Rio Tinto Alcan announces their plans to reboot the Kemano Completion Project as a risk mitigation strategy, as part of the $3.3 billion Kitimat smelter expansion project (Kitimat Modernization Project)

Appendix B: MATLAB Code

3D Stress Tensor Rotation and Calculation of Tangential Stresses for T1

```
close all

clear all

clc


%this script performs 3D stress tensor rotation about the z-axis, gets the 2D
stress tensor in YZ plane, the calculates sig1, sig3 and theta in a plane
perpendicular to the tunnel


%T1

RawData = xlsread('Raw_fromAbaqus',1,'A1:J324');


%add an extra column that calculates the rotation angle (alpha) depending on
chainage


for i = 1:size(RawData,1),

  if RawData(i,1) <= 270; %for tunnel chainage 0+000 (Tahtsa portal) to 0+270

    RawData(i,11) = -15;

  elseif (RawData(i,1) > 270 && RawData(i,1) <= 570); %for tunnel chainage
0+270 to 0+570

    RawData(i,11) = -2;

  elseif (RawData(i,1) > 570 && RawData(i,1) <= 7880); %for tunnel chainage
0+570 to 7+880

    RawData(i,11) = 7;

  elseif (RawData(i,1) > 7880 && RawData(i,1) <= 7890); %for tunnel chainage
7+880 to 7+890

    RawData(i,11) = 16;

  elseif (RawData(i,1) > 7890 && RawData(i,1) <= 8960); %for tunnel chainage
7+890 to 8+960

    RawData(i,11) = 26;

  elseif (RawData(i,1) > 8960 && RawData(i,1) <= 16400); %for tunnel chainage
8+960 to 16+400 (1600' portal)

    RawData(i,11) = 30;
```

```
  else
    fprintf('This chainage is not valid for the T1 tunnel.');
  end

end

%create matrix to contain calculate values
OutputData = zeros(size(RawData,1),7);

%get 2D stress tensor and principal stress for entire length of tunnel in 50
m segments

for i = 1:size(RawData,1)

%rotation matrix about z axis, calculated using alpha which is based on
chainage
theta = RawData(i,11);
R = [cos(theta) -sin(theta) 0; sin(theta) cos(theta) 0; 0 0 1];
R_T = [cos(theta) sin(theta) 0; -sin(theta) cos(theta) 0; 0 0 1];

%get 3D stress tensor from raw data (from Abaqus)
stress_tensor = [RawData(i,2) RawData(i,3) RawData(i,4); RawData(i,5)
RawData(i,6) RawData(i,7); RawData(i,8) RawData(i,9) RawData(i,10)];

%rotate stress tensor about the z-axis using the rotation matrix
Rotated_A = stress_tensor*R*R_T;

%get 2D tensor in YZ plane and write to file
OutputData(i,1) = Rotated_A(2,2);
OutputData(i,2) = Rotated_A(2,3);
OutputData(i,3) = Rotated_A(3,2);
OutputData(i,4) = Rotated_A(3,3);
```

```
%redundant calcs but keeps the following equations cleaner

sig_y = Rotated_A(2,2);

tau_zy = Rotated_A(2,3);

tau_yz = Rotated_A(3,2);

sig_z = Rotated_A(3,3);


%complete 2D coordinate transformation to obtain sig_1, sig_3, theta

OutputData(i,5) = ((sig_y + sig_z)/2) + 0.5*sqrt(((sig_y - sig_z)^2 +
4*tau_zy^2));

OutputData(i,6) = ((sig_y + sig_z)/2) - 0.5*sqrt(((sig_y - sig_z)^2 +
4*tau_zy^2));

OutputData(i,7) = 2*atand((2*tau_zy)/(sig_y - sig_z));




end


fprintf('Finished computing principal stresses and orientations.');
```

3D Stress Tensor Rotation and Calculation of Tangential Stresses for T2

```
close all

clear all

clc


%this script performs 3D stress tensor rotation about the z-axis, gets the 2D
stress tensor in YZ plane, the calculates sig1, sig3 and theta in a plane
perpendicular to the tunnel


%T2

RawData = xlsread('Raw_fromAbaqus',2,'A1:J307');


%add an extra column that calculates the rotation angle (alpha) depending on
chainage


for i = 1:size(RawData,1),

  if RawData(i,1) <= 7610; %for tunnel chainage 0+000 (Tahtsa portal) to
7+610

    RawData(i,11) = 6;

  elseif (RawData(i,1) > 7610 && RawData(i,1) <= 7640); %for tunnel chainage
7+610 to 7+640

    RawData(i,11) = 10;

  elseif (RawData(i,1) > 7640 && RawData(i,1) <= 7665); %for tunnel chainage
7+640 to 7+665

    RawData(i,11) = 8;

  elseif (RawData(i,1) > 7665 && RawData(i,1) <= 7695); %for tunnel chainage
7+665 to 7+695

    RawData(i,11) = 15;

  elseif (RawData(i,1) > 7695 && RawData(i,1) <= 16200); %for tunnel chainage
7+695 to 16+200 (1600' Portal)

    RawData(i,11) = 30;

   else

    fprintf('This chainage is not valid for the T1 tunnel.');

  end
```

```
end


%create matrix to contain calculate values

OutputData = zeros(size(RawData,1),7);


%get 2D stress tensor and principal stress for entire length of tunnel in 50
m segments


for i = 1:size(RawData,1)




%rotation matrix about z axis, calculated using alpha which is based on
chainage

theta = RawData(i,11);

R = [cos(theta) -sin(theta) 0; sin(theta) cos(theta) 0; 0 0 1];

R_T = [cos(theta) sin(theta) 0; -sin(theta) cos(theta) 0; 0 0 1];


%get 3D stress tensor from raw data (from Abaqus)

stress_tensor = [RawData(i,2) RawData(i,3) RawData(i,4); RawData(i,5)
RawData(i,6) RawData(i,7); RawData(i,8) RawData(i,9) RawData(i,10)];


%rotate stress tensor about the z-axis using the rotation matrix

Rotated_A = stress_tensor*R*R_T;


%get 2D tensor in YZ plane and write to file

OutputData(i,1) = Rotated_A(2,2);

OutputData(i,2) = Rotated_A(2,3);

OutputData(i,3) = Rotated_A(3,2);

OutputData(i,4) = Rotated_A(3,3);


%redundant calcs but keeps the following equations cleaner
```

```
sig_y = Rotated_A(2,2);

tau_zy = Rotated_A(2,3);

tau_yz = Rotated_A(3,2);

sig_z = Rotated_A(3,3);


%complete 2D coordinate transformation to obtain sig_1, sig_3, theta

OutputData(i,5) = ((sig_y + sig_z)/2) + 0.5*sqrt(((sig_y - sig_z)^2 +
4*tau_zy^2));

OutputData(i,6) = ((sig_y + sig_z)/2) - 0.5*sqrt(((sig_y - sig_z)^2 +
4*tau_zy^2));

OutputData(i,7) = 2*atand((2*tau_zy)/(sig_y - sig_z));




end


fprintf('Finished computing principal stresses and orientations.');
```

Appendix C: Conditional Probability Tables

Joint Shear Strength CPT

Roughness	*Infilling*	*Weathering*	*High*	*Medium*	*Low*
Very rough	*None*	*Unweathered*	100	0	0
Very rough	*None*	*Slightly weathered*	100	0	0
Very rough	*None*	*Moderately weathered*	100	0	0
Very rough	*None*	*Highly weathered*	100	0	0
Very rough	*None*	*Decomposed*	50	50	0
Very rough	*Hard more than 5mm*	*Unweathered*	100	0	0
Very rough	*Hard more than 5mm*	*Slightly weathered*	100	0	0
Very rough	*Hard more than 5mm*	*Moderately weathered*	0	100	0
Very rough	*Hard more than 5mm*	*Highly weathered*	0	100	0
Very rough	*Hard more than 5mm*	*Decomposed*	0	100	0
Very rough	*Hard less than 5mm*	*Unweathered*	100	0	0
Very rough	*Hard less than 5mm*	*Slightly weathered*	100	0	0
Very rough	*Hard less than 5mm*	*Moderately weathered*	100	0	0
Very rough	*Hard less than 5mm*	*Highly weathered*	0	100	0
Very rough	*Hard less than 5mm*	*Decomposed*	0	100	0
Very rough	*Soft more than 5mm*	*Unweathered*	50	50	0
Very rough	*Soft more than 5mm*	*Slightly weathered*	0	100	0
Very rough	*Soft more than 5mm*	*Moderately weathered*	0	100	0
Very rough	*Soft more than 5mm*	*Highly weathered*	0	100	0
Very rough	*Soft more than 5mm*	*Decomposed*	0	50	50
Very rough	*Soft less than 5mm*	*Unweathered*	100	0	0
Very rough	*Soft less than 5mm*	*Slightly weathered*	100	0	0
Very rough	*Soft less than 5mm*	*Moderately weathered*	0	100	0
Very rough	*Soft less than 5mm*	*Highly weathered*	0	100	0
Very rough	*Soft less than 5mm*	*Decomposed*	0	100	0
Rough	*None*	*Unweathered*	100	0	0
Rough	*None*	*Slightly weathered*	100	0	0
Rough	*None*	*Moderately weathered*	100	0	0
Rough	*None*	*Highly weathered*	50	50	0
Rough	*None*	*Decomposed*	0	100	0
Rough	*Hard more than 5mm*	*Unweathered*	100	0	0
Rough	*Hard more than 5mm*	*Slightly weathered*	50	50	0
Rough	*Hard more than 5mm*	*Moderately weathered*	0	100	0
Rough	*Hard more than 5mm*	*Highly weathered*	0	100	0
Rough	*Hard more than 5mm*	*Decomposed*	0	100	0
Rough	*Hard less than 5mm*	*Unweathered*	100	0	0
Rough	*Hard less than 5mm*	*Slightly weathered*	100	0	0
Rough	*Hard less than 5mm*	*Moderately weathered*	50	50	0

Roughness	***Infilling***	***Weathering***	***High***	***Medium***	***Low***
Rough	*Hard less than 5mm*	*Highly weathered*	0	100	0
Rough	*Hard less than 5mm*	*Decomposed*	0	100	0
Rough	*Soft more than 5mm*	*Unweathered*	0	100	0
Rough	*Soft more than 5mm*	*Slightly weathered*	0	100	0
Rough	*Soft more than 5mm*	*Moderately weathered*	0	100	0
Rough	*Soft more than 5mm*	*Highly weathered*	0	50	50
Rough	*Soft more than 5mm*	*Decomposed*	0	0	100
Rough	*Soft less than 5mm*	*Unweathered*	100	0	0
Rough	*Soft less than 5mm*	*Slightly weathered*	50	50	0
Rough	*Soft less than 5mm*	*Moderately weathered*	0	100	0
Rough	*Soft less than 5mm*	*Highly weathered*	0	100	0
Rough	*Soft less than 5mm*	*Decomposed*	0	100	0
Slightly rough	*None*	*Unweathered*	100	0	0
Slightly rough	*None*	*Slightly weathered*	100	0	0
Slightly rough	*None*	*Moderately weathered*	50	50	0
Slightly rough	*None*	*Highly weathered*	0	100	0
Slightly rough	*None*	*Decomposed*	0	100	0
Slightly rough	*Hard more than 5mm*	*Unweathered*	0	100	0
Slightly rough	*Hard more than 5mm*	*Slightly weathered*	0	100	0
Slightly rough	*Hard more than 5mm*	*Moderately weathered*	0	100	0
Slightly rough	*Hard more than 5mm*	*Highly weathered*	0	50	50
Slightly rough	*Hard more than 5mm*	*Decomposed*	0	0	100
Slightly rough	*Hard less than 5mm*	*Unweathered*	100	0	0
Slightly rough	*Hard less than 5mm*	*Slightly weathered*	50	50	0
Slightly rough	*Hard less than 5mm*	*Moderately weathered*	0	100	0
Slightly rough	*Hard less than 5mm*	*Highly weathered*	0	100	0
Slightly rough	*Hard less than 5mm*	*Decomposed*	0	100	0
Slightly rough	*Soft more than 5mm*	*Unweathered*	0	100	0
Slightly rough	*Soft more than 5mm*	*Slightly weathered*	0	100	0
Slightly rough	*Soft more than 5mm*	*Moderately weathered*	0	50	50
Slightly rough	*Soft more than 5mm*	*Highly weathered*	0	0	100
Slightly rough	*Soft more than 5mm*	*Decomposed*	0	0	100
Slightly rough	*Soft less than 5mm*	*Unweathered*	0	100	0
Slightly rough	*Soft less than 5mm*	*Slightly weathered*	0	100	0
Slightly rough	*Soft less than 5mm*	*Moderately weathered*	0	100	0
Slightly rough	*Soft less than 5mm*	*Highly weathered*	0	50	50
Slightly rough	*Soft less than 5mm*	*Decomposed*	0	0	100
Smooth	*None*	*Unweathered*	100	0	0
Smooth	*None*	*Slightly weathered*	50	50	0
Smooth	*None*	*Moderately weathered*	0	100	0

Roughness	*Infilling*	*Weathering*	*High*	*Medium*	*Low*
Smooth	*None*	*Highly weathered*	0	100	0
Smooth	*None*	*Decomposed*	0	100	0
Smooth	*Hard more than 5mm*	*Unweathered*	0	100	0
Smooth	*Hard more than 5mm*	*Slightly weathered*	0	100	0
Smooth	*Hard more than 5mm*	*Moderately weathered*	0	50	50
Smooth	*Hard more than 5mm*	*Highly weathered*	0	0	100
Smooth	*Hard more than 5mm*	*Decomposed*	0	0	100
Smooth	*Hard less than 5mm*	*Unweathered*	0	100	0
Smooth	*Hard less than 5mm*	*Slightly weathered*	0	100	0
Smooth	*Hard less than 5mm*	*Moderately weathered*	0	100	0
Smooth	*Hard less than 5mm*	*Highly weathered*	0	50	50
Smooth	*Hard less than 5mm*	*Decomposed*	0	0	100
Smooth	*Soft more than 5mm*	*Unweathered*	0	100	0
Smooth	*Soft more than 5mm*	*Slightly weathered*	0	50	50
Smooth	*Soft more than 5mm*	*Moderately weathered*	0	0	100
Smooth	*Soft more than 5mm*	*Highly weathered*	0	0	100
Smooth	*Soft more than 5mm*	*Decomposed*	0	0	100
Smooth	*Soft less than 5mm*	*Unweathered*	0	100	0
Smooth	*Soft less than 5mm*	*Slightly weathered*	0	100	0
Smooth	*Soft less than 5mm*	*Moderately weathered*	0	50	50
Smooth	*Soft less than 5mm*	*Highly weathered*	0	0	100
Smooth	*Soft less than 5mm*	*Decomposed*	0	0	100
Slickensided	*None*	*Unweathered*	50	50	0
Slickensided	*None*	*Slightly weathered*	0	100	0
Slickensided	*None*	*Moderately weathered*	0	100	0
Slickensided	*None*	*Highly weathered*	0	100	0
Slickensided	*None*	*Decomposed*	0	50	50
Slickensided	*Hard more than 5mm*	*Unweathered*	0	100	0
Slickensided	*Hard more than 5mm*	*Slightly weathered*	0	100	0
Slickensided	*Hard more than 5mm*	*Moderately weathered*	0	0	100
Slickensided	*Hard more than 5mm*	*Highly weathered*	0	0	100
Slickensided	*Hard more than 5mm*	*Decomposed*	0	0	100
Slickensided	*Hard less than 5mm*	*Unweathered*	0	100	0
Slickensided	*Hard less than 5mm*	*Slightly weathered*	0	100	0
Slickensided	*Hard less than 5mm*	*Moderately weathered*	0	100	0
Slickensided	*Hard less than 5mm*	*Highly weathered*	0	0	100
Slickensided	*Hard less than 5mm*	*Decomposed*	0	0	100
Slickensided	*Soft more than 5mm*	*Unweathered*	0	50	50
Slickensided	*Soft more than 5mm*	*Slightly weathered*	0	0	100
Slickensided	*Soft more than 5mm*	*Moderately weathered*	0	0	100

Roughness	*Infilling*	*Weathering*	*High*	*Medium*	*Low*
Slickensided	*Soft more than 5mm*	*Highly weathered*	0	0	100
Slickensided	*Soft more than 5mm*	*Decomposed*	0	0	100
Slickensided	*Soft less than 5mm*	*Unweathered*	0	100	0
Slickensided	*Soft less than 5mm*	*Slightly weathered*	0	100	0
Slickensided	*Soft less than 5mm*	*Moderately weathered*	0	0	100
Slickensided	*Soft less than 5mm*	*Highly weathered*	0	0	100
Slickensided	*Soft less than 5mm*	*Decomposed*	0	0	100

Geological Strength Index CPT

Structure	Joint shear strength	Very poor rock	Poor rock	Fair rock	Good rock	Very good rock
Intact or massive	*High*	0.00	0.00	0.00	33.33	66.67
Intact or massive	*Medium*	0.00	0.00	20.00	80.00	0.00
Intact or massive	*Low*	x	x	x	x	x
Blocky	*High*	0.00	0.00	0.00	80.00	20.00
Blocky	*Medium*	0.00	0.00	66.67	33.33	0.00
Blocky	*Low*	0.00	60.00	40.00	0.00	0.00
Very blocky	*High*	0.00	0.00	40.00	60.00	0.00
Very blocky	*Medium*	0.00	25.00	75.00	0.00	0.00
Very blocky	*Low*	20.00	80.00	0.00	0.00	0.00
Disturbed	*High*	0.00	0.00	80.00	20.00	0.00
Disturbed	*Medium*	0.00	75.00	25.00	0.00	0.00
Disturbed	*Low*	50.00	50.00	0.00	0.00	0.00
Disintegrated	*High*	0.00	25.00	75.00	0.00	0.00
Disintegrated	*Medium*	0.00	100.00	0.00	0.00	0.00
Disintegrated	*Low*	75.00	25.00	0.00	0.00	0.00
Laminated or sheared	*High*	x	x	x	x	x
Laminated or sheared	*Medium*	33.33	66.67	0.00	0.00	0.00
Laminated or sheared	*Low*	100.00	0.00	0.00	0.00	0.00

Material property, *s* CPT

GSI	*a low*	*a common*	*a high*
Very poor rock	0	0	100
Poor rock	0	0	100
Fair rock	0	80	20
Good rock	0	100	0
Very good rock	100	0	0

Material property, *a* CPT

GSI	*Disturbance factor*	*s low*	*s common*	*s high*
Very poor rock	*Excellent*	100	0	0
Very poor rock	*Minimal*	100	0	0
Very poor rock	*Severe damage*	100	0	0
Poor rock	*Excellent*	30	70	0
Poor rock	*Minimal*	90	10	0
Poor rock	*Severe damage*	100	0	0
Fair rock	*Excellent*	0	80	20
Fair rock	*Minimal*	0	100	0
Fair rock	*Severe damage*	10	90	0
Good rock	*Excellent*	0	0	100
Good rock	*Minimal*	0	20	80
Good rock	*Severe damage*	0	50	50
Very good rock	*Excellent*	0	0	100
Very good rock	*Minimal*	0	0	100
Very good rock	*Severe damage*	0	0	100

Rock Mass Strength CPT

UCS	s	a	Rock Mass Strength
Low	*Low*	*Low*	Medium
Low	*Normal*	*Low*	Medium
Low	*High*	*Low*	Medium
Low	*Low*	*Common*	Low
Low	*Normal*	*Common*	Medium
Low	*High*	*Common*	Medium
Low	*Low*	*High*	Low
Low	*Normal*	*High*	Low
Low	*High*	*High*	Medium
Medium	*Low*	*Low*	Medium
Medium	*Normal*	*Low*	Medium
Medium	*High*	*Low*	Medium
Medium	*Low*	*Common*	Low
Medium	*Normal*	*Common*	Medium
Medium	*High*	*Common*	Medium

UCS	s	a	Rock Mass Strength
Medium	*Low*	*High*	Low
Medium	*Normal*	*High*	Low
Medium	*High*	*High*	Medium
High	*Low*	*Low*	Medium
High	*Normal*	*Low*	Medium
High	*High*	*Low*	High
High	*Low*	*Common*	Low
High	*Normal*	*Common*	Medium
High	*High*	*Common*	High
High	*Low*	*High*	Low
High	*Normal*	*High*	Low
High	*High*	*High*	Medium

σ_{max} CPT

σ_1	σ_3	*High*	*Medium*	*Low*
High	*High*	33.333	66.667	0
High	*Med*	40	60	0
High	*Low*	43.333	56.667	0
Med	*High*	0	43.333	56.667
Med	*Med*	0	53.333	46.667
Med	*Low*	0	60	40
Low	*High*	0	0	100
Low	*Med*	0	0	100
Low	*Low*	0	0	100

σ_{min} CPT

σ1	*σ3*	*High*	*Medium*	*Low*	*In tension*
High	*High*	0	6.667	20	73.333
High	*Med*	0	0	0	100
High	*Low*	0	0	0	100
Med	*High*	0	0	46.667	53.333
Med	*Med*	0	0	46.667	53.333
Med	*Low*	0	0	0	100
Low	*High*	66.667	33.333	0	0
Low	*Med*	0	53.333	40	6.667
Low	*Low*	0	0	0	100

Depth of spalling CPT

RMS	σ_{max}	*Tunnel radius*	*None*	*Low*	*Medium*	*Deep*
Low	*High*	*Small*	0	0	100	0
Low	*High*	*Medium*	0	0	0	100
Low	*High*	*Large*	0	0	0	100
Low	*Medium*	*Small*	0	0	100	0

RMS	σ_{max}	*Tunnel radius*	*None*	*Low*	*Medium*	*Deep*
Low	*Medium*	*Medium*	0	0	0	100
Low	*Medium*	*Large*	0	0	0	100
Low	*Low*	*Small*	0	100	0	0
Low	*Low*	*Medium*	0	0	100	0
Low	*Low*	*Large*	0	0	100	0
Medium	*High*	*Small*	0	100	0	0
Medium	*High*	*Medium*	0	100	0	0
Medium	*High*	*Large*	0	100	0	0
Medium	*Medium*	*Small*	100	0	0	0
Medium	*Medium*	*Medium*	100	0	0	0
Medium	*Medium*	*Large*	100	0	0	0
Medium	*Low*	*Small*	100	0	0	0
Medium	*Low*	*Medium*	100	0	0	0
Medium	*Low*	*Large*	100	0	0	0
High	*High*	*Small*	100	0	0	0
High	*High*	*Medium*	0	100	0	0
High	*High*	*Large*	100	0	0	0
High	*Medium*	*Small*	100	0	0	0
High	*Medium*	*Medium*	100	0	0	0
High	*Medium*	*Large*	100	0	0	0
High	*Low*	*Small*	100	0	0	0
High	*Low*	*Medium*	100	0	0	0
High	*Low*	*Large*	100	0	0	0

Location of Spalling CPT

σ_1 *orientation*	*Right springline*	*Right shoulder*	*Crown*	*Left shoulder*	*Left springline*
Right springline	0	0	100	0	0
Right shoulder	0	0	0	100	0
Crown	50	0	0	0	50
Left shoulder	0	100	0	0	0
Left springline	0	0	100	0	0

Ravelling CPT

Joint Shear Strength	*Groundwater*	*Joint Orientation*	*Ravelling Potential*	*Rock Load*	*Depth of Ravelling*
High	*Dry*	*Very Fav.*	*Five*	*Massive*	None
High	*Dry*	*Very Fav.*	*Ten*	*Massive*	None
High	*Dry*	*Very Fav.*	*Seventy*	*Massive*	None
High	*Dry*	*Very Fav.*	*One Hundred*	*Massive*	None

Joint Shear Strength	*Groundwater*	*Joint Orientation*	*Ravelling Potential*	*Rock Load*	*Depth of Ravelling*
High	*Dry*	*Very Fav.*	*Five*	*Blocky*	Low
High	*Dry*	*Very Fav.*	*Ten*	*Blocky*	Low
High	*Dry*	*Very Fav.*	*Seventy*	*Blocky*	Deep
High	*Dry*	*Very Fav.*	*One Hundred*	*Blocky*	Deep
High	*Dry*	*Very Fav.*	*Five*	*Very Blocky*	Low
High	*Dry*	*Very Fav.*	*Ten*	*Very Blocky*	Low
High	*Dry*	*Very Fav.*	*Seventy*	*Very Blocky*	Deep
High	*Dry*	*Very Fav.*	*One Hundred*	*Very Blocky*	Deep
High	*Dry*	*Fav.*	*Five*	*Massive*	None
High	*Dry*	*Fav.*	*Ten*	*Massive*	None
High	*Dry*	*Fav.*	*Seventy*	*Massive*	None
High	*Dry*	*Fav.*	*One Hundred*	*Massive*	None
High	*Dry*	*Fav.*	*Five*	*Blocky*	Low
High	*Dry*	*Fav.*	*Ten*	*Blocky*	Low
High	*Dry*	*Fav.*	*Seventy*	*Blocky*	Deep
High	*Dry*	*Fav.*	*One Hundred*	*Blocky*	Deep
High	*Dry*	*Fav.*	*Five*	*Very Blocky*	Low
High	*Dry*	*Fav.*	*Ten*	*Very Blocky*	Low
High	*Dry*	*Fav.*	*Seventy*	*Very Blocky*	Deep
High	*Dry*	*Fav.*	*One Hundred*	*Very Blocky*	Deep
High	*Dry*	*Fair*	*Five*	*Massive*	None
High	*Dry*	*Fair*	*Ten*	*Massive*	None
High	*Dry*	*Fair*	*Seventy*	*Massive*	None
High	*Dry*	*Fair*	*One Hundred*	*Massive*	None
High	*Dry*	*Fair*	*Five*	*Blocky*	Low
High	*Dry*	*Fair*	*Ten*	*Blocky*	Low
High	*Dry*	*Fair*	*Seventy*	*Blocky*	Deep
High	*Dry*	*Fair*	*One Hundred*	*Blocky*	Deep
High	*Dry*	*Fair*	*Five*	*Very Blocky*	Low

Joint Shear Strength	*Groundwater*	*Joint Orientation*	*Ravelling Potential*	*Rock Load*	*Depth of Ravelling*
High	*Dry*	*Fair*	*Ten*	*Very Blocky*	Low
High	*Dry*	*Fair*	*Seventy*	*Very Blocky*	Deep
High	*Dry*	*Fair*	*One Hundred*	*Very Blocky*	Deep
High	*Dry*	*Unfav.*	*Five*	*Massive*	None
High	*Dry*	*Unfav.*	*Ten*	*Massive*	None
High	*Dry*	*Unfav.*	*Seventy*	*Massive*	None
High	*Dry*	*Unfav.*	*One Hundred*	*Massive*	None
High	*Dry*	*Unfav.*	*Five*	*Blocky*	Low
High	*Dry*	*Unfav.*	*Ten*	*Blocky*	Low
High	*Dry*	*Unfav.*	*Seventy*	*Blocky*	Deep
High	*Dry*	*Unfav.*	*One Hundred*	*Blocky*	Deep
High	*Dry*	*Unfav.*	*Five*	*Very Blocky*	Low
High	*Dry*	*Unfav.*	*Ten*	*Very Blocky*	Low
High	*Dry*	*Unfav.*	*Seventy*	*Very Blocky*	Deep
High	*Dry*	*Unfav.*	*One Hundred*	*Very Blocky*	Deep
High	*Dry*	*Very Unfav.*	*Five*	*Massive*	None
High	*Dry*	*Very Unfav.*	*Ten*	*Massive*	None
High	*Dry*	*Very Unfav.*	*Seventy*	*Massive*	None
High	*Dry*	*Very Unfav.*	*One Hundred*	*Massive*	None
High	*Dry*	*Very Unfav.*	*Five*	*Blocky*	Low
High	*Dry*	*Very Unfav.*	*Ten*	*Blocky*	Low
High	*Dry*	*Very Unfav.*	*Seventy*	*Blocky*	Deep
High	*Dry*	*Very Unfav.*	*One Hundred*	*Blocky*	Deep
High	*Dry*	*Very Unfav.*	*Five*	*Very Blocky*	Low
High	*Dry*	*Very Unfav.*	*Ten*	*Very Blocky*	Low
High	*Dry*	*Very Unfav.*	*Seventy*	*Very Blocky*	Deep
High	*Dry*	*Very Unfav.*	*One Hundred*	*Very Blocky*	Deep

Joint Shear Strength	*Groundwater*	*Joint Orientation*	*Ravelling Potential*	*Rock Load*	*Depth of Ravelling*
High	*Damp*	*Very Fav.*	*Five*	*Massive*	None
High	*Damp*	*Very Fav.*	*Ten*	*Massive*	None
High	*Damp*	*Very Fav.*	*Seventy*	*Massive*	None
High	*Damp*	*Very Fav.*	*One Hundred*	*Massive*	None
High	*Damp*	*Very Fav.*	*Five*	*Blocky*	Low
High	*Damp*	*Very Fav.*	*Ten*	*Blocky*	Low
High	*Damp*	*Very Fav.*	*Seventy*	*Blocky*	Deep
High	*Damp*	*Very Fav.*	*One Hundred*	*Blocky*	Deep
High	*Damp*	*Very Fav.*	*Five*	*Very Blocky*	Low
High	*Damp*	*Very Fav.*	*Ten*	*Very Blocky*	Low
High	*Damp*	*Very Fav.*	*Seventy*	*Very Blocky*	Deep
High	*Damp*	*Very Fav.*	*One Hundred*	*Very Blocky*	Deep
High	*Damp*	*Fav.*	*Five*	*Massive*	None
High	*Damp*	*Fav.*	*Ten*	*Massive*	None
High	*Damp*	*Fav.*	*Seventy*	*Massive*	None
High	*Damp*	*Fav.*	*One Hundred*	*Massive*	None
High	*Damp*	*Fav.*	*Five*	*Blocky*	Low
High	*Damp*	*Fav.*	*Ten*	*Blocky*	Low
High	*Damp*	*Fav.*	*Seventy*	*Blocky*	Deep
High	*Damp*	*Fav.*	*One Hundred*	*Blocky*	Deep
High	*Damp*	*Fav.*	*Five*	*Very Blocky*	Low
High	*Damp*	*Fav.*	*Ten*	*Very Blocky*	Low
High	*Damp*	*Fav.*	*Seventy*	*Very Blocky*	Deep
High	*Damp*	*Fav.*	*One Hundred*	*Very Blocky*	Deep
High	*Damp*	*Fair*	*Five*	*Massive*	None
High	*Damp*	*Fair*	*Ten*	*Massive*	None
High	*Damp*	*Fair*	*Seventy*	*Massive*	None
High	*Damp*	*Fair*	*One Hundred*	*Massive*	None
High	*Damp*	*Fair*	*Five*	*Blocky*	Low

Joint Shear Strength	***Groundwater***	***Joint Orientation***	***Ravelling Potential***	***Rock Load***	***Depth of Ravelling***
High	*Damp*	*Fair*	*Ten*	*Blocky*	Low
High	*Damp*	*Fair*	*Seventy*	*Blocky*	Deep
High	*Damp*	*Fair*	*One Hundred*	*Blocky*	Deep
High	*Damp*	*Fair*	*Five*	*Very Blocky*	Low
High	*Damp*	*Fair*	*Ten*	*Very Blocky*	Low
High	*Damp*	*Fair*	*Seventy*	*Very Blocky*	Deep
High	*Damp*	*Fair*	*One Hundred*	*Very Blocky*	Deep
High	*Damp*	*Unfav.*	*Five*	*Massive*	None
High	*Damp*	*Unfav.*	*Ten*	*Massive*	None
High	*Damp*	*Unfav.*	*Seventy*	*Massive*	None
High	*Damp*	*Unfav.*	*One Hundred*	*Massive*	None
High	*Damp*	*Unfav.*	*Five*	*Blocky*	Low
High	*Damp*	*Unfav.*	*Ten*	*Blocky*	Low
High	*Damp*	*Unfav.*	*Seventy*	*Blocky*	Deep
High	*Damp*	*Unfav.*	*One Hundred*	*Blocky*	Deep
High	*Damp*	*Unfav.*	*Five*	*Very Blocky*	Low
High	*Damp*	*Unfav.*	*Ten*	*Very Blocky*	Low
High	*Damp*	*Unfav.*	*Seventy*	*Very Blocky*	Deep
High	*Damp*	*Unfav.*	*One Hundred*	*Very Blocky*	Deep
High	*Damp*	*Very Unfav.*	*Five*	*Massive*	None
High	*Damp*	*Very Unfav.*	*Ten*	*Massive*	None
High	*Damp*	*Very Unfav.*	*Seventy*	*Massive*	None
High	*Damp*	*Very Unfav.*	*One Hundred*	*Massive*	None
High	*Damp*	*Very Unfav.*	*Five*	*Blocky*	Low
High	*Damp*	*Very Unfav.*	*Ten*	*Blocky*	Low
High	*Damp*	*Very Unfav.*	*Seventy*	*Blocky*	Deep
High	*Damp*	*Very Unfav.*	*One Hundred*	*Blocky*	Deep
High	*Damp*	*Very Unfav.*	*Five*	*Very Blocky*	Low

Joint Shear Strength	*Groundwater*	*Joint Orientation*	*Ravelling Potential*	*Rock Load*	*Depth of Ravelling*
High	*Damp*	*Very Unfav.*	*Ten*	*Very Blocky*	Low
High	*Damp*	*Very Unfav.*	*Seventy*	*Very Blocky*	Deep
High	*Damp*	*Very Unfav.*	*One Hundred*	*Very Blocky*	Deep
High	*Wet*	*Very Fav.*	*Five*	*Massive*	None
High	*Wet*	*Very Fav.*	*Ten*	*Massive*	None
High	*Wet*	*Very Fav.*	*Seventy*	*Massive*	None
High	*Wet*	*Very Fav.*	*One Hundred*	*Massive*	None
High	*Wet*	*Very Fav.*	*Five*	*Blocky*	Low
High	*Wet*	*Very Fav.*	*Ten*	*Blocky*	Low
High	*Wet*	*Very Fav.*	*Seventy*	*Blocky*	Deep
High	*Wet*	*Very Fav.*	*One Hundred*	*Blocky*	Deep
High	*Wet*	*Very Fav.*	*Five*	*Very Blocky*	Low
High	*Wet*	*Very Fav.*	*Ten*	*Very Blocky*	Low
High	*Wet*	*Very Fav.*	*Seventy*	*Very Blocky*	Deep
High	*Wet*	*Very Fav.*	*One Hundred*	*Very Blocky*	Deep
High	*Wet*	*Fav.*	*Five*	*Massive*	None
High	*Wet*	*Fav.*	*Ten*	*Massive*	None
High	*Wet*	*Fav.*	*Seventy*	*Massive*	None
High	*Wet*	*Fav.*	*One Hundred*	*Massive*	None
High	*Wet*	*Fav.*	*Five*	*Blocky*	Low
High	*Wet*	*Fav.*	*Ten*	*Blocky*	Low
High	*Wet*	*Fav.*	*Seventy*	*Blocky*	Deep
High	*Wet*	*Fav.*	*One Hundred*	*Blocky*	Deep
High	*Wet*	*Fav.*	*Five*	*Very Blocky*	Low
High	*Wet*	*Fav.*	*Ten*	*Very Blocky*	Low
High	*Wet*	*Fav.*	*Seventy*	*Very Blocky*	Deep
High	*Wet*	*Fav.*	*One Hundred*	*Very Blocky*	Deep

Joint Shear Strength	*Groundwater*	*Joint Orientation*	*Ravelling Potential*	*Rock Load*	*Depth of Ravelling*
High	*Wet*	*Fair*	*Five*	*Massive*	None
High	*Wet*	*Fair*	*Ten*	*Massive*	None
High	*Wet*	*Fair*	*Seventy*	*Massive*	None
High	*Wet*	*Fair*	*One Hundred*	*Massive*	None
High	*Wet*	*Fair*	*Five*	*Blocky*	Low
High	*Wet*	*Fair*	*Ten*	*Blocky*	Low
High	*Wet*	*Fair*	*Seventy*	*Blocky*	Deep
High	*Wet*	*Fair*	*One Hundred*	*Blocky*	Deep
High	*Wet*	*Fair*	*Five*	*Very Blocky*	Low
High	*Wet*	*Fair*	*Ten*	*Very Blocky*	Low
High	*Wet*	*Fair*	*Seventy*	*Very Blocky*	Deep
High	*Wet*	*Fair*	*One Hundred*	*Very Blocky*	Deep
High	*Wet*	*Unfav.*	*Five*	*Massive*	None
High	*Wet*	*Unfav.*	*Ten*	*Massive*	None
High	*Wet*	*Unfav.*	*Seventy*	*Massive*	None
High	*Wet*	*Unfav.*	*One Hundred*	*Massive*	None
High	*Wet*	*Unfav.*	*Five*	*Blocky*	Low
High	*Wet*	*Unfav.*	*Ten*	*Blocky*	Low
High	*Wet*	*Unfav.*	*Seventy*	*Blocky*	Deep
High	*Wet*	*Unfav.*	*One Hundred*	*Blocky*	Deep
High	*Wet*	*Unfav.*	*Five*	*Very Blocky*	Low
High	*Wet*	*Unfav.*	*Ten*	*Very Blocky*	Low
High	*Wet*	*Unfav.*	*Seventy*	*Very Blocky*	Deep
High	*Wet*	*Unfav.*	*One Hundred*	*Very Blocky*	Deep
High	*Wet*	*Very Unfav.*	*Five*	*Massive*	None
High	*Wet*	*Very Unfav.*	*Ten*	*Massive*	None
High	*Wet*	*Very Unfav.*	*Seventy*	*Massive*	None
High	*Wet*	*Very Unfav.*	*One Hundred*	*Massive*	None
High	*Wet*	*Very Unfav.*	*Five*	*Blocky*	Low

Joint Shear Strength	***Groundwater***	***Joint Orientation***	***Ravelling Potential***	***Rock Load***	***Depth of Ravelling***
High	*Wet*	*Very Unfav.*	*Ten*	*Blocky*	Low
High	*Wet*	*Very Unfav.*	*Seventy*	*Blocky*	Deep
High	*Wet*	*Very Unfav.*	*One Hundred*	*Blocky*	Deep
High	*Wet*	*Very Unfav.*	*Five*	*Very Blocky*	Low
High	*Wet*	*Very Unfav.*	*Ten*	*Very Blocky*	Low
High	*Wet*	*Very Unfav.*	*Seventy*	*Very Blocky*	Deep
High	*Wet*	*Very Unfav.*	*One Hundred*	*Very Blocky*	Deep
High	*Dripping*	*Very Fav.*	*Five*	*Massive*	None
High	*Dripping*	*Very Fav.*	*Ten*	*Massive*	None
High	*Dripping*	*Very Fav.*	*Seventy*	*Massive*	None
High	*Dripping*	*Very Fav.*	*One Hundred*	*Massive*	None
High	*Dripping*	*Very Fav.*	*Five*	*Blocky*	Low
High	*Dripping*	*Very Fav.*	*Ten*	*Blocky*	Low
High	*Dripping*	*Very Fav.*	*Seventy*	*Blocky*	Deep
High	*Dripping*	*Very Fav.*	*One Hundred*	*Blocky*	Deep
High	*Dripping*	*Very Fav.*	*Five*	*Very Blocky*	Low
High	*Dripping*	*Very Fav.*	*Ten*	*Very Blocky*	Low
High	*Dripping*	*Very Fav.*	*Seventy*	*Very Blocky*	Deep
High	*Dripping*	*Very Fav.*	*One Hundred*	*Very Blocky*	Deep
High	*Dripping*	*Fav.*	*Five*	*Massive*	None
High	*Dripping*	*Fav.*	*Ten*	*Massive*	None
High	*Dripping*	*Fav.*	*Seventy*	*Massive*	None
High	*Dripping*	*Fav.*	*One Hundred*	*Massive*	None
High	*Dripping*	*Fav.*	*Five*	*Blocky*	Low
High	*Dripping*	*Fav.*	*Ten*	*Blocky*	Low
High	*Dripping*	*Fav.*	*Seventy*	*Blocky*	Deep
High	*Dripping*	*Fav.*	*One Hundred*	*Blocky*	Deep
High	*Dripping*	*Fav.*	*Five*	*Very Blocky*	Low

Joint Shear Strength	***Groundwater***	***Joint Orientation***	***Ravelling Potential***	***Rock Load***	***Depth of Ravelling***
High	*Dripping*	*Fav.*	*Ten*	*Very Blocky*	Low
High	*Dripping*	*Fav.*	*Seventy*	*Very Blocky*	Deep
High	*Dripping*	*Fav.*	*One Hundred*	*Very Blocky*	Deep
High	*Dripping*	*Fair*	*Five*	*Massive*	None
High	*Dripping*	*Fair*	*Ten*	*Massive*	None
High	*Dripping*	*Fair*	*Seventy*	*Massive*	None
High	*Dripping*	*Fair*	*One Hundred*	*Massive*	None
High	*Dripping*	*Fair*	*Five*	*Blocky*	Low
High	*Dripping*	*Fair*	*Ten*	*Blocky*	Low
High	*Dripping*	*Fair*	*Seventy*	*Blocky*	Deep
High	*Dripping*	*Fair*	*One Hundred*	*Blocky*	Deep
High	*Dripping*	*Fair*	*Five*	*Very Blocky*	Low
High	*Dripping*	*Fair*	*Ten*	*Very Blocky*	Low
High	*Dripping*	*Fair*	*Seventy*	*Very Blocky*	Deep
High	*Dripping*	*Fair*	*One Hundred*	*Very Blocky*	Deep
High	*Dripping*	*Unfav.*	*Five*	*Massive*	None
High	*Dripping*	*Unfav.*	*Ten*	*Massive*	None
High	*Dripping*	*Unfav.*	*Seventy*	*Massive*	None
High	*Dripping*	*Unfav.*	*One Hundred*	*Massive*	None
High	*Dripping*	*Unfav.*	*Five*	*Blocky*	Low
High	*Dripping*	*Unfav.*	*Ten*	*Blocky*	Low
High	*Dripping*	*Unfav.*	*Seventy*	*Blocky*	Deep
High	*Dripping*	*Unfav.*	*One Hundred*	*Blocky*	Deep
High	*Dripping*	*Unfav.*	*Five*	*Very Blocky*	Low
High	*Dripping*	*Unfav.*	*Ten*	*Very Blocky*	Low
High	*Dripping*	*Unfav.*	*Seventy*	*Very Blocky*	Deep
High	*Dripping*	*Unfav.*	*One Hundred*	*Very Blocky*	Deep

Joint Shear Strength	*Groundwater*	*Joint Orientation*	*Ravelling Potential*	*Rock Load*	*Depth of Ravelling*
High	*Dripping*	*Very Unfav.*	*Five*	*Massive*	None
High	*Dripping*	*Very Unfav.*	*Ten*	*Massive*	None
High	*Dripping*	*Very Unfav.*	*Seventy*	*Massive*	None
High	*Dripping*	*Very Unfav.*	*One Hundred*	*Massive*	None
High	*Dripping*	*Very Unfav.*	*Five*	*Blocky*	Low
High	*Dripping*	*Very Unfav.*	*Ten*	*Blocky*	Low
High	*Dripping*	*Very Unfav.*	*Seventy*	*Blocky*	Deep
High	*Dripping*	*Very Unfav.*	*One Hundred*	*Blocky*	Deep
High	*Dripping*	*Very Unfav.*	*Five*	*Very Blocky*	Low
High	*Dripping*	*Very Unfav.*	*Ten*	*Very Blocky*	Low
High	*Dripping*	*Very Unfav.*	*Seventy*	*Very Blocky*	Deep
High	*Dripping*	*Very Unfav.*	*One Hundred*	*Very Blocky*	Deep
High	*Flowing*	*Very Fav.*	*Five*	*Massive*	None
High	*Flowing*	*Very Fav.*	*Ten*	*Massive*	None
High	*Flowing*	*Very Fav.*	*Seventy*	*Massive*	None
High	*Flowing*	*Very Fav.*	*One Hundred*	*Massive*	None
High	*Flowing*	*Very Fav.*	*Five*	*Blocky*	Low
High	*Flowing*	*Very Fav.*	*Ten*	*Blocky*	Low
High	*Flowing*	*Very Fav.*	*Seventy*	*Blocky*	Deep
High	*Flowing*	*Very Fav.*	*One Hundred*	*Blocky*	Deep
High	*Flowing*	*Very Fav.*	*Five*	*Very Blocky*	Low
High	*Flowing*	*Very Fav.*	*Ten*	*Very Blocky*	Low
High	*Flowing*	*Very Fav.*	*Seventy*	*Very Blocky*	Deep
High	*Flowing*	*Very Fav.*	*One Hundred*	*Very Blocky*	Deep
High	*Flowing*	*Fav.*	*Five*	*Massive*	None
High	*Flowing*	*Fav.*	*Ten*	*Massive*	None
High	*Flowing*	*Fav.*	*Seventy*	*Massive*	None
High	*Flowing*	*Fav.*	*One Hundred*	*Massive*	None
High	*Flowing*	*Fav.*	*Five*	*Blocky*	Low

Joint Shear Strength	***Groundwater***	***Joint Orientation***	***Ravelling Potential***	***Rock Load***	***Depth of Ravelling***
High	*Flowing*	*Fav.*	*Ten*	*Blocky*	Low
High	*Flowing*	*Fav.*	*Seventy*	*Blocky*	Deep
High	*Flowing*	*Fav.*	*One Hundred*	*Blocky*	Deep
High	*Flowing*	*Fav.*	*Five*	*Very Blocky*	Low
High	*Flowing*	*Fav.*	*Ten*	*Very Blocky*	Low
High	*Flowing*	*Fav.*	*Seventy*	*Very Blocky*	Deep
High	*Flowing*	*Fav.*	*One Hundred*	*Very Blocky*	Deep
High	*Flowing*	*Fair*	*Five*	*Massive*	None
High	*Flowing*	*Fair*	*Ten*	*Massive*	None
High	*Flowing*	*Fair*	*Seventy*	*Massive*	None
High	*Flowing*	*Fair*	*One Hundred*	*Massive*	None
High	*Flowing*	*Fair*	*Five*	*Blocky*	Low
High	*Flowing*	*Fair*	*Ten*	*Blocky*	Low
High	*Flowing*	*Fair*	*Seventy*	*Blocky*	Deep
High	*Flowing*	*Fair*	*One Hundred*	*Blocky*	Deep
High	*Flowing*	*Fair*	*Five*	*Very Blocky*	Low
High	*Flowing*	*Fair*	*Ten*	*Very Blocky*	Low
High	*Flowing*	*Fair*	*Seventy*	*Very Blocky*	Deep
High	*Flowing*	*Fair*	*One Hundred*	*Very Blocky*	Deep
High	*Flowing*	*Unfav.*	*Five*	*Massive*	None
High	*Flowing*	*Unfav.*	*Ten*	*Massive*	None
High	*Flowing*	*Unfav.*	*Seventy*	*Massive*	None
High	*Flowing*	*Unfav.*	*One Hundred*	*Massive*	None
High	*Flowing*	*Unfav.*	*Five*	*Blocky*	Low
High	*Flowing*	*Unfav.*	*Ten*	*Blocky*	Low
High	*Flowing*	*Unfav.*	*Seventy*	*Blocky*	Medium
High	*Flowing*	*Unfav.*	*One Hundred*	*Blocky*	Deep
High	*Flowing*	*Unfav.*	*Five*	*Very Blocky*	Low

Joint Shear Strength	***Groundwater***	***Joint Orientation***	***Ravelling Potential***	***Rock Load***	***Depth of Ravelling***
High	*Flowing*	*Unfav.*	*Ten*	*Very Blocky*	Low
High	*Flowing*	*Unfav.*	*Seventy*	*Very Blocky*	Deep
High	*Flowing*	*Unfav.*	*One Hundred*	*Very Blocky*	Deep
High	*Flowing*	*Very Unfav.*	*Five*	*Massive*	None
High	*Flowing*	*Very Unfav.*	*Ten*	*Massive*	None
High	*Flowing*	*Very Unfav.*	*Seventy*	*Massive*	None
High	*Flowing*	*Very Unfav.*	*One Hundred*	*Massive*	None
High	*Flowing*	*Very Unfav.*	*Five*	*Blocky*	Low
High	*Flowing*	*Very Unfav.*	*Ten*	*Blocky*	Low
High	*Flowing*	*Very Unfav.*	*Seventy*	*Blocky*	Medium
High	*Flowing*	*Very Unfav.*	*One Hundred*	*Blocky*	Deep
High	*Flowing*	*Very Unfav.*	*Five*	*Very Blocky*	Low
High	*Flowing*	*Very Unfav.*	*Ten*	*Very Blocky*	Low
High	*Flowing*	*Very Unfav.*	*Seventy*	*Very Blocky*	Deep
High	*Flowing*	*Very Unfav.*	*One Hundred*	*Very Blocky*	Deep
Medium	*Dry*	*Very Fav.*	*Five*	*Massive*	Low
Medium	*Dry*	*Very Fav.*	*Ten*	*Massive*	Low
Medium	*Dry*	*Very Fav.*	*Seventy*	*Massive*	Deep
Medium	*Dry*	*Very Fav.*	*One Hundred*	*Massive*	Deep
Medium	*Dry*	*Very Fav.*	*Five*	*Blocky*	Low
Medium	*Dry*	*Very Fav.*	*Ten*	*Blocky*	Low
Medium	*Dry*	*Very Fav.*	*Seventy*	*Blocky*	Deep
Medium	*Dry*	*Very Fav.*	*One Hundred*	*Blocky*	Deep
Medium	*Dry*	*Very Fav.*	*Five*	*Very Blocky*	Low
Medium	*Dry*	*Very Fav.*	*Ten*	*Very Blocky*	Low
Medium	*Dry*	*Very Fav.*	*Seventy*	*Very Blocky*	Deep
Medium	*Dry*	*Very Fav.*	*One Hundred*	*Very Blocky*	Deep

Joint Shear Strength	*Groundwater*	*Joint Orientation*	*Ravelling Potential*	*Rock Load*	*Depth of Ravelling*
Medium	*Dry*	*Fav.*	*Five*	*Massive*	Low
Medium	*Dry*	*Fav.*	*Ten*	*Massive*	Low
Medium	*Dry*	*Fav.*	*Seventy*	*Massive*	Deep
Medium	*Dry*	*Fav.*	*One Hundred*	*Massive*	Deep
Medium	*Dry*	*Fav.*	*Five*	*Blocky*	Low
Medium	*Dry*	*Fav.*	*Ten*	*Blocky*	Low
Medium	*Dry*	*Fav.*	*Seventy*	*Blocky*	Deep
Medium	*Dry*	*Fav.*	*One Hundred*	*Blocky*	Deep
Medium	*Dry*	*Fav.*	*Five*	*Very Blocky*	Low
Medium	*Dry*	*Fav.*	*Ten*	*Very Blocky*	Low
Medium	*Dry*	*Fav.*	*Seventy*	*Very Blocky*	Deep
Medium	*Dry*	*Fav.*	*One Hundred*	*Very Blocky*	Deep
Medium	*Dry*	*Fair*	*Five*	*Massive*	Low
Medium	*Dry*	*Fair*	*Ten*	*Massive*	Low
Medium	*Dry*	*Fair*	*Seventy*	*Massive*	Deep
Medium	*Dry*	*Fair*	*One Hundred*	*Massive*	Deep
Medium	*Dry*	*Fair*	*Five*	*Blocky*	Low
Medium	*Dry*	*Fair*	*Ten*	*Blocky*	Low
Medium	*Dry*	*Fair*	*Seventy*	*Blocky*	Deep
Medium	*Dry*	*Fair*	*One Hundred*	*Blocky*	Deep
Medium	*Dry*	*Fair*	*Five*	*Very Blocky*	Low
Medium	*Dry*	*Fair*	*Ten*	*Very Blocky*	Low
Medium	*Dry*	*Fair*	*Seventy*	*Very Blocky*	Deep
Medium	*Dry*	*Fair*	*One Hundred*	*Very Blocky*	Deep
Medium	*Dry*	*Unfav.*	*Five*	*Massive*	Low
Medium	*Dry*	*Unfav.*	*Ten*	*Massive*	Low
Medium	*Dry*	*Unfav.*	*Seventy*	*Massive*	Medium
Medium	*Dry*	*Unfav.*	*One Hundred*	*Massive*	Deep
Medium	*Dry*	*Unfav.*	*Five*	*Blocky*	Low

Joint Shear Strength	***Groundwater***	***Joint Orientation***	***Ravelling Potential***	***Rock Load***	***Depth of Ravelling***
Medium	*Dry*	*Unfav.*	*Ten*	*Blocky*	Low
Medium	*Dry*	*Unfav.*	*Seventy*	*Blocky*	Medium
Medium	*Dry*	*Unfav.*	*One Hundred*	*Blocky*	Deep
Medium	*Dry*	*Unfav.*	*Five*	*Very Blocky*	Low
Medium	*Dry*	*Unfav.*	*Ten*	*Very Blocky*	Low
Medium	*Dry*	*Unfav.*	*Seventy*	*Very Blocky*	Medium
Medium	*Dry*	*Unfav.*	*One Hundred*	*Very Blocky*	Deep
Medium	*Dry*	*Very Unfav.*	*Five*	*Massive*	Low
Medium	*Dry*	*Very Unfav.*	*Ten*	*Massive*	Low
Medium	*Dry*	*Very Unfav.*	*Seventy*	*Massive*	Medium
Medium	*Dry*	*Very Unfav.*	*One Hundred*	*Massive*	Deep
Medium	*Dry*	*Very Unfav.*	*Five*	*Blocky*	Low
Medium	*Dry*	*Very Unfav.*	*Ten*	*Blocky*	Low
Medium	*Dry*	*Very Unfav.*	*Seventy*	*Blocky*	Medium
Medium	*Dry*	*Very Unfav.*	*One Hundred*	*Blocky*	Deep
Medium	*Dry*	*Very Unfav.*	*Five*	*Very Blocky*	Low
Medium	*Dry*	*Very Unfav.*	*Ten*	*Very Blocky*	Low
Medium	*Dry*	*Very Unfav.*	*Seventy*	*Very Blocky*	Medium
Medium	*Dry*	*Very Unfav.*	*One Hundred*	*Very Blocky*	Deep
Medium	*Damp*	*Very Fav.*	*Five*	*Massive*	Low
Medium	*Damp*	*Very Fav.*	*Ten*	*Massive*	Low
Medium	*Damp*	*Very Fav.*	*Seventy*	*Massive*	Deep
Medium	*Damp*	*Very Fav.*	*One Hundred*	*Massive*	Deep
Medium	*Damp*	*Very Fav.*	*Five*	*Blocky*	Low
Medium	*Damp*	*Very Fav.*	*Ten*	*Blocky*	Low
Medium	*Damp*	*Very Fav.*	*Seventy*	*Blocky*	Deep
Medium	*Damp*	*Very Fav.*	*One Hundred*	*Blocky*	Deep
Medium	*Damp*	*Very Fav.*	*Five*	*Very Blocky*	Low

Joint Shear Strength	*Groundwater*	*Joint Orientation*	*Ravelling Potential*	*Rock Load*	*Depth of Ravelling*
Medium	*Damp*	*Very Fav.*	*Ten*	*Very Blocky*	Low
Medium	*Damp*	*Very Fav.*	*Seventy*	*Very Blocky*	Deep
Medium	*Damp*	*Very Fav.*	*One Hundred*	*Very Blocky*	Deep
Medium	*Damp*	*Fav.*	*Five*	*Massive*	Low
Medium	*Damp*	*Fav.*	*Ten*	*Massive*	Low
Medium	*Damp*	*Fav.*	*Seventy*	*Massive*	Deep
Medium	*Damp*	*Fav.*	*One Hundred*	*Massive*	Deep
Medium	*Damp*	*Fav.*	*Five*	*Blocky*	Low
Medium	*Damp*	*Fav.*	*Ten*	*Blocky*	Low
Medium	*Damp*	*Fav.*	*Seventy*	*Blocky*	Deep
Medium	*Damp*	*Fav.*	*One Hundred*	*Blocky*	Deep
Medium	*Damp*	*Fav.*	*Five*	*Very Blocky*	Low
Medium	*Damp*	*Fav.*	*Ten*	*Very Blocky*	Low
Medium	*Damp*	*Fav.*	*Seventy*	*Very Blocky*	Deep
Medium	*Damp*	*Fav.*	*One Hundred*	*Very Blocky*	Deep
Medium	*Damp*	*Fair*	*Five*	*Massive*	Low
Medium	*Damp*	*Fair*	*Ten*	*Massive*	Low
Medium	*Damp*	*Fair*	*Seventy*	*Massive*	Medium
Medium	*Damp*	*Fair*	*One Hundred*	*Massive*	Deep
Medium	*Damp*	*Fair*	*Five*	*Blocky*	Low
Medium	*Damp*	*Fair*	*Ten*	*Blocky*	Low
Medium	*Damp*	*Fair*	*Seventy*	*Blocky*	Medium
Medium	*Damp*	*Fair*	*One Hundred*	*Blocky*	Deep
Medium	*Damp*	*Fair*	*Five*	*Very Blocky*	Low
Medium	*Damp*	*Fair*	*Ten*	*Very Blocky*	Low
Medium	*Damp*	*Fair*	*Seventy*	*Very Blocky*	Medium
Medium	*Damp*	*Fair*	*One Hundred*	*Very Blocky*	Deep

Joint Shear Strength	*Groundwater*	*Joint Orientation*	*Ravelling Potential*	*Rock Load*	*Depth of Ravelling*
Medium	*Damp*	*Unfav.*	*Five*	*Massive*	Low
Medium	*Damp*	*Unfav.*	*Ten*	*Massive*	Low
Medium	*Damp*	*Unfav.*	*Seventy*	*Massive*	Medium
Medium	*Damp*	*Unfav.*	*One Hundred*	*Massive*	Deep
Medium	*Damp*	*Unfav.*	*Five*	*Blocky*	Low
Medium	*Damp*	*Unfav.*	*Ten*	*Blocky*	Low
Medium	*Damp*	*Unfav.*	*Seventy*	*Blocky*	Medium
Medium	*Damp*	*Unfav.*	*One Hundred*	*Blocky*	Deep
Medium	*Damp*	*Unfav.*	*Five*	*Very Blocky*	Low
Medium	*Damp*	*Unfav.*	*Ten*	*Very Blocky*	Low
Medium	*Damp*	*Unfav.*	*Seventy*	*Very Blocky*	Medium
Medium	*Damp*	*Unfav.*	*One Hundred*	*Very Blocky*	Deep
Medium	*Damp*	*Very Unfav.*	*Five*	*Massive*	Low
Medium	*Damp*	*Very Unfav.*	*Ten*	*Massive*	Low
Medium	*Damp*	*Very Unfav.*	*Seventy*	*Massive*	Medium
Medium	*Damp*	*Very Unfav.*	*One Hundred*	*Massive*	Deep
Medium	*Damp*	*Very Unfav.*	*Five*	*Blocky*	Low
Medium	*Damp*	*Very Unfav.*	*Ten*	*Blocky*	Low
Medium	*Damp*	*Very Unfav.*	*Seventy*	*Blocky*	Medium
Medium	*Damp*	*Very Unfav.*	*One Hundred*	*Blocky*	Deep
Medium	*Damp*	*Very Unfav.*	*Five*	*Very Blocky*	Low
Medium	*Damp*	*Very Unfav.*	*Ten*	*Very Blocky*	Low
Medium	*Damp*	*Very Unfav.*	*Seventy*	*Very Blocky*	Medium
Medium	*Damp*	*Very Unfav.*	*One Hundred*	*Very Blocky*	Deep
Medium	*Wet*	*Very Fav.*	*Five*	*Massive*	Low
Medium	*Wet*	*Very Fav.*	*Ten*	*Massive*	Low
Medium	*Wet*	*Very Fav.*	*Seventy*	*Massive*	Deep
Medium	*Wet*	*Very Fav.*	*One Hundred*	*Massive*	Deep
Medium	*Wet*	*Very Fav.*	*Five*	*Blocky*	Low

Joint Shear Strength	*Groundwater*	*Joint Orientation*	*Ravelling Potential*	*Rock Load*	*Depth of Ravelling*
Medium	*Wet*	*Very Fav.*	*Ten*	*Blocky*	Low
Medium	*Wet*	*Very Fav.*	*Seventy*	*Blocky*	Deep
Medium	*Wet*	*Very Fav.*	*One Hundred*	*Blocky*	Deep
Medium	*Wet*	*Very Fav.*	*Five*	*Very Blocky*	Low
Medium	*Wet*	*Very Fav.*	*Ten*	*Very Blocky*	Low
Medium	*Wet*	*Very Fav.*	*Seventy*	*Very Blocky*	Deep
Medium	*Wet*	*Very Fav.*	*One Hundred*	*Very Blocky*	Deep
Medium	*Wet*	*Fav.*	*Five*	*Massive*	Low
Medium	*Wet*	*Fav.*	*Ten*	*Massive*	Low
Medium	*Wet*	*Fav.*	*Seventy*	*Massive*	Medium
Medium	*Wet*	*Fav.*	*One Hundred*	*Massive*	Deep
Medium	*Wet*	*Fav.*	*Five*	*Blocky*	Low
Medium	*Wet*	*Fav.*	*Ten*	*Blocky*	Low
Medium	*Wet*	*Fav.*	*Seventy*	*Blocky*	Medium
Medium	*Wet*	*Fav.*	*One Hundred*	*Blocky*	Deep
Medium	*Wet*	*Fav.*	*Five*	*Very Blocky*	Low
Medium	*Wet*	*Fav.*	*Ten*	*Very Blocky*	Low
Medium	*Wet*	*Fav.*	*Seventy*	*Very Blocky*	Medium
Medium	*Wet*	*Fav.*	*One Hundred*	*Very Blocky*	Deep
Medium	*Wet*	*Fair*	*Five*	*Massive*	Low
Medium	*Wet*	*Fair*	*Ten*	*Massive*	Low
Medium	*Wet*	*Fair*	*Seventy*	*Massive*	Medium
Medium	*Wet*	*Fair*	*One Hundred*	*Massive*	Deep
Medium	*Wet*	*Fair*	*Five*	*Blocky*	Low
Medium	*Wet*	*Fair*	*Ten*	*Blocky*	Low

Location of Ravelling CPT

σ_1 orientation	**Right springline**	**Right shoulder**	**Crown**	**Left shoulder**	**Left springline**

Right springline	100	0	0	0	0
Right shoulder	0	100	0	0	0
Crown	0	0	100	0	0
Left shoulder	0	0	0	100	0
Left springline	0	0	0	0	100

Ground Class CPT

Depth of Ravelling	***Depth of Spalling***	***I***	***IIa***	***IIb***	***III***	***IV***
None	*None*	100	0	0	0	0
None	*Low*	50	50	0	0	0
None	*Medium*	20	60	0	20	0
None	*Deep*	0	20	0	40	40
Low	*None*	50	0	50	0	0
Low	*Low*	60	20	20	0	0
Low	*Medium*	0	50	20	30	0
Low	*Deep*	0	10	0	30	60
Medium	*None*	20	0	50	30	0
Medium	*Low*	0	20	40	40	0
Medium	*Medium*	0	20	20	60	0
Medium	*Deep*	0	10	10	30	50
Deep	*None*	0	0	40	40	20
Deep	*Low*	0	10	20	30	40
Deep	*Medium*	0	0	0	40	60
Deep	*Deep*	0	0	0	20	80

Appendix D: Kemano Specific Database

Chainage	*Rock type*	*σ_1*	*σ_3*	*θ*	*Structure*	*J_infill*	*J_weather*	*Groundwater*	*J_orient*
16+186	Mortella Pluton	4.0	3.4	-54.29	4.3	None	Unweathered	Dry	Very unfavourable
16+175	Mortella Pluton	4.0	3.4	-54.29	4.3	None	Unweathered	Dry	Very unfavourable
16+150	Mortella Pluton	4.0	3.4	-54.29	4.3	None	Unweathered	Dry	Very unfavourable
16+125	Mortella Pluton	4.0	3.4	-54.29	4.3	None	Moderately weathered	Dry	Unfavourable
16+100	Mortella Pluton	4.0	3.4	-54.29	4.3	None	Moderately weathered	Dry	Unfavourable
16+075	Mortella Pluton	4.0	3.4	-54.29	3.85	None	Decomposed	Dry	Unfavourable
16+050	Mortella Pluton	4.9	3.8	64.00	3.85	None	Decomposed	Dry	Fair
16+025	Mortella Pluton	4.9	3.8	64.00	3.85	None	Highly weathered	Damp	Unfavourable
16+000	Mortella Pluton	5.9	4.1	43.89	3.85	None	Highly weathered	Dry	Unfavourable
15+975	Mortella Pluton	5.9	4.1	43.89	3.57	None	Unweathered	Dry	Fair
15+950	Mortella Pluton	5.9	4.1	43.89	3.57	Soft more than 5mm	Unweathered	Dry	Fair
15+925	Mortella Pluton	6.9	4.3	36.51	3.57	None	Unweathered	Dry	Fair
15+900	Mortella Pluton	6.9	4.3	36.51	3.57	Soft more than 5mm	Unweathered	Dry	Unfavourable
15+875	Mortella Pluton	7.6	4.4	33.10	8.33	None	Unweathered	Dry	Unfavourable
15+850	Mortella Pluton	7.6	4.4	33.10	8.33	None	Unweathered	Dry	Unfavourable
15+825	Mortella Pluton	8.3	4.6	30.97	8.33	None	Unweathered	Dry	Fair
15+800	Mortella Pluton	8.3	4.6	30.97	8.33	None	Unweathered	Dry	Very unfavourable
15+775	Mortella Pluton	8.9	4.7	29.25	6.67	Soft more than 5mm	Unweathered	Dry	Unfavourable
15+750	Mortella Pluton	8.9	4.7	29.25	6.67	None	Unweathered	Dry	Unfavourable
15+725	Mortella Pluton	9.5	4.8	26.69	6.67	None	Unweathered	Dry	Fair
15+700	Mortella Pluton	9.5	4.8	26.69	6.67	None	Unweathered	Damp	Unfavourable
15+675	Mortella Pluton	10.0	4.9	24.59	6.67	None	Unweathered	Dry	Fair
15+650	Mortella Pluton	10.0	4.9	24.59	6.67	None	Unweathered	Dry	Unfavourable
15+625	Mortella Pluton	10.4	5.0	22.93	6.67	None	Slightly weathered	Dry	Fair
15+600	Mortella Pluton	10.4	5.0	22.93	6.67	Soft more than 5mm	Slightly weathered	Damp	Unfavourable
15+575	Mortella Pluton	10.9	5.1	21.67	4.76	None	Unweathered	Dry	Fair
15+550	Mortella Pluton	10.9	5.1	21.67	4.76	None	Unweathered	Dry	Fair
15+525	Mortella Pluton	11.3	5.2	20.39	4.76	None	Unweathered	Dry	Fair
15+500	Mortella Pluton	11.3	5.2	20.39	4.76	None	Unweathered	Dry	Fair
15+475	Mortella Pluton	11.3	5.2	20.39	6.67	None	Unweathered	Dry	Fair
15+450	Mortella Pluton	11.6	5.3	19.45	6.67	None	Unweathered	Dry	Fair
15+425	Mortella Pluton	11.6	5.3	19.45	6.67	Soft more than 5mm	Moderately weathered	Dry	Fair
15+400	Mortella Pluton	11.9	5.3	19.08	6.67	None	Moderately weathered	Damp	Fair
15+375	Mortella Pluton	11.9	5.3	19.08	4.55	None	Moderately weathered	Dry	Unfavourable
15+350	Mortella Pluton	12.2	5.4	18.53	4.55	Soft more than 5mm	Moderately weathered	Dry	Fair
15+325	Mortella Pluton	12.2	5.4	18.53	4.55	Soft more than 5mm	Moderately weathered	Damp	Unfavourable
15+300	Mortella Pluton	12.4	5.4	17.80	4.55	Hard more than 5mm	Moderately weathered	Damp	Unfavourable
15+275	Mortella Pluton	12.4	5.4	17.80	2.94	None	Slightly weathered	Damp	Fair
15+250	Mortella Pluton	12.7	5.5	16.80	2.94	None	Slightly weathered	Damp	Fair

Chainage	*Rock type*	*σ_1*	*σ_3*	*θ*	*Structure*	*J_infill*	*J_weather*	*Groundwater*	*J_orient*
15+225	Mortella Pluton	12.7	5.5	16.80	2.94	None	Slightly weathered	Damp	Fair
15+200	Mortella Pluton	12.9	5.5	15.92	2.94	None	Slightly weathered	Damp	Fair
15+175	Mortella Pluton	12.9	5.5	15.92	3.45	None	Slightly weathered	Damp	Fair
15+150	Mortella Pluton	13.0	5.5	15.51	3.45	None	Slightly weathered	Wet	Fair
15+125	Mortella Pluton	13.0	5.5	15.51	3.45	None	Slightly weathered	Damp	Fair
15+100	Mortella Pluton	13.2	5.6	15.14	3.45	None	Slightly weathered	Damp	Unfavourable
15+075	Mortella Pluton	13.2	5.6	15.14	6.67	Soft more than 5mm	Highly weathered	Damp	Fair
15+050	Mortella Pluton	13.3	5.6	14.37	6.67	None	Highly weathered	Dripping	Unfavourable
15+025	Mortella Pluton	13.3	5.6	14.37	6.67	None	Unweathered	Dry	Unfavourable
15+000	Mortella Pluton	13.5	5.6	13.73	6.67	None	Unweathered	Dry	Fair
14+975	Mortella Pluton	13.5	5.6	13.73	20	None	Unweathered	Dry	Fair
14+950	Mortella Pluton	13.5	5.6	13.73	20	None	Unweathered	Dry	Unfavourable
14+925	Mortella Pluton	13.5	5.6	13.23	20	None	Unweathered	Dry	Unfavourable
14+900	Mortella Pluton	13.5	5.6	13.23	20	None	Unweathered	Dry	Unfavourable
14+875	Mortella Pluton	13.6	5.6	12.87	20	None	Unweathered	Dry	Unfavourable
14+850	Mortella Pluton	13.6	5.6	12.87	20	None	Unweathered	Dry	Fair
14+825	Mortella Pluton	13.7	5.6	12.74	20	None	Unweathered	Dry	Unfavourable
14+800	Mortella Pluton	13.7	5.6	12.74	20	None	Unweathered	Dry	Fair
14+775	Mortella Pluton	13.7	5.6	12.62	16.67	None	Unweathered	Dry	Unfavourable
14+750	Mortella Pluton	13.7	5.6	12.62	16.67	None	Unweathered	Damp	Unfavourable
14+725	Mortella Pluton	13.8	5.7	12.61	16.67	None	Unweathered	Dry	Unfavourable
14+700	Mortella Pluton	13.8	5.7	12.61	16.67	None	Unweathered	Dry	Fair
14+675	Mortella Pluton	13.9	5.7	12.63	10	None	Unweathered	Dry	Fair
14+650	Mortella Pluton	13.9	5.7	12.63	10	None	Unweathered	Dry	Fair
14+625	Mortella Pluton	13.9	5.7	12.58	10	None	Slightly weathered	Dry	Fair
14+600	Mortella Pluton	13.9	5.7	12.58	10	None	Slightly weathered	Dry	Fair
14+575	Mortella Pluton	14.0	5.7	12.63	5.56	None	Slightly weathered	Dry	Fair
14+550	Mortella Pluton	14.0	5.7	12.63	5.56	None	Slightly weathered	Dry	Unfavourable
14+525	Mortella Pluton	14.0	5.7	12.63	5.56	None	Slightly weathered	Dry	Fair
14+500	Mortella Pluton	14.0	5.7	12.63	5.56	None	Slightly weathered	Dry	Unfavourable
14+475	Mortella Pluton	14.0	5.7	12.63	8.33	None	Unweathered	Dry	Unfavourable
14+450	Mortella Pluton	14.0	5.7	12.64	8.33	None	Unweathered	Dry	Fair
14+425	Mortella Pluton	14.0	5.7	12.64	8.33	Hard more than 5mm	Unweathered	Dry	Very unfavourable
14+400	Mortella Pluton	14.1	5.7	12.70	8.33	None	Unweathered	Dry	Unfavourable
14+375	Mortella Pluton	14.1	5.7	12.70	9.09	None	Unweathered	Dry	Unfavourable
14+350	Mortella Pluton	14.1	5.7	12.87	9.09	None	Unweathered	Dry	Very unfavourable
14+325	Mortella Pluton	14.1	5.7	12.87	9.09	None	Slightly weathered	Dry	Unfavourable
14+300	Mortella Pluton	14.1	5.8	13.11	9.09	Hard more than 5mm	Slightly weathered	Dry	Unfavourable
14+275	Mortella Pluton	14.1	5.8	13.11	7.14	Soft more than 5mm	Highly weathered	Dry	Unfavourable
14+250	Mortella Pluton	14.1	5.8	13.46	7.14	None	Highly weathered	Dry	Fair

Chainage	*Rock type*	σ_1	σ_3	*θ*	*Structure*	*J_infill*	*J_weather*	*Groundwater*	*J_orient*
14+225	Mortella Pluton	14.1	5.8	13.46	7.14	None	Moderately weathered	Dry	Fair
14+200	Mortella Pluton	14.1	5.8	13.87	7.14	None	Moderately weathered	Dry	Unfavourable
14+175	Mortella Pluton	14.1	5.8	13.87	12.5	None	Slightly weathered	Dry	Unfavourable
14+150	Mortella Pluton	14.1	5.8	14.25	12.5	None	Slightly weathered	Dry	Unfavourable
14+125	Mortella Pluton	14.1	5.8	14.25	12.5	Soft more than 5mm	Moderately weathered	Dry	Fair
14+100	Mortella Pluton	14.1	5.8	14.65	12.5	Soft less than 5mm	Moderately weathered	Dry	Unfavourable
14+075	Mortella Pluton	14.1	5.8	14.65	8.33	Soft less than 5mm	Moderately weathered	Damp	Unfavourable
14+050	Mortella Pluton	14.1	5.8	14.97	8.33	Soft less than 5mm	Moderately weathered	Dry	Unfavourable
14+025	Mortella Pluton	14.1	5.8	14.97	8.33	None	Unweathered	Dry	Unfavourable
14+000	Mortella Pluton	14.1	5.8	15.20	8.33	None	Unweathered	Dry	Very unfavourable
13+975	Mortella Pluton	14.1	5.8	15.20	14.29	None	Unweathered	Dry	Fair
13+950	Mortella Pluton	14.1	5.8	15.20	14.29	None	Unweathered	Damp	Unfavourable
13+925	Mortella Pluton	14.1	5.8	15.39	14.29	Soft more than 5mm	Unweathered	Dry	Unfavourable
13+900	Mortella Pluton	14.1	5.8	15.39	14.29	None	Unweathered	Dry	Unfavourable
13+875	Mortella Pluton	14.1	5.8	15.61	7.69	None	Highly weathered	Dry	Unfavourable
13+850	Mortella Pluton	14.1	5.8	15.61	7.69	Soft more than 5mm	Highly weathered	Dry	Unfavourable
13+825	Mortella Pluton	14.1	5.8	15.85	7.69	Soft less than 5mm	Unweathered	Dry	Unfavourable
13+800	Mortella Pluton	14.1	5.8	15.85	7.69	None	Unweathered	Dry	Unfavourable
13+775	Mortella Pluton	14.1	5.8	16.10	12.5	None	Unweathered	Dry	Fair
13+750	Mortella Pluton	14.1	5.8	16.10	12.5	None	Unweathered	Damp	Fair
13+725	Mortella Pluton	14.1	5.8	16.28	12.5	None	Unweathered	Dry	Very unfavourable
13+700	Mortella Pluton	14.1	5.8	16.28	12.5	Soft more than 5mm	Unweathered	Dry	Fair
13+675	Mortella Pluton	14.1	5.8	16.40	30	Soft less than 5mm	Unweathered	Dry	Unfavourable
13+650	Mortella Pluton	14.1	5.8	16.40	30	None	Unweathered	Dry	Fair
13+625	Mortella Pluton	14.1	5.8	16.40	30	None	Slightly weathered	Dry	Unfavourable
13+600	Mortella Pluton	14.1	5.8	16.40	30	None	Slightly weathered	Dry	Fair
13+575	Mortella Pluton	14.1	5.8	16.12	14.29	None	Unweathered	Dry	Unfavourable
13+550	Mortella Pluton	14.1	5.8	16.12	14.29	None	Unweathered	Dry	Unfavourable
13+525	Mortella Pluton	14.1	5.8	15.60	14.29	None	Unweathered	Dry	Unfavourable
13+500	Mortella Pluton	14.1	5.8	15.60	14.29	None	Unweathered	Dry	Fair
13+475	Mortella Pluton	14.1	5.8	15.60	6.67	None	Unweathered	Dry	Unfavourable
13+450	Mortella Pluton	14.1	5.9	14.85	6.67	None	Unweathered	Dry	Unfavourable
13+425	Mortella Pluton	14.1	5.9	14.85	6.67	None	Unweathered	Dry	Unfavourable
13+400	Horetzky Dyke	14.0	5.9	14.16	6.67	None	Unweathered	Dry	Unfavourable
13+375	Horetzky Dyke	14.0	5.9	14.16	20	None	Slightly weathered	Dry	Unfavourable
13+350	Horetzky Dyke	14.0	5.9	13.95	20	None	Slightly weathered	Dry	Fair
13+325	Horetzky Dyke	14.0	5.9	13.95	20	None	Slightly weathered	Dry	Unfavourable
13+300	Horetzky Dyke	14.0	6.0	13.54	20	None	Slightly weathered	Dry	Unfavourable
13+275	Horetzky Dyke	14.0	6.0	13.54	16.67	None	Unweathered	Dry	Fair
13+250	Horetzky Dyke	14.0	6.0	12.85	16.67	None	Unweathered	Dry	Unfavourable

Chainage	*Rock type*	σ_1	σ_3	*θ*	*Structure*	*J_infill*	*J_weather*	*Groundwater*	*J_orient*
13+225	Horetzky Dyke	14.0	6.0	12.85	16.67	None	Slightly weathered	Dry	Fair
13+200	Horetzky Dyke	14.0	6.0	12.00	16.67	None	Slightly weathered	Dry	Fair
13+175	Horetzky Dyke	14.0	6.0	12.00	14.29	None	Slightly weathered	Dry	Unfavourable
13+150	Horetzky Dyke	14.0	6.0	11.15	14.29	None	Slightly weathered	Dry	Fair
13+125	Horetzky Dyke	14.0	6.0	11.15	14.29	None	Unweathered	Dry	Fair
13+100	Horetzky Dyke	14.0	6.1	9.90	14.29	None	Unweathered	Dry	Unfavourable
13+075	Horetzky Dyke	14.0	6.1	9.90	50	None	Unweathered	Dry	Fair
13+050	Horetzky Dyke	13.9	6.1	8.66	50	None	Unweathered	Dry	Fair
13+025	Horetzky Dyke	13.9	6.1	8.66	50	None	Unweathered	Dry	Unfavourable
13+000	Horetzky Dyke	13.9	6.2	7.43	50	None	Unweathered	Dry	Unfavourable
12+975	Horetzky Dyke	13.9	6.2	7.43	14.29	None	Slightly weathered	Dry	Fair
12+950	Horetzky Dyke	13.9	6.2	7.43	14.29	None	Slightly weathered	Dry	Fair
12+925	Horetzky Dyke	13.9	6.2	6.19	14.29	None	Moderately weathered	Dry	Fair
12+900	Horetzky Dyke	13.9	6.2	6.19	14.29	None	Moderately weathered	Dry	Fair
12+875	Horetzky Dyke	13.8	6.2	4.98	16.67	None	Moderately weathered	Dry	Unfavourable
12+850	Horetzky Dyke	13.8	6.2	4.98	16.67	None	Moderately weathered	Damp	Unfavourable
12+825	Horetzky Dyke	13.8	6.3	3.80	16.67	None	Unweathered	Dry	Fair
12+800	Horetzky Dyke	13.8	6.3	3.80	16.67	None	Unweathered	Dry	Fair
12+775	Horetzky Dyke	13.7	6.3	2.72	9.09	None	Slightly weathered	Dry	Fair
12+750	Horetzky Dyke	13.7	6.3	2.72	9.09	Hard more than 5mm	Slightly weathered	Dry	Fair
12+725	Horetzky Dyke	13.6	6.3	1.41	9.09	None	Unweathered	Damp	Unfavourable
12+700	Horetzky Dyke	13.6	6.3	1.41	9.09	None	Unweathered	Dry	Fair
12+675	Horetzky Dyke	13.6	6.4	-0.09	11.11	None	Unweathered	Dry	Fair
12+650	Horetzky Dyke	13.6	6.4	-0.09	11.11	None	Unweathered	Damp	Fair
12+625	Horetzky Dyke	13.4	6.4	-1.97	11.11	None	Slightly weathered	Dry	Fair
12+600	Horetzky Dyke	13.4	6.4	-1.97	11.11	None	Slightly weathered	Dry	Fair
12+575	Horetzky Dyke	13.3	6.4	-4.79	10	None	Slightly weathered	Dry	Fair
12+550	Horetzky Dyke	13.3	6.4	-4.79	10	Hard more than 5mm	Slightly weathered	Dry	Fair
12+525	Horetzky Dyke	13.1	6.4	-7.68	10	None	Unweathered	Dry	Fair
12+500	Horetzky Dyke	13.1	6.4	-7.68	10	None	Unweathered	Dry	Fair
12+475	Horetzky Dyke	13.1	6.4	-7.68	14.29	None	Slightly weathered	Dry	Fair
12+450	Horetzky Dyke	13.0	6.4	-9.33	14.29	None	Slightly weathered	Dry	Fair
12+425	Horetzky Dyke	13.0	6.4	-9.33	14.29	None	Unweathered	Dry	Fair
12+400	Horetzky Dyke	12.8	6.4	-11.66	14.29	None	Unweathered	Dry	Fair
12+375	Horetzky Dyke	12.8	6.4	-11.66	8.33	Hard more than 5mm	Unweathered	Damp	Fair
12+350	Horetzky Dyke	12.5	6.4	-13.89	8.33	None	Unweathered	Damp	Fair
12+325	Horetzky Dyke	12.5	6.4	-13.89	8.33	None	Unweathered	Damp	Fair
12+300	Horetzky Dyke	12.3	6.4	-16.00	8.33	None	Unweathered	Dry	Fair
12+275	Horetzky Dyke	12.3	6.4	-16.00	8.33	None	Moderately weathered	Dry	Fair
12+250	Horetzky Dyke	12.1	6.4	-18.04	8.33	None	Moderately weathered	Dry	Unfavourable

Chainage	*Rock type*	*σ_1*	*σ_3*	*θ*	*Structure*	*J_infill*	*J_weather*	*Groundwater*	*J_orient*
12+225	Horetzky Dyke	12.1	6.4	-18.04	8.33	Soft less than 5mm	Slightly weathered	Dry	Unfavourable
12+200	Horetzky Dyke	11.8	6.4	-18.86	8.33	None	Slightly weathered	Damp	Fair
12+175	Horetzky Dyke	11.8	6.4	-18.86	6.25	None	Slightly weathered	Dry	Fair
12+150	Horetzky Dyke	11.5	6.4	-19.40	6.25	None	Slightly weathered	Damp	Fair
12+125	Horetzky Dyke	11.5	6.4	-19.40	6.25	None	Slightly weathered	Dry	Fair
12+100	Horetzky Dyke	11.3	6.3	-18.95	6.25	None	Slightly weathered	Damp	Fair
12+075	Horetzky Dyke	11.3	6.3	-18.95	5.26	None	Unweathered	Dry	Fair
12+050	Horetzky Dyke	11.1	6.3	-18.28	5.26	None	Unweathered	Dry	Fair
12+025	Horetzky Dyke	11.1	6.3	-18.28	5.26	None	Unweathered	Dry	Fair
12+000	Horetzky Dyke	10.9	6.3	-17.92	5.26	None	Unweathered	Dry	Fair
11+975	Horetzky Dyke	10.9	6.3	-17.92	8.33	None	Highly weathered	Damp	Fair
11+950	Horetzky Dyke	10.7	6.3	-16.44	8.33	None	Slightly weathered	Dry	Fair
11+900	Horetzky Dyke	10.7	6.3	-16.44	8.33	None	Slightly weathered	Dry	Fair
11+875	Horetzky Dyke	10.6	6.3	-13.73	7.14	None	Moderately weathered	Dry	Fair
11+850	Horetzky Dyke	10.6	6.3	-13.73	7.14	Soft more than 5mm	Moderately weathered	Dry	Unfavourable
11+825	Horetzky Dyke	10.5	6.3	-10.08	7.14	None	Moderately weathered	Dry	Fair
11+800	Horetzky Dyke	10.5	6.3	-10.08	7.14	None	Moderately weathered	Dry	Fair
11+775	Horetzky Dyke	10.4	6.2	-7.20	5.88	None	Moderately weathered	Dry	Fair
11+750	Horetzky Dyke	10.4	6.2	-7.20	5.88	Hard less than 5mm	Moderately weathered	Damp	Fair
11+725	Horetzky Dyke	10.4	6.2	-5.20	5.88	Hard more than 5mm	Moderately weathered	Dry	Fair
11+700	Horetzky Dyke	10.4	6.2	-5.20	5.88	None	Moderately weathered	Dry	Fair
11+675	Horetzky Dyke	10.3	6.2	-3.01	10	None	Unweathered	Dry	Fair
11+650	Horetzky Dyke	10.3	6.2	-3.01	10	None	Unweathered	Dry	Fair
11+625	Horetzky Dyke	10.3	6.2	-1.44	10	None	Slightly weathered	Dry	Fair
11+600	Horetzky Dyke	10.3	6.2	-1.44	10	None	Slightly weathered	Damp	Fair
11+575	Horetzky Dyke	10.3	6.2	-0.24	5.56	None	Moderately weathered	Damp	Fair
11+550	Horetzky Dyke	10.3	6.2	-0.24	5.56	None	Moderately weathered	Dry	Unfavourable
11+525	Horetzky Dyke	10.3	6.1	0.38	5.56	None	Unweathered	Dry	Fair
11+500	Horetzky Dyke	10.3	6.1	0.38	5.56	Hard more than 5mm	Unweathered	Dry	Fair
11+475	Horetzky Dyke	10.3	6.1	0.38	5.88	None	Slightly weathered	Dry	Fair
11+450	Horetzky Dyke	10.4	6.0	0.48	5.88	None	Slightly weathered	Dry	Fair
11+425	Horetzky Dyke	10.4	6.0	0.48	5.88	None	Unweathered	Dry	Fair
11+400	Horetzky Dyke	10.4	6.0	0.66	5.88	None	Unweathered	Dry	Fair
11+375	Horetzky Dyke	10.4	6.0	0.66	5.56	None	Slightly weathered	Dry	Fair
11+350	Horetzky Dyke	10.5	5.9	-0.31	5.56	None	Slightly weathered	Dry	Fair
11+325	Horetzky Dyke	10.5	5.9	-0.31	5.56	None	Slightly weathered	Dry	Fair
11+300	Horetzky Dyke	10.5	5.9	-2.49	5.56	Soft less than 5mm	Slightly weathered	Dry	Fair
11+275	Horetzky Dyke	10.5	5.9	-2.49	5	None	Moderately weathered	Dry	Fair
11+250	Horetzky Dyke	10.5	5.8	-4.10	5	None	Moderately weathered	Dry	Fair

Chainage	*Rock type*	σ_1	σ_3	*θ*	*Structure*	*J_infill*	*J_weather*	*Groundwater*	*J_orient*
11+225	Horetzky Dyke	10.5	5.8	-4.10	5	None	Moderately weathered	Dry	Fair
11+200	Horetzky Dyke	10.6	5.8	-5.73	5	None	Moderately weathered	Dry	Fair
11+175	Horetzky Dyke	10.6	5.8	-5.73	50	None	Moderately weathered	Dry	Fair
11+150	Horetzky Dyke	10.6	5.7	-7.36	50	None	Moderately weathered	Damp	Fair
11+125	Horetzky Dyke	10.6	5.7	-7.36	50	Soft more than 5mm	Moderately weathered	Damp	Fair
11+100	Horetzky Dyke	10.7	5.7	-9.02	50	Soft less than 5mm	Moderately weathered	Dry	Fair
11+075	Horetzky Dyke	10.7	5.7	-9.02	33.33	Soft more than 5mm	Moderately weathered	Dry	Fair
11+050	Horetzky Dyke	10.7	5.6	-10.52	33.33	None	Moderately weathered	Dry	Fair
11+025	Horetzky Dyke	10.7	5.6	-10.52	33.33	Soft less than 5mm	Unweathered	Dry	Fair
11+000	Horetzky Dyke	10.8	5.5	-11.86	33.33	None	Unweathered	Dry	Fair
10+975	Horetzky Dyke	10.8	5.5	-11.86	10	None	Slightly weathered	Dry	Fair
10+950	Horetzky Dyke	10.9	5.5	-12.78	10	Soft more than 5mm	Slightly weathered	Dry	Fair
10+900	Horetzky Dyke	10.9	5.5	-12.78	10	Soft more than 5mm	Slightly weathered	Dry	Fair
10+875	Horetzky Dyke	10.9	5.4	-13.20	12.5	Hard more than 5mm	Moderately weathered	Dry	Fair
10+850	Horetzky Dyke	10.9	5.4	-13.20	12.5	None	Moderately weathered	Dry	Fair
10+825	Horetzky Dyke	10.9	5.4	-13.95	12.5	None	Moderately weathered	Dry	Fair
10+800	Horetzky Dyke	10.9	5.4	-13.95	12.5	None	Moderately weathered	Dry	Unfavourable
10+775	Horetzky Dyke	10.8	5.3	-15.22	8.33	Hard less than 5mm	Moderately weathered	Dry	Fair
10+750	Horetzky Dyke	10.8	5.3	-15.22	8.33	None	Moderately weathered	Damp	Fair
10+725	Horetzky Dyke	10.8	5.2	-16.52	8.33	None	Moderately weathered	Damp	Fair
10+700	Horetzky Dyke	10.8	5.2	-16.52	8.33	None	Moderately weathered	Damp	Fair
10+675	Horetzky Dyke	10.7	5.2	-17.78	6.67	None	Unweathered	Dry	Fair
10+650	Horetzky Dyke	10.7	5.2	-17.78	6.67	None	Unweathered	Dry	Fair
10+625	Horetzky Dyke	10.6	5.1	-18.65	6.67	None	Moderately weathered	Damp	Fair
10+600	Horetzky Dyke	10.6	5.1	-18.65	6.67	None	Moderately weathered	Damp	Fair
10+575	Horetzky Dyke	10.4	5.0	-19.25	7.14	None	Highly weathered	Dry	Fair
10+550	Horetzky Dyke	10.4	5.0	-19.25	7.14	None	Highly weathered	Damp	Fair
10+525	Horetzky Dyke	10.2	4.9	-20.44	7.14	None	Moderately weathered	Damp	Unfavourable
10+500	Horetzky Dyke	10.2	4.9	-20.44	7.14	Hard more than 5mm	Moderately weathered	Dry	Fair
10+475	Horetzky Dyke	10.2	4.9	-20.44	4.76	Hard more than 5mm	Unweathered	Dry	Fair
10+450	Horetzky Dyke	10.0	4.8	-21.93	4.76	Hard less than 5mm	Unweathered	Dry	Unfavourable
10+425	Horetzky Dyke	10.0	4.8	-21.93	4.76	Soft more than 5mm	Slightly weathered	Damp	Fair
10+400	Horetzky Dyke	9.8	4.8	-23.71	4.76	None	Slightly weathered	Damp	Fair
10+375	Horetzky Dyke	9.8	4.8	-23.71	10	None	Unweathered	Dry	Unfavourable
10+350	Horetzky Dyke	9.5	4.6	-25.38	10	None	Unweathered	Wet	Unfavourable
10+325	Horetzky Dyke	9.5	4.6	-25.38	10	Hard less than 5mm	Unweathered	Damp	Unfavourable
10+300	Horetzky Dyke	9.2	4.5	-27.16	10	None	Unweathered	Dry	Fair
10+275	Horetzky Dyke	9.2	4.5	-27.16	4.55	None	Slightly weathered	Dry	Fair
10+250	Horetzky Dyke	8.8	4.4	-29.93	4.55	None	Slightly weathered	Damp	Fair

Chainage	*Rock type*	σ_1	σ_3	*θ*	*Structure*	*J_infill*	*J_weather*	*Groundwater*	*J_orient*
10+225	Horetzky Dyke	8.8	4.4	-29.93	4.55	None	Slightly weathered	Dry	Fair
10+200	Horetzky Dyke	8.5	4.3	-32.12	4.55	None	Slightly weathered	Dry	Fair
10+175	Horetzky Dyke	8.5	4.3	-32.12	7.14	None	Unweathered	Dry	Fair
10+150	Horetzky Dyke	8.1	4.1	-34.07	7.14	None	Unweathered	Dry	Fair
10+125	Horetzky Dyke	8.1	4.1	-34.07	7.14	None	Unweathered	Dry	Fair
10+100	Horetzky Dyke	7.8	4.0	-36.57	7.14	None	Unweathered	Damp	Unfavourable
10+075	Horetzky Dyke	7.8	4.0	-36.57	11.11	Hard more than 5mm	Unweathered	Dry	Fair
10+050	Horetzky Dyke	7.4	3.9	-39.52	11.11	None	Unweathered	Dry	Fair
10+025	Horetzky Dyke	7.4	3.9	-39.52	11.11	Soft more than 5mm	Moderately weathered	Dry	Fair
10+000	Horetzky Dyke	7.0	3.8	-42.72	11.11	None	Moderately weathered	Damp	Very unfavourable
09+975	Horetzky Dyke	7.0	3.8	-42.72	16.67	None	Moderately weathered	Damp	Fair
09+950	Horetzky Dyke	7.0	3.8	-42.72	16.67	None	Moderately weathered	Dry	Fair
09+925	Horetzky Dyke	6.7	3.6	-42.70	16.67	None	Moderately weathered	Dry	Unfavourable
09+900	Horetzky Dyke	6.7	3.6	-42.70	16.67	None	Moderately weathered	Dry	Fair
09+875	Horetzky Dyke	6.3	3.4	-42.83	8.33	None	Moderately weathered	Damp	Fair
09+850	Horetzky Dyke	6.3	3.4	-42.83	8.33	None	Moderately weathered	Dry	Unfavourable
09+825	Horetzky Dyke	6.0	3.3	-43.02	8.33	None	Highly weathered	Dry	Fair
09+800	Horetzky Dyke	6.0	3.3	-43.02	8.33	None	Highly weathered	Dry	Fair
09+775	Horetzky Dyke	5.7	3.2	-43.48	20	None	Unweathered	Dry	Fair
09+750	Horetzky Dyke	5.7	3.2	-43.48	20	Hard less than 5mm	Unweathered	Dry	Unfavourable
09+725	Horetzky Dyke	5.3	3.1	-43.47	20	Hard more than 5mm	Slightly weathered	Dry	Unfavourable
09+700	Gamsby Group	5.3	3.1	-43.47	20	None	Slightly weathered	Dry	Unfavourable
09+675	Gamsby Group	5.1	3.0	-48.71	6.67	None	Slightly weathered	Dry	Unfavourable
09+650	Gamsby Group	5.1	3.0	-48.71	6.67	Soft more than 5mm	Slightly weathered	Dry	Unfavourable
09+625	Gamsby Group	4.8	2.9	-54.00	6.67	None	Slightly weathered	Dry	Fair
09+600	Gamsby Group	4.8	2.9	-54.00	6.67	None	Slightly weathered	Dry	Unfavourable
09+575	Gamsby Group	4.5	2.6	-58.29	16.67	Soft more than 5mm	Slightly weathered	Dry	Unfavourable
09+550	Gamsby Group	4.5	2.6	-58.29	16.67	None	Slightly weathered	Dry	Fair
09+525	Gamsby Group	4.2	2.4	-66.54	16.67	Soft more than 5mm	Unweathered	Dry	Fair
09+500	Gamsby Group	4.2	2.4	-66.54	16.67	None	Unweathered	Dry	Unfavourable
09+475	Gamsby Group	4.2	2.4	-66.54	10	None	Unweathered	Dry	Unfavourable
09+450	Gamsby Group	4.0	2.3	-77.64	10	None	Unweathered	Dry	Unfavourable
09+425	Gamsby Group	4.0	2.3	-77.64	10	Soft more than 5mm	Unweathered	Dry	Fair
09+400	Gamsby Group	3.9	2.3	-83.14	10	Soft more than 5mm	Unweathered	Dry	Fair
09+375	Gamsby Group	3.9	2.3	-83.14	6.25	Hard more than 5mm	Unweathered	Dry	Fair
09+350	Gamsby Group	3.9	2.3	-82.47	6.25	Soft more than 5mm	Unweathered	Damp	Fair
09+325	Gamsby Group	3.9	2.3	-82.47	6.25	None	Unweathered	Dry	Fair
09+300	Gamsby Group	3.8	2.2	-86.42	6.25	None	Unweathered	Dry	Fair
09+275	Gamsby Group	3.8	2.2	-86.42	9.09	Soft more than 5mm	Slightly weathered	Dry	Fair
09+250	Gamsby Group	3.8	2.2	88.39	9.09	None	Slightly weathered	Dry	Fair

Chainage	*Rock type*	σ_1	σ_3	θ	*Structure*	*J_infill*	*J_weather*	*Groundwater*	*J_orient*
09+225	Gamsby Group	3.8	2.2	88.39	9.09	None	Unweathered	Dry	Fair
09+200	Gamsby Group	3.8	2.1	83.47	9.09	Hard less than 5mm	Unweathered	Dry	Fair
09+175	Gamsby Group	3.8	2.1	83.47	6.25	None	Unweathered	Damp	Fair
09+150	Gamsby Group	3.8	2.1	79.94	6.25	None	Unweathered	Damp	Unfavourable
09+125	Gamsby Group	3.8	2.1	79.94	6.25	None	Unweathered	Damp	Unfavourable
09+100	Gamsby Group	3.9	2.1	79.37	6.25	None	Unweathered	Dry	Unfavourable
09+075	Gamsby Group	3.9	2.1	79.37	7.14	Soft more than 5mm	Unweathered	Dry	Unfavourable
09+050	Gamsby Group	3.9	2.0	80.33	7.14	None	Unweathered	Dry	Fair
09+025	Gamsby Group	3.9	2.0	80.33	7.14	Hard more than 5mm	Slightly weathered	Dry	Fair
09+000	Gamsby Group	4.0	2.0	79.70	7.14	None	Slightly weathered	Dry	Unfavourable
08+975	Gamsby Group	4.0	2.0	79.70	7.69	Hard less than 5mm	Moderately weathered	Damp	Unfavourable
08+950	Gamsby Group	4.0	2.0	79.70	7.69	Hard more than 5mm	Moderately weathered	Damp	Fair
08+925	Gamsby Group	4.1	2.1	77.15	7.69	None	Highly weathered	Damp	Fair
08+900	Gamsby Group	4.1	2.1	77.15	7.69	None	Highly weathered	Wet	Unfavourable
08+875	Gamsby Group	4.2	2.1	73.48	7.69	Hard less than 5mm	Highly weathered	Wet	Fair
08+850	Gamsby Group	4.2	2.1	73.48	7.69	Soft more than 5mm	Highly weathered	Damp	Unfavourable
08+825	Gamsby Group	4.3	2.1	67.19	7.69	None	Moderately weathered	Damp	Unfavourable
08+800	Gamsby Group	4.3	2.1	67.19	7.69	None	Moderately weathered	Dry	Unfavourable
08+775	Gamsby Group	4.5	2.0	66.58	5.56	None	Highly weathered	Dry	Fair
08+750	Gamsby Group	4.5	2.0	66.58	5.56	None	Highly weathered	Dry	Unfavourable
08+725	Gamsby Group	4.7	1.9	64.91	5.56	Hard less than 5mm	Highly weathered	Dry	Fair
08+700	Gamsby Group	4.7	1.9	64.91	5.56	Hard more than 5mm	Highly weathered	Dry	Unfavourable
08+675	Gamsby Group	5.0	2.0	63.13	10	None	Moderately weathered	Dry	Unfavourable
08+650	Gamsby Group	5.0	2.0	63.13	10	None	Moderately weathered	Dry	Fair
08+625	Gamsby Group	5.3	2.0	63.47	10	None	Slightly weathered	Damp	Unfavourable
08+600	Gamsby Group	5.3	2.0	63.47	10	Hard more than 5mm	Slightly weathered	Damp	Fair
08+575	Gamsby Group	5.6	2.0	61.35	5.88	Hard more than 5mm	Moderately weathered	Dripping	Fair
08+550	Gamsby Group	5.6	2.0	61.35	5.88	None	Moderately weathered	Damp	Fair
08+525	Gamsby Group	5.7	2.1	57.78	5.88	Hard more than 5mm	Moderately weathered	Damp	Unfavourable
08+500	Gamsby Group	5.7	2.1	57.78	5.88	None	Moderately weathered	Flowing	Fair
08+475	Gamsby Group	5.7	2.1	57.78	9.09	None	Unweathered	Flowing	Fair
08+450	Gamsby Group	5.7	2.1	54.49	9.09	None	Unweathered	Dry	Unfavourable
08+425	Gamsby Group	5.7	2.1	54.49	9.09	Soft more than 5mm	Unweathered	Damp	Very unfavourable
08+400	Gamsby Group	5.7	2.0	53.20	9.09	None	Unweathered	Damp	Unfavourable
08+375	Gamsby Group	5.7	2.0	53.20	4.17	None	Moderately weathered	Damp	Unfavourable
08+350	Gamsby Group	5.7	1.9	51.91	4.17	None	Moderately weathered	Dry	Fair
08+325	Gamsby Group	5.7	1.9	51.91	4.17	None	Slightly weathered	Dry	Unfavourable
08+300	Gamsby Group	5.6	1.9	48.26	4.17	None	Slightly weathered	Dry	Unfavourable
08+275	Gamsby Group	5.6	1.9	48.26	6.25	Hard more than 5mm	Moderately weathered	Damp	Fair
08+250	Gamsby Group	5.4	1.9	47.68	6.25	None	Moderately weathered	Damp	Unfavourable

Chainage	*Rock type*	σ_1	σ_3	*θ*	*Structure*	*J_infill*	*J_weather*	*Groundwater*	*J_orient*
08+225	Gamsby Group	5.4	1.9	47.68	6.25	None	Highly weathered	Dry	Unfavourable
08+200	Gamsby Group	5.4	1.9	44.40	6.25	None	Highly weathered	Dry	Fair
08+175	Gamsby Group	5.4	1.9	44.40	4.35	Soft more than 5mm	Decomposed	Dry	Fair
08+150	Gamsby Group	5.3	1.8	40.39	4.35	Soft less than 5mm	Decomposed	Damp	Unfavourable
08+125	Gamsby Group	5.3	1.8	40.39	4.35	Soft more than 5mm	Slightly weathered	Damp	Unfavourable
08+100	Gamsby Group	5.3	1.8	35.60	4.35	Soft less than 5mm	Slightly weathered	Dry	Unfavourable
08+075	Gamsby Group	5.3	1.8	35.60	4.17	None	Unweathered	Dry	Fair
08+050	Gamsby Group	5.3	1.7	33.22	4.17	Soft more than 5mm	Unweathered	Dry	Fair
08+025	Gamsby Group	5.3	1.7	33.22	4.17	None	Highly weathered	Wet	Fair
08+000	Gamsby Group	5.3	1.7	32.43	4.17	None	Highly weathered	Wet	Fair
07+975	Gamsby Group	5.3	1.7	32.43	4.17	None	Unweathered	Dry	Unfavourable
07+950	Gamsby Group	5.3	1.7	32.43	4.17	None	Unweathered	Damp	Fair
07+925	Gamsby Group	5.5	1.7	29.01	4.17	None	Unweathered	Damp	Unfavourable
07+900	Gamsby Group	5.5	1.7	29.01	4.17	Soft more than 5mm	Unweathered	Dripping	Unfavourable
07+875	Gamsby Group	5.7	1.6	26.00	7.46	Soft less than 5mm	Unweathered	Dripping	Fair
07+850	Gamsby Group	5.7	1.6	26.00	7.46	None		Damp	
07+825	Gamsby Group	6.0	1.7	29.12	7.46	None		Damp	
07+800	Gamsby Group	6.0	1.7	29.12	7.46	None		Damp	
07+775	Gamsby Group	6.3	1.7	34.21	7.46	None		Damp	
07+750	Gamsby Group	6.3	1.7	34.21	7.46	None		Damp	
07+725	Gamsby Group	6.6	1.8	40.86	Massive	None		Damp	
07+700	Tahtsa Complex	6.6	1.8	40.86	Massive	Hard less than 5mm			
07+675	Tahtsa Complex	7.2	1.9	44.61	Massive	Soft more than 5mm			
07+650	Tahtsa Complex	7.2	1.9	44.61	Massive	Soft more than 5mm			
07+625	Tahtsa Complex	7.8	2.0	45.17	Massive				
07+600	Tahtsa Complex	7.8	2.0	45.17	Massive				
07+575	Tahtsa Complex	8.3	2.1	45.93	Massive				
07+550	Tahtsa Complex	8.3	2.1	45.93	Massive				
07+525	Tahtsa Complex	8.8	2.0	45.67	Massive				
07+500	Tahtsa Complex	8.8	2.0	45.67	Massive				
07+475	Tahtsa Complex	8.8	2.0	45.67	Massive				
07+450	Tahtsa Complex	9.2	2.0	44.32	Massive				
07+425	Tahtsa Complex	9.2	2.0	44.32	Massive				
07+400	Tahtsa Complex	9.2	1.9	38.23	Massive				
07+375	Tahtsa Complex	9.2	1.9	38.23	Massive				
07+350	Tahtsa Complex	9.3	1.8	32.52	Massive				
07+325	Tahtsa Complex	9.3	1.8	32.52	Massive				
07+300	Tahtsa Complex	9.3	1.7	28.53	Massive				
07+275	Tahtsa Complex	9.3	1.7	28.53	Massive				
07+250	Tahtsa Complex	9.4	1.8	24.33	Massive				

Chainage	*Rock type*	*σ_1*	*σ_3*	*θ*	*Structure*	*J_infill*	*J_weather*	*Groundwater*	*J_orient*
07+225	Tahtsa Complex	9.4	1.8	24.33	Massive				
07+200	Tahtsa Complex	9.4	1.9	23.30	Massive				
07+175	Tahtsa Complex	9.4	1.9	23.30	Massive				
07+150	Tahtsa Complex	9.5	1.9	25.21	Massive				
07+125	Tahtsa Complex	9.5	1.9	25.21	Massive				
07+100	Tahtsa Complex	9.6	2.0	27.13	Massive				
07+075	Tahtsa Complex	9.6	2.0	27.13	Massive				
07+050	Tahtsa Complex	9.7	2.1	29.17	Massive				
07+025	Tahtsa Complex	9.7	2.1	29.17	Massive				
07+000	Tahtsa Complex	9.8	2.2	32.21	Very blocky				
06+975	Tahtsa Complex	9.8	2.2	32.21	Very blocky				
06+950	Tahtsa Complex	9.8	2.2	32.21	Very blocky				
06+925	Tahtsa Complex	10.0	2.3	34.07	Very blocky				
06+900	Tahtsa Complex	10.0	2.3	34.07	Very blocky				
06+875	Tahtsa Complex	10.1	2.4	37.68	Very blocky				
06+850	Tahtsa Complex	10.1	2.4	37.68	Very blocky				
06+825	Tahtsa Complex	10.3	2.4	40.04	Very blocky				
06+800	Tahtsa Complex	10.3	2.4	40.04	Very blocky				
06+775	Tahtsa Complex	10.5	2.5	41.82	Very blocky				
06+750	Tahtsa Complex	10.5	2.5	41.82	Very blocky				
06+725	Tahtsa Complex	10.6	2.5	42.21	Very blocky				
06+700	Tahtsa Complex	10.6	2.5	42.21	Very blocky				
06+675	Horetzky Dyke	10.7	2.6	41.39	Very blocky				
06+650	Horetzky Dyke	10.7	2.6	41.39	Very blocky				
06+625	Horetzky Dyke	10.8	2.6	41.58	Very blocky				
06+600	Horetzky Dyke	10.8	2.6	41.58	Very blocky				
06+575	Horetzky Dyke	10.6	2.7	42.38	Very blocky				
06+550	Horetzky Dyke	10.6	2.7	42.38	Very blocky				
06+525	Horetzky Dyke	10.6	2.7	44.44	Very blocky				
06+500	Horetzky Dyke	10.6	2.7	44.44	Blocky				
06+475	Horetzky Dyke	10.6	2.7	44.44	Blocky				
06+450	Horetzky Dyke	10.6	2.8	46.32	Blocky				
06+425	Horetzky Dyke	10.6	2.8	46.32	Blocky				
06+400	Horetzky Dyke	10.7	2.9	49.53	Blocky				
06+375	Horetzky Dyke	10.7	2.9	49.53	Blocky				
06+350	Horetzky Dyke	10.9	3.0	53.22	Blocky				
06+325	Horetzky Dyke	10.9	3.0	53.22	Blocky				
06+300	Horetzky Dyke	11.0	3.1	57.07	Blocky				
06+275	Horetzky Dyke	11.0	3.1	57.07	Blocky				
06+250	Horetzky Dyke	11.2	3.2	59.21	Blocky				

Chainage	*Rock type*	*σ_1*	*σ_3*	*θ*	*Structure*	*J_infill*	*J_weather*	*Groundwater*	*J_orient*
06+225	Horetzky Dyke	11.2	3.2	59.21	Blocky				
06+200	Horetzky Dyke	11.3	3.2	61.46	Blocky				
06+175	Horetzky Dyke	11.3	3.2	61.46	Blocky				
06+150	Horetzky Dyke	11.4	3.3	63.72	Blocky				
06+125	Horetzky Dyke	11.4	3.3	63.72	Blocky				
06+100	Horetzky Dyke	11.5	3.3	65.60	Blocky				
06+075	Horetzky Dyke	11.5	3.3	65.60	Blocky				
06+050	Horetzky Dyke	11.6	3.4	67.18	Blocky				
06+025	Horetzky Dyke	11.6	3.4	67.18	Blocky				
06+000	Horetzky Dyke	11.6	3.4	68.61	Blocky				
05+975	Horetzky Dyke	11.6	3.4	68.61	Blocky				
05+950	Horetzky Dyke	11.6	3.4	68.61	Blocky				
05+925	Horetzky Dyke	11.6	3.4	70.01	Blocky				
05+900	Horetzky Dyke	11.6	3.4	70.01	Blocky				
05+875	Horetzky Dyke	11.6	3.5	69.78	Blocky				
05+850	Horetzky Dyke	11.6	3.5	69.78	Blocky				
05+825	Horetzky Dyke	11.5	3.4	70.56	Blocky				
05+800	Horetzky Dyke	11.5	3.4	70.56	Blocky				
05+775	Horetzky Dyke	11.4	3.4	70.21	Blocky				
05+750	Horetzky Dyke	11.4	3.4	70.21	Blocky				
05+725	Horetzky Dyke	11.2	3.4	68.83	Blocky				
05+700	Horetzky Dyke	11.2	3.4	68.83	Blocky				
05+675	Horetzky Dyke	11.1	3.4	65.66	Blocky				
05+650	Horetzky Dyke	11.1	3.4	65.66	Blocky				
05+625	Horetzky Dyke	10.8	3.3	61.30	Blocky				
05+600	Horetzky Dyke	10.8	3.3	61.30	Blocky				
05+575	Horetzky Dyke	10.5	3.3	57.00	Blocky				
05+550	Horetzky Dyke	10.5	3.3	57.00	Blocky				
05+525	Horetzky Dyke	10.0	3.4	57.09	Blocky				
05+500	Horetzky Dyke	10.0	3.4	57.09	Blocky				
05+475	Horetzky Dyke	10.0	3.4	57.09	Blocky				
05+450	Horetzky Dyke	9.3	3.6	59.12	Blocky				
05+425	Horetzky Dyke	9.3	3.6	59.12	Blocky				
05+400	Horetzky Dyke	9.1	3.9	67.03	Blocky				
05+375	Horetzky Dyke	9.1	3.9	67.03	Blocky				
05+350	Horetzky Dyke	9.1	4.1	77.22	Blocky				
05+325	Horetzky Dyke	9.1	4.1	77.22	Blocky				
05+300	Horetzky Dyke	9.2	4.2	-89.96	Blocky				
05+275	Horetzky Dyke	9.2	4.2	-89.96	Blocky				
05+250	Horetzky Dyke	9.6	4.2	-79.72	Blocky				

Chainage	*Rock type*	*σ_1*	*σ_3*	*θ*	*Structure*	*J_infill*	*J_weather*	*Groundwater*	*J_orient*
05+225	Horetzky Dyke	9.6	4.2	-79.72	Blocky				
05+200	Horetzky Dyke	10.0	4.2	-73.54	Blocky				
05+175	Horetzky Dyke	10.0	4.2	-73.54	Blocky				
05+150	Horetzky Dyke	10.4	4.2	-70.40	Blocky				
05+125	Horetzky Dyke	10.4	4.2	-70.40	Blocky				
05+100	Horetzky Dyke	10.8	4.2	-68.39	Blocky				
05+075	Horetzky Dyke	10.8	4.2	-68.39	Blocky				
05+050	Horetzky Dyke	11.1	4.2	-67.51	Blocky				
05+025	Horetzky Dyke	11.1	4.2	-67.51	Blocky				
05+000	Horetzky Dyke	11.4	4.2	-67.52	Very blocky				
04+975	Horetzky Dyke	11.4	4.2	-67.52	Very blocky				
04+950	Horetzky Dyke	11.6	4.2	-69.94	Very blocky				
04+925	Horetzky Dyke	11.6	4.2	-69.94	Very blocky				
04+900	Horetzky Dyke	11.8	4.2	-72.19	Very blocky				
04+875	Horetzky Dyke	11.8	4.2	-72.19	Very blocky				
04+850	Horetzky Dyke	11.9	4.2	-74.14	Very blocky				
04+825	Horetzky Dyke	11.9	4.2	-74.14	Very blocky				
04+800	Horetzky Dyke	12.0	4.3	-76.04	Very blocky				
04+775	Horetzky Dyke	12.0	4.3	-76.04	Very blocky				
04+750	Horetzky Dyke	12.0	4.3	-77.95	Very blocky				
04+725	Horetzky Dyke	12.0	4.3	-77.95	Very blocky	Soft more than 5mm	Slightly weathered	Dry	
04+700	Horetzky Dyke	12.1	4.3	-79.87	Very blocky				
04+675	Horetzky Dyke	12.1	4.3	-79.87	Very blocky				
04+650	Horetzky Dyke	12.1	4.3	-81.21	Very blocky				
04+625	Horetzky Dyke	12.1	4.3	-81.21	Very blocky				
04+600	Horetzky Dyke	12.2	4.3	-81.64	Very blocky				
04+575	Horetzky Dyke	12.2	4.3	-81.64	Very blocky				
04+550	Horetzky Dyke	12.2	4.5	-79.48	Very blocky				
04+525	Horetzky Dyke	12.2	4.5	-79.48	Massive				
04+500	Horetzky Dyke	12.2	4.5	-79.48	Massive				
04+475	Horetzky Dyke	12.3	4.6	-76.61	Massive				
04+450	Horetzky Dyke	12.3	4.6	-76.61	Massive				
04+425	Horetzky Dyke	12.3	4.7	-73.13	Massive				
04+400	Horetzky Dyke	12.3	4.7	-73.13	Massive				
04+375	Horetzky Dyke	12.6	4.8	-70.58	Massive				
04+350	Horetzky Dyke	12.6	4.8	-70.58	Massive				
04+325	Horetzky Dyke	13.0	4.9	-68.17	Massive				
04+300	Horetzky Dyke	13.0	4.9	-68.17	Massive				
04+275	Horetzky Dyke	13.4	4.9	-63.67	Massive				
04+250	Horetzky Dyke								

Chainage	*Rock type*	*σ_1*	*σ_3*	*θ*	*Structure*	*J_infill*	*J_weather*	*Groundwater*	*J_orient*
04+225	Horetzky Dyke	13.4	4.9	-63.67	Massive				
04+200	Horetzky Dyke	13.9	5.0	-60.02	Massive				
04+175	Horetzky Dyke	13.9	5.0	-60.02	Massive				
04+150	Horetzky Dyke	14.3	5.0	-58.46	Massive				
04+125	Horetzky Dyke	14.3	5.0	-58.46	Massive				
04+100	Horetzky Dyke	14.7	5.1	-58.08	Massive				
04+075	Horetzky Dyke	14.7	5.1	-58.08	Massive				
04+050	Horetzky Dyke	15.0	5.1	-57.64	Massive				
04+025	Horetzky Dyke	15.0	5.1	-57.64	Massive				
04+000	Horetzky Dyke	15.3	5.2	-57.39	Massive				
03+975	Horetzky Dyke	15.3	5.2	-57.39	Massive				
03+950	Horetzky Dyke	15.6	5.2	-58.03	Massive				
03+925	Horetzky Dyke	15.6	5.2	-58.03	Massive				
03+900	Horetzky Dyke	15.6	5.2	-58.03	Massive				
03+875	Horetzky Dyke	15.9	5.3	-58.67	Massive				
03+850	Horetzky Dyke	15.9	5.3	-58.67	Massive				
03+825	Horetzky Dyke	16.2	5.3	-59.22	Massive				
03+800	Horetzky Dyke	16.2	5.3	-59.22	Massive				
03+775	Horetzky Dyke	16.4	5.3	-59.27	Massive				
03+750	Horetzky Dyke	16.4	5.3	-59.27	Massive				
03+725	Horetzky Dyke	16.6	5.3	-59.92	Massive				
03+700	Horetzky Dyke	16.6	5.3	-59.92	Massive				
03+675	Horetzky Dyke	16.7	5.4	-59.93	Massive				
03+650	Horetzky Dyke	16.7	5.4	-59.93	Massive				
03+625	Horetzky Dyke	16.9	5.4	-59.81	Massive				
03+600	Horetzky Dyke	16.9	5.4	-59.81	Massive				
03+575	Horetzky Dyke	17.0	5.5	-59.58	Massive				
03+550	Horetzky Dyke	17.0	5.5	-59.58	Massive				
03+525	Horetzky Dyke	17.1	5.5	-59.31	Massive				
03+500	Horetzky Dyke	17.1	5.5	-59.31	Blocky				
03+475	Horetzky Dyke	17.1	5.5	-59.31	Blocky				
03+450	Horetzky Dyke	17.2	5.5	-59.42	Blocky				
03+425	Horetzky Dyke	17.2	5.5	-59.42	Blocky				
03+400	Horetzky Dyke	17.2	5.5	-59.43	Blocky				
03+375	Horetzky Dyke	17.2	5.5	-59.43	Blocky				
03+350	Horetzky Dyke	17.2	5.5	-59.37	Blocky				
03+325	Horetzky Dyke	17.2	5.5	-59.37	Blocky				
03+300	Horetzky Dyke	17.2	5.6	-59.74	Blocky				
03+275	Horetzky Dyke	17.2	5.6	-59.74	Blocky				
03+250	Horetzky Dyke	17.2	5.6	-60.28	Blocky				

Chainage	*Rock type*	*σ_1*	*σ_3*	*θ*	*Structure*	*J_infill*	*J_weather*	*Groundwater*	*J_orient*
03+225	Horetzky Dyke	17.2	5.6	-60.28	Blocky				
03+200	Horetzky Dyke	17.1	5.6	-60.81	Blocky				
03+175	Horetzky Dyke	17.1	5.6	-60.81	Blocky				
03+150	Horetzky Dyke	17.0	5.6	-61.21	Blocky				
03+125	Horetzky Dyke	17.0	5.6	-61.21	Blocky				
03+100	Horetzky Dyke	16.9	5.6	-61.71	Blocky				
03+075	Horetzky Dyke	16.9	5.6	-61.71	Blocky				
03+050	Horetzky Dyke	16.7	5.6	-62.23	Blocky				
03+025	Horetzky Dyke	16.7	5.6	-62.23	Blocky				
03+000	Horetzky Dyke	16.6	5.6	-62.74	Blocky				
02+975	Horetzky Dyke	16.6	5.6	-62.74	Blocky				
02+950	Horetzky Dyke	16.5	5.6	-63.26	Blocky				
02+900	Horetzky Dyke	16.5	5.6	-63.26	Blocky				
02+875	Horetzky Dyke	16.3	5.6	-63.78	Blocky				
02+850	Horetzky Dyke	16.3	5.6	-63.78	Blocky				
02+825	Horetzky Dyke	16.2	5.6	-64.31	Blocky				
02+800	Horetzky Dyke	16.2	5.6	-64.31	Blocky				
02+775	Horetzky Dyke	16.0	5.6	-64.93	Blocky				
02+750	Horetzky Dyke	16.0	5.6	-64.93	Blocky				
02+725	Horetzky Dyke	15.8	5.5	-65.67	Blocky				
02+700	Horetzky Dyke	15.8	5.5	-65.67	Blocky				
02+675	Horetzky Dyke	15.6	5.5	-65.99	Blocky				
02+650	Horetzky Dyke	15.6	5.5	-65.99	Blocky				
02+625	Horetzky Dyke	15.4	5.5	-66.36	Blocky				
02+600	Horetzky Dyke	15.4	5.5	-66.36	Blocky				
02+575	Horetzky Dyke	15.2	5.5	-66.84	Blocky				
02+550	Horetzky Dyke	15.2	5.5	-66.84	Blocky				
02+525	Horetzky Dyke	15.0	5.4	-67.63	Blocky				
02+500	Horetzky Dyke	15.0	5.4	-67.63	Very blocky				
02+475	Horetzky Dyke	15.0	5.4	-67.63	Very blocky				
02+450	Horetzky Dyke	14.8	5.4	-67.91	Very blocky				
02+425	Horetzky Dyke	14.8	5.4	-67.91	Very blocky				
02+400	Horetzky Dyke	14.5	5.4	-68.43	Very blocky				
02+375	Horetzky Dyke	14.5	5.4	-68.43	Very blocky				
02+350	Horetzky Dyke	14.3	5.3	-69.00	Very blocky				
02+325	Horetzky Dyke	14.3	5.3	-69.00	Very blocky				
02+300	Horetzky Dyke	14.0	5.3	-69.53	Very blocky				
02+275	Horetzky Dyke	14.0	5.3	-69.53	Very blocky				
02+250	Horetzky Dyke	13.8	5.3	-69.97	Very blocky				

Chainage	*Rock type*	*σ_1*	*σ_3*	*θ*	*Structure*	*J_infill*	*J_weather*	*Groundwater*	*J_orient*
02+225	Horetzky Dyke	13.8	5.3	-69.97	Very blocky				
02+200	Horetzky Dyke	13.5	5.2	-70.35	Very blocky				
02+175	Horetzky Dyke	13.5	5.2	-70.35	Very blocky				
02+150	Horetzky Dyke	13.3	5.2	-70.46	Very blocky				
02+125	Horetzky Dyke	13.3	5.2	-70.46	Very blocky				
02+100	Horetzky Dyke	13.1	5.2	-69.92	Very blocky				
02+075	Horetzky Dyke	13.1	5.2	-69.92	Very blocky				
02+050	Horetzky Dyke	12.9	5.1	-69.57	Very blocky				
02+025	Horetzky Dyke	12.9	5.1	-69.57	Very blocky				
02+000	Horetzky Dyke	12.6	5.1	-69.64	Very blocky				
01+975	Horetzky Dyke	12.6	5.1	-69.64	Very blocky				
01+950	Horetzky Dyke	12.4	5.0	-69.45	Very blocky				
01+925	Horetzky Dyke	12.4	5.0	-69.45	Very blocky				
01+900	Horetzky Dyke	12.4	5.0	-69.45	Very blocky				
01+875	Horetzky Dyke	12.1	5.0	-69.11	Very blocky				
01+850	Horetzky Dyke	12.1	5.0	-69.11	Very blocky				
01+825	Horetzky Dyke	11.9	4.9	-68.74	Very blocky				
01+800	Horetzky Dyke	11.9	4.9	-68.74	Very blocky				
01+775	Horetzky Dyke	11.7	4.8	-68.27	Very blocky				
01+750	Horetzky Dyke	11.7	4.8	-68.27	Very blocky				
01+725	Horetzky Dyke	11.5	4.8	-67.72	Very blocky				
01+700	Horetzky Dyke	11.5	4.8	-67.72	Very blocky				
01+675	Horetzky Dyke	11.3	4.7	-67.38	Very blocky				
01+650	Horetzky Dyke	11.3	4.7	-67.38	Very blocky				
01+625	Horetzky Dyke	11.2	4.6	-67.72	Very blocky				
01+600	Horetzky Dyke	11.2	4.6	-67.72	Very blocky				
01+575	Horetzky Dyke	11.0	4.6	-68.34	Very blocky				
01+550	Horetzky Dyke	11.0	4.6	-68.34	Very blocky				
01+525	Horetzky Dyke	10.8	4.5	-69.11	Very blocky				
01+500	Horetzky Dyke	10.8	4.5	-69.11	Massive				
01+475	Horetzky Dyke	10.8	4.5	-69.11	Massive				
01+450	Horetzky Dyke	10.6	4.4	-70.03	Massive				
01+425	Horetzky Dyke	10.6	4.4	-70.03	Massive				
01+400	Horetzky Dyke	10.4	4.4	-71.13	Massive				
01+375	Horetzky Dyke	10.4	4.4	-71.13	Massive				
01+350	Horetzky Dyke	10.1	4.3	-72.84	Massive				
01+325	Horetzky Dyke	10.1	4.3	-72.84	Massive				
01+300	Horetzky Dyke	9.9	4.2	-76.09	Massive				
01+275	Horetzky Dyke	9.9	4.2	-76.09	Massive				
01+250	Horetzky Dyke	9.6	4.2	-79.21	Massive				

Chainage	*Rock type*	*σ_1*	*σ_3*	*θ*	*Structure*	*J_infill*	*J_weather*	*Groundwater*	*J_orient*
01+225	Horetzky Dyke	9.6	4.2	-79.21	Massive				
01+200	Horetzky Dyke	9.4	4.1	-82.51	Massive				
01+175	Horetzky Dyke	9.4	4.1	-82.51	Massive				
01+150	Horetzky Dyke	9.1	4.0	-86.10	Massive				
01+125	Horetzky Dyke	9.1	4.0	-86.10	Massive				
01+100	Horetzky Dyke	8.9	4.0	-89.49	Massive				
01+075	Horetzky Dyke	8.9	4.0	-89.49	Massive				
01+050	Horetzky Dyke	8.7	3.9	87.21	Massive				
01+025	Horetzky Dyke	8.7	3.9	87.21	Massive				
01+000	Horetzky Dyke	8.4	3.8	84.91	Very blocky				
00+975	Horetzky Dyke	8.4	3.8	84.91	Very blocky				
00+950	Horetzky Dyke	8.4	3.8	84.91	Very blocky				
00+925	Horetzky Dyke	8.1	3.7	82.52	Very blocky				
00+900	Horetzky Dyke	8.1	3.7	82.52	Very blocky				
00+875	Horetzky Dyke	7.8	3.6	77.70	Very blocky				
00+850	Horetzky Dyke	7.8	3.6	77.70	Very blocky				
00+825	Horetzky Dyke	7.5	3.4	71.25	Very blocky				
00+800	Horetzky Dyke	7.5	3.4	71.25	Very blocky				
00+775	Horetzky Dyke	7.2	3.3	64.75	Very blocky				
00+750	Horetzky Dyke	7.2	3.3	64.75	Very blocky				
00+725	Horetzky Dyke	6.9	3.2	59.52	Very blocky				
00+700	Horetzky Dyke	6.9	3.2	59.52	Very blocky				
00+675	Horetzky Dyke	6.6	3.1	52.81	Very blocky				
00+650	Horetzky Dyke	6.6	3.1	52.81	Very blocky				
00+625	Horetzky Dyke	6.3	3.0	45.70	Very blocky				
00+600	Horetzky Dyke	6.3	3.0	45.70	Very blocky				
00+575	Horetzky Dyke	6.0	2.9	40.06	Very blocky				
00+550	Horetzky Dyke	6.0	2.9	40.06	Very blocky				
00+525	Horetzky Dyke	5.7	2.8	32.79	Very blocky				
00+500	Horetzky Dyke	5.7	2.8	32.79	Very blocky				
00+475	Horetzky Dyke	5.7	2.8	32.79	Very blocky				
00+450	Horetzky Dyke	5.4	2.6	23.30	Very blocky				
00+425	Horetzky Dyke	5.4	2.6	23.30	Very blocky				
00+400	Horetzky Dyke	5.1	2.5	11.90	Very blocky				
00+375	Horetzky Dyke	5.1	2.5	11.90	Very blocky				
00+350	Horetzky Dyke	4.8	2.3	-2.29	Very blocky				
00+325	Horetzky Dyke	4.8	2.3	-2.29	Very blocky				
00+300	Horetzky Dyke	4.6	2.2	-16.66	Very blocky				
00+275	Horetzky Dyke	4.6	2.2	-16.66	Very blocky				
00+250	Horetzky Dyke	4.3	2.0	-32.31	Very blocky				

Chainage	***Rock type***	***σ_1***	***σ_3***	***θ***	***Structure***	***J_infill***	***J_weather***	***Groundwater***	***J_orient***
00+225	Horetzky Dyke	4.3	2.0	-32.31	Very blocky				
00+200	Horetzky Dyke	4.0	1.7	-55.24	Very blocky				
00+175	Horetzky Dyke	4.0	1.7	-55.24	Very blocky				
00+150	Horetzky Dyke	3.8	1.5	-78.91	Very blocky				
00+125	Horetzky Dyke	3.8	1.5	-78.91	Very blocky				
00+100	Horetzky Dyke	3.4	1.1	80.97	Very blocky				
00+075	Horetzky Dyke	3.4	1.1	80.97	Very blocky				
00+050	Horetzky Dyke	3.0	0.7	64.35	Very blocky				
00+025	Horetzky Dyke	3.0	0.7	64.35	Very blocky				
00+000	Horetzky Dyke	3.0	0.7	64.35	Very blocky				

Appendix E: Copyright Permissions

SPRINGER LICENSE
TERMS AND CONDITIONS

Jun 27, 2016

This Agreement between Josephine Morgenroth ("You") and Springer ("Springer") consists of your license details and the terms and conditions provided by Springer and Copyright Clearance Center.

License Number	3897250371134
License date	Jun 27, 2016
Licensed Content Publisher	Springer
Licensed Content Publication	Bulletin of Engineering Geology and the Environment
Licensed Content Title	The geological strength index: applications and limitations
Licensed Content Author	V. Marinos
Licensed Content Date	Jan 1, 2005
Licensed Content Volume Number	64
Licensed Content Issue Number	1
Type of Use	Thesis/Dissertation
Portion	Figures/tables/illustrations
Number of figures/tables /illustrations	1
Author of this Springer article	No
Order reference number	
Original figure numbers	Fig.1
Title of your thesis / dissertation	Elastic stress modelling and prediction of ground class using a Bayesian Belief Network at the Kemano tunnels
Expected completion date	Aug 2016
Estimated size(pages)	120
Requestor Location	Josephine Morgenroth EME 3203 1137 Alumni Ave Kelowna, BC v1v1v7 Canada Attn: Josephine Morgenroth
Billing Type	Invoice
Billing Address	Josephine Morgenroth EME 3203 1137 Alumni Ave Kelowna, BC v1v1v7 Canada Attn: Josephine Morgenroth

Total 0.00 CAD

Terms and Conditions

Introduction
The publisher for this copyrighted material is Springer. By clicking "accept" in connection with completing this licensing transaction, you agree that the following terms and conditions apply to this transaction (along with the Billing and Payment terms and conditions established by Copyright Clearance Center, Inc. ("CCC"), at the time that you opened your Rightslink account and that are available at any time at http://myaccount.copyright.com).
Limited License
With reference to your request to reuse material on which Springer controls the copyright, permission is granted for the use indicated in your enquiry under the following conditions:
- Licenses are for one-time use only with a maximum distribution equal to the number stated in your request.
- Springer material represents original material which does not carry references to other sources. If the material in question appears with a credit to another source, this permission is not valid and authorization has to be obtained from the original copyright holder.
- This permission
• is non-exclusive
• is only valid if no personal rights, trademarks, or competitive products are infringed.
• explicitly excludes the right for derivatives.
- Springer does not supply original artwork or content.
- According to the format which you have selected, the following conditions apply accordingly:
• **Print and Electronic:** This License include use in electronic form provided it is password protected, on intranet, or CD-Rom/DVD or E-book/E-journal. It may not be republished in electronic open access.
• **Print:** This License excludes use in electronic form.
• **Electronic:** This License only pertains to use in electronic form provided it is password protected, on intranet, or CD-Rom/DVD or E-book/E-journal. It may not be republished in electronic open access.
For any electronic use not mentioned, please contact Springer at permissions.springer@spi-global.com.
- Although Springer controls the copyright to the material and is entitled to negotiate on rights, this license is only valid subject to courtesy information to the author (address is given in the article/chapter).
- If you are an STM Signatory or your work will be published by an STM Signatory and you are requesting to reuse figures/tables/illustrations or single text extracts, permission is granted according to STM Permissions Guidelines: http://www.stm-assoc.org/permissions-guidelines/
For any electronic use not mentioned in the Guidelines, please contact Springer at permissions.springer@spi-global.com. If you request to reuse more content than stipulated in the STM Permissions Guidelines, you will be charged a permission fee for the excess content.
Permission is valid upon payment of the fee as indicated in the licensing process. If permission is granted free of charge on this occasion, that does not prejudice any rights we might have to charge for reproduction of our copyrighted material in the future.

-If your request is for reuse in a Thesis, permission is granted free of charge under the following conditions:
This license is valid for one-time use only for the purpose of defending your thesis and with a maximum of 100 extra copies in paper. If the thesis is going to be published, permission needs to be reobtained.
- includes use in an electronic form, provided it is an author-created version of the thesis on his/her own website and his/her university's repository, including UMI (according to the definition on the Sherpa website: http://www.sherpa.ac.uk/romeo/);
- is subject to courtesy information to the co-author or corresponding author.
Geographic Rights: Scope
Licenses may be exercised anywhere in the world.
Altering/Modifying Material: Not Permitted
Figures, tables, and illustrations may be altered minimally to serve your work. You may not alter or modify text in any manner. Abbreviations, additions, deletions and/or any other alterations shall be made only with prior written authorization of the author(s).
Reservation of Rights
Springer reserves all rights not specifically granted in the combination of (i) the license details provided by you and accepted in the course of this licensing transaction and (ii) these terms and conditions and (iii) CCC's Billing and Payment terms and conditions.
License Contingent on Payment
While you may exercise the rights licensed immediately upon issuance of the license at the end of the licensing process for the transaction, provided that you have disclosed complete and accurate details of your proposed use, no license is finally effective unless and until full payment is received from you (either by Springer or by CCC) as provided in CCC's Billing and Payment terms and conditions. If full payment is not received by the date due, then any license preliminarily granted shall be deemed automatically revoked and shall be void as if never granted. Further, in the event that you breach any of these terms and conditions or any of CCC's Billing and Payment terms and conditions, the license is automatically revoked and shall be void as if never granted. Use of materials as described in a revoked license, as well as any use of the materials beyond the scope of an unrevoked license, may constitute copyright infringement and Springer reserves the right to take any and all action to protect its copyright in the materials.
Copyright Notice: Disclaimer
You must include the following copyright and permission notice in connection with any reproduction of the licensed material:
"Springer book/journal title, chapter/article title, volume, year of publication, page, name(s) of author(s), (original copyright notice as given in the publication in which the material was originally published) "With permission of Springer"
In case of use of a graph or illustration, the caption of the graph or illustration must be included, as it is indicated in the original publication.
Warranties: None
Springer makes no representations or warranties with respect to the licensed material and adopts on its own behalf the limitations and disclaimers established by CCC on its behalf in its Billing and Payment terms and conditions for this licensing transaction.
Indemnity
You hereby indemnify and agree to hold harmless Springer and CCC, and their respective officers, directors, employees and agents, from and against any and all claims arising out of

your use of the licensed material other than as specifically authorized pursuant to this license.

No Transfer of License

This license is personal to you and may not be sublicensed, assigned, or transferred by you without Springer's written permission.

No Amendment Except in Writing

This license may not be amended except in a writing signed by both parties (or, in the case of Springer, by CCC on Springer's behalf).

Objection to Contrary Terms

Springer hereby objects to any terms contained in any purchase order, acknowledgment, check endorsement or other writing prepared by you, which terms are inconsistent with these terms and conditions or CCC's Billing and Payment terms and conditions. These terms and conditions, together with CCC's Billing and Payment terms and conditions (which are incorporated herein), comprise the entire agreement between you and Springer (and CCC) concerning this licensing transaction. In the event of any conflict between your obligations established by these terms and conditions and those established by CCC's Billing and Payment terms and conditions, these terms and conditions shall control.

Jurisdiction

All disputes that may arise in connection with this present License, or the breach thereof, shall be settled exclusively by arbitration, to be held in the Federal Republic of Germany, in accordance with German law.

Other conditions:

V 12AUG2015

Questions? customercare@copyright.com or +1-855-239-3415 (toll free in the US) or +1-978-646-2777.

ELSEVIER LICENSE
TERMS AND CONDITIONS

Jun 20, 2016

This Agreement between Josephine Morgenroth ("You") and Elsevier ("Elsevier") consists of your license details and the terms and conditions provided by Elsevier and Copyright Clearance Center.

License Number	3893151227255
License date	Jun 20, 2016
Licensed Content Publisher	Elsevier
Licensed Content Publication	Tunnelling and Underground Space Technology
Licensed Content Title	Risk analysis during tunnel construction using Bayesian Networks: Porto Metro case study
Licensed Content Author	Rita L. Sousa,Herbert H. Einstein
Licensed Content Date	January 2012
Licensed Content Volume Number	27
Licensed Content Issue Number	1
Licensed Content Pages	15
Start Page	86
End Page	100
Type of Use	reuse in a thesis/dissertation
Intended publisher of new work	other
Portion	figures/tables/illustrations
Number of figures/tables /illustrations	1
Format	electronic
Are you the author of this Elsevier article?	No
Will you be translating?	No
Order reference number	
Original figure numbers	Figure 3
Title of your thesis/dissertation	Elastic stress modelling and prediction of ground class using a Bayesian Belief Network at the Kemano tunnels
Expected completion date	Aug 2016
Estimated size (number of pages)	120
Elsevier VAT number	GB 494 6272 12

Requestor Location	Josephine Morgenroth EME 3203 1137 Alumni Ave Kelowna, BC v1v1v7 Canada Attn: Josephine Morgenroth
Total	0.00 USD

Terms and Conditions

INTRODUCTION

1. The publisher for this copyrighted material is Elsevier. By clicking "accept" in connection with completing this licensing transaction, you agree that the following terms and conditions apply to this transaction (along with the Billing and Payment terms and conditions established by Copyright Clearance Center, Inc. ("CCC"), at the time that you opened your Rightslink account and that are available at any time at http://myaccount.copyright.com).

GENERAL TERMS

2. Elsevier hereby grants you permission to reproduce the aforementioned material subject to the terms and conditions indicated.
3. Acknowledgement: If any part of the material to be used (for example, figures) has appeared in our publication with credit or acknowledgement to another source, permission must also be sought from that source. If such permission is not obtained then that material may not be included in your publication/copies. Suitable acknowledgement to the source must be made, either as a footnote or in a reference list at the end of your publication, as follows:
"Reprinted from Publication title, Vol /edition number, Author(s), Title of article / title of chapter, Pages No., Copyright (Year), with permission from Elsevier [OR APPLICABLE SOCIETY COPYRIGHT OWNER]." Also Lancet special credit - "Reprinted from The Lancet, Vol. number, Author(s), Title of article, Pages No., Copyright (Year), with permission from Elsevier."
4. Reproduction of this material is confined to the purpose and/or media for which permission is hereby given.
5. Altering/Modifying Material: Not Permitted. However figures and illustrations may be altered/adapted minimally to serve your work. Any other abbreviations, additions, deletions and/or any other alterations shall be made only with prior written authorization of Elsevier Ltd. (Please contact Elsevier at permissions@elsevier.com)
6. If the permission fee for the requested use of our material is waived in this instance, please be advised that your future requests for Elsevier materials may attract a fee.
7. Reservation of Rights: Publisher reserves all rights not specifically granted in the combination of (i) the license details provided by you and accepted in the course of this licensing transaction, (ii) these terms and conditions and (iii) CCC's Billing and Payment terms and conditions.
8. License Contingent Upon Payment: While you may exercise the rights licensed immediately upon issuance of the license at the end of the licensing process for the transaction, provided that you have disclosed complete and accurate details of your proposed use, no license is finally effective unless and until full payment is received from you (either by publisher or by CCC) as provided in CCC's Billing and Payment terms and conditions. If full payment is not received on a timely basis, then any license preliminarily granted shall be

deemed automatically revoked and shall be void as if never granted. Further, in the event that you breach any of these terms and conditions or any of CCC's Billing and Payment terms and conditions, the license is automatically revoked and shall be void as if never granted. Use of materials as described in a revoked license, as well as any use of the materials beyond the scope of an unrevoked license, may constitute copyright infringement and publisher reserves the right to take any and all action to protect its copyright in the materials.

9. Warranties: Publisher makes no representations or warranties with respect to the licensed material.

10. Indemnity: You hereby indemnify and agree to hold harmless publisher and CCC, and their respective officers, directors, employees and agents, from and against any and all claims arising out of your use of the licensed material other than as specifically authorized pursuant to this license.

11. No Transfer of License: This license is personal to you and may not be sublicensed, assigned, or transferred by you to any other person without publisher's written permission.

12. No Amendment Except in Writing: This license may not be amended except in a writing signed by both parties (or, in the case of publisher, by CCC on publisher's behalf).

13. Objection to Contrary Terms: Publisher hereby objects to any terms contained in any purchase order, acknowledgment, check endorsement or other writing prepared by you, which terms are inconsistent with these terms and conditions or CCC's Billing and Payment terms and conditions. These terms and conditions, together with CCC's Billing and Payment terms and conditions (which are incorporated herein), comprise the entire agreement between you and publisher (and CCC) concerning this licensing transaction. In the event of any conflict between your obligations established by these terms and conditions and those established by CCC's Billing and Payment terms and conditions, these terms and conditions shall control.

14. Revocation: Elsevier or Copyright Clearance Center may deny the permissions described in this License at their sole discretion, for any reason or no reason, with a full refund payable to you. Notice of such denial will be made using the contact information provided by you. Failure to receive such notice will not alter or invalidate the denial. In no event will Elsevier or Copyright Clearance Center be responsible or liable for any costs, expenses or damage incurred by you as a result of a denial of your permission request, other than a refund of the amount(s) paid by you to Elsevier and/or Copyright Clearance Center for denied permissions.

LIMITED LICENSE

The following terms and conditions apply only to specific license types:

15. **Translation**: This permission is granted for non-exclusive world **English** rights only unless your license was granted for translation rights. If you licensed translation rights you may only translate this content into the languages you requested. A professional translator must perform all translations and reproduce the content word for word preserving the integrity of the article.

16. **Posting licensed content on any Website**: The following terms and conditions apply as follows: Licensing material from an Elsevier journal: All content posted to the web site must maintain the copyright information line on the bottom of each image; A hyper-text must be included to the Homepage of the journal from which you are licensing at http://www.sciencedirect.com/science/journal/xxxxx or the Elsevier homepage for books at http://www.elsevier.com; Central Storage: This license does not include permission for a

scanned version of the material to be stored in a central repository such as that provided by Heron/XanEdu.
Licensing material from an Elsevier book: A hyper-text link must be included to the Elsevier homepage at http://www.elsevier.com . All content posted to the web site must maintain the copyright information line on the bottom of each image.

Posting licensed content on Electronic reserve: In addition to the above the following clauses are applicable: The web site must be password-protected and made available only to bona fide students registered on a relevant course. This permission is granted for 1 year only. You may obtain a new license for future website posting.
17. **For journal authors:** the following clauses are applicable in addition to the above:
Preprints:
A preprint is an author's own write-up of research results and analysis, it has not been peer-reviewed, nor has it had any other value added to it by a publisher (such as formatting, copyright, technical enhancement etc.).
Authors can share their preprints anywhere at any time. Preprints should not be added to or enhanced in any way in order to appear more like, or to substitute for, the final versions of articles however authors can update their preprints on arXiv or RePEc with their Accepted Author Manuscript (see below).
If accepted for publication, we encourage authors to link from the preprint to their formal publication via its DOI. Millions of researchers have access to the formal publications on ScienceDirect, and so links will help users to find, access, cite and use the best available version. Please note that Cell Press, The Lancet and some society-owned have different preprint policies. Information on these policies is available on the journal homepage.
Accepted Author Manuscripts: An accepted author manuscript is the manuscript of an article that has been accepted for publication and which typically includes author-incorporated changes suggested during submission, peer review and editor-author communications.
Authors can share their accepted author manuscript:

- immediately
    - via their non-commercial person homepage or blog
    - by updating a preprint in arXiv or RePEc with the accepted manuscript
    - via their research institute or institutional repository for internal institutional uses or as part of an invitation-only research collaboration work-group
    - directly by providing copies to their students or to research collaborators for their personal use
    - for private scholarly sharing as part of an invitation-only work group on commercial sites with which Elsevier has an agreement
- after the embargo period
    - via non-commercial hosting platforms such as their institutional repository
    - via commercial sites with which Elsevier has an agreement

In all cases accepted manuscripts should:

- link to the formal publication via its DOI
- bear a CC-BY-NC-ND license - this is easy to do

- if aggregated with other manuscripts, for example in a repository or other site, be shared in alignment with our hosting policy not be added to or enhanced in any way to appear more like, or to substitute for, the published journal article.

Published journal article (JPA): A published journal article (PJA) is the definitive final record of published research that appears or will appear in the journal and embodies all value-adding publishing activities including peer review co-ordination, copy-editing, formatting, (if relevant) pagination and online enrichment.
Policies for sharing publishing journal articles differ for subscription and gold open access articles:
Subscription Articles: If you are an author, please share a link to your article rather than the full-text. Millions of researchers have access to the formal publications on ScienceDirect, and so links will help your users to find, access, cite, and use the best available version.
Theses and dissertations which contain embedded PJAs as part of the formal submission can be posted publicly by the awarding institution with DOI links back to the formal publications on ScienceDirect.
If you are affiliated with a library that subscribes to ScienceDirect you have additional private sharing rights for others' research accessed under that agreement. This includes use for classroom teaching and internal training at the institution (including use in course packs and courseware programs), and inclusion of the article for grant funding purposes.
Gold Open Access Articles: May be shared according to the author-selected end-user license and should contain a CrossMark logo, the end user license, and a DOI link to the formal publication on ScienceDirect.
Please refer to Elsevier's posting policy for further information.
18. **For book authors** the following clauses are applicable in addition to the above: Authors are permitted to place a brief summary of their work online only. You are not allowed to download and post the published electronic version of your chapter, nor may you scan the printed edition to create an electronic version. **Posting to a repository:** Authors are permitted to post a summary of their chapter only in their institution's repository.
19. **Thesis/Dissertation**: If your license is for use in a thesis/dissertation your thesis may be submitted to your institution in either print or electronic form. Should your thesis be published commercially, please reapply for permission. These requirements include permission for the Library and Archives of Canada to supply single copies, on demand, of the complete thesis and include permission for Proquest/UMI to supply single copies, on demand, of the complete thesis. Should your thesis be published commercially, please reapply for permission. Theses and dissertations which contain embedded PJAs as part of the formal submission can be posted publicly by the awarding institution with DOI links back to the formal publications on ScienceDirect.

Elsevier Open Access Terms and Conditions
You can publish open access with Elsevier in hundreds of open access journals or in nearly 2000 established subscription journals that support open access publishing. Permitted third party re-use of these open access articles is defined by the author's choice of Creative Commons user license. See our open access license policy for more information.
Terms & Conditions applicable to all Open Access articles published with Elsevier:
Any reuse of the article must not represent the author as endorsing the adaptation of the article nor should the article be modified in such a way as to damage the author's honour or

reputation. If any changes have been made, such changes must be clearly indicated.
The author(s) must be appropriately credited and we ask that you include the end user license and a DOI link to the formal publication on ScienceDirect.
If any part of the material to be used (for example, figures) has appeared in our publication with credit or acknowledgement to another source it is the responsibility of the user to ensure their reuse complies with the terms and conditions determined by the rights holder.
Additional Terms & Conditions applicable to each Creative Commons user license:
CC BY: The CC-BY license allows users to copy, to create extracts, abstracts and new works from the Article, to alter and revise the Article and to make commercial use of the Article (including reuse and/or resale of the Article by commercial entities), provided the user gives appropriate credit (with a link to the formal publication through the relevant DOI), provides a link to the license, indicates if changes were made and the licensor is not represented as endorsing the use made of the work. The full details of the license are available at http://creativecommons.org/licenses/by/4.0.
CC BY NC SA: The CC BY-NC-SA license allows users to copy, to create extracts, abstracts and new works from the Article, to alter and revise the Article, provided this is not done for commercial purposes, and that the user gives appropriate credit (with a link to the formal publication through the relevant DOI), provides a link to the license, indicates if changes were made and the licensor is not represented as endorsing the use made of the work. Further, any new works must be made available on the same conditions. The full details of the license are available at http://creativecommons.org/licenses/by-nc-sa/4.0.
CC BY NC ND: The CC BY-NC-ND license allows users to copy and distribute the Article, provided this is not done for commercial purposes and further does not permit distribution of the Article if it is changed or edited in any way, and provided the user gives appropriate credit (with a link to the formal publication through the relevant DOI), provides a link to the license, and that the licensor is not represented as endorsing the use made of the work. The full details of the license are available at http://creativecommons.org/licenses/by-nc-nd/4.0.
Any commercial reuse of Open Access articles published with a CC BY NC SA or CC BY NC ND license requires permission from Elsevier and will be subject to a fee.
Commercial reuse includes:

- Associating advertising with the full text of the Article
- Charging fees for document delivery or access
- Article aggregation
- Systematic distribution via e-mail lists or share buttons

Posting or linking by commercial companies for use by customers of those companies.

20. **Other Conditions**:

v1.8

Questions? customercare@copyright.com or +1-855-239-3415 (toll free in the US) or +1-978-646-2777.

JOHN WILEY AND SONS LICENSE TERMS AND CONDITIONS

Jun 20, 2016

This Agreement between Josephine Morgenroth ("You") and John Wiley and Sons ("John Wiley and Sons") consists of your license details and the terms and conditions provided by John Wiley and Sons and Copyright Clearance Center.

License Number	3893150602997
License date	Jun 20, 2016
Licensed Content Publisher	John Wiley and Sons
Licensed Content Publication	Computer-Aided Civil and Infrastructure Engineering
Licensed Content Title	Dynamic Bayesian Network for Probabilistic Modeling of Tunnel Excavation Processes
Licensed Content Author	Olga Špačková,Daniel Straub
Licensed Content Date	Apr 9, 2012
Licensed Content Pages	21
Type of use	Dissertation/Thesis
Requestor type	University/Academic
Format	Electronic
Portion	Figure/table
Number of figures/tables	2
Original Wiley figure/table number(s)	Figure 4 Table 1
Will you be translating?	No
Title of your thesis / dissertation	Elastic stress modelling and prediction of ground class using a Bayesian Belief Network at the Kemano tunnels
Expected completion date	Aug 2016
Expected size (number of pages)	120
Requestor Location	Josephine Morgenroth EME 3203 1137 Alumni Ave Kelowna, BC v1v1v7 Canada Attn: Josephine Morgenroth
Publisher Tax ID	EU826007151
Billing Type	Invoice
Billing Address	Josephine Morgenroth EME 3203 1137 Alumni Ave Kelowna, BC v1v1v7 Canada

Attn: Josephine Morgenroth

Total 0.00 CAD

Terms and Conditions

TERMS AND CONDITIONS

This copyrighted material is owned by or exclusively licensed to John Wiley & Sons, Inc. or one of its group companies (each a"Wiley Company") or handled on behalf of a society with which a Wiley Company has exclusive publishing rights in relation to a particular work (collectively "WILEY"). By clicking "accept" in connection with completing this licensing transaction, you agree that the following terms and conditions apply to this transaction (along with the billing and payment terms and conditions established by the Copyright Clearance Center Inc., ("CCC's Billing and Payment terms and conditions"), at the time that you opened your RightsLink account (these are available at any time at http://myaccount.copyright.com).

Terms and Conditions

- The materials you have requested permission to reproduce or reuse (the "Wiley Materials") are protected by copyright.

- You are hereby granted a personal, non-exclusive, non-sub licensable (on a stand-alone basis), non-transferable, worldwide, limited license to reproduce the Wiley Materials for the purpose specified in the licensing process. This license, **and any CONTENT (PDF or image file) purchased as part of your order,** is for a one-time use only and limited to any maximum distribution number specified in the license. The first instance of republication or reuse granted by this license must be completed within two years of the date of the grant of this license (although copies prepared before the end date may be distributed thereafter). The Wiley Materials shall not be used in any other manner or for any other purpose, beyond what is granted in the license. Permission is granted subject to an appropriate acknowledgement given to the author, title of the material/book/journal and the publisher. You shall also duplicate the copyright notice that appears in the Wiley publication in your use of the Wiley Material. Permission is also granted on the understanding that nowhere in the text is a previously published source acknowledged for all or part of this Wiley Material. Any third party content is expressly excluded from this permission.

- With respect to the Wiley Materials, all rights are reserved. Except as expressly granted by the terms of the license, no part of the Wiley Materials may be copied, modified, adapted (except for minor reformatting required by the new Publication), translated, reproduced, transferred or distributed, in any form or by any means, and no derivative works may be made based on the Wiley Materials without the prior permission of the respective copyright owner.**For STM Signatory Publishers clearing permission under the terms of the STM Permissions Guidelines only, the terms of the license are extended to include subsequent editions and for editions in other languages, provided such editions are for the work as a whole in situ and does not involve the separate exploitation of the permitted figures or extracts,** You may not alter, remove or suppress in any manner any copyright, trademark or other notices displayed by the Wiley Materials. You may not license, rent, sell, loan,

lease, pledge, offer as security, transfer or assign the Wiley Materials on a stand-alone basis, or any of the rights granted to you hereunder to any other person.

- The Wiley Materials and all of the intellectual property rights therein shall at all times remain the exclusive property of John Wiley & Sons Inc, the Wiley Companies, or their respective licensors, and your interest therein is only that of having possession of and the right to reproduce the Wiley Materials pursuant to Section 2 herein during the continuance of this Agreement. You agree that you own no right, title or interest in or to the Wiley Materials or any of the intellectual property rights therein. You shall have no rights hereunder other than the license as provided for above in Section 2. No right, license or interest to any trademark, trade name, service mark or other branding ("Marks") of WILEY or its licensors is granted hereunder, and you agree that you shall not assert any such right, license or interest with respect thereto

- NEITHER WILEY NOR ITS LICENSORS MAKES ANY WARRANTY OR REPRESENTATION OF ANY KIND TO YOU OR ANY THIRD PARTY, EXPRESS, IMPLIED OR STATUTORY, WITH RESPECT TO THE MATERIALS OR THE ACCURACY OF ANY INFORMATION CONTAINED IN THE MATERIALS, INCLUDING, WITHOUT LIMITATION, ANY IMPLIED WARRANTY OF MERCHANTABILITY, ACCURACY, SATISFACTORY QUALITY, FITNESS FOR A PARTICULAR PURPOSE, USABILITY, INTEGRATION OR NON-INFRINGEMENT AND ALL SUCH WARRANTIES ARE HEREBY EXCLUDED BY WILEY AND ITS LICENSORS AND WAIVED BY YOU.

- WILEY shall have the right to terminate this Agreement immediately upon breach of this Agreement by you.

- You shall indemnify, defend and hold harmless WILEY, its Licensors and their respective directors, officers, agents and employees, from and against any actual or threatened claims, demands, causes of action or proceedings arising from any breach of this Agreement by you.

- IN NO EVENT SHALL WILEY OR ITS LICENSORS BE LIABLE TO YOU OR ANY OTHER PARTY OR ANY OTHER PERSON OR ENTITY FOR ANY SPECIAL, CONSEQUENTIAL, INCIDENTAL, INDIRECT, EXEMPLARY OR PUNITIVE DAMAGES, HOWEVER CAUSED, ARISING OUT OF OR IN CONNECTION WITH THE DOWNLOADING, PROVISIONING, VIEWING OR USE OF THE MATERIALS REGARDLESS OF THE FORM OF ACTION, WHETHER FOR BREACH OF CONTRACT, BREACH OF WARRANTY, TORT, NEGLIGENCE, INFRINGEMENT OR OTHERWISE (INCLUDING, WITHOUT LIMITATION, DAMAGES BASED ON LOSS OF PROFITS, DATA, FILES, USE, BUSINESS OPPORTUNITY OR CLAIMS OF THIRD PARTIES), AND WHETHER OR NOT THE PARTY HAS BEEN ADVISED OF THE POSSIBILITY OF SUCH DAMAGES. THIS LIMITATION SHALL APPLY NOTWITHSTANDING ANY FAILURE OF ESSENTIAL PURPOSE OF ANY LIMITED REMEDY PROVIDED HEREIN.

- Should any provision of this Agreement be held by a court of competent jurisdiction to be illegal, invalid, or unenforceable, that provision shall be deemed amended to achieve as nearly as possible the same economic effect as the original provision, and the legality, validity and enforceability of the remaining provisions of this Agreement shall not be affected or impaired thereby.

- The failure of either party to enforce any term or condition of this Agreement shall not constitute a waiver of either party's right to enforce each and every term and condition of this Agreement. No breach under this agreement shall be deemed waived or excused by either party unless such waiver or consent is in writing signed by the party granting such waiver or consent. The waiver by or consent of a party to a breach of any provision of this Agreement shall not operate or be construed as a waiver of or consent to any other or subsequent breach by such other party.

- This Agreement may not be assigned (including by operation of law or otherwise) by you without WILEY's prior written consent.

- Any fee required for this permission shall be non-refundable after thirty (30) days from receipt by the CCC.

- These terms and conditions together with CCC's Billing and Payment terms and conditions (which are incorporated herein) form the entire agreement between you and WILEY concerning this licensing transaction and (in the absence of fraud) supersedes all prior agreements and representations of the parties, oral or written. This Agreement may not be amended except in writing signed by both parties. This Agreement shall be binding upon and inure to the benefit of the parties' successors, legal representatives, and authorized assigns.

- In the event of any conflict between your obligations established by these terms and conditions and those established by CCC's Billing and Payment terms and conditions, these terms and conditions shall prevail.

- WILEY expressly reserves all rights not specifically granted in the combination of (i) the license details provided by you and accepted in the course of this licensing transaction, (ii) these terms and conditions and (iii) CCC's Billing and Payment terms and conditions.

- This Agreement will be void if the Type of Use, Format, Circulation, or Requestor Type was misrepresented during the licensing process.

- This Agreement shall be governed by and construed in accordance with the laws of the State of New York, USA, without regards to such state's conflict of law rules. Any legal action, suit or proceeding arising out of or relating to these Terms and Conditions or the breach thereof shall be instituted in a court of competent jurisdiction in New York County in the State of New York in the United States of America and each party hereby consents and submits to the personal jurisdiction of such court, waives any

objection to venue in such court and consents to service of process by registered or certified mail, return receipt requested, at the last known address of such party.

WILEY OPEN ACCESS TERMS AND CONDITIONS

Wiley Publishes Open Access Articles in fully Open Access Journals and in Subscription journals offering Online Open. Although most of the fully Open Access journals publish open access articles under the terms of the Creative Commons Attribution (CC BY) License only, the subscription journals and a few of the Open Access Journals offer a choice of Creative Commons Licenses. The license type is clearly identified on the article.

The Creative Commons Attribution License

The Creative Commons Attribution License (CC-BY) allows users to copy, distribute and transmit an article, adapt the article and make commercial use of the article. The CC-BY license permits commercial and non-

Creative Commons Attribution Non-Commercial License

The Creative Commons Attribution Non-Commercial (CC-BY-NC)License permits use, distribution and reproduction in any medium, provided the original work is properly cited and is not used for commercial purposes.(see below)

Creative Commons Attribution-Non-Commercial-NoDerivs License

The Creative Commons Attribution Non-Commercial-NoDerivs License (CC-BY-NC-ND) permits use, distribution and reproduction in any medium, provided the original work is properly cited, is not used for commercial purposes and no modifications or adaptations are made. (see below)

Use by commercial "for-profit" organizations

Use of Wiley Open Access articles for commercial, promotional, or marketing purposes requires further explicit permission from Wiley and will be subject to a fee.

Further details can be found on Wiley Online Library http://olabout.wiley.com/WileyCDA/Section/id-410895.html

Other Terms and Conditions:

v1.10 Last updated September 2015

Questions? customercare@copyright.com or +1-855-239-3415 (toll free in the US) or +1-978-646-2777.